WAP

NATIONAL ACADEMIES OF SCIENCES AND ENGINEERING

NATIONAL RESEARCH COUNCIL

of the

UNITED STATES OF AMERICA

UNITED STATES NATIONAL COMMITTEE

International Union of Radio Science

National Radio Science Meeting

4–8 January 2000

Sponsored by USNC/URSI

University of Colorado
Boulder, Colorado
U.S.A.

United States National Committee

INTERNATIONAL UNION OF RADIO SCIENCE

PROGRAM AND ABSTRACTS

National Radio Science Meeting
4–8 January 2000

Sponsored by USNC/URSI

NOTE:

Programs and Abstracts of the USNC/URSI Meetings are available from:

USNC/URSI
National Academy of Sciences
2101 Constitution Avenue, N.W.
Washington, DC 20418

at $5 for 1983–1999 meetings.

The full papers are not published in any collected format; requests for them should be addressed to the authors who may have them published on their own initiative. Please note that these meetings are national. They are not organized by the International Union, nor are the programs available from the International Secretariat.

MEMBERSHIP

United States National Committee
INTERNATIONAL UNION OF RADIO SCIENCE

Chair:	Gary Brown *
Secretary & Chair-Elect:	Umran S. Inan*
Immediate Past Chair:	Susan K. Avery*

Members Representing Societies, Groups, and Institutes:

American Astronomical Society	Thomas G. Phillips
American Geophysical Union	Donald T. Farley
American Meteorological Society	vacant
IEEE Antennas and Propagation Society	Linda P.B. Katehi
IEEE Geosciences and Remote Sensing Society	Roger Lang
IEEE Microwave Theory and Techniques Society	Arthur A. Oliner

Members-at-Large:

Amalia Barrios
J. Richard Fisher
Melinda Picket-May
Ronald Pogorzelski
W. Ross Stone
Richard Ziolkowski

Chairs of the USNC/URSI Commissions:

Commission A	Moto Kanda
Commission B	Piergiorgio L. E. Uslenghi
Commission C	Alfred O. Hero
Commission D	Alan Mickelson
Commission E	Jon Schoenberg
Commission F	Edgeworth R. Westwater
Commission G	John C. Foster
Commission H	Min-Chang Lee
Commission J	Peter Napier
Commission K	Frank S. Barnes

Officers, Chairs and Vice Chairs of Commissions of URSI residing in the United States:

Past President	Thomas B. A. Senior
Chair, Commission E	Robert L. Gardner
Chair, Commission J	Jackie N. Hewitt
Vice Chair, Commission A	Quirino Balzano
Vice Chair, Commission H	Umran S. Inan

* Member of USNC/URSI Executive Committee

DESCRIPTION OF THE INTERNATIONAL UNION OF RADIO SCIENCE

The International Union of Radio Science is one of the world scientific unions organized under the International Council of Scientific Unions (ICSU). It is commonly designated as URSI (from its French name, Union Radio Scientifique Internationale). Its aims are (1) to promote the scientific study of radio communications, (2) to aid and organize radio research requiring cooperation on an international scale and to encourage the discussion and publication of the results, (3) to facilitate agreement upon common methods of measurement and the standardization of measuring instruments, and (4) to stimulate and to coordinate studies of the scientific aspects of telecommunications using electromagnetic waves, guided and unguided. The International Union itself is an organizational framework to aid in promoting these objectives. The actual technical work is largely done by the National Committee in the various countries.

The new officers of the International Union are:

President:	Hiroshi Matsumoto (Japan)
Past President:	Thomas B. A. Senior (U.S.A.)
Vice Presidents:	Kristian Schlegel (Germany) Joseph Shapira (Israel) Andrzej W. Wernik (Poland Paul H. Wittke (Canada)
Secretary-General:	Paul Lagasse (Belgium)
Assistant Secretary-General:	Peter Van Daele
Administrative Secretary:	Inge Heleu

The Secretary-General's office and the headquarters of the organization are located at Avenue Albert Lancaster, 32, B-1180 Brussels, Belgium. The Union is supported by contributions (dues) from 38 member countries. Additional funds for symposia and other scientific activities of the Union are provided by ICSU from contributions received for this purpose from UNESCO.

The international Union, as of the XXVth General Assembly held in Kyoto, Japan, August 13–September 2, 1999, has ten bodies called Commissions for centralizing studies in the principal technical fields.

Every three years the International Union holds a meeting called the General Assembly. The next is the XXVIth, to be held in August, 2002, in Maastricht, the Netherlands. The Secretariat prepares and distributes the Proceedings of the General Assemblies. The International Union

arranges international symposia on specific subjects pertaining to the work of one or several Commissions and also cooperates with other Unions in international symposia on subjects of joint interest.

Radio is unique among the fields of scientific work in having a specific adaptability to large-scale international research programs, since many of the phenomena that must be studied are worldwide in extent and yet are in a measure subject to control by experimenters. Exploration of space and the extension of scientific observations to the space environment are dependent on radio for their research. One branch, radio astronomy, involves cosmic phenomena. URSI thus has a distinct field of usefulness in furnishing a meeting ground for the numerous workers in the manifold aspects of radio research; its meetings and committee activities furnish valuable means of promoting research through exchange of ideas.

Steering Committee:

D. Cook	P. L. Jensen	D. Thorsen	
R. Frehlich	J. McKie		

Technical Program Committee:

G.S. Brown, Chairperson

S.K. Avery	U. Inan	M. Picket-May	D. Wilton
F. Barnes	M. Kanda	L. Scharf	R. Frehlich
M.-C. Lee	J. Schoenberg	A. Gasiewski	P. Napier
D. Thorsen			

Session A1, 08:55 AM, Wed., Room 151

METROLOGY FOR DETECTION OF BURIED OBJECTS

Chairpersons: L.S. Riggs, Auburn Univ (riggs@eng.auburn.edu)
J. Harvey, Army Research Office (harvey@arl.mil)

A1-1 09:00 **UXOCOE MASTER PLAN FOR QUANTITATIVE TESTING OF UXO SENSOR TECHNOLOGIES**

Richard Weaver, Director
Joint Unexploded Ordnance Coordinating Office
Attn: AMSEL-RD-UXO-CO
10221 Burbeck Road
Ft. Belvoir, VA 22060-5806

Denis M. Reidy
E-OIR Measurements, Inc.
P.O. Box 1240
Spotsylvania, VA 22553-1240

Fairly comparing the detection and discrimination performance of sensors or systems is always difficult. A useful comparison is nearly impossible in uncontrolled test situations. The Unexploded Ordnance Center of Excellence (UXOCOE) proposes measuring performance using a set of standard test locations, targets, and protocols that are administered by an impartial entity. This paper briefly outlines a master plan to establish standard test sites, protocols, and procedures for Unexploded Ordnance (UXO) sensors.

Since the 1990's, significant investments by both the government and private industry have produced an exciting array of promising developments in sensors for detection of buried munitions, both ordnance and mines. Technologies such as ground penetrating radar (GPR), magnetometry, electro-magnetic induction (EMI) and synthetic aperture radar (SAR) are just a few examples that form the basis for many UXO detection sensors under development. Within each of these technology categories of UXO sensors, there are a number of different technical approaches being sold as the "best" way to exploit the respective technology. In addition, sensor fusion concepts (i.e. using more than one sensor technology) are being explored in an effort to bring the best of each technology to bear in solving the UXO problem.

The UXO industry (both military and civilian) cannot reasonably equally support every technology and sensor type being explored and promoted today. Rather, a tradeoff must occur in which only those technologies that are the most superior (both technically and economically) will become the *de facto* industry standards. Since it is unclear at this point which technologies and sensors types are superior, deciding how to wisely invest scarce R&D funds in this environment is complex.

A1-2
09:20

SPLITTING OF DEGERATE NATURAL MODES FOR BURIED TARGETS WITH ALMOST-O_2 SYMMETRY

Carl E. Baum
Air Force Research Laboratory DEHP
3550 Aberdeen Ave. SE
Kirtland AFB, NM 87117-5776

A recent paper [C.E. Baum, Interaction Note 523, 1996] has introduced a target signature based on continuous two-dimensional rotational symmetry with axial symmetry planes ($C_{\infty a}$ =O_2 symmetry). For wavelengths on the order of the target dimensions, this is sufficient to give zero backscattering cross polarization in the usual radar h,v coordinates where the axis of rotation is perpendicular to the $\hat{1}_h$ direction: Furthermore this property remains as the radar is moved around the target. For targets on or under the ground surface, this also allows for a vertically stratified earth which maintains the above symmetry. Note that it is the lack of something (the h,v backscattering) which is the signature. As such this can be referred to as a vampire signature, a vampire not seeing its reflection in a mirror (in this case the h,v mirror), at least according to legend. This signature has now been experimentally observed [L. Carin, R. Kapoor, and C.E. Baum, IEEE Trans. Geoscience and Remote Sensing, pp. 1985-1988, 1998]. Note that for SAR (synthetic aperture radar) measurements the O_2 symmetry is important since measurements are made from many azimuthal angles around the target.

For buried targets and associated lossy dielectric half space with O_2 symmetry (vertical rotation axis and axial symmetry planes, infinite in number) there is a two-fold degeneracy of the natural modes (for $m \geq 1$ in the $\cos(m\phi)$, $\sin(m\phi)$ decomposition), both with the same natural frequency. If the symmetry is not perfect, there is a splitting of these natural frequencies. Such asymmetry can come from many sources including target tilting and ground inhomogeneities.

As this signature is exploited, one should consider various theoretical and experimental aspects. No measurement is perfect; various sources of noise (errors) are present. One needs to quantify the amount of cross polarization present in the data, and compare it to the h,h and v,v components. This can be approached via the norms discussed in [C.E. Baum, Interaction Note 538, 1998]. Furthermore, the target may not possess the O_2 symmetry in perfect form, particularly when one considers the target's relation to the nearby soil which may not be uniform (e.g., rocks) and may not have the ground surface perfectly perpendicular to the target's rotation axis. This last problem is considered in this paper.

A1-3 09:40 ELECTROMAGNETIC INDUCTION SPECTROSCOPY FOR DETECTING AND IDENTIFYING BURIED OBJECTS

I. J. Won and Dean Keiswetter
Geophex, Ltd.
605 Mercury Street
Raleigh, North Carolina 27603
Phone: (919) 839-8515
Fax: (919) 839-8528
Email: ijwon@geophex.com or Keiswetter@geophex.com

An object, made partly or wholly of metals, has distinct combination of electrical conductivity, magnetic permeability, and geometrical shape and size. When the object is exposed to a low-frequency electromagnetic field, it produces a secondary magnetic field. By measuring the broadband spectrum of the secondary field, we obtain a distinct spectral signature that may uniquely identify the object. Based on the response spectrum, we attempt to "fingerprint" the object. This is the basic concept of *Electromagnetic Induction Spectroscopy* (EMIS).

From numerous surveys that we have conducted using our multifrequency electromagnetic sensors (GEM-2 and GEM-3 developed by Geophex), we have accumulated significant evidence that a metallic object undergoes continuous changes in response as the transmitter frequency changes. These observations made over many UXO targets suggest strongly that the EMI anomaly measured in a broad band offers an ability to both detect and identify a target.

Conventional metal detectors are not designed to do any more than simply detect the presence of buried metal objects, because most of them operate at a factory-set single frequency. A few detectors may have capability of operating at two or more discrete frequencies. These detectors have no ability to discriminate ordnance from trash metals and, therefore, the false alarm rate is unacceptably high. We believe that the EMIS technology can provide both detection and identification capabilities.

EMIS technology can be particularly useful for detecting buried landmines and unexploded ordnance. By fully characterizing and identifying an object without excavation, we should be able to reduce significantly the number of false targets. EMIS is applicable to many other problems where target identification and recognition (without intrusive search) are important. For instance, someday, an advanced EMIS devise at an airport security gate may be able to recognize a particular weapon by its maker and type.

A1-4 10:00 STATISTICAL SIGNAL PROCESSING FOR IMPROVED SUBSURFACE OBJECT DETECTION AND DISCRIMINATION

Stacy Tantum and Leslie Collins
Department of Electrical and Computer Engineering, Duke University
Box 90291, Durham, NC, 27708-0291

Several sensor modalities are currently being explored for the detection and identification of buried objects such as unexploded ordnance (UXO) and landmines. These include electromagnetic induction (EMI), magnetometers, radar, and seismic sensors. In our research program we are developing physics-based signal processing algorithms for each of the aforementioned sensor modalities and have demonstrated dramatic improvements in sensor performance (quantified in terms of the receiver operating characteristic, or ROC) by rigorously building the underlying physics into the signal processing algorithm. We are also utilizing the physical models to place performance bounds on the various systems. In addition to incorporating the physics directly into the signal processing architecture, uncertainties manifested in the subsurface sensing problem are also accounted for in an optimal framework. In the context of the UXO and landmine detection problem, the target depth, orientation, conductivity and permeability are generally unknown, and are treated statistically based on the their anticipated distributions. Such uncertainties, as well as a statistical characterization of clutter, are accounted for optimally through use of a Bayesian framework. The integration of a computational model into the statistical signal processing framework along with consideration of the uncertainty in the sensing environment results in a computationally intensive algorithm. Because of this fact, we have also considered several alternative approaches that, while sub-optimal, have significantly lowered the computational burden.

In this paper, we will discuss the underlying physical nature of the EMI-based UXO and landmine detection problem and briefly describe the range of computational models that have been developed by our colleagues. The tradeoffs between time- and frequency-domain sensor operation, as well as common approaches for sampling the received waveforms will also be summarized. We will present new theoretical results that quantify the performance bounds for several well-established time-domain sampling designs. Next, we describe an approach for determining the optimal sampling design and apply this approach to time-domain EMI systems. Finally, the relevance of these theoretical results will be demonstrated on field data by illustrating the improvements that have been obtained for the problem of UXO detection and discrimination from clutter. Tradeoffs between optimal and sub-optimal processing will also be discussed.

A1-5 10:40 ON DISCRIMINATING BETWEEN BURIED METALLIC MINES AND METALLIC CLUTTER USING SPATIAL SYMMETRY AND TEMPORAL EXPONENTIAL DECAY RATES

Lloyd Riggs, Tom Barnett, Larry Lowe, Jon Mooney, Steven Cash, and James Elkins
Electrical and Computer Engineering Department 200 Broun Hall
Auburn University, Alabama 36849

Last year we collected data at the JUXOCO test site located at Fort A. P. Hill with the U. S. Army's standard metal detector the AN/PSS-12. The AN/PSS-12 is a pulse-induction metal detector, and our instrumentation allowed us to collect "raw" data by amplifying and recording the time-domain response immediately following the metal detector's receiver coil. The JUXOCO test site has a calibration area and a large test grid made up of 980 adjacent 1 m square test locations (20 adjacent rows and each row has 49 test squares). At the center of each square there is nothing at all (a blank), a mine, or a clutter item (metallic trash). Time domain response data was collected at a number of different positions on an x-y grid centered over each square in the large test grid. Our presentation describes the signal processing algorithms that were used to discriminate among blanks, metallic mines, and metallic clutter.

The baseline receiver operating characteristic (ROC) curve (probability-of-detection versus probability-of-false alarm curve) for the AN/PSS-12 is shown to lie along the chance diagonal indicating that the instrument has no ability to discriminate between mines and clutter when used in its normal mode of operation (*i.e.* as a metal detector). We discovered that the *spatial* energy signature for mines is symmetrical, almost without exception, whereas in many instances the metallic clutter did not demonstrate this symmetry. This finding lead us to develop a very simple "symmetry detector" (algorithm) that enjoys a ROC curve well above the chance diagonal. Thus, by taking advantage of spatial information we were able to transform the AN/PSS-12 from a simple metal detector into a mine detector! Our paper will describe in greater detail the signal processing techniques that lead to the baseline and improved symmetry ROCs.

As pointed out by Baum (C. E. Baum, Interaction Note 499, November 1993) the low frequency response of highly, but not perfectly, conducting bodies is characterized by negative real natural frequencies that correspond to a damped exponential response in time domain. There is a unique correspondence between a metallic object's geometry (shape) and constitutive parameters (conductivity and permittivity) and its poles or time domain decay rates. This unique correspondence affords an opportunity for discrimination among metallic objects based on their negative real natural frequencies – a method referred to as magnetic singularity identification (MSI). We are currently working to use MSI to improve our symmetry ROC, and our presentation will summarize progress on this front.

A1-6
11:00

TARGET-VICINITY SCATTERING PARAMETERS

Carl E. Baum
Air Force Research Laboratory DEHP
3550 Aberdeen Ave SE
Kirtland AFB, NM 87117-5776

The scattering of an electromagnetic wave from a target in a complex nonuniform medium, and using the scattered fields to identify the target is quite a challenging problem. Even with a finite library of target types (e.g., mine or unexploded ordnance (UXO)) the various types of clutter (e.g., rocks rough ground surface, etc.) can greatly distort the signal one is trying to receive from the target. One would like to separate the clutter signals from the target signals to the extent possible.

One approach to this problem is to separate out the scattering phenomena at the target (volume V_s) and in its immediate vicinity V_v, from the scattering of both incident and target-scattered fields at more distant positions (clutter, ground surface, etc.). So we would like to concentrate on parameters which are associated with the target itself, and not the propagation to and from the target through a scattering medium. We can call such parameters *target-vicinity parameters*. Of course, such parameters still have to be measured by the scattered field as received by our antennas.

In the analysis let us assume that the target vicinity V_v has a simple or "uncluttered" characteristic. It might be uniform and isotropic, or at least of a simpler character than that of the medium farther away. In our approach to this problem we will define a canonical or background problem and compare this to the more realistic problem with the clutter. By such we may be able to see what remains the same, or nearly so. This can even lead to a perturbation analysis to approximately quantify the changes.

By looking at the medium in V_v (the target vicinity), one can extend this medium through the target and on to infinity to define a canonical scattering problem. Then one can often treat the difference from this canonical problem as a difference problem containing the clutter. Such distant contributions can be considered as a small change to the Green functions *at the target*, where both source and observation coordinates are in the target volume V_s. This is reflected in small changes to things like natural frequencies, natural modes, eigenvalues, eigenmodes, etc. that are properties of the integral-equation operator in the target domain V_s. Such are the target-vicinity scattering parameters. A useful way to evaluate the desired insensitivity of the target-scattering parameters to distant clutter is perturbation theory.

A1-7
11:20

SIMULATIONS OF GPR BACKSCATTER FROM BURIED DRUMS

John F. Aurand
ITT Industries, Systems Division
6400 Uptown Blvd. NE, Suite 300E
Albuquerque, NM 87110
(Work Performed at the University of New Mexico, EECE Dept.)

As part of a ground-penetrating radar project at Sandia National Laboratories, we recently completed numerical simulations of the electromagnetic backscatter propagation from buried 55-gal. drums. These simulations were based on prior numerical modeling by Duke University. This presentation describes the modeling effort and the resulting predictions of backscatter propagation from drums buried at several depths.

The Duke University modeling work yielded datasets for the electromagnetic backscatter from a buried PEC right circular cylinder with a diameter of 60 cm and a length of 90 cm, in a variety of orientations and at depths up to 3 m. This was performed with a unique frequency-domain method-of-moments code designed for a perfectly-conducting target buried in a lossy, dispersive half-space.

Based on those frequency-domain datasets, we extended the backscatter data to higher frequencies to cover the spectral content of the transient GPR pulses used in our simulations. The extended-frequency datasets were then used in GPR system simulations to predict the transient backscatter from the buried targets at the specified depths and orientations.

The backscatter transfer function was formed for a normally-incident plane wave impinging on flat earth, propagating down to the buried drum, scattering off the drum, and propagating back up and out of the earth surface. This was done for vertically oriented drums and horizontally oriented drums (with axis either parallel to or perpendicular to the incident wave polarization). The backscatter transfer function was then used with a variety of transient incident pulses to simulate the backscattered wave from the buried target. In addition, the reflected wave off the surface of the earth was computed, for realistic prediction of the overall time-domain signals which would be measured by a VHF/UHF high-power GPR system.

B/F1-1
09:00

SURFACE PLASMON POLARITON PROPAGATION NEAR AN INDEX STEP

Alexei A. Maradudin*
University of California
Irvine, CA 92697
T. A. Leskova
Institute of Spectroscopy, Moscow Region 142092
Troitsk, Russia
W. Zierau
Universität Muenster,
Muenster, Germany

In this work we study theoretically the scattering of p-polarized light of frequency ω from a system consisting of a dielectric medium (prism) characterized by a real positive isotropic dielectric constant ϵ_0 in the region $x_3 > D$; a metal film characterized by a complex isotropic dielectric function $\epsilon(\omega)$ in the region $0 < x_3 < D$; a dielectric film characterized by a coordinate-dependent dielectric constant $\epsilon(x_1)$ in the region $-d < x_3 < 0$; and vacuum in the region $x_3 < -d$. The light, whose plane of incidence is the x_1x_3-plane, is incident through the prism. For the dielectric constant $\epsilon(x_1)$ we assume the form $\epsilon(x_1) = \epsilon\theta(x_1)$, where $\theta(x_1)$ is the Heaviside unit step function. Thus, we have a dielectric film of dielectric constant ϵ covering the half of the lower surface ($x_3 = 0$) of the metal film defined by $x_1 > 0$. The reduced Rayleigh equation for the amplitude of the light scattered back into the prism, $R(q|k)$, is solved numerically, and the result is used to calculate the intensity of the scattered field in the far-field region as a function of x_1 for a fixed value of x_3 for several values of the wavelength of the incident light. The results provide information about the scattering of the surface plasmon polariton on the metal-vacuum interface, excited by the incident light, from an index step on that interface, and are compared with the results of a recent experimental study of this scattering (C. E. H. Berger, R. P. H. Kooyman, and J. Greve, Opt. Commun. **167**, 183, 1999).). The agreement is good. Some discussion of the transmission of light through this system will also be given.

B/F1-2
09:20

LOCALIZATION OF SURFACE PLASMON POLARITONS ON A RANDOM SURFACE

I. Simonsen*
Norwegian University of Science and Technology,
Trondheim, Norway
T. A. Leskova
Institute of Spectroscopy, Moscow Region 142092
Troitsk, Russia
Alexei A. Maradudin
University of California
Irvine, CA 92697

The Anderson localization length of a surface plasmon polariton of frequency ω propagating along a one-dimensional randomly rough surface of a metal in contact with vacuum can be determined by calculating the amplitude $t(\omega)$ of the surface plasmon polariton transmitted through a finite length L of the random surface. The surface plasmon polariton transmission coefficient is then given by $T(\omega) = |t(\omega)|^2$. For large L the average of the self-averaging quantity $\ell n T(\omega)$ over the ensemble of realizations of the random surface, $\langle \ell n T(\omega) \rangle$, is expected to display the behavior L, $\langle \ell n T(\omega) \rangle = \text{const.} - L/\ell_T(\omega)$, where the characteristic length $\ell_T(\omega)$ is called the Lyapunov exponent. It is not the localization length of the surface plasmon polariton $\ell(\omega)$ because there are two other mechanisms besides localization that can lead to such a behavior: ohmic losses due to the imaginary part of the dielectric function of the metal, and the roughness-induced conversion of the surface plasmon polariton into volume waves in the vacuum propagating away from the surface. This radiative damping of the surface plasmon polariton is called leakage. If the characteristic decay lengths associated with ohmic losses and with leakage are denoted by $\ell_\epsilon(\omega)$ and $\ell_{\rm rad}(\omega)$, respectively, we have $\ell_T^{-1}(\omega) = \ell^{-1}(\omega) + \ell_\epsilon^{-1}(\omega) + \ell_{\rm rad}^{-1}(\omega)$. We have carried out computer simulation calculations of $\langle \ell n T(\omega) \rangle$ as a function of L, and hence $\ell_T(\omega)$, for a weakly rough one-dimensional surface that suppresses leakage, i.e. one for which $\ell_{\rm rad}^{-1}(\omega) = 0$. The reciprocal decay rate $\ell_\epsilon^{-1}(\omega)$ is readily calculated perturbatively for the weakly rough random metal surfaces we consider here. We are therefore able to calculate the Anderson localization length $\ell(\omega)$ from the calculated values of $\ell_T(\omega)$.

B/F1-3
09:40

REFLECTIVITY OF AN AMPLIFYING SURFACE

I. Simonsen*
Norwegian University of Science and Technology,
Trondheim, Norway
T. A. Leskova
Institute of Spectroscopy, Moscow Region 142092
Troitsk, Russia
Alexei A. Maradudin
University of California
Irvine, CA 92697

The overwhelming majority of the theoretical and experimental studies of the scattering of light from randomly rough surfaces have been devoted to scattering from the surfaces of passive, i.e. absorbing, media. The scattering of light from a randomly rough surface bounding an active, i.e. an amplifying, medium, has been little studied until now. In this work we calculate the reflectivity when a system consisting of vacuum in the region $x_3 > \zeta(x_1)$, an amplifying medium in the region $-d < x_3 < \zeta(x_1)$, and a perfect conductor in the region $x_3 < -d$, is illuminated from the vacuum side by s-polarized light of frequency ω. The surface profile function $\zeta(x_1)$ is assumed to be a single-valued function of x_1 that is differentiable as many times as is necessary, and that constitutes a zero-mean, stationary Gaussian random process characterized by a Gaussian height autocorrelation function. The amplifying medium is modeled by a dielectric medium whose dielectric constant ϵ has an imaginary part ϵ_2 that is negative, while its real part ϵ_1 is positive. The values of ϵ_2 are chosen such that they correspond to gains in the medium that are physically realizable. The assumption of a negative imaginary part to ϵ is the simplest way of modeling stimulated emission in this system. The reflectivity is given by $|R(k)|^2$, where $R(k)$ is defined in terms of the scattering amplitude $R(q|k)$ by $|\langle R(q|k)\rangle|^2 = L_1 2\pi\delta(q-k)|R(k)|^2$. In this relation the wavenumbers k and q are related to the angles of incidence and scattering by $k = (\omega/c)\sin\theta_0$ and $q = (\omega/c)\sin\theta_s$, respectively, L_1 is the length of the x_1-axis covered by the random surface, and the angle brackets denote an average over the ensemble of realizations of the surface profile function $\zeta(x_1)$. The scattering amplitude $R(q|k)$ is obtained by solving numerically the reduced Rayleigh equation it satisfies for a large number of realizations of $\zeta(x_1)$, and $\langle R(q|k)\rangle$ is obtained by averaging the results. As expected, the reflectivity of the amplifying medium with a random surface is larger than that of the corresponding absorbing medium, viz. a medium with the same value of $|\epsilon_2|$ but with ϵ_2 positive, for all angles of incidence.

B/F1-4
10:00

THE ANGULAR INTENSITY CORRELATION FUNCTION $C^{(10)}(q,k|q',k')$ OF LIGHT SCATTERED FROM SURFACES WITH EVEN AND ODD SYMMETRY

T. A. Leskova*
Institute of Spectroscopy, Moscow Region 142092
Troitsk, Russia
Alexei A. Maradudin
University of California
Irvine, CA 92697
I. Simonsen
Norwegian University of Science and Technology,
Trondheim, Norway

Existing theoretical and experimental studies of the angular intensity correlation function $C^{(10)}(q,k|q',k')$ for the scattering of p-polarized light from a weakly rough, one-dimensional, random metal surface have shown that its envelope function $C_0^{(10)}(q,k|q',q'+q-k)$, defined by $C^{(10)}(q,k|q',k') = 2\pi\delta(q+q'-k'-k')\ C_0^{(10)}(q,k|q',q'+q-k)$, is a structureless function of θ_s' for fixed values of θ_0 and θ_s, subject to the condition $\sin\theta_0' = \sin\theta_s' + \sin\theta_s - \sin\theta_0$. In the preceding expressions the wavenumbers k and q are related to the angles of incidence and scattering by $k = (\omega/c)\sin\theta_0$ and $q = (\omega/c)\sin\theta_s$, respectively, where ω is the frequency of the incident light. In the present work we examine the question of whether structure, e.g. peaks or dips, can be induced into $C_0^{(10)}(q,k|q',q'+q-k)$ by the use of a suitably designed one-dimensional random surface. In particular, by small-amplitude perturbation theory and by a computer simulation approach, we calculate $C_0^{(10)}(q,k|q',q'+q-k)$ for a one-dimensional, random, metal surface whose surface profile function $\zeta(x_1)$ is an even or an odd function of x_1, $\zeta(-x_1) = \pm\zeta(x_1)$, respectively. Such a surface can be obtained by first generating a one-dimensional surface profile function $\zeta(x_1)$ that is a zero-mean, stationary, Gaussian random process, characterized by a surface height autocorrelation function that is either of Gaussian or West-O'Donnell form. The surface profile function $\zeta(x_1)$ is then defined by $\zeta(x_1) = \frac{1}{2}[s(x_1) \pm s(-x_1)]$. It is no longer a stationary random process, because the point $x_1 = 0$ is a distinguished point. The results of our calculations show that $C_0^{(10)}(q,k|q',q'+q-k)$ displays peaks analogous to the memory effect peak and to the reciprocal memory effect peak, for scattering from surfaces of both even and odd symmetry.

B/F1-5
10:40

LASER EXCITATION OF POLARIZATION WAVES IN A FROZEN GAS

V. Celli* J. S. Frasier
University of Virginia
Charlottesville, VA 22903

Laser experiments with optically excited frozen gases entail the excitation of polarization waves that, neglecting retardation, can be described as Frenkel excitons in the presence of an applied electric field. The atoms are initially in an s state and the field, in the z direction, is strong enough that the p_z state is well separated from the p_x and p_y states. Therefore only transitions to the p_z state need to be considered. In a continuum approximation the waves are dispersionless, but their frequency depends on the direction of propagation according to $P_2(\cos\theta_k)$, where θ_k is the angle between the propagation vector and the direction of the electric field. A question of interest for the interpretation of the experiments is the frequency spectrum of these excitons in the frozen gas, assuming that the atoms are randomly distributed.

In the experiments, the excitation occurs through energy transfer from a pair of initial states, s and s', to two states p_z and p'_z via dipole-dipole interactions. Thus a p'_z exciton is created at the same time as a p_z exciton, but the dispersion of the p'_z exciton is small. We are able to describe exactly the probability of the initial $ss' \rightarrow p_z p'_z$ transfer in the discrete random medium. To describe the subsequent time development, we need to know not only the spectrum of the p_z excitons, but also whether and how they are localized. The exciton spectrum and localization have been discussed previously when no E_z field is present (D. E. Logan and P. G. Wolynes, *J. Chem. Phys.*, **87**, 7199–7207, 1987). We are applying similar techniques in the presence of an electric field and also carrying out direct numerical simulations of time evolution. In these simulations we do not make any further approximations, but solve the coupled system of differential equations numerically for many possible realizations and average the results.

We have shown in a previous publication (J. S. Frasier, V. Celli, and T. Blum, *Phys. Rev. A*, **59**, 4358–4367, 1999) how a system of atoms interacting via dipole-dipole potentials is mathematically equivalent to a system of interacting spins. The particular system which we are studying is equivalent to the problem of a random ferromagnetic alloy with dipolar interactions, and in that system the polarization waves we discuss here correspond to spin waves. We actually have two interpenetrating spin systems, one initially with all spins up corresponding to the atoms in the s state, and one initially with all spins down corresponding to the atoms in the s' state. As the two spin systems interact, many spin waves are created and mode-mode coupling could be important. We have developed a simple average magnetization picture that leads to Bloch-type equations of time evolution. This picture will be tested against the spin-wave picture and numerical simulations.

B/F1-6
11:00

ROUGH SURFACE RADAR BACKSCATTER CROSS SECTIONS BASED ON A STATIONARY TWO-SCALE FULL WAVE APPROACH

Ezekiel Bahar and Paul Crittenden
Electrical Engineering Department and the
Center for Electro-Optics
Mathematics Department
University of Nebraska-Lincoln
Lincoln, NE 68588-0511

The new unified full wave approach is used to determine the vertically and horizontally polarized radar scatter cross sections for composite, multiple scale random rough surfaces. The radar cross sections are expressed as weighted sums of two cross sections associated with the larger and smaller components of the rough surface height spectral density function. This analysis is based on the original full wave solutions which are restricted to rough surface with moderate slopes. However, unlike the small perturbation solution, the original full wave solutions are not limited to surfaces with small root mean square heights (compared to wave length) since the surface height fluctuations do no appear as coefficients in the expressions for the diffuse scattered fields. The surface height appears in the phase term as in the physical optics solution.

Extensive use has been made here of the full wave scattering cross section modulation for arbitrarily oriented composite rough surfaces, in order to account for larger undulations of the rough scale surface. Thus the radar cross section of the multiple scale rough surface is obtained by regarding the composite rough surface as an ensemble of patches (consisting of smaller spectral components) with arbitrary orientation that ride upon the larger scale (spatially filtered) rough surface. The contribution to the cross section from the slope modulated patches is obtained by averaging over the slopes of the larger scale surface. The contribution to the cross section from the larger scale surface is reduced by a factor equal to the magnitude squared of the characteristic function of the smaller scale surface.

The patch size is linked to the spatial wave number that separates the larger scale rough surface from the smaller scale rough surface. A smooth filtering of the patch surface height density function is assumed here. The unified full wave scatter cross sections of the composite rough surfaces are relatively stationary over a broad range of patch sizes.

B/F1-7
11:20

SOMMERFELD AND ZENNECK WAVE PROPAGATION FOR A FINITELY CONDUCTING ONE-DIMENSIONAL ROUGH SURFACE — COHERENT FIELD

Akira Ishimaru, John D. Rockway, Yasuo Kuga, and Seung-Woo Lee
Department of Electrical Engineering
University of Washington, Box 352500
Seattle, WA 98195-2500

Starting with Zenneck and Sommerfeld, wave propagation over a flat finitely conducting surface has been extensively studied by Wait and many other authors. In this paper, we examine propagation over a finitely conducting rough surface. The theory developed here applies to rough surfaces with small rms heights ($\sigma < \lambda$). We limit ourselves to the one-dimensional rough surface with finite conductivity excited by a magnetic line source which is equivalent to the Sommerfeld dipole problem in two dimensions (x-z plane). With the presence of finite roughness, the total field decomposes into the coherent field and the incoherent field. We examine the coherent field in detail. The coherent (average) field is obtained by using Dyson's equation, a fundamental integral equation based on the modified perturbation method. Once the coherent field has been obtained, we determine the Sommerfeld pole, the surface impedance and the Zenneck wave for rough surfaces of small rms heights. The coherent field is written in terms of the Fourier transform, which is equivalent to the Sommerfeld integral. Numerical examples of the attenuation function, Sommerfeld pole and surface impedance are shown to contrast the flat and rough surface cases. These cases are given to compare the effects of the rough surface to the flat surface case. It is shown that the attenuation of the Zenneck wave increases with roughness and that the surface reactance is inductive and also increases with roughness. The theory presented here applies to small rough surface heights of less then .1λ. Therefore, for a given rms height, the effects of rough surface diminish at the lower frequencies, while at the higher frequencies, the theory is not applicable. In the intermediate frequencies when the rms height is of the order of .1λ, the rough surface effects are significant with increasing attenuation.

B/F1-8
11:40

FDTD SIMULATIONS OF ZENNECK WAVE PROPAGATION OVER A FINITE CONDUCTING ONE-DIMENSIONAL ROUGH SURFACE

Seung-Woo Lee, John D. Rockway, Akira Ishimaru, and Yasuo Kuga
Department of Electrical Engineering
University of Washington, Box 352500
Seattle, WA 98195-2500

Many authors, starting with Zenneck and Sommerfeld, have studied wave propagation over a finitely conducting surface. The theory has been developed through the description of the half-space Green's function. Recently, we have developed a "smooth" rough surface Green's function which describes the wave propagation over a finitely conducting rough surface with small *rms* heights. This Green's function decomposes into coherent (average) and incoherent (diffuse) wave propagation. From the description of the coherent Green's function, ground wave propagation or the Zenneck wave may be determined and the propagation factor (attenuation function) calculated. The results indicate that the Zenneck wave propagating along a finitely conducting rough surface with small *rms* height attenuates faster than in the equivalent flat-surface problem. To confirm these results, a FDTD simulation was conducted for a magnetic line source located near the surface radiating over a large numerical rough surface (30 – 400 λ). The numerical simulation of the surface wave required an elongated thin computational domain resulting in near grazing angles incident on the PML. To achieve numerical accuracy of the field, a large number of boundary layers are needed, and the PML parameters (σ_{max}, κ_{max}) should be carefully chosen. We measure the field along the surface and compare the attenuation factor for both flat and finite roughness for both land ($\varepsilon = 10, \sigma = 9 \times 10^{-3}$) and sea ($\varepsilon = 80, \sigma = 4$). The frequency range varies from 1 MHz to 100 MHz and the rough surface *rms* varies from 0.0 to .3 meters. The numerical simulation is then compared to the analytical description of the Zenneck wave propagation described by the "smooth" rough surface Green's function for a rough surface up to 0.1 λ. To further pursue the subject of surface wave propagation, we investigate the attenuation function due to increasing surface heights beyond that described by our theory (0.1 – 1 λ).

B/J1-1 09:00 DISTORTION COMPENSATION OF LARGE SPACE ANTENNAS: A CASE STUDY OF ARISE ANTENNA

Yahya Rahmat-Samii
Department of Electrical Engineering
University of California, Los Angeles
Los Angeles, CA 90095-1594, U.S.A.
e-mail: rahmat@ee.ucla.edu

Among one of the potential new millennium radio astronomy missions, ARISE (Advanced Radio Interfrometry between Space and Earth) has been receiving some attention (J. S. Ulvestad, et at, AIAA Symp., Sept. 1995). The antenna system for this mission is projected to utilize a 25-m dual offset Gregorian optics operating from 8 GHz to 86 GHz. The key scientific objective of this mission is to create a space-based VLBI system (integrated with ground based antennas) for high resolution mapping of the black holes. One of the fundamental challenges in achieving the desired performance is to adaptively correct the unwanted surface distortions on the 25-m main reflector antenna envisioned to be an inflatable structure. Among various compensating options, application of deformable subreflector and focal plane array of feeds are getting much attention. The objective of this paper is to assess the performance improvement based on subreflector shaping and to demonstrate a novel hybrid computational technique to synthesize the desired shape of the subreflector for simulation purposes. This hybrid technique uses the machinery of *GO/Fourier-Jacobi surface expansion/PO* computational technique to evaluate the role of a shaped subreflector for this class of applications.

Three computational options are typically available to synthesize the desired shape of the subreflector [D. Duan and Y. Rahmat-Samii, IEEE Antennas and Propagation Transactions, Jan. 1995]. These are GO/GO, PO/PO and the hybrid technique based on GO/PO. The disadvantage of GO/GO is that it does not allow one to directly define the optimization cost function based on the antenna radiation pattern. The PO/PO optimization technique is the ultimate approach; however, it suffers from considerable amount of required computation time. The hybrid GO/PO method effectively combines the advantages of the other two methods. Computationally it is attractive because of the GO implementation, and performance wise it is effective because of the PO computation of the secondary pattern. Once the subreflector shape is determined through the optimization technique, the PO/PO is finally used to characterize the overall antenna performance.

The machinery of the Fourier-Jacobi (related to Zernike polynomials) expansion of the subreflector surface is used to parametrize the surface with unknown coefficients yet to be determined. To implement the hybrid technique, one needs to first determine the GO field from this parametrized subreflector. It is shown that all of the required parameters for the implementation of GO, such as, curvature matrices, divergence factor, etc., can be constructed in a closed form. This computation machinery is then incorporated into an optimization process to ultimately determine the surface expansion coefficients for the characterization of the subreflector surface. Representative numerical results will be shown to demonstrate the utility of this hybrid technique. Simulation results will clearly show that the deformable subreflector could effectively overcome the unwanted distortion effects of the inflatable main reflector. Some of the challenging issues in the actual implementation of the concept will be highlighted.

B/J1-2
09:20

ADVANCES IN THE DEEP SPACE NETWORK – ADDING KA-BAND TO THE 70-METER ANTENNA

William A. Imbriale and Daniel J. Hoppe
California Institute of Technology
Jet Propulsion Laboratory
Pasadena, CA 91109

With the advent of faster, cheaper planetary missions, the coming decade promises a significant growth in the number of missions that will be simultaneously supported by NASA's Deep Space Network (DSN). Ambitious outer planet missions, with extremely tenuous communications links due to their great distances, and data-intensive orbiter or in situ missions incorporating high-bandwidth science instruments will demand improved telecommunications capabilities. The Telecommunications and Mission Operations Directorate (TMOD) at the Jet Propulsion Laboratory, which operates NASA's Deep Space Network, has developed a road map for deep-space telecommunications through the year 2010 that meets these challenges. One key aspect of this road map is the rapid infusion of Ka-band (32-GHz) into the DSN and into future spacecraft.

The gain performance of the 70-meter antenna at Ka-band falls off rapidly as the antenna is pointed at targets either above or below the elevation angle for which the antenna was optimized. This antenna roll-off was measured to be 3.6 dB at low elevation and 6.5 dB at high elevation angles. Techniques for improving the antenna's performance include a deformable mirror and an array feed. The deformable flat plate, which is inserted in the optical ray path of the antenna, compensates for the gravity distortion of the antenna main surface by phase conjugate deformation, thus restoring the focal point of the antenna. The Array Feed Compensation System (AFCS) utilizes signal combining and tracking from a seven element array feed. It combines the distributed energy in the focal plane of the antenna due to a gravity induced defocusing, and also provides for closed loop tracking. The AFCS combines the two functions of gravity distortion compensation and closed loop tracking into one system. The DFP combined with a monopulse tracking system also provides the same two functions. A theoretical and experimental study compared the deformable flat plate (DFP) and an array feed compensation system (AFCS) performances on the DSS-14 70-meter antenna at Ka-Band (32-GHz).

In addition to adding Ka-band, it is necessary to maintain the existing transmit and receive functions at S- and X-band. This paper shows how the results of the study led to the currently proposed system for adding Ka-band to the existing 70-meter antenna.

B/J1-3 09:40 THE SECOND ARECIBO UPGRADE: PERFORMANCE AND PROSPECTS

Paul F. Goldsmith, Lynn A. Baker and Donald B. Campbell
National Astronomy and Ionosphere Center
Cornell University, Ithaca, NY and
Michael M. Davis
National Astronomy and Ionosphere Center
Arecibo Observatory, Arecibo, Puerto Rico

A major upgrade of the Arecibo 305-m radio telescope has recently been completed (P.F. Goldsmith, "The Second Arecibo Upgrade", *IEEE Potentials*, *15*, No. 3, Aug./Sept. 1996). The most important component of the upgrade is a dual shaped reflector system that corrects the aberration of the spherical primary. The design of the system has been well documented in the antenna literature (P.S. Kildal, L. Baker, and T. Hagfors, "Development of a Dual-Reflector Feed for the Arecibo Radio Telescope: An Overview", *IEEE Antennas and Propag. Magazine*, *33*, No. 5, Oct. 1991; P.S. Kildal, L.A. Baker, and T. Hagfors, "The Arecibo Upgrading: Electrical Design and Expected Performance of the Dual-Reflector Feed System", *Proc. IEEE*, *82*, No. 5, May 1994; extensive bibliographies of related topics can be found in these two papers). Other major components of this "Second Arecibo Upgrade" include a doubling of the S-band radar transmitter power to 1 megawatt, completely rebuilding the telescope drive systems, and adding a ground screen to minimize pickup of stray radiation.

This unique reflector system is now in full time use at L and S bands with steady progress being made toward realizing the full potential of the system at frequencies up to 10 GHz. This presentation will briefly review the design and implementation of the Arecibo Upgrade, will present the most recent measured results of the telescope performance, and will conclude with a brief overview of planned future improvements.

The dual shaped subreflectors that comprise the Gregorian corrector system feeding the spherical primary of the Arecibo telescope are unique. Designing this optical system required development of new shaping methods and analysis techniques. The mounting of the corrector system on a cable suspended structure is unusual and has necessitated innovative mechanical and drive system solutions. The complete system provides the world's largest filled aperture telescope with high efficiency, low noise, and broad instantaneous bandwidth over a wide frequency range.

We have carried out extensive modeling to predict the performance of the Arecibo telescope at various frequencies. We will compare theory and measurements, and will discuss differences in terms of surveyed errors and tolerance theory. Other factors affecting the performance such as the aperture blockage are included in the performance budget. We will also describe a plan to improve the reflector surface accuracy.

Radio telescopes should be very low noise systems and the Arecibo optical system has been designed to satisfy this criterion. The various factors contributing to the total system noise temperature will be presented in a noise temperature budget. We will also present a plan to lower the overall system noise temperature.

B/J1-4
10:00

FIRST TEST OBSERVATIONS WITH THE SMA

J. M. Moran
Harvard-Smithsonian Center for Astrophysics
60 Garden Street
Cambridge MA 02138

The Submillimeter Array (SMA) is a collaborative project of the Smithsonian Astrophysical Observatory and the Institute of Astronomy and Astrophysics of the Academy of Science (Taiwan). The status of the construction and early observations with the array will be discussed.

The array will be sited on Mauna Kea, approximately 150 and 300 m from the JCMT and CSO telescopes, respectively. The array will consist of eight 6 m antennas arranged in four configurations, with diameters of approximately 24, 64, 171, and 470 m. Each antenna will be equipped with a cryostat at its Nasmyth focus holding up to eight receivers covering all usable bands from 190 to 850 GHz. The maximum angular resolution will vary from 0.1″ to 0.4″ over the frequency range. Signals will be distributed by buried Sumitomo fiber optic cable, operating without phase compensation. Signal processing will be performed on a hybrid XF correlator using the Haystack Mark IV chip. The correlator will accept two channels (for either dual-polarization or dual-frequency operation) from each antenna of 2 GHz bandwidth each. Provisions are being made to include the JCMT and CSO instruments as elements in the array.

Two operational prototype antennas were tested at the Westford construction site in 1998. The antennas have reflector backup structures constructed of carbon fiber tubes and steel nodes. The machined aluminum panels have rms accuracies of 5 μm and the overall surface accuracy is expected to be 12 μm rms. The surfaces of the antennas have been adjusted to an rms accuracy of about 18 μm using 90 GHz holography. In fall 1998, initial interferometric tests were conducted at 230 GHz with two antennas on a 15 m baseline at the Westford site. Although the zenith opacity at this frequency was generally greater than one, strong fringes were obtained on several planets and compact CO sources. The rms phase deviation over several hours was generally less than 20°.

As of 1 September 1999, the civil work on Mauna Kea, including the installation of 24 pads, the assembly building, and the control building, is complete. The first antenna has been erected on the mountain, and after one round of holography, its surface accuracy was 31 μm. The second antenna will be deployed with 230 and 345 GHz receivers before 15 September 1999, and the first fringe tests are expected to be conducted before the end of that month. Extensive changes are being made to the cabin design and servo system. The third antenna and the two antennas now under construction in Taiwan are expected to be operational on Mauna Kea by the middle of 2000. The rest of the antennas and the full correlator will be in place in early 2001.

B/J1-5
10:40

ANTENNA DESIGNS FOR THE ALMA PROJECT

P.J. Napier
NRAO
PO Box 0
Socorro, NM 87801

The Atacama Large Millimeter Array (ALMA) is a new radio telescope that is currently in its design and development phase. The telescope, which will operate in the frequency range 30-900 GHz, will be built on a site at 5000m altitude in Northern Chile by an international partnership consisting of the US and a consortium of European countries. The goal for the array is sixtyfour 12m diameter transportable antennas located in reconfigurable arrays with diameters from 160m to 10km.

The antennas will be exposed to the environment and will be required to meet their performance specifications in a 9m/s wind and under full solar loading. The principal performance requirements include:

Elevation range: 2-125 degrees
Rms surface accuracy: 25 microns
Absolute pointing accuracy: 2 arcsec rms
Offset pointing accuracy (2 degrees of sky, 15 min. of time): 0.6 arcsec rms
Pathlength errors over 2 degrees of sky, 3 min. of time: 15 microns rms
Azimuth velocity/acceleration: 6 deg/sec, 24 deg/sec/sec
Elevation velocity/acceleration: 3 deg/sec, 12 deg/sec/sec
Minimum antenna spacing: 15m between azimuth axis
Solar observations: direct observation of the sun allowed

Current project plans call for both the US and European groups to issue contracts to different companies for the design and fabrication of prototype antennas. A progress report on the status of this work will be given as well as a review of some of the design concepts investigated to meet the demanding performance requirements.

B/J1-6
11:00

THE SARDINIA RADIO TELESCOPE

G. Grueff
Department of Physics, University of Bologna, Bologna, Italy
G. Tofani*
Arcetri Astrophysical Observatory, Largo Fermi 5, Florence, Italy

Sardinia Radio Telescope (SRT) is a flexible, high performance instrument for Radio Astronomy and Space Research. The project, led by the Istituto di Radio Astronomia (IRA) of the Consiglio Nazionale delle Ricerche (CNR) with the support of the Italian Space Agency (ASI) and of the Sardinia Regional Governement, aims to build a fully steerable 64m paraboloid.

Planned operating frequencies span from 300 MHz up to 100 GHz. Telescope optics has a Gregorian symmetrical configuration. Primary and secondary surfaces will consist of precision trapezoidal panels with fabrication error not greater than 100 micron rms. A quasi-homologous structure on a wheel-and track mounting supports the primary surface. The structure by itself will allow the antenna to operate with good efficiency up to about 22 GHz. Beyond this limit, computer controlled actuators, on the panel supports, will optimize primary and secondary surfaces, according to a loop system which reacts to gravitational, temperature and wind deformations. High frequency operations require pointing errors be kept less than 2 arcsecs at the best. In order to gradually approach this limit, different steps in the metrology of structural errors are foreseen, starting from the use of electronic levels, to laser metrology and optical star trackers. All systems will refer to a central stable reference structure.

Most of the science with SRT deals with radioastronomy techniques. VLBI will continue to play a major role. SRT may improve the sensitivity and the u-v plane coverage of existing networks (EVN, ground-to-space VLBI, etc.). As a single dish, SRT will provide high sensitive spectroscopy of molecular and recombination lines and sensitive continuum analysis of selected galactic and extragalactic sources.

Important applications of SRT are foreseen in Space Research, in the fields of Radio Science and Deep Space Telecommunications. ASI is planning the use of the antenna in on-going and future space missions, jointly with ESA and NASA projects. For the complex instrumentation needed in space radiolinks, two mirrors will refocus the radiation after the secondary focus, via a partial Beam Wave Guide system, to a third focal position in a separate room below the elevation axis.

The selected site is a small flat valley near S. Basilio village, about 50 km from the city of Cagliari, at an elevation of 560 m. A site survey has shown a relatively radio quiet environment. The area is quite dry, with moderate wind activity. Water vapour radiometric data indicate a good percentage of time with low atmospheric attenuation.

B/J1-7
11:20

PROGRESS ON THE LARGE MILLIMETER TELESCOPE

Jacob W.M. Baars
LMT Project - 815 Lederle Graduate Research Center
University of Massachusetts, Amherst, MA 01003

The Large Millimeter Telescope (LMT) Project was introduced to the National Radio Science Meeting 1999 (Abstract Book, p. 240). The present paper is concerned with the current state of the project, in particular the telescope. The LMT is a full aperture telescope of 50 m diameter for operation to a shortest wavelength of 1 mm. The major specifications are 75 micrometers reflector accuracy and 1 arcsec pointing accuracy under operational conditions (10 m/s windspeed) at the 4600 m high site in Central Mexico. The LMT is being designed by MAN Technology of Germany. The preliminary design is completed and detailed design and shop fabrication has been started.

The LMT is an exposed, alt-azimuth antenna with a wheel-on-track azimuth drive and double bull-gear elevation drive. An advanced servo-system will aid in achieving the pointing accuracy. A spacious receiver cabin behind the reflector, stationary in elevation, allows the deployment of and easy access to several, large receiver systems. The reflector is a space-frame structure, supporting 180 reflector "subframes" of about 5x3 m2, each of which carries six reflector surface panels. The panels will be made by Mexican industry in a technology transfer from MAN. They are composite panels of about 2 m^2, made of carbon fiber reinforced plastic top and bottom sheets bonded to a 50 mm thick aluminium honeycomb core. The will be replicated from steel molds with an accuracy of 15 micrometers.

The subframes are supported on actuators to enable real-time correction of the reflector surface for deformations, caused by gravity, temperature gradients and the quasi-static wind component. These deformations will be computed from the finite element model with the aid of an "adaptive controller", using measured data from temperature sensors and strain gauges. The pointing of 1 arcsec will be achieved with a similar adaptive system. To reach the goal of 0.6 arcsec (one tenth of the beamwidth at 1.2 mm wavelength), an optical system is under development at UMass, in collaboration with Lincoln Laboratory, to measure and control the position of the subreflector in order to correct small and relatively fast pointing variations. Variable atmospheric refraction might limit the achievable pointing accuracy. We plan to incorporate a 183 GHz wavefront sensor to ameliorate this effect.

The LMT Project is a collaboration between the Mexican Instituto Nacional de Astrofisica, Optica and Electronica (INAOE) in Puebla and the University of Massachusetts at Amherst. It is sponsored by the Defense Advanced Research Projects Agency, Sensor Technology Office - DARPA Order N0. C134, Program Code N0. 63226E. Issued by DARPA/CMO under contract MDA972-95-C-0004.

B/J1-8
11:40

THE GREEN BANK TELESCOPE

M. M. McKinnon
National Radio Astronomy Observatory
Green Bank, WV 24944

The Green Bank Telescope (GBT) is a 100-meter diameter offset parabolic reflector that is currently under construction at the National Radio Astronomy Observatory in Green Bank, West Virginia. Construction of the telescope should be complete by the end of 1999, and its commissioning will continue into the year 2000.

The principle components of the GBT structure are its tipping structure and alidade. The tipping structure consists of the solid reflector surface and its supporting backup structure (BUS), the box structure which supports the BUS, and an offset feed support arm. The tipping structure can move between elevations of 5 and 95 degrees at a rate of up to 20 degrees per minute. The alidade supports the tipping structure and moves the telescope in azimuth at a maximum rate of 40 degrees per minute.

The primary reflecting surface of the GBT is a 100×110 m section of a 208 m parent paraboloid. The focus of the primary reflecting surface lies 60 m above the vertex of the parent parabaloid, giving an F/D of 0.29. A retractable boom will be used to position receivers at prime focus for observations at frequencies below 1.2 GHz. For observations above 1.2 GHz, the prime focus boom will be retracted, and an 8 m Gregorian subreflector will redirect radiation to a secondary focus at the top of a receiver room. A large turret in the roof of the receiver room can be rotated to position any one of more than ten receiving systems into the secondary focal plane.

The initial suite of GBT receivers consists of prime focus receivers which can cover frequencies ranging from 290 MHz to 1.2 GHz and a set of eight receivers at the Gregorian focus which are spaced throughout a frequency range of 1.2 GHz to 52.0 GHz. The data recording instruments available on the GBT include the new GBT spectrometer, the NRAO spectral processor, a digital continuum receiver, a holography receiver, and a VLBA data acquisition system.

The telescope will be equipped with actuators beneath the reflector surface panels to correct for deformations in the surface and thus maintain high aperture efficiency over the full range of telescope elevation angles. Precise locations of the surface panels and other parts of the telescope structure will be measured with a system of laser rangefinders. The rangefinder data will be used to optimize the shape of the reflector surface and refine the pointing of the telescope.

B/J1-9
12:00

NOVEL METHODS FOR PRACTICAL MICROWAVE HOLOGRAPHY OF ANTENNAS

Wonchalerm Chalodhorn* David R. DeBoer
School of Electrical and Computer Engineering
Georgia Institute of Technology
Atlanta, GA

The Georgia Tech Woodbury Research Facility consists of a pair of 30-meter Cassegrain antennas located approximately 65 miles south of Georgia Tech's Atlanta campus (DeBoer and Steffes, *Radio Sci.*, **34**, 991-1004, 1999). The facility has been primarily used for radio astronomy, engineering research and education.

The technique of microwave holography has been conducted at the Woodbury facility to characterize the condition of the antenna surface (*ibid.*, Chalodhorn *et al.*, *URSI abstract*, 119, 1999). The implementation employed phase coherent holography whereby the complex far-field antenna pattern is directly measured. Two sets of measurements at C-band (4.2 GHz) have been obtained using two different geostationary satellite beacons at slightly different elevation angles serving as signal sources. The similar features shown in both measurements indicate the reproducibility and validity of the measurement system. Some of the errors appearing in the previous measurement (*ibid.*) were corrected leading to the more recent result.

A different method employing phase retrieval has been considered and implemented by many of the microwave holography measurement systems. It involves retrieving the phase information from amplitude-only antenna patterns (Morris, *IEEE A&P Trans.*, **AP-33**, 749-755, 1985). A popular phase retrieval algorithm (Misell, *J. Phys. D: Appl. Phys.*, **6**, L6-L9, 1973) requires the measurement of a defocused intensity pattern of the antenna under test for retrieving the aperture phase distribution. Defocusing typically implies axial displacement of either the feed or the sub-reflector. Unfortunately, these elements of the Woodbury antennas are not amenable to this type of displacement. Since the primary effect of the slight defocusing is a phase shift between ray paths reflecting on the antenna surface, there is therefore a motivation to employ some kind of microwave lens in front of the feed to delay the phase by the desired amount. A metal plate lens (Kock, *Pr! oc. IRE*, **34**, 828-836, 1946) is currently being designed and implemented to achieve this. The lens' surface shape, size, and spacing between the metal plates are dictated by several important factors such as the desired amount of phase shift, matching, measurement frequency, output pattern, and construction. In addition to the metal plate lens, a "bed" of circular waveguides and a Fresnel zone plate are also being considered as possible solutions. This method is well suited to those facilities that are not able or willing to move the sub-reflector or feed and should afford an advantage over setting up a reference antenna and coherent phase measurement system.

Session F1, 08:55 AM-Wed., Room 1B-40
MICROWAVE RADIOMETRY — CM TO SUBMILLIMETER WAVE
Chairpersons: E.R. Westwater, CIRES/NOAA (ewestwater@etl.noaa.gov)
A.J. Gasiewski, NOAA ETL (agasiewski@etl.noaa.gov)

F1-1
09:00

A COMPARISON OF CLEAR-SKY EMISSION MODELS WITH DATA TAKEN DURING THE 1999 MILLIMETER-WAVE RADIOMETRIC ARCTIC WINTER WATER VAPOR EXPERIMENT

E. R. Westwater[1], Y. Han[1], P. E. Racette[2], A. J. Gasiewski[3], and M. Klein[1]
[1] CIRES, University of Colorado/NOAA Environmental Technology Laboratory, Boulder, CO
[2] NASA/ Goddard Space Flight Center, Greenbelt, MD
[3] NOAA Environmental Technology Laboratory, Boulder, CO

Remote sounding of atmospheric temperature and moisture requires accurate absorption/emission models for input to parameter or profile retrieval algorithms. Data from surface-based radiometers and co-located radiosondes provide a useful supplement to laboratory data for validating and even refining, absorption models. In March 1999, The NASA Goddard Space Flight Center and the NOAA Environmental Technology Laboratory conducted a comprehensive radiometric experiment at the Department of Energy's Atmospheric Radiation Measurements' (ARM) field site near Barrow, Alaska. Angular scanning radiometers, with a total of twenty-four frequencies between 20 and 350 GHz, were deployed in the experiment. Data taken by ARM during the experiment included daily radiosonde releases that used Vaisala Humicap RS-80 humidity sensors, measurements of cloud heights by two independent lidar systems, and measurements of cloud heights and thicknesses by a 35 GHz cloud radar. In addition to radiosondes launched at the field site, we also had access to radiosondes that were launched twice daily by the National Weather Service, at a location about five kilometers away. Although the cloud measurements are important in their own right, they were used in our study to determine the presence of clear skies. Using data taken during clear conditions, vertical profiles of temperature, pressure, and water vapor can be inserted into radiative transfer models to compute radiance or brightness temperature that can then be compared with well-calibrated radiometer data. Thus, the accuracy of absorption/emission models can be determined on how well the models agree with measured radiometric data. Our radiometric calibration procedures relied on both internal and external calibration reference sources, and, in transmission window regions, by calibrations based on the tipping curve method. In our work, we will compare the absorption models of Liebe's Microwave Propagation Models of 1989 and 1993, as well as a recent model of Rosenkranz (P. Rosenkranz, *Radio Science*, **33**, 919-928, 1998). Calculations based on the radiosondes indicated as much as 20 K differences between the models at sub-millimeter wavelengths.

F1-2
09:20

OBSERVATIONS OF ARCTIC WINTER ATMOSPHERE BY TWO GROUND-BASED 183-GHZ RADIOMETERS DURING MARCH 1999 AT THE NORTH SLOPE OF ALASKA

Y. Han[1], E. R. Westwater[1], P. E. Racette[2], A. J. Gasiewski[3], and M. Klein[1]
[1] CIRES, University of Colorado/NOAA Environmental Technology Laboratory, Boulder, CO
[2] NASA/ Goddard Space Flight Center, Greenbelt, MD
[3] NOAA Environmental Technology Laboratory, Boulder, CO

It has been generally recognized that arctic climate conditions have strong influence on the world climate. Among many influential factors, water vapor and clouds are particularly important because of their ability to regulate the polar energy budgets. Precipitable water vapor (PWV) and integrated cloud liquid (ICL) have been successfully measured using dual-channel microwave radiometers on the wings of the 22.231 GHz water vapor absorption line and in the absorption window region around 31 GHz at the middle and low latitudes. However, due to the relatively weak absorption at the 22 GHz band, the relative errors of the PWV measurements become large under extremely dry weather conditions, such as the Arctic winter environments in which PWV is below 5mm for most of the periods. In order to improve the PWV measurements, the NASA Goddard Space Flight Center (GSFC) and the NOAA Environmental Technology Laboratory (ETL) jointly conducted an experiment during March 1999 at the North Slope of Alaska/Adjacent Arctic Ocean Cloud and Radiation Testbed site. During the experiment, the NASA's Millimeter-wave Imaging Radiometer (MIR) and the NOAA's Circularly Scanning Radiometer (CSR) were operated together. Both MIR and CSR have several channels on the 183 GHz water vapor absorption band, which are stronger than the 22 GHz water vapor absorption band. In addition, over 20 additional channels, ranging from 20 GHz to 340 GHz, were provided by the two instruments and other radiometers.

In this presentation, we discuss the inter-comparisons of the MIR and CSR measurements, the calibration issues, and the responses of the 183-GHz channels to variations of water vapor, temperature, and clouds, as well as the comparisons between measurements and radiative transfer models. The inter-comparisons include analyses of data from other frequency channels, radiosondes, surface in situ temperature and humidity sensors, and active remote sensors, such as ceilometer which identifies the presences of clouds.

F1-3
09:40

GROUND-BASED MILLIMETER-WAVE RADIOMETRIC OBSERVATIONS DURING VERY DRY ATMOSPHERIC CONDITIONS

Paul Racette
NASA/GSFC, Mail Code 555
Greenbelt, Maryland 20770
Phone: 301-286-4756
Fax: 301-286-1750
per@meneg.gsfc.nasa.gov

Ed Westwater, Yong Han, and Marian Klein
CIRES
325 Broadway
MS R/E/ET1
Boulder, CO 80303
303-497-6527

Albin Gasiewski
NOAA/ETL
325 Broadway
MS R/E/ET1
Boulder, CO 80303
303-497-7275

Nadir-viewing millimeter-wave radiometry has been applied to measuring the distribution of water vapor in the troposphere for nearly two decades. The application of millimeter-wave radiometry for making ground-based estimates of precipitable water vapor (PWV) is not as well developed. The strength associated with the 183 GHz water vapor absorption line makes radiometry in this frequency regime suitable for measuring low amounts of water vapor. However, these frequencies also respond to the vertical temperature distribution as well as liquid and ice clouds. A better understanding of these influences must be developed before operational measurements and retrievals are possible. Pacific Northwest National Laboratories under the auspices of the DoE Atmospheric Radiation Measurement (ARM) program sponsored NASA Goddard Space Flight Center and NOAA Environmental Technology Laboratory to conduct an experiment to investigate the utility of millimeter wave measurements for making ground-based estimates of PWV during the very dry conditions that predominate during the winter months in high latitude regions.

NASA and NOAA deployed a suite of radiometers covering 25 channels in the frequency range of 20 GHz up to 340 GHz. Twenty three days of nearly consecutive radiometer data were collected during March 1999 at the DoE's ARM program's North Slope of Alaska/Adjacent Arctic Ocean Cloud and Radiation Testbed site (DoE ARM NSA/AAO CaRT) located just outside Barrow, Alaska. In addition to the usual CaRT site instrumentation the NOAA Depolarization and Backscatter Unattended Lidar (DABUL), the SUNY Rotating Shadowband Spectroradiometer (RSS) and other surface based meteorological instrumentation were deployed during the intensive observation period. Vaisala RS80 radiosondes were launched daily as well as nearby National Weather Service VIZ sondes. The experiment benefited from a range of atmospheric conditions ranging from clear calm skies to blowing snow and heavy multi-layer cloud coverage. Measurements made by the radiosondes indicate the PWV varied from ~1 to ~5 mm during the experiment. The near-surface temperature varied between about -40 °C to -15 °C.

The data set obtained during this experiment is applicable to assessing the potential and limitations of millimeter-wave radiometry to retrieving very low amounts of PWV. The data are also valuable for studying discrepancies in the different absorption models for water vapor, oxygen, and super cooled liquid water. However, before such studies can be performed with confidence the uncertainty in the calibration of the data must be addressed. To assess the calibration of the instrument, measurements of three blackbody references at different temperatures were made throughout the experiment. Continuous elevation scans were also performed providing a means of constraining the calibration using the "tip curve" technique. Comparison between similar radiometer channels provides another means of assigning confidence limits to the data. In this presentation, an overview of the experiment with examples of data collected and a review of the on going analysis will be presented.

F1-4
10:00

SUBMILLIMETER-WAVE REMOTE SENSING OF CIRRUS: NEW INSTRUMENTS AND RECENT RESULTS

K. F. Evans* A. H. Evans
University of Colorado Boulder, CO 80309-0311
I. G. Nolt M. D. Vanek
NASA Langley Research Center, Hampton, VA
P. A. R. Ade
Queen Mary and Westfield Colllege, London, UK
S. J. Walter
Jet Propulsion Laboratory, Pasadena, CA

Submillimeter-wave (submm) radiometry is a new technique for remote sensing ice clouds in the atmosphere. Submm radiation, emitted by water vapor in the lower troposphere, propagates to the upper troposphere where it interacts with cirrus cloud ice particles primarily by scattering. Some of the radiation is scattered backwards, which causes a decrease in the observed radiation (relative to clear sky) for a downward viewing radiometer and an increase in signal for an upward viewing radiometer. Submillimeter wavelengths are close in size to cirrus ice crystals, and so scatter much more strongly than microwave frequencies. The amount of scattering, and hence the brightness temperature change from clear sky, is closely related to the integrated ice mass, but also depends on the characteristic ice particle size. Multiple radiometer frequencies can be used to obtain information about particle size and accurately retrieve IWP (Evans, et al., *J. Appl. Met.*, **37**, 184-205, 1998).

Two instrument approaches are being pursued to realize submm remote sensing of cirrus. The first is an aircraft-based Fourier transform spectrometer (FTS) designed by I. G. Nolt and P. A. R. Ade. The Far InfraRed Sensor for Cirrus (FIRSC) is a Martin-Puplett interferometer, which incorporates a polarizer for the beamsplitter, and has a spectral resolution of 0.1 cm^{-1}. A cryogenic (0.3 K) bolometer channel for 10 to 33 cm^{-1} (300 to 1000 GHz) achieves a noise equivalent temperature of approximately 1 K at 30 cm^{-1} in one 4 second FTS scan. A series of aircraft flights were made in 1998 and 1999. The spectra showed the expected cirrus scattering effect and the first detection of submm polarization due to ice clouds.

The Submillimeter-Wave Cloud Ice Radiometer (SWCIR) is being built at the Jet Propulsion Laboratory under the direction of Steven J. Walter. This heterodyne instrument has four receivers each with a Schottky diode mixer. The 183, 325, and 448 GHz receivers are centered on water vapor absorption lines and have harmonic mixers to give an IF bandpass within 1 GHz of the center. There will be three double-sideband channels for each of these three receivers. The 643 GHz receiver uses a Fabry-Perot diplexer to couple in the local oscillator. The expected noise temperatures are about 0.5 K for a 0.1 second integration time. The instrument will fly on the NASA DC-8 in a window mount with cross track scanning from +90° (zenith) to -70°.

F1-5
10:40

THE INFLUENCE OF OZONE ON THE CLEAR AIR TEMPERATURE AND MOISTURE SOUNDING CAPABILITIES OF MILLIMETER AND SUB-MILLIMETER WAVE CHANNELS.

M. Klein[1] and A. J. Gasiewski[2]
[1]CIRES, NOAA/ETL, R/E/ET1, 325 Broadway, 80303 Boulder, Colorado
[2] NOAA/ETL, R/E/ET1, 325 Broadway, 80303 Boulder, Colorado

To obtain adequate spatial resolution using reasonably sized antennas a future geosynchronous microwave sounder could be based upon the use of sub-millimeter wavelength sounding and imaging channels. To support the development of such instrument, a sensitivity study of the clear air nadir sounding capabilities in the millimeter and sub-millimeter wave spectral range for significant water vapor and oxygen absorption lines was recently performed. Part of this study was focused on the impact of ozone (O_3) on the incremental weighting functions (IWF) for temperature and water vapor. Several key parameters for sounding are influenced by ozone at particular frequencies, among them the brightness temperature difference and standard deviation spectra for ozone versus ozone-free atmospheres, the effective sounding height, the natural available bandwidth (B_N), and the minimum integration time for a total power radiometer. The influence of ozone lines on temperature and water vapor sounding over the frequency range from ~10 to 1000 GHz will be presented.

The impact of absorption by upper tropospheric and stratospheric ozone on water vapor sounding is to reduce the sensitivity to low-altitude water vapor and moisture variations but only over spectral intervals much narrower than typically encountered in sounding. At most, the screening effects of ozone lines are moderate and warrant no special concern unless the sensing bandwidth is restricted below B_N for either technological or spectral allocation reasons. Stratospheric ozone also impacts temperature sounding by slightly increasing channel sensitivity in the stratosphere. The amount of this increase is variable (depending on the O_3 density), but for the strongest ozone lines can be expected to cause a complete shift of the support of the IWF to the stratosphere or even mesosphere. Such excursions, however, will occur over relatively narrow bands. Over bands of width B_N (or comparable) the sounding effects of ozone are again negligible.

F1-6
11:00

POLARIMETRIC C-BAND IMAGING OF SOIL MOISTURE SIGNATURES USING A CONICAL-SCANNED MICROWAVE RADIOMETER

A.J. Gasiewski[1], M. Klein[2], S. Christiani[3], A. Francavilla[1], A. Yevgrafov[2], M. Falls[1], and T. Jackson[4]

[1] NOAA Environmental Technology Laboratory, Boulder, CO

[2] CIRES, University of Colorado/NOAA Environmental Technology Laboratory, Boulder, CO

[3] University of Karlsruhe, Institute for High Frequency Electronics Karlsruhe, Germany

[4] U.S. Department of Agriculture Hydrology Lab, Beltsville, MD

The effective microwave dielectric constant, and hence the emissivity, of soil is greatly influenced by its volumetric moisture content (VMC). Monotonic decreases in the upwelling brightness temperature of over ~140 K at L-band can occur as soil moisture increases from ~5 to ~40% VMC. Such changes can potentially be measured to ~1 K precision over large areas using space-borne imaging radiometers, and mapped at much higher spatial resolution using airborne imaging radiometers. The principal advantage of the use of L-band for VMC mapping lies in its ability to penetrate vegetation cover, while the use of higher frequencies (S-through W-bands) provide higher spatial resolution at reduced aperture costs but with progressively greater sensitivity to scattering and absorption by vegetation.

The NASA Advanced Microwave Scanning Radiometer (AMSR) on the EOS-PM platform ("Terra") is a conically-scanned imaging sensor that will support a dual-polarization channel at 6.92 GHz. The use of this AMSR band for soil moisture retrieval depends on the degree to which both beam-filling and vegetation effects can be compensated. To study these effects as well as those of anthropogenic interference at this band, a polarimetric C-band scanhead for the conically-scanning Polarimetric Scanning Radiometer (PSR) instrument was developed and flown on the NASA P-3 aircraft as part of the 1999 Southern Great Plains experiment (SGP99). The data from the PSR over the Oklahoma area clearly show 50-70 K decreases in upwelling horizontally-polarized brightness temperature as the result of a major precipitation event that deposited 1-2" of rain, and increases of similar magnitude during the subsequent dry down phase. The high-resolution (~2 x 3 km footprints) imagery clearly shows differences in the rate of brightness change during the dry down depending on the location of the pixel within the watershed. Anthropogenic interference at C-band is also seen to be common and several interference mitigation techniques will be discussed.

F1-7 11:20 ELECTROMAGNETIC AND THERMAL ANALYSES OF RADIOMETER CALIBRATION TARGETS

D.M. Jackson[1] and A.J. Gasiewski[2]
[1] Central Intelligence Agency, Washington, DC
[2] NOAA Environmental Technology Laboratory, Boulder, CO

A novel approach for the analysis of millimeter-wave radiometer calibration target performance is presented. An ideal calibration target is a blackbody with a known uniform thermometric (or kinetic) temperature distribution. In practice, however, a target exhibits a nonuniform and non-unity emissivity and a nonuniform temperature distribution, and therefore, is not simply, or even directly, related to the target's measured physical temperature at some reference location. The measurement of target brightness temperature represents an important component in a typical radiometer's overall calibration uncertainty budget.

We demonstrate an accurate calculation of the thermal emission from a one-dimensional wedge-profile calibration target by performing both an electromagnetic and thermal analysis of the structure. The scattered, transmitted, and internal fields of the wedge target (a lossy periodic absorber) illuminated in the principal direction by a plane wave, are analyzed using the coupled-wave (CW) algorithm (T.K. Gaylord and M.G. Moharam, Proc. IEEE, vol. 73, pp. 894-937, 1985). From knowledge of these fields the wedge trough-to-tip absorptivity profile is computed. IN addition, the two-dimensional wedge temperature distribution is determined using a finite-element solution to the steady-state heat equation. The temperature solution's self-consistency is verified with conservation of heat flux calculations and its results are compared with those of two other numerical techniques. Using the absorptivity and temperature profiles, the radiative transfer equation is solved to obtain the thermal emission from the wedge calibration target. Significant effects resulting from the inhomogeneous temperature distribution are quantified and heuristic arguments are presented to extend the analyses to two-dimensionally periodic pyramidal-profile structures.

F1-8
11:40

THE SCANNING OZONE RADIOMETER (SCOR): A GROUND-BASED WIDEBAND ATMOSPHERIC TRACE CONSTITUENT SENSOR

David R. DeBoer
School of Electrical and Computer Engineering
Georgia Institute of Technology
Atlanta, GA

A new instrument to measure the total ozone profile throughout the atmosphere is currently under development at the Georgia Institute of Technology in the School of Electrical and Computer Engineering. This passive millimeter-wave instrument, called the Scanning Ozone Radiometer (SCOR), will detect ozone by observing spectral lines in an instantaneous bandwidth of 100 - 118 GHz (primarily near the 110 GHz ozone line). In addition, a 118 GHz pressure/temperature (P/T) sounder is incorporated directly into the radiometer for continuous and colocated P/T sounding.

SCOR will employ a front-end low noise amplifier (LNA) and a double mixer/local oscillator (LO) in a classic heterodyne configuration. The design employing a second, tunable synthesized local oscillator will allow any and all frequencies within the 100-118 GHz band to be observed at any of the resolution bandwidths. The P/T sounder incorporates an image rejection filter, limiting the bandwidth to frequencies greater than 114 GHz.

The ozone sounder will have eight resolution channels, including a digital channel that will yield a continuously variable bandwidth ranging from about 50 kHz (the lowest reasonable bandwidth to yield mesospheric ozone) to 20 MHz (the widest bandwidth without aliasing for reasonable sampling rates). The remaining channels range to bandwidths of about 1 GHz. The narrowband channels will typically be used about the 110 GHz ozone line center (or other line within 100-118 GHz) to measure the stratospheric and mesospheric ozone profiles, while the wider channels will be used to measure the wings for tropospheric ozone. The P/T sounder will also have eight channels, the exact bandwidths of which are still to be determined, however, with the inclusion of the image rejection filter, they will be single-sided and constrained to frequencies above about 114 GHz. Again, any frequency in this reduced band (114-118 GHz) may be viewed with any of the P/T resolution bandwidths by changing the LO frequency.

The instrument will also have an incorporated weather station to determine local temperature, pressure and relative humidity, as well as an ozone contact sensor to characterize the a priori information needed for the retrieval. In addition a water vapor radiometer (WVR) operating near the 22 GHz water line will be integrated into the instrument to retrieve water content. The scene water content, pressure and temperature will be needed to successfully retrieve tropospheric ozone.

F1-9 12:00 OBSERVATIONS ON INFRASONIC PRESSURES VARIATION DURING THE SOLAR ECLIPSE OF 11 AUG 1999

M. Lal, S. Gurubaran, C. Paneerselvam, K.U. Nair, C. Selvaraj, and R. Rajaram
Equatorial Geophysical Research Laboratory
Indian Institute of Geomagnetism
Krishnapuram, Tirunelveli-627011, India
e-mail: egrl@vsnl.com

We have made an attempt to study the infrasonic pressure variation during the solar Eclipse of 11 Aug 1999, at low latitude northern hemisphere, Tirunelveli, India (8.7 deg N, 77.8 deg E). We have measured the surface pressure variation by using microbarograph. We have also measured weather parameters such as surface temperature and humidity by using Physcrometer. At low latitude station, convection activity and wind variation is very large and it is being modulated in the surface pressure variation. Therefore, to minimise the convection and wind variation effect in the microbarograph record, we have fabricated noise-reducing lines of pipe typically consisting of about 150 feet of pipe of various diameters, tapering from 3 inch (inside diameter) pipe at the center in steps to 0.5 inch (inside diameter) pipe at the ends. The pipe line is equipped with capillary ports to the atmosphere usually set at 5 ft intervals, and the input to the microphone is connected to the center of this spatial filter. The maximum obscuration of the eclipse at this location was 70%. We have taken continous observations on the eclipse as well as on control days. The surface pressure has been recorded at the interval of one seconds. The dry and wet bulb temperature has been recorded at five minutes interval. The weather parameter has been recorded from 1600 hrs IST (Indian Standard Time) to 1900 hrs IST, during the eclipse as well as on control days. We have found the decrease in surface pressure by about 600 microbar between the beginning of the eclipse and the maximum obscuration. The surface temperature on the eclipse day has been found to be 2-3 deg C less than the control days. The surface humdity on the eclipse day is about 8% higher than the control days. We have also made an attempt to study the signature of gravity waves produced by the supersonic movements of the lunar shadow during the eclipse. The power spectral analysis of the surface pressure variation has been done. We have found the significantly larger amplitude of waves of periodicity 2.13 and 2.63 minutes on the eclipse day. This feature has not been observed on the control days. These waves might have been generated by the surface level observed such as H2O and CO2 due to decrease in surface temperature and has been recorded by the microbarograph at the ground.

Session G1, 08:55 AM-Wed., Room 245
DATA ASSIMILATION AND MODELS
Chairperson: D. Anderson, NOAA/SEC (danderson@sec.noaa.gov)

G1-1
09:00

AN ASSIMILATING MODEL FOR THE IONOSPHERE

Robert P. McCoy
Code 321SR
Office of Naval Research
800 N. Quincy St.
Arlington, VA 22217
703 323 7444

The Office of Naval Research in conjunction with the Air Force Office of Scientific Research is managing a new program to develop an assimilating model for the ionosphere. This effort is one of the 1999 Multidisciplinary University Research Initiative (MURI) awards granted by the Director Defense Research and Engineering (DDR&E). The MURI award goes to two consortia of universities with principal investigators from Utah State University (Bob Schunk) and the University of Southern California (Chunming Wang). The 99 MURI entitled "Models for Improved Specification and Forecast of the Global Ionosphere" is a three to five year program focussing on new techniques for the development of a real-time data driven ionospheric model. This research investigation will combine the state of the art in several areas including ionospheric physics, data assimilation and ionospheric remote and in situ sensing. The wealth of experience with data assimilation in meteorology and lessons learned will be used to help guide the present initiative. Data candidates for real time ionospheric assimilation will include radio remote sensing techniques (GPS, computer ionospheric tomography), optical (primarily ultraviolet) remote sensing, ground-based soundings and in situ satellite observations of ionospheric composition and variability. The emphasis will be on ionospheric data sources available to the DoD with the plan to develop a model that can transition into DoD operations.

G1-2 09:20 DEVELOPMENT OF GLOBAL DATA ASSIMILATIVE IONOSPHERIC MODEL

C.Wang[1], G. Hajj[1,2] , X. Pi[1,2], G. Bailey[3], L.J. Romans[1,2], I.G. Rosen[1]

[1]Department of Mathematics, University of Southern California, CA 90089-1113
[2]Jet Propulsion Laboratory, California Institute of Technology, 4800 Oak Grove Dr. Pasadena, CA 91109
[3]School of Mathematics and Statistics, University of Sheffield, Sheffield, S3 7RH, England

As the number of ground and space based receivers tracking the global positioning system (GPS) increases steadily and, as other remote sensing data of the ionosphere such as the measurements of airglow become available, it is now possible to monitor the changes in the ionosphere continuously and on a global scale with unprecedented accuracy and reliability. However, in order to make best use of such a large volume of data for both ionospheric specification and forecast, it is important to develop a data driven ionospheric model which is consistent with the underlying physical principles governing ionosphere dynamics. In this paper, we present a summary of research effort currently underway at the University of Southern California and at the Jet Propulsion Laboratory to develop a Global Assimilative Ionospheric Model (GAIM).

The main focus of our research is to demonstrate the feasibility of combining various data sources to improve ionospheric specification and forecast. The two most important aspects of our efforts are the estimation of ion densities distributions and the estimation of driving forces which are involved in the theoretical models of the ionosphere. The later is particularly critical for ionosphere forecast applications. The underlying theoretical ionospheric model for the current phase of our investigation is a modified version of USPIM from the University of Sheffield. The data assimilation problem is formulated mathematically as a nonlinear least square minimization problem with the initial state of ionosphere and driving forces as parameters to be estimated.

In addition to the discussion of the mathematical framework in which the ionospheric data assimilation problem is formulated, we shall present our where the electron density distribution is estimated using the method of Kalman filter driving forces such as the electrical field and the neutral wind in the ionospheric model are estimated using the method of adjoint equation. Because our current effort is focused upon the demonstration of our technical approach for data assimilation, we have primarily used the Observation System Simulation Experiment (OSSE) procedure to evaluate the performance of our data assimilation algorithms.

Acknowledgement: Research supported in part by the grant MURI N00014-99-1-0743 from the Office of Naval Research

G1-3
09:40

GLOBAL ASSIMILATION OF IONOSPHERIC MEASUREMENTS (GAIM)

R. W. Schunk
Center for Atmospheric and Space Sciences
Utah State University
Logan UT 84322-4405

A university consortium composed of Utah State University (USU), the University of Colorado in Boulder (CU), the University of Texas in Dallas (UTD), and the University of Washington (UW) has been funded to construct a specification and forecast model for the Earth's ionosphere called GAIM. GAIM will use a physics-based ionosphere-plasmasphere model as a basis for assimilating a diverse set of real-time (or near real-time) measurements. The assimilative ionospheric model will provide specifications and forecasts on a spatial grid that can be global, regional, or local (50 km x 50 km). The specifications/forecasts will be in the form of 3-dimensional electron density distributions from 90 km to geosynchronous altitudes (35,000 km). In its specification mode, GAIM will provide quantitative estimates for the accuracy of the reconstructed ionospheric densities. More than 4000 measurements/day will be assimilated by GAIM when the model is completed in three years. The data sets that will be incorporated in GAIM include: (1) slant path Total Electron Content (TEC) measurements from 24 GPS satellites and 90 ground-based receivers; (2) occultation measurements between 8 low-Earth-orbit (COSMIC) satellites and the GPS satellites; (3) bottomside electron density (N_e) profiles from several ground-based ionosondes; (4) line-of-site ultraviolet (UV) emissions and in situ N_e measurements obtained from DoD satellites; and (5) high-quality TEC measurements between selected ground-based sites and satellites with radio beacons (2-D ionospheric tomography). The overall program involves model construction, data quality assessment, data assimilation, construction of an executive system to automatically run the model, validation, and science. The technical and science objectives of the new program will be discussed.

G1-4
10:00

A DATA ASSIMILATIVE IONOSPHERIC TOMOGRAPHY ALGORITHM

G. S. Bust* D. S. Coco
Center for Ionospheric Research
Applied Research Laboratories
University of Texas at Austin
10000 Burnet
Austin, TX 78758

We have developed a new tomography algorithm designed to be compatitable with data assimilation models. This algorithm is based on objective analysis methods and the three dimensional spatial component of the algorithm is consistent with the statistical minimization "3dvar" approach taken by at NRL West (R. Daley, and E. Barker, *The NRL 3DVAR Source Book*, NRL West Internal Document, 1998). We make use of the data and forecast model error covariance matrices to produce a weighted estimate of electron density on a three dimensional grid. This estimate is an optimal estimate when the covariances are known exactly. All of the apriori information necessary for the tomography algorithm is carried in the two error covariances and the model forecast of electron density. Thus, at least in principle, all the apriori information can be determined from fundamental physics - no ad-hoc assumptions are necessary.

Our 3dvar tomography algorithm uses beacon TEC, GPS TEC from both ground and LEO receivers, ionosonde density profiles, DMSP in-situ density and EUV limb scans as input data. The algorithm can also take ISR data as input, but the ISR data is usually used to validate the algorithm. In principle, any model can be used as the forecast model. The current version of the algorithm uses the climatological model IRI and the first principle physics model FLIP. To extend the algorithm in time, we adopt a kalman filter approach. For IRI we use a method similar to that described by B. Howe (B. M. Howe, K. Runciman and J. A. Secan, *Radio Science*, **33**, 109-128, 1998). For FLIP, we update the model with results from the tomography algorithm at user selectable time intervals - 24 hours currently. We also use a simple method of updating the FLIP error covariance. Rather than do a full model update, we update the variance and assume that the spatial correlations do not change with data assimilation.

We will present a description of the algorithm and results from our tomography campaigns. We will compare results from using IRI as the forecast model with results from using FLIP as the forecast model.

G1-5
10:40

SAMI2: A NEW IONOSPHERIC MODEL

J.D. Huba* G. Joyce
Plasma Physics Division
Naval Research Laboratory
Washington, DC
20375
J.A. Fedder
Sachs-Freeman
Landover, MD

SAMI2 (Sami2 is Another Model of the Ionosphere) is a self-consistent, low-latitude model of the ionosphere recently developed at the Naval Research Laboratory. It is an outgrowth of a mid-latitude ionospheric model developed at the Naval Research Laboratory in the mid 1970's. SAMI2 treats the dynamic plasma and chemical evolution of seven ion species (H^+, He^+, N^+, O^+, N_2^+, NO^+, and O_2^+). The neutral species are modeled using MSIS86 and HWM93. The ion temperature equation is solved for three species: H^+, He^+, and O^+. The electron temperature equation is also solved. SAMI2 models the plasma along the earth's dipole field from hemisphere to hemisphere, includes the $\mathbf{E} \times \mathbf{B}$ drift of a flux tube (both in altitude and in longitude), and includes ion inertia in the ion momentum equation for plasma motion along the dipole field line. This last point insures that the plasma dynamics at high altitudes is treated correctly. Existing ionospheric models assume the ions are collisional at all altitudes. To our knowledge, SAMI2 is the first low latitude ionospheric model to include ion inertia. In this paper we report the possibility of a high altitude electron hole that has been found with SAMI2. The hole forms in the altitude range 1000 - 2000 km at geomagnetic equatorial latitudes. The electron hole is produced by transhemispheric flows of O^+ that transports H^+ to lower altitudes thereby reducing the electron density. The transhemispheric flows are caused by an interhemispheric pressure anisotropy that is generated by the neutral wind. The electron hole has a strong seasonal and longitudinal dependence.

G1-6
11:00

FURTHER ANALYSIS OF GPS/MET RADIO OCCULTATION DATA IN THE IONOSPHERE

W. S. Schreiner* Sergey V. Sokolovskiy Christian Rocken
Douglas C. Hunt
GPS Science and Technology Program
University Corporation for Atmospheric Research
Boulder, CO 80301
Ming-Quey Chen
Institute of Space Science
National Central University
Chung-Li, Taiwan

Ground and space-based dual frequency amplitude and phase measurements from the Global Positioning System (GPS) are useful for monitoring the distribution and variability of the Earth's ionospheric electron density. A GPS receiver in low Earth orbit (LEO) can precisely measure the total electron content (TEC) along the signal paths to all visible GPS satellites, even those at negative elevation angles which profile the ionospheric electron density from orbit altitude downwards. We examine two different profiling algorithms and compare the GPS occultation results from the GPS/MET experiment to correlative data. The two profiling algorithms that are discussed in detail include: 1) the traditional Abel inversion which assumes spherical symmetry; and 2) a 3D inversion that is constrained with the horizontal structure of an a priori 3D electron density field. The retrieved profiles are validated by statistically comparing two years (> 36,000 profiles) of GPS/MET inversions to f_oF_2 data from a network of 66 ionosonde stations, to vertical TEC data derived from the global network of GPS ground receivers, and to TOPEX vertical TEC data. Globally, the results of the Abel inversion agree with the ionosonde f_oF_2 data (1,674 matches within 1,000 km, and 30 minutes) at the 0.80 MHz rms level with a negligible mean difference. When these data are culled to allow only matches in low gradient regions, then the agreement is near the 0.25 MHz rms level. Analysis of correlative matches in high gradient regions (near the equatorial anomaly) indicates that horizontal gradients can introduce errors into the Abel retrievals with magnitudes greater than 1 MHz in f_oF_2. In an effort to estimate the magnitude of the Abel retrieval errors, simulations of these erorrs with NCAR's TIME-GCM model will be presented for solar minimum and maximum conditions. Current attemps to improve upon the Abel inversion with the constrained inversion algorithm in high gradient regions using real data will also be presented.

G1-7
11:20

THE CHARACTERIZATION OF THE IONOSPHERE USING DIVERSE DATA AND MODELS

S. Ganguly* G. H. Van Bavel A. Brown
Center for Remote Sensing, Inc
11350 Random Hills Rd, Suite 710
Fairfax, VA 22030

The complete description of the spatial distribution of the ionospheric plasma is necessary for scientific understanding and for several practical applications involving communication, radar, navigation, etc. Ionospheric diagnostic techniques, on the other hand, provide information piecemeal. A framework is needed that would provide for the consistent fusion of various input data that differ in spatial and temporal resolution. We have implemented an approach in which an ionospheric model serves as basis for the assimilation of ionospheric data. The free parameters of the ionospheric model are adjusted using observations and then the adjusted model is used to specify the state of the ionosphere over a 3D region of interest. The models available in the current implementation include the International Reference Ionosphere (IRI) and the Parameterized Ionospheric Model (PIM). A subsequent reconstruction utilizes an adaptive tomographic technique that combines ionosonde measurements with TEC observations from ground and/or satellite borne receivers and beacons. Any satellite constellation (including GPS, NNSS, GLONASS, etc.) and ionosonde configuration may be specified, and the method can be extended to include other data sources, such as oblique sounders, radar, radio propagation, incoherent scatter, optical observations, etc. The reconstruction provides a 3D description of the ionosphere that is self-consistent in terms of ionospheric physics and various observational data. The assimilation is based upon basic principles of data analysis. A weighted best-fit reconstruction of the electron distribution provides a robust means to organize the data in terms of spatially varying uncertainties and, thereby, yields an ionosphere that satisfies the diverse data in accordance with their reliability.

G1-8
11:40

IONOSPHERIC DATA QUALITY ISSUES FOR IONOSPHERIC MEASUREMENTS; A GAIM STRATEGY

J. J. Sojka, D. Thompson, and R. W. Schunk
Center for Atmospheric and Space Sciences
Utah State University
Logan UT 84322-4405

Observations of the ionosphere are an essential ingredient in data assimilation modeling of the ionosphere. At the same time, these data are potentially the unseen weakness of operational models. Unlike a scientific study in which experts evaluate each element of the data and model prior to reaching a scientific conclusion, an operational assimilation model must perform continuously without expert supervision. In this paper, we present and discuss data issues specifically associated with the Global Assimilation of Ionospheric Measurements (GAIM) project. These issues apply equally well to other efforts in which observations are acquired and used without expert supervision. The objective in each case is to ensure that the autonomous data handling and processing software has adequate intelligence to prevent the situation of 'bad' data being passed into an assimilation utility.

The philosophy of data quality determination depends heavily on an individual's relationship to the data stream. An instrument builder understands the nuances of the instrument which may or may not be reflected in a meaningful way to data handling engineers tasked with delivering a contracted product and so leads to an immediate disconnect occurring in the product's quality tracking. A further level of diffusiveness occurs in the final computational environment where this data product needs to be packaged into a state-of-the-art database. By this stage, the tracking of quality documentation from instrument developer, to transmission engineer, to database manager has pretty much become an impossibility because no project funding is available to bring these individuals and the assimilation team together to establish the final data quality.

Examples of operational 'data' problems will be shown and discussed. In almost every case, the problem arose because as data gets handed off at each stage, an assumption about quality and requirements has been made. However, no final overview of maintenance of the quality is required at the application end.

The data ingest process is further confounded by selective availability and mixed types of data. These concerns will also be discussed. Selective availability arises in many ways; on DMSP, for example, instrument duty cycle, delayed tape recorder dumps, unique orbit geometry, data transfer delays, and ray data extraction are but a few. Some instruments perform most poorly under conditions, such as storms, when the application most heavily depends upon them. Are high resolution, but infrequent, in situ measurements of an ionospheric density more valuable than an almost continuous line-of-sight integral? Can the subsequent inversion of the line-of-sight data produce ionospheric densities that are an adequate substitute for key ionospheric parameters?

We will provide an overview of the GAIM data handling strategy targeting future operational assimilation.

G1-9
12:00

THE POSSIBILITY TO MODEL IONOSPHERIC PERTURBED CONDITIONS THROUGH EMPIRICAL MODELS

E. A. Araujo-Pradere, T. J. Fuller-Rowell, M. V. Codrescu

CIRES – University of Colorado. SEC – NOAA.

325 Broadway. R/E/SE. CO 80303

While the ionospheric behavior during quiet conditions is well know and efficiently modeled, the knowledge about ionospheric response during geomagnetic storms, and related process, still remain unclear. Because there is currently no empirical storm-time correction algorithm in use that as shown improvement over climatological references models such as International Reference Ionosphere (D. Bilitza, IRI 1990, *Nat. Space Sci. Data.* NGDC), to obtain a model to predict the ionospheric response during storms is a priority ionospheric task.

This work presents a empirical model that starting from the integral of the auroral power or the integral of the tri-hourly index ap, predict Φ (= foF2obs/foF2mm) changes during perturbed conditions.

Based in the theory developed by Prölss (G.W. Prölss, *J. Geophys. Res.*, **98**, 5981-5991, 1993) and extended by Fuller-Rowell et al. (T.J. Fuller-Rowell, D. Rees, S. Quegan, R.J. Moffett, M.V. Codrescu, and G.H. Millward, STEP: Handbook of Ionospheric Models. 1996), which suggested that negative storm effects are due to regions in which the neutral composition is changed, we proposed an empirical algorithm to capture the ionospheric response under different dependences (seasonal, local time, latitudinal):

$$\Phi = a + b_1\left[X(t_0)\right] + b_2\left[X(t_0)\right]^2 + \ldots. + c\left[X(t_0)\right] sen(LT + \phi_1)$$

where $X(t_0) = \int F(\tau) P(t_0 - \tau) d\tau$, and $F(\tau)$ is the filter weighting function of auroral power, P, over the 30 previous hours or the weighting function of the ap index over the 36 previous hours. "a", "b_1" y "b_2" are coefficients for the polynomial fit to the non-linear relationship between the ionospheric response and the integral of the power. ϕ_1 is selected to peak at down.

The optimum of the filter was obtained by a multi linear regression technique, minimizing the mean square error between the filter input (aurora power or ap index) and filter output (ionospheric ratios). The power values have equal weight for the first 24 hours prior to the time of interest, and reduce to zero linearly between 24 and 30 hours, while the ap values has a remarkable peak in the second part. The absolute magnitudes are not important. This implies that, at mid-latitudes, the ionosphere is dependent on geomagnetic or auroral activity up to 30 hours in the past.

The RMSEs for the eighteen storms intervals using the empirical algorithm show a significant improvement over the first attempt and climatology. The algorithm reduces the variance to values between 0.13 and 0.15, close to the quiet-time reference level (0.12756).

Session H1, 08:55 AM-Wed., Room 265
DIAGNOSTICS IN LABORATORY AND SPACE PLASMAS
Chairperson: W.E. Amatucci, Naval Research Laboratory (amatucci@ccf.nrl.navy.mil)

H1-1
09:00

SPACE PLASMA DIAGNOSTICS: WHAT WE MEASURE AND WHY

J. Bonnell
Space Sciences Laboratory
University of California
Berkeley, CA 94720

In an effort to set the stage for a comparison between and discussion of plasma diagnostic techniques in laboratory and space plasmas, we will discuss the various methods used to diagnose plasma properties in the space plasma context. We will concentrate on examples drawn from phenomena observed in the auroral ionosphere (large-scale convection, ion acceleration, coherent wave structures) which also have applications in the magnetospheric context. We will review techniques for the measurement of DC and wave electric and magnetic fields, bulk plasma density and temperature, particle distributions and ion composition. Electric field measurements in space plasmas are typically done using double-probe antennas, either singly, or in Interferometric arrays. Fluxgate and searchcoil magnetometers take care of magnetic field measurements. DC field measurements are typically sampled waveforms, while wave measurements use a combination of on-board spectral analysis, and sampled waveform (full-time and capture mode) analysis. Bulk plasma density and temperature measurements are done using various types of Langmuir probes, while bulk density and composition can often be inferred from cutoffs and resonances in the measured electric field spectrum. Particle energy-pitch angle spectra are measured using electrostatic E/q analyzers, with mass spectrometry typically done using time-of-flight or magnetic analyzers.

We will also review the constraints on interpretation imposed by the typically single-point, non-repeatable nature of space plasma measurements, as well as common models used to aid in interpretation. The primary constraint imposed by the single-point nature of most space plasma measurements is the familiar one of whether spatial or temporal variation of the quantities measured is observed. Recent missions flying either multiple sensors per payload, or multiple payloads, have begun to remove this constraint, although the methods for analyzing the resulting data are still in development.

H1-2
09:20

LABORATORY SIMULATION OF SPACE PLASMA PHENOMENA[†]

W. E. Amatucci*
Plasma Physics Division, Code 6755
Naval Research Laboratory
Washington, DC 20375

Throughout the past 40+ years of *in situ* research in near-Earth space plasmas, a rich variety of phenomena has been observed. Improvements in the temporal resolution of each successive generation of spacecraft have revealed that the space plasma environment is more rich and complicated than first thought. However, there are several underlying difficulties with the data obtained from the space measurements. The data are often single point measurements, frequently causing space-time ambiguities to complicate interpretation. Typically, the data are either snapshots in time or statistical compilations from many satellite passes which are subject to varying plasma conditions. Given these operational realities, further insight into the details of the processes can often be obtained through laboratory simulation of space plasma phenomena.

Laboratory experiments can compliment *in situ* space experimentation in several important ways. The main advantage offered by laboratory experiments is the ability to create controlled, *reproducible* conditions in which the important space plasma parameters can be scaled and maintained. By producing scaled space-like conditions, diagnosis of the physics involved in these processes can be performed with a level of detail that is not possible in space. In addition to studies of fundamental plasma processes, laboratory devices that can reproduce space-like conditions are excellent testing grounds for development of improved *in situ* diagnostics. This is particularly important since space physics has progressed to the point where the ability to make accurate, quantitative measurements in space is required (L. R. O. Storey, *Measurement Techniques in Space Plasmas: Particles*, Geophys. Monograph **102**, Amer. Geophys. Union, 1998, p. 17).

A number of different facilities are currently being used to perform space-related laboratory experiments. Plasmas are created in these laboratory devices by several distinct methods. In this talk, the ways in which laboratory plasmas are created, the range of characteristics that these plasmas have and their scaling to space plasmas will be reviewed, along with a brief overview of the standard types of diagnostics available to the laboratory plasma experimentalist.

[†]Work supported by the Office of Naval Research.

H1-3
09:40

ELECTRIC FIELD DOUBLE PROBE MEASUREMENTS FOR IONOSPHERIC SPACE PLASMA EXPERIMENTS

R. Pfaff*
NASA/Goddard Space Flight Center
Greenbelt, MD 20771

Double probes represent a well-proven technique for gathering high quality DC and AC electric field measurements in a variety of space plasma regimes including the magnetosphere, ionosphere, and mesosphere. Such experiments have been successfully flown on a variety of spacecraft including sounding rockets and satellites. Typical instrument designs involve a series of trades, depending on the science objectives, type of platform (e.g., spinning or 3-axis stabilized), expected plasma regime where the measurements will be made, available telemetry, budget, etc. In general, ionospheric DC electric field instruments that achieve accuracies of 0.1 mV/m or better, place spherical sensors at large distances (10m or more) from the spacecraft body in order to extend well beyond the spacecraft wake and sheath and to achieve large signal-to-noise ratios for DC and long wavelength measurements. Additional sets of sensors inboard of the primary, outermost sensors provide useful additional information, both for diagnostics of the plasma contact potentials, which particularly enhance the DC electric field measurements on non-spinning spacecraft, and for wavelength and phase velocity measurements that use the spaced receiver or "interferometer" technique. Accurate attitude knowledge enables $\mathbf{V} \times \mathbf{B}$ contributions to be subtracted from the measured potentials, and permits the measured components to be rotated into meaningful geophysical reference frames. We review the measurement technique for both DC and wave electric field measurements in the ionosphere discussing recent advances involving high resolution burst memories, multiple baseline double probes, new sensor surface materials, biasing techniques, and other considerations.

H1-4
10:00

ELECTRIC FIELD MEASUREMENTS IN LABORATORY PLASMAS

Robert L. Merlino
Department of Physics and Astronomy
The University of Iowa
Iowa City, IA 52242

The Langmuir probe remains the most widely used diagnostic for the measurement of electric fields in laboratory plasmas. They are relatively inexpensive and easy to construct and implement, and they provide point measurements with very good spatial resolution. They can be used to measure both steady-state (DC) and fluctuating (AC) electric fields, and thus provide information on both the equilibrium (zero-order) state of the plasma and the presence of waves and instabilities (perturbed state).

Langmuir probes do not provide a direct determination of electric fields but rather a localized measurement of the space potential of the plasma. Electric field profiles can then be constructed from spatial profiles of the space potential. Ideally, this process requires that the full current-voltage characteristic of the probe be obtained at many spatial points within the plasma. A more direct, although somewhat approximate mapping of DC electric field profiles in a plasma can be obtained using a emissive probe. An emissive probe is a fine tungsten wire inserted into the plasma and heated to thermionically emit electrons. When sufficient electron emission occurs, the floating potential of the probe is a very close approximation to the actual space potential. The advantage of this technique is that the floating potential can be continuously measured (with a high impedance voltmeter) as the probe is moved to different locations in the plasmas. Thus the entire potential structure (and hence the electric field) can be mapped out.

A relatively non-perturbing technique for direct measurement of the electric field in a plasma is based on the deflection of a very low current, energetic, diagnostic electron beam.

Examples of measurements of DC and AC electric fields in laboratory plasmas using the techniques mentioned above will be presented.

This work was supported by ONR and NSF.

H1-5
10:40

INTERFEROMETRIC COHERENCY DETERMINATION OF WAVELENGTH OR WHAT ARE BB-ELF WAVES?

P. M. Kintner* J. Franz P. Schuck E. Klatt
School of Electrical Engineering
Cornell University
Ithaca, NY, 14853

To determine the wavelength of waves within a random, isotropic wave field we introduce the observable of wave coherency measured with plasma wave interferometers. We show generally that wavelengths large compared to the interferometer length produce large coherency (nearly one), but wavelengths the order of a few times the interferometer length, or smaller, produce small coherency (close to zero). We apply this principle first to examining auroral hiss and lower hybrid waves measured by the PHAZE 2 and TOPAZ 3 experiments and show that the implied wavelengths are consistent with the expected dispersion relations and with other, different estimates of wavelength for these modes. Next we apply the principle to a plasma wave phenomena called broadband extra low frequency (BB-ELF) electric fields observed in both experiments. BB-ELF electric fields have been established as the wave measurements most often associated with the most significant transverse ion acceleration up to an altitude of at least 1700 km within the auroral ionosphere. Our analysis indicates that the wavelengths of the BB-ELF are quite small. In one case we calculate the coherency of BB-ELF electric fields using an ensemble average of 7889 data samples and demonstrate that the coherency near the oxygen gyrofrequency is very small ($\simeq 0.15$), corresponding to wavelengths of 10 m and the order of the ion gyroradius. We conclude that because of the short wavelengths, previous satellite measurements of BB-ELF electric fields likely underestimated the electric field amplitudes. Although the wavelengths and frequencies of BB-ELF electric fields are now known, we are unable to assign the wave to a known normal mode of homogeneous plasmas. This suggests that inhomogeneities may be essential for describing BB-ELF electric fields.

H1-6
11:00

TWO-PROBE TECHNIQUES TO MEASURE WAVENUMBER-FREQUENCY SPECTRUM OF VTF PLASMA

R.J. Riddolls* M.C. Lee N.E. Dalrymple
Plasma Science and Fusion Center
NW16-229
Massachusetts Institute of Technology
Cambridge, MA 02139

The Versatile Toroidal Facility (VTF) is a large plasma device located at the MIT Plasma Science and Fusion Center. Plasma is produced by either Electron Cyclotron Resonance Heating (ECRH) or by the injection of electron beams. Plasma densities of 5×10^{17} m^{-3} can be produced in a magnetic field of 800 G, allowing one to appropriately simulate the ionospheric plasma. An experiment has been designed to allow one to estimate the frequency-wavenumber spectrum of turbulence generated by the injection of large-amplitude whistler waves.

An in-plasma crossed-dipole antenna has been mounted in the VTF. The antenna is oriented and phased to launch waves in the whistler mode. Approximately 100 W of radiation is launched at a frequency slightly above the lower hybrid resonance. In that frequency range, it is expected that the whistler waves will undergo mode conversion into lower hybrid waves (K.M. Groves *et al.*, *J. Geophys. Res.*, **93**, 14683–14687, 1988) and possibly excite lower hybrid waves and zero-frequency modes via a parametric instability (M.C. Lee *et al.*, *J. Geophys. Res.*, **89**, 10873–10880, 1984).

Two-probe techniques have been used to investigate the whistler-produced plasma turbulence. The probes have been given several degrees of spatial freedom in order to allow one to estimate the frequency-wavenumber spectrum by various means. First, conventional interferometry (P.M. Bellan *et al.*, *Phys. of Fluids.*, **19**, 995-1006, 1976) has been implemented by scanning the probes during wave injection. Second, the statistics of phase-lag measurements have been computed from fixed probe pair positions (J.M. Beall *et al.*, *J. Appl. Phys.*, **53**, 3933–3940, 1982). Finally, the space-time cross-correlation function has been transformed (D.B. Ilic *et al.*, *Rev. Sci. Instrum.*, **46**, 1197–1200, 1975). Presented are results of VTF laboratory experiments using the second method. The role of lower hybrid waves in the high-power radio wave heating experiments at Arecibo is discussed.

H1-7
11:20

HIGH RESOLUTION PHOTOMETRY OF FLICKERING AURORA

Matthew G. McHarg*
Department of Physics
United States Air Force Academy CO 80840
Hans Stenbæk-Nielsen
Geophysical Institute
University of Alaska, Fairbanks
Fairbanks AK 99775

The exact mechanisms for auroral electron acceleration are not fully understood. A comparison of experimentally determined arc thicknesses with 22 different theoretical predictions of arc thicknesses shows very poor agreement (Borovsky, *J. Geophys. Res*, 1993). Of the possible theories examined by Borovsky approximately a third would have temporal fluctuations of the auroral intensity associated with them. Ground based narrow field TV and high speed photometry offer a unique perspective on the spatial and temporal scales of the aurora. Narrow field TV data are used to evaluate the spatial extent, and variations in auroral morphology. A high-speed photometer boresighted to narrow field TV is used to explore the fast intensity fluctuations of the auroral light. We observe auroral intensity fluctuations at frequencies above the Nyquist frequency of the TV camera in flickering aurora. We present data that shows a band limited tone of ~50 Hertz, that decreases in frequency to ~30 Hertz in approximately 3 minutes. Immediately following the band limited tone becomes broad band up to ~50 Hertz, followed by a narrow band tone at ~7 Hertz. This narrow band 7-Hertz tone is seen in the narrow field TV camera as flickering aurora. A possible interpretation of the observed data in terms of a wave particle modulation of the primary electrons causing the auroral light is presented. Possible sources of the wave field are electromagnetic ion cyclotron waves (Temerin et al. *J. Geophys. Res* 1986), and inhomogeneous energy density driven (IEDD) waves (Ganguli et al., *J. Geophys. Res* 1994, Ganguli in *Cross Scale Coupling in Space Plasma*, Geophysical Monograph No. 93, 1995 and Gavrishchaka et al. *Phys. Plasmas* 1996). While ground based high spatial and temporal resolution observations alone can not alone determine the modulation mechanism of auroral electrons they represent a new important contribution to the remote sensing of space plasmas.

H1-8
11:40

DESIGN STRATEGIES FOR MINIATURIZING CHARGED-PARTICLE ENERGY ANALYZERS

C. L. Enloe
Integrated Science and Technology Program, MSC 4102
James Madison University
Harrisonburg, VA 22807

Electrostatic charged-particle energy analyzers are often used in applications where miniaturization can be a substantial benefit. In spaceborne applications, where payload mass is a major consideration, the size of an instrument is directly related to the cost of fielding it on orbit. In laboratory applications, reducing the size of a probe typically reduces the level of perturbation the probe introduces to a system.

Certain analyzer configurations, although simple conceptually, are unsuitable for miniaturization. The gridded, planar retarding potential analyzer is one such design. Although conducting meshes of high fineness are readily available from which to construct such a miniature device, the feature size of these meshes on the miniature scale introduces such undesirable behaviors as a non-monotonic filter response. Attempting to refine the electric field structure using multiple meshes adds mechanical complexity, reduces the sensitivity of the analyzer, and can introduce additional complications such as moir patters into the spatial response.

Better success can be had with miniature analyzer designs that rely on electric field relaxation to establish electrostatic potential structures. One such device presented here, the "cone-in-a-can" configuration, offers high energy resolution in a design whose performance is insensitive to the precise dimensions of the analyzer. It is therefore suitable for fabrication methods where manufacturing tolerances may be large relative to the dimensions of the analyzer itself.

The ready availability of three-dimensional numerical modeling tools for charged particle optics has opened the possibility of unique analyzer designs that would be difficult to describe analytically. One configuration presented here, the "pac-man" configuration, proved to have an unusable filter response when fabricated symmetrically. Breaking symmetry in the z-axis (an approach suggested by numerical modeling of the analyzer) yielded a successful design with a wide field of view and good spatial and energy resolution.

Numerical modeling is an enabling tool for the micro-electrostatic analyzer (MESA) concept. Reducing analyzer size to very small dimensions means that the designer must consider the analyzer's configuration and the processes by which it will be manufactured simultaneously. The final analyzer configuration presented here is currently being tested as a macro-scale prototype for a micro-fabricated instrument. Numerical simulation has allowed multiple iterations of the design concept to proceed efficiently before testing of the prototype was initiated.

A/D1-1
14:00

NEW TRENDS IN GLOBAL MODELING TECHNIQUES: ARTIFICIAL NEURAL NETWORK AND WAVELET BASED APPROACH

S. Goasguen and S. M. El-Ghazaly
Telecommunications Research Center
Department of Electrical Engineering
Arizona State University, AZ 85287-5706 USA
Email: sme@asu.edu

The global modeling approach was demonstrated recently. In general, it requires intensive computation to solve the full hydrodynamic model that characterizes the active device, and computationally expensive techniques to connect the passive and the active components, such as the diakoptics approach. In this paper, we present two new trends to obtain efficient global modeling simulation: The use of neural network and the use of wavelets.

On one hand, we propose to model the steady state solution of the hydrodynamic equations by an artificial neural network that accurately and efficiently predicts the behavior of the simulated MESFET. The transistor is implemented in an extended FDTD code to simulate an amplifier. The non-linearities of the MESFET are described by the ANN which update the circuit parameters values inside the FDTD mesh according to the electromagnetic field computed. As a result, large-signal characterization is obtained as fast as small-signal characterization. This new approach provides a very efficient and practical first order global modeling of a MMIC.

On the other hand, we propose to use a wavelet-based numerical technique to create an adaptive irregular grid over the complete physical domain. This allows us to avoid using diakoptics techniques and greatly reduces the computation time. The multiresolution property of wavelet bases reduces the number of grid points. A fine mesh is used in regions of strongly varying fields and a coarse mesh is used in regions of slowly varying fields. The choice of wavelet bases will be discussed to deal appropriately with the non-linear equations that characterize the active device.

A/D1-2 14:20 INTEGRATED ACTIVE ANTENNA USING RESONANT TUNNELING DIODE

Kai Liu, Samir M. El-Ghazaly
Vijay Nair*, Nada El-Zein*, Herb Coronkin*
Department of Electrical Engineering
Telecommunication Research Center
Arizona State University
Tempe, AZ 85287-7206
Email: sme@asu.edu
*PCRL, Motorola, Inc.,2100 E.Elliot Road
Tempe, AZ 85284

Wireless communications have been playing an important role in modern society, either in outdoor or indoor applications. To that end, wireless systems are facing the challenges of larger bandwidth as well as better service quality. As the computing capabilities advance, the programming oriented Soft Radio proves itself to be the likely candidate of wireless communication means. Smart antennas incorporated in Soft Radio are finding more and more applications. The array antennas not only enhance the signal level in service area, but also increase the flexibilities of associated signal processing algorithm. In this paper, we investigate the potential use of Heterojuncture Interband Tunneling Diode (HITD) in wireless communications. The integrated active antenna can be used to perform several functionalities (e.g., switch, oscillator, amplifier, and mixer) while it still has regular antenna performance

To realize a significant simplification of the circuit topology, we choose planar geometry for antenna structure. Spectral Domain Approach (SDA) is utilized to simulate the antenna characteristics. The RTD can be either inside or outside slot antenna. The design data for grounded substrate and half space infinite substrate are obtained through the SDA. The impedance of slot antenna is sensitive to the substrate thickness. The DC and AC properties of RTD are measured or extracted from measured data after the RTD's have been fabricated. The DC and AC characteristics are very consistent with each other. For example, at the bias (from 0.2V~0.5V) where DC characteristics IV curve has Negative Differential Resistance, the RTD's RF resistance always appears negative. To validate the simulation result, we designed and fabricated several integrated active antennas. Theoretical and experimental results will be presented.

A/D1-3 14:40 QUANTUM MMICs: TECHNOLOGY AND APPLICATIONS

V. Nair, N. El-Zein, M. Deshpande, J. Lewis, K. Kramer and H. Goronkin
Physical Sciences Research Laboratories, Motorola Inc.
2100 E. Elliot Road, MD EL508
Tempe, Az. 85284, USA
Tel: 480-413-5922, Fax: 480-413-5934, e-mail:
avac90@email.mot.com

Recent advancement in device and IC technology based on InP material system have shown that high performance MMICs that consume less power can be fabricated at milli-meter wave frequencies [C. Pobanz *et. al.*, IEEE JSSC, pp. 1219-1224, Sept.199]. In addition, the integration of hetero-junction inter-band tunnelling diode and HEMT has shown that ICs with even smaller die size can be realised by utilising the negative differential resistance behaviour of the diode along with the amplification characteristics of the HEMT [V. Nair *et al* IEEE GaAs IC Digest, pp. 191-194, Nov. 1998].

A three terminal device, known as Hetero-structure Inter-band Tunnelling FET (HITFET), is realised by integration of an hetero-junction inter-band tunnelling diode that exhibits the quantum tunnelling phenomenon and a HEMT that has very high electron mobility. Quantum MMICs based on the quantum tunnelling FETs exhibit many desirable characteristics that can be exploited to realise multifunctional ICs at high frequencies. The availability of negative resistance elements in the QMMIC fabrication process enables the development of high frequency circuits such as VCOs; frequency multipliers, LNAs and power amplifiers that have smaller die size superior RF performance VCOs designed with HITFET device technology can reduce the complexity of the up-down converters. Utilisation of these devices that have inherent negative resistance region in the design of low noise amplifiers and power amplifiers also lead ICs with better performance. Low noise amplifiers will have better RF characteristics and lower power consumption. Power amplifiers will have higher power added efficiencies and suitable for operation at lower voltage. A HITFET based circuit approach can be implemented to generate square like waveform required to switch the class E power amplifier output stage. The RF signal is used to initiate the square wave form generation of the driver stage device. Higher power added efficiency could be realised with this type of circuit configuration. An overview of the device characteristics and examples of RF applications will be presented at the conference.

This work was performed in part under the management of Research and Development Association for Future Electron Devices within the MITI R&D Program on Quantum Functional Devices supported by NEDO

A/D1-4 THE GENERATION OF SYNTHETIC LOAD PULL DATA
15:00

Peter A. Blakey and Eric M. Johnson
Motorola MD: EL720
GaAs Technology Department
2100 E. Elliot Road,
Tempe, AZ 85284

Load-pull measurements assist the development of semiconductor technologies for wireless power amplifiers. These measurements characterize RF behavior as a function of load impedance, with some RF parameter (often input power) held constant. The behaviors that can be measured include output power, power-added efficiency, and linearity (e.g. ACPR). Measured quantities are plotted on a Smith chart, yielding a convenient graphical view of performance tradeoffs as functions of load impedance.

The time required to perform load-pull measurements is quite long, and the resources associated with acquiring and operating load-pull measurement systems are significant. Some organizations that own load-pull systems face a measurement bottle-neck; and other organizations that could benefit from load-pull measurements do not have access to a load-pull measurement system. Synthetic load-pull (SLP) was developed in response to these issues.

SLP uses I-V characteristics, sometimes supplemented by small-signal data, to predict the results of large-signal load-pull measurements. The DC and small-signal data may be obtained from measurements or simulation. The accuracy of SLP is found to be very good when pulsed I-V characteristics, rather than DC I-V characteristics are used. This is because pulsed I-V characteristics account for both self-heating and carrier trapping.

The basic SLP system extends techniques developed by Cripps [S. C. Cripps, *MTT-S Digest*, pp. 221-223, 1983] and Kushner [L. J. Kushner, *Technical Report 812*, Lincoln Laboratory, MIT, 1988]. In essence, Cripps algorithm is generalized to include a self-consistent load-line, and Kushner's approach is generalized to handle arbitrary output characteristics. The SLP algorithm uses I-V data to calculate contours of constant output power, drain efficiency and load resistance in the input voltage - output voltage plane. The superposition of these contours makes it easy to select optimum operating conditions and to determine the corresponding load resistances. Comparisons between calculated and measured load-pull data for three different PA technologies demonstrate excellent agreement.

The calculation of input power, and hence gain and power-added efficiency, requires knowledge of small-signal s-parameters. SLP calculations of gain as a function of input power have yielded very good agreement with measured data. Extensions of SLP that support harmonic termination, automatic bias optimization, and the calculation of linearity figures of merit will also be outlined.

A/D1-5
15:40

Collisional Accelerations and Hot Carrier Metrology

Robert O. Grondin
Department of Electrical Engineering
Arizona State University
Tempe, AZ 85287

For several decades electromagnetic emissions from semiconductors have been interpreted as possibly resulting from Bremstrahhlung like sources. However, this has been a controversial subject, and one needs to be careful to make a distinction between "hot carrier Bremstrahhlung" and "intraband radiative transitions". Early work involved models in which the radiation was associated with ionized impurity scattering of carriers in the semiconductor. However, much of the data involves structures which are lightly doped and therefore do not have much ionized impurity scattering. In these structures the radiation must originate from intraband radiative transitions associated with phonons. In the presentation we will first quickly review the existing experimental data on this broad band electromagnetic radiation of submillimeter wavelengths often referred to as "hot carrier Bremstrahhlung" and discuss how it possibly might be used to prove the internal physics of semiconductor devices. Then, we will quickly review experiments in which ultrafast optical devices are used to make Hertzian dipole like structures that serve as both as sources and as detectors of broadband electromagnetic radiation of submillimeter wavelengths. These optically induced Hertzian dipole structures also are lightly doped structures in which impurity scattering is unimportant and where the transport models therefore are dominated by phonon scattering. We will show that in some instances a detailed explanation of these experiments suggests that one needs to include the presence of electromagnetic radiation due to collisional accelerations. Then, we will ask if the two sets of experimental data are related and explore implications for the development of models.

A/D1-6 16:00 ANALYSIS AND DESIGN OF OPTICAL MODULATORS

N Alkhdour, M M Tomeh, and S. El-Ghazaly
Telecommunications Research Center (TRC)
Department of Electrical Engineering,
Arizona State University
Tempe, AZ 85287

The high bandwidth requirements of modern technologies have made optical communications systems a necessity. There is, therefore, a clear need for optical modulators acting as a link between local electronic systems and optical communications signals.

The most viable proposal for such a modulator is a $LiNbO_3$ traveling wave optical modulator. It consists of a coplanar waveguide (CPW) on a $LiNbO_3$ substrate terminated by a ground plane. Light is fed through $LiNbO_3$ optical waveguides imbedded in the ($LiNbO_3$) substrate underneath the gaps between the central conductor and CPW ground planes. This device exploits the dependence of dielectric permittivity in $LiNbO_3$ on electric fields. Microwave signals travelling in the CPW change the dielectric constant in the optical waveguides embedded underneath them allowing for modulation.

The primary design considerations for such a modulator are matching the speeds of the microwave and optical signals, low microwave electrode losses, and optimization of the electrode characteristic impedance. Optical-microwave velocity matching enhances the broadband performance of this device. The presence in the structure of bends increases the chance for losses due to radiation. Impedance mismatching further hinders performance, as reflections must then be accounted for. Numerical techniques are used to provide an accurate model for the device to enhance its performance and design.

A/D1-7
16:20

WIDEBAND FERROELECTRIC COPLANAR WAVEGUIDE PHASE SHIFTERS

Jeffrey M. Pond, Steven W. Kirchoefer, Edward J. Cukauskas, Won-Jeong Kim, and James S. Horwitz
Naval Research Laboratory
Washington, DC 20375

We are developing room temperature thin-film ferroelectric materials for use in distributed microwave components such as phase shifters. Phase shifter applications of ferroelectric thin films are more compatible with the present state of refinement of ferroelectric thin films than other applications, such as ferroelectric varactors (S.W. Kirchoefer, et al., *Micro. and Opt. Tech. Lett., 18*, 168-171, 1998). This offers the possibility of yielding components that are competitive with the best results of conventional approaches, yet does not depend critically upon significant new materials advances. Success has already been documented in the literature for phase shifters using a narrow-band design on ferroelectric thin films, with insertion losses on the order of 5 dB. (van Kuels et al., *Micro. and Opt. Tech. Lett. 20*, 53, 1999). Initial results on broadband phase shifters, although not achieving an optimal match, show very promising results.

Our effort involve several different approaches to obtaining ferroelectric thin films which simultaneously possess low dielectric loss tangent and reasonable modulation of the relative permittivity with an applied dc field. Pulsed-laser-deposition is the most extensively studied deposition system for ferroelectric thin films and considerable progress has been made in correlating the microstructure of the material with its microwave properties. More recently, magnetron sputtering techniques have demonstrated the potential to produce ferroelectric films with properties suitable to microwave device applications. Comparisons between the deposition techniques and the measured properties are providing useful information to help refine both deposition processes.

In addition to a discussion of measured results and design issues for phase shifter applications, the potential to use these elements as building blocks for tapped delay lines to realize transversal filters, will be addressed. Tunable filter and oscillator applications are other possible applications which will become highly desirable as modest improvements are made in the material properties of the ferroelectric thin films.

A/D1-8
16:40

RADIO FREQUENCY LNA ON CMOS

Arif Mahmud* David Allee Samir El-Ghazaly
Electrical Engineering
Arizona State University
Tempe, AZ 85287

Although the signal processing in many modern receivers occurs in the digital realm, analog circuits are still needed to amplify weak incoming signals from the antenna to a voltage which can be conveniently digitized. With the rapidly growing consumer market for portable wireless communicators, there is increasing cost incentive to implement RF analog circuits using conventional VLSI CMOS technologies. The conventional paradigm is to employ high-speed $GaAs$ FET and Si bipolar technologies since analog Si MOS alternatives are considered incapable of operating in the near GHz regime. However, the performance of Si CMOS devices has emerged to a point where analog CMOS is now a strong cost-effective contender to challenge existing solutions to realize highly integrated RF communication components.

This article consists primarily of the basic concepts useful in the analysis and design of RF Low Noise Amplifiers (LNAs). In addition, design considerations and existing topologies for CMOS low noise amplifiers are discussed in brief. The design of an LNA involves numerous tradeoffs. Important RF parameters include noise performance, intermodulation performance, and overall level. Gain stability over temperature and supply voltage variation is important as this affects worst case system specifications. Finally, supply current is critical in portable applications and must be minimized.

Since low power consumption is the key driving force for the present day portable and wireless communication all analog as well as digital circuits are designed keeping this additional constraint in mind. The LNA circuit needs to provide the required gain at low enough noise figure while keeping the DC power dissipation to a minimum. Fortunately, the possibility to achieve lower noise figure by reducing the device width lends itself to the fact that low power and low noise can be achieved at the same time without a trade-off between the two.

Our present work is intended to come up with a fully-monolithic LNA that can be used in the GPS (Global Positioning System) receiver. A 1.8V, 1.57542GHz LNA has been designed for a 0.6μm CMOS process. This amplifier provides a forward gain 19dB with a noise figure better than 3dB while drawing only 17mW DC power. The employment of CAD optimization tool is expected to help achieve improved circuit performance.

Session B/D1, 13:15 PM-Wed., 1B-40
PHOTONIC BANDGAP STRUCTURES
Chairperson: Richard Ziolkowski, Univ. of Arizona (ziolkowski@ece.arizona.edu)

B/D1-1
13:20

PHOTONIC BAND STRUCTURE DIAGRAMS FOR TWO-DIMENSIONAL FINITE-HEIGHT FINITE-LENGTH GROUNDED ELECTROMAGNETIC CRYSTALS

P. Keith Kelly*, Ted Kutrumbos, Melinda Piket-May
Department of Electrical and Computer Engineering
Campus Box 425
University of Colorado
Boulder, CO 80309 USA

Susan C. Hagness
Department of Electrical and Computer Engineering
University of Wisconsin-Madison
1415 Engineering Drive, Madison, WI 53706-1691 USA

There exist a number of electromagnetic problems where guided surface waves can affect the performance of guiding, radiating, or scattering devices. Microstrip patch antennas are known to suffer reduced efficiency from surface wave excitation, especially for thick, high dielectric, homogeneous substrates. However, increased substrate thickness is very desirable to obtain wider bandwidth performance to support higher capacity in communication applications. Another structure suffering performance degradation is printed antenna arrays on substrates. The array can suffer an E-plane scan blindness when the wavenumber of the desired space wave matches the propagation constant of the dominant surface-wave mode. It has been shown that the coupling to the surface wave mode can be mitigated through use of an electromagnetic crystal (P.K. Kelly, et. al., "Investigation of Scan Blindness Mitigation using Photonic Bandgap Structure in Phased Arrays", Proc. of SPIE, vol. 3464, pp. 239-248, July 1998).

We have been investigating surface wave mitigation on dielectric-loaded perfectly conducting surfaces using electromagnetic crystals (P. K. Kelly, et. al., *Proc. of National Radio Science Meeting*, 215, 1999). The findings of this research have shown effective reduction of surface wave propagation on finite height grounded electromagnetic crystals. The photonic band structure diagram (the dispersion diagram) was shown for one-dimensional periodic structures. However, most practical applications will require a two-dimensional periodicity. Here, the finite-difference time-domain (FDTD) method is used to simulate the surface wave propagation for a two-dimensional substrate. The scattering parameters are derived from the incident, reflected, transmitted, and radiated probe measurements. Since the scattering parameters are determined with the phase preserved, band structure diagrams can be calculated using the insertion phase of the finite height crystal compared to the insertion phase of a solid substrate. Furthermore, the band structure can be determined over the complete irreducible Brillouin zone.

The numerical processing techniques for obtaining the complete band structure diagram from FDTD data, as well as results for grounded substrate finite-height finite-length hexagonal-lattice crystals, will be presented.

B/D1-2
13:40

PASSIVE AND ACTIVE ELECTROMAGNETIC BANDGAP STRUCTURE MODELING AND EXPERIMENTS

Michael J. Hill* Richard W. Ziolkowski
Department of Electrical and Computer Engineering
The University of Arizona
1230 E. Speedway
Tucson, AZ 85721-0104

Nanometer and micron sized optical devices are currently being explored for their applications in a variety of systems associated with communications, data storage, optical computing, etc. It has been demonstrated that photonic bandgap (PBG) structures can be used at these sizes to form extremely narrow bandwidth filters and extremely small waveguiding structures by a variety of research groups. The ability of the FDTD approach to model finite-sized PBG structures with the defects required to form these filters and waveguides, and to recover known behaviors has been demonstrated. The FDTD scheme provides a PBG simulation environment that is quite flexible in terms of the allowed variations in the PBG structure and the excitation pulses.

One electromagnetic bandgap (EBG) structure that has received attention both in the microwave and the optical regimes is the log cabin PBG. We have simulated and built a finite sized log cabin EBG from square metallic rods. A wide bandgap region where little electromagnetic energy is transmitted through the structure has been demonstrated both numerically and experimentally. The structure has also been modeled with a set of passive defects by removing one partial row of rods in the center of the structure. The difference between the structure without and with the defects has been studied numerically. It has been demonstrated that a narrow microwave frequency filter can be achieved with the defective EBG structure. We are in the process of confirming this behavior experimentally. We will report comparisons between the simulations and experiments as they are available.

It has also been found that additional defects can be used to control actively the flow of the power in the EBG structures. In particular, by attaching diodes to control several of the rods in the log cabin structure, one can actively initiate the frequency filtering effects of the EBG structure. This allows one to achieve an active microwave switch. These effects are being studied numerically. We are concurrently fielding the required components to perform the corresponding microwave experiments.

The results from all of these simulations and experiments will be reviewed in our presentation. The performance of these EBG structures for use in practical microwave applications will be addressed.

B/D1-3
14:00

SCATTERING FROM CYLINDERS LOADED BY ELECTROMAGNETIC CRYSTALS

P. Keith Kelly*, Ted Kutrumbos, Melinda Piket-May
Department of Electrical and Computer Engineering
Campus Box 425
University of Colorado
Boulder, CO 80309

Scattering from infinitely long circular cylinders is well understood using series solutions. These solutions have been formulated for both perfectly conducting and dielectrically loaded circular cylinders (G. T. Ruck, et. al., *Radar Cross Section Handbook*, chapter 4, 1970). Researchers have investigated the effects of periodic surface profiles for infinite radius of curvature, i.e. flat (J. Kiang, *IEEE Trans. APS*, 46, no. 2, 176-180, 1998), with the goal of reducing the backscattering cross section. This cross section reduction is accomplished, in part, by preventing surface wave excitation. Since the scattering from cylinders is a result of a specular response (initial reflection) and a creeping wave response (latent radiation from surface wave excitation), a surface treatment may allow the reduction of the scattering cross section of the cylinder. This paper presents findings on the backscattering cross section of infinitely long perfectly conducting circular cylinders loaded by electromagnetic crystals.

Recently, researchers have been investigating surface wave mitigation on dielectrically loaded perfectly conducting surfaces using electromagnetic crystals (P. K. Kelly, et. al., *Proc. of National Radio Science Meeting*, 215, 1999). The findings of this research have shown effective reduction of surface wave propagation on finite height grounded electromagnetic crystals. When examining the spectral density of the creeping wave response from dielectrically loaded cylinders, one finds that the creeping wave has a preferred center frequency. If this center frequency is aligned with the center frequency of the bandgap of the electromagnetic crystal, the creeping wave propagation around the cylinder will be changed. By properly designing the crystal, reduction of the creeping wave component to the backscattering direction is possible.

The finite-difference time-domain method is used to simulate the scattering response of these cylinders using a two-dimensional formulation. The code has been validated against the exact solution for both metallic and dielectrically loaded cylinders. Since the simulation is performed in the time domain with fine time resolution, the frequency domain response from the specular return and the creeping wave returns can be separated using gated post processing techniques. Simulated data will be presented showing the frequency domain and time domain responses for metal, dielectrically loaded and electromagnetic crystal loaded circular cylinders. The crystal performance will be shown for its surface wave propagation characteristics and the design methodology will be explained. Additionally, a description of the data processing methods will be covered, specifically the near to far field transformation scheme.

B/D1-4
14:20

COUPLING SUPPRESSION BETWEEN MICROSTRIP LINES USING PHOTONIC-BANDGAP STRUCTURES

A. C. Guyette, K. M. K. H. Leong, and W. A. Shiroma*
Department of Electrical Engineering
2540 Dole St., Holmes Hall 483
University of Hawaii at Manoa
Honolulu, HI 96822

One of the major obstacles to increasing the circuit density of monolithic microwave integrated circuits is the parasitic coupling and crosstalk that arises between neighboring transmission lines.

This presentation will discuss a coupling-reduction scheme for high-density, multi-frequency circuits that allows adjacent lines to lie closer or even intersect each other. The concept does not involve any additional top-layer filtering circuitry, but instead incorporates planar photonic-bandgap (PBG) structures in the normally unused ground plane, thus saving valuable chip real-estate area. The PBG structure consists of a square lattice of holes etched in the ground plane of a microstrip line (V. Radisić, Y. Qian, R. Coccioli, and T. Itoh, *IEEE Microwave and Guided Wave Lett.*, **8**, 69–71, Feb. 1998).

For the first example, two adjacent microstrip lines are fabricated on a common substrate. One line is intended to guide an X-band signal, and the other a Ku-band signal, *e.g.*, as in a transmit/receive module. In the ground plane of the X-band line, a PBG structure is etched with a stopband at Ku-band, and vice-versa. This allows the intended X-band signal to propagate unimpeded, but suppresses the coupling of Ku-band signals from the neighboring line. Compared to the case of a standard ground plane, 40-dB coupling suppression is measured at 16.6 GHz and 26-dB suppression is measured at 9.1 GHz.

As a second example, two intersecting microstrip lines are fabricated on a common substrate, with PBG structures etched in the ground plane of each line as before. Compared to the case of a standard ground plane, coupling reductions of 9 dB and 24 dB are measured at 11 and 18 GHz, respectively.

B/D1-5 NOVEL DESIGNS WITH FREQUENCY SELECTIVE SURFACES:
14:40 T. Lammers, A. Holley, J. Huang, P.K. Kelly, M. Piket-May, Electrical Engineering, Univ. of Colorado

B/D1-6
15:00

ACTIVE GRIDS ON PHOTONIC-BANDGAP STRUCTURES

W. A. Shiroma*
Department of Electrical Engineering
2540 Dole St., Holmes Hall 483
University of Hawaii at Manoa
Honolulu, HI 96822

Active grids are a class of spatial power combiners in which solid-state devices load a periodic grating that serves as a dc-biasing circuit, RF-embedding network, and a radiating structure. The period of the grating is typically small compared to a wavelength, allowing potentially hundreds of devices to be packed in a small area.

This presentation reviews oscillator grids that incorporate photonic-bandgap (PBG) structures into their design for power, polarization, and frequency control. Photonic-bandgap structures are periodic dielectric or metallo-dielectric structures that prohibit electromagnetic wave propagation in certain frequency bands.

One example demonstrates how replacing the metal mirror of a conventional grid oscillator with a PBG mirror results in improved output power, cross-polarization, and locking characteristics (Q. Sun, J. B. Horiuchi, S. R. Haynes, K. W. Miyashiro, and W. A. Shiroma, *IEEE Trans. Microwave Theory Tech.*, **46**, 2324–2329, Dec. 1998). The oscillator operates at a frequency that lies along the stopband edge of the PBG mirror, allowing the proper feedback level to be set for maximum power. The PBG lattice spacing is designed to reflect only the vertical polarization generated by the grid oscillator, resulting in improved cross-polarization. By confining the oscillator to operate only within the narrow stopband of the PBG mirror, multiple oscillation modes upon turn-on are suppressed.

Another example demonstrates a three-dimensional power-combining structure consisting of four active grids mounted on a PBG dielectric cube. A quasi-optical source consisting of 64 transistors is designed for multidirectional operation, with the backlobe of one grid serving as the injection-locking signal for additional grids on opposite faces of the cube (J. Mazotta, K. S. Ching, and W. A. Shiroma, *1999 IEEE MTT-S Int. Microwave Symp. Dig.*, 547–550, June 1999).

This source can also be used in receive-mode as a three-dimensional self-oscillating mixer (B. Elamaran, K. Y. Sung, D. M. K. Ah Yo, K. S. Ching, and W. A. Shiroma, *J. Lightwave Tech.*, Nov. 1999). Since the free-running oscillation frequency is restricted to lie within the narrow stopband of the PBG structure, injection locking to an external source is minimized, thereby extending the operating range of the mixer.

Session B/D2, 15:35 PM-Wed., Room 1B-40
ACTIVE ANTENNAS
Chairperson: W. Pearson, Clemson (wilson.pearson@ces.clemson.edu)

B/D2-1 LOW NOISE ACTIVE INTEGRATED ANTENNAS FOR RECEIVERS
15:40

Jonathan D. Fredrick, Yongxi Qian and Tatsuo Itoh
Department of Electrical Engineering
University of California, Los Angeles
405 Hilgard Avenue, Los Angeles, CA 90095
Phone: (310) 206-1024 Fax: (310) 206-4819 mail: fredrick@ee.ucla.edu

Introduction

This abstract describes the use of active integrated antennas for receiver purposes. Much attention has been paid to the integration of antennas into active transmitters. Several benefits can be realized through the integration of antennas into receiver systems. These benefits include improved signal to noise ratio and receiver gain.

In the transmitter mode active integrated antennas are exploited to maximize power efficiency and harmonic suppression. (J. Lin and T. Itoh, *IEEE Trans. Microwave Theory Tech.*, vol. MTT-42, pp. 2186-2194, Dec. 1994.) (V. Schulz, S. T. Chew, Y. Qian and T. Itoh, *IEEE Microwave and Guided Wave Lett.*, vol. 7, pp. 39-41, Feb. 1997.)

In the case of a receiver, however, the designer is concerned with the link budget and hence, the receiver's noise performance. In this abstract a circularly polarized patch antenna is integrated with a pair of low noise receivers to eliminate the losses, and associated degradation of noise figure, of the combining network.

Low Noise Integrated Receiver

The low noise integrated receiver is shown in Figure 1. Through the integration of low noise amplifiers into the circularly polarized antenna, losses in the transmission lines and quadrature hybrid are rendered negligible. Since the noise performance is dominated by the first stage these losses do not have an appreciable effect on overall performance.

Measured Results

Figure 2 shows the gain performance of the integrated low noise receiver. At the patch's resonance frequency (5.75 GHz) a peak power gain of 17 dB (over passive version) and minimum noise figure of 0.91 dB is measured.

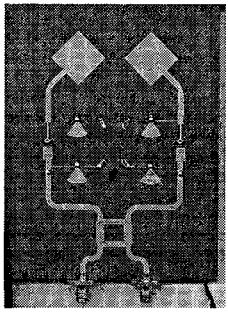

Fig. 1 Low Noise Antenna

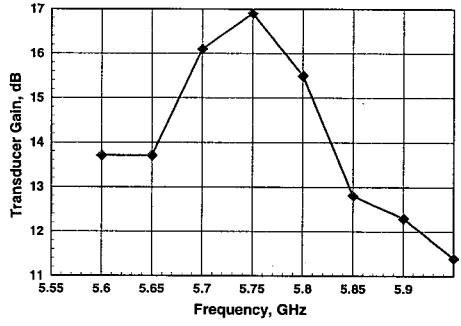

Fig. 2 Gain Performance of Low Noise Antenna

B/D2-2
16:00

ACTIVE ANTENNA INTEGRATED WITH DIODE LASER MODULATION

Joseph Tustin, Peter Kirkpatrick, and Zoya Popović
University of Colorado at Boulder
Campus Box 425, Boulder, CO 80309-0425 USA
Tel: 303-492-8998, Fax: 303-492-5323
Email: tustin@Colorado.EDU

Due to the large bandwidth and natural atmospheric attenuation of microwave signals, microwave links show promise for use in local area networks. However, due to this attenuation, a low-loss, guided mode link must be employed to connect the microwave LAN to a wide area network. Because of the low propogation loss inherent in optical fibers, recent reductions in the cost of optical components, and development of RF modulation capabilities in commercial diode lasers, an optical fiber channel is a viable choice for a high bandwidth, long distance transmission medium. In the system discussed here, wireless local communication is achieved in the microwave spectrum, and long range communication is achieved in a low loss optical fiber.

The component developed for this task is an active antenna which directly modulates a diode laser. The operational block diagram of the active antenna/optical modulator is shown in Figure 1. The RF signal is received by a microstrip patch antenna and amplified by a MMIC low noise amplifier (LNA). The LO signal is received by a microstrip fed slot antenna. These two signals are combined in a 90° hybrid coupler and mixed by a packaged Schottky diode to a 1 GHz IF. This IF is amplified by a packaged transistor and is used to amplitude modulate the DC current of the laser diode. The 1310 nm laser module is pigtailed to an optical fiber which is used to remote the IF signal to an InGaAs photodetector. The output from this detector is observable on an oscilloscope, or may be mixed to demodulate the signal.

The individual components in both the microwave and optical regimes will be discussed in this talk. Design, implementation, and characterization of each microwave component and characterization of the commercial optical components used in the system will be presented. The task of system integration and characterization will be developed and presented along with performance results. The authors also expect to demonstrate an array of such active antennas whose outputs may be combined to produce an optical interference pattern for angle of arrival detection of the incident RF signal.

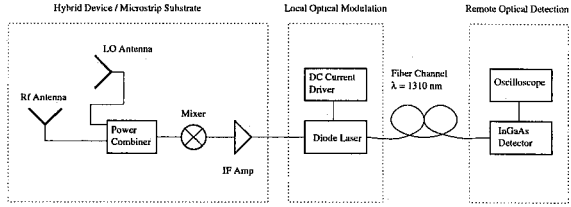

Figure 1: Block Diagram of an Active Antenna Optical Modulator

B/D2-3 16:20 ON THE MODULATION OF COUPLED OSCILLATOR ARRAYS IN PHASED ARRAY BEAM CONTROL

R. J. Pogorzelski
Mail Stop 138-307
Jet Propulsion Laboratory
Calif. Institute of Technology
4800 Oak Grove Drive
Pasadena, CA 91109

J. S. Acorn
Department of Electrical and Computer Engineering
Worcester Polytechnic Institute
100 Institute Road
Worcester, MA 01609

Over the past several years, coupled oscillator arrays have been under development as a means of providing, in a simple manner, control over the aperture phase of an array antenna thus achieving steering of the beam. The oscillators are arranged in linear or planar arrays in which they are each coupled via transmission lines to their nearest neighbors in such a manner as to cause them to mutually injection lock and oscillate as an ensemble. It has been shown that in the absence of any external injection signals they oscillate at the average of their free running frequencies. Under these conditions the relative phases of the oscillator output signals is a function of the free running frequencies of the oscillators. Assuming that they are voltage controlled oscillators (VCOs), the phase control is accomplished by application of appropriate biasing voltages. It has been shown that the slope of linear phase progressions across the array can be controlled by adjustment of the bias on only the end oscillators of a linear array. [R. A. York, IEEE Trans., MTT-41, 1799-1809, 1993][P. Liao and R. A. York, IEEE Trans., MTT-41, 1810-1815, 1993] Analogously, such slope control can be accomplished by biasing only the perimeter oscillators of a planar array. A body of theory capable of predicting the dynamic behavior of such arrays has also been developed. [R. J. Pogorzelski, P. F. Maccarini, and R. A. York, IEEE Trans. MTT-47, 463-470, 1999] [R. J. Pogorzelski, P. F. Maccarini, and R. A. York, IEEE Trans. MTT-47, 471-478, 1999][R. J. Pogorzelski, Nat. Radio Sci. Mtg Dig., pg. 296, Boulder, CO, Jan. 1999][R. J. Pogorzelski, IEEE AP-S/URSI Int'l Symp. Dig., pg. 2382, Orlando, FL, July 1999] In addition, a seven element experimental array has been fabricated and tested. This array is used in the work described here.

The primary objective of the work to be presented is investigation of the modulation characteristics of a linear coupled oscillator controlled phased array. It is shown that modulation cannot be effectively applied unless all of the oscillators are modulated simultaneously. Using the seven element experimental array, a low frequency square wave was applied simultaneously to all of the oscillator tuning ports and the resulting phase dynamics observed on a multi-channel oscilloscope. These measurements verify certain aspects of the theoretical predictions concerning the modulation dynamics of the array under both free running and externally injection locked conditions and thus enhance the credibility of the continuum model underlying the theory.

B/D2-4 16:40 **BEAM POINTING ERRORS IN COUPLED OSCILLATOR ACTIVE ARRAYS**

Jinjin Shen and L. Wilson Pearson
Holcombe Department of Electrical and Computer Engineering
Clemson University
Clemson, SC 29634-0915
jshen@clemson.edu, pearson@ces.clemson.edu

Coupled-oscillator arrays demonstrate beam steering that is controllable through signals applied at the elements on the perimeter of the array alone. Recent work by York, Pogorzelski, Itoh, and the authors of this abstract has been directed toward fuller understanding of this phenomenon and toward defining means whereby a low-cost replacement for a phased array might be derived based on the beam steering principle.

Phase errors are present across the array aperture through two different mechanisms. First, random errors in the free-running frequency of each oscillator in array introduce random phase errors from element to element. (The free-running frequency is defined for each oscillator acting singly.) This error is diminished in proportion to the ration Q/K, where Q is the quality factor of the entire oscillator circuit in its free-running configuration and K is the element-to-element coupling factor in the array configuration. The second source of phase error is the extent to which the phase of the coupling factor differs from zero (or π, depending on the coupling scheme). Both of these phase errors result in beam pointing error in the field radiated by the array.

We present results of numerical studies of errors arising through both of the mechanisms indicated above. These results are computed from York's full nonlinear model of coupled oscillator systems. Errors in the free-running frequency of individual oscillators are introduced in a Monte Carlo fashion. The error in coupling factor phase is systematic and is introduced in a fashion consistent with that which we observe in extended-resonance coupled systems. The computed results provide phase and amplitude distributions across the array from which radiation patterns are obtained.

We demonstrate that the beam pointing error can be adjusted out through pre-biasing the control signal that is applied to the perimeter elements in the array. Thus the entire array can be fabricated without tuning of individual devices during assembly. The pre-biasing of the control signal is determined in a single calibration of the fully configured array. An unwanted consequence of this procedure is a narrowing of the scan range of the antenna array.

Some observations are made regarding the practical realization of a matched set of oscillators for use in beam-steered arrays.

B/D2-5
17:00

10 GHZ WAVEGUIDE CAVITY EO PHASE MODULATOR

Peter E. Kirkpatrick and Zoya B. Popović
University of Colorado at Boulder
Campus Box 425, Boulder, CO 80309-0425 USA
Tel: 303-492-8998, Fax: 303-492-5323
Email: kirkpatp@colorado.edu

An electrooptic (EO) phase modulator based on a resonant waveguide cavity has been designed and fabricated. Figure 1(a) shows an isometric view of the EO. The Lithium Niobate ($LiNbO_3$) cavity is designed to be $\frac{3\lambda_g}{4}$ in length at 10 GHz. The z-component of the electrical permittivity of $LiNbO_3$ is ϵ_z=34, which was used to determine the guided wavelength in the cavity. The z-axis of the $LiNbO_3$ crystal is oriented in the vertical direction, normal to the waveguide plates and co-axial with the RF electric field. This configuration takes advantage of the high value of the corresponding EO coefficient in $LiNbO_3$, $r_{33} = 30.8 \times 10^{-12} \frac{m}{V}$. The feed for the cavity was fabricated on a Duroid substrate with ϵ_r=10.2 and thickness t=1.27 mm. The feed consists of a 100 Ω parallel plate waveguide (PPWG) matched to 50 Ω through an exponentially tapered impedance matching section. The width of the PPWG, which is given by the impedance of the line, determines the width of the crystal and thus the interaction distance for the microwave and optical electric fields. This impedance was chosen to be higher than 50 Ω to increase the strength of the electric field for a given amount of power. The width also determines the cutoff frequency for higher order transverse modes, which in this case was well above the frequency of operation. Similarly, the thickness of the substrate determines the thickness of the crystal. The thickness also determines the strength of the electric field in the crystal, so a thinner substrate improves the coupling of the RF and optical electric fields, given that light may still be coupled into the crystal.

A heterodyne (interferometric) measurement technique is used to measure the modulator performance. The interferometer is realized using polarization maintaining fibers and components, as shown in Figure 1(b). The detector used is a 20 GHz InGaAs photodetector operating at 1.3 μm.

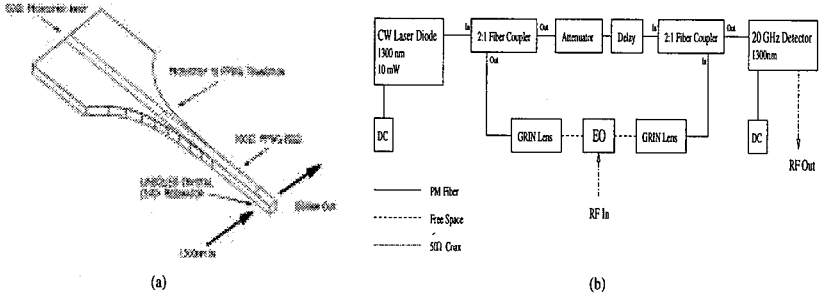

Figure 1: (a) Isometric view of resonant EO phase modulator
(b) Fiber interferometer for phase measurement

B/D2-6
17:20

FM NOISE IN INJECTION LOCKED PLANAR RADIATING OSCILLATOR

Akiko KISHI Masami MURATA Shingo OHMORI Toshiaki MATSUI
University of Electro-Communications Communications Research Laboratory
1-5-1, Choufugaoka, Choufu-shi, Japan Ministry of Posts and Telecommunications
E-mail: akiko@net.is.uec.ac.jp 4-2-1, Nukui-Kitamachi, Koganei-shi, Japan

Recently, active integrated antennas [Y. Qian and T. Itoh, "Progress in Active Integrated Antennas and Their Applications," *IEEE Trans. Microwave Theory Tech.*, vol. MTT 46, pp 1891-1900, November. 1998] have received much attention for millimeter-wave application because of their simplicity and the possibility of versatility. Since the oscillation type active antenna is free-running oscillator integrated with antenna, injection locking for stabilization is required. Many researchers have reported the radiating oscillator design and its characteristics of injection locking in the literature [for example, R.A.York and T. Itoh, "Injection-and phase-locking Techniques for Beam Control," *IEEE Trans. Microwave Theory Tech.*, vol. MTT 46, pp 1920-1929, November. 1998]. We proposed a planar radiating oscillator using butterfly-shaped patch (B-PRO)[M. Murata and T. Matsui, " 2X2 Spatial power combining array of planar radiating oscillator using butterfly-shaped patch element," to be published in *Proc.29th European Microwave Conf.*, Sept. 1999], which can control injection locking range by changing flare angle. In this paper, we report the characteristics of FM noise through the injection locking of the B-PRO. Fig. 1 shows top and side view of the B-PRO that has injection transmission line. The B-PRO uses a two sided microstrip structure, with a common ground plane in the center. The patch was located on one side of the structure, while the directly injection feed line was on the opposite side. The circuit was designed for operation at frequency of 8.3GHz on a 3.2mm thick glasscross teflon with a relative dielectric constant of 2.17. We measured FM noise as a function of offset carrier frequencies from 100KHz to 500KHz for fundamental injection locking case and free-running case. A dramatic FM noise reduction for the fundamental injection locked oscillator was observed. The larger the injection power the better the noise reduction. There is no influence on the oscillation, since the microstrip line for injection locking is on non-radiation plane.

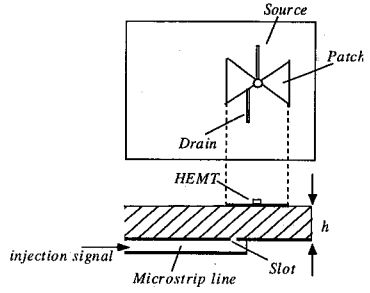

Fig. 1 Top and side view of planar radiating oscillator

Session B/F2, 13:15 PM-Wed., Room 1B-51
ROUGH SURFACE SCATTERING APPLICATIONS AND METHODS
Chairperson: J.A. DeSanto, Colorado School of Mines (jdesanto@mines.edu)

B/F2-1 13:20 **SCATTERING CROSS SECTION FROM A ROUGH SURFACE AT SMALL GRAZING ANGLES**

Iosif M. Fuks, Valerian I. Tatarskii, Donald E. Barrick*)
Cooperative Institute for Research in Environmental Sciences,
University of Colorado/NOAA, Environmental Technology Laboratory,
325 Broadway, Boulder, CO 80303
*)CODAR Ocean Sensors, Fremont Avenue, Suite K, Los Altos, CA 94024

The particular problem of wave scattering at low grazing angles is of great interest because of it importance for long distance propagation of radio waves along the Earth surface, radar observation of near surface objects, and for solving many other fundamental and applied problems. One of the main questions is - how the specific cross section behaves for extremely small grazing angles? In the paper (V.I. Tatarskii and M.I. Charnotskii, *Trans. IEEE*, **AP-46,** 67-72, 1998) a general answer to this question was obtained for the scattering cross section by arbitrary rough surfaces of two types: with Dirichlet and Neumann boundary condition. For the last case the main result of such general consideration, obtained there, is the following: the scattering amplitude tends to a constant without any assumptions on the relationship between wavelength and the geometrical scales of surface roughness. The results of (D.E. Barrick, *Trans. IEEE*, **AP-46,** 73-83, 1998), including both numerical calculations and a general proof, contains the opposite statement: the scattering amplitude for both surface types mentioned above tends to zero as the second power of a grazing angle.

We consider the process of wave scattering by a statistically rough surface with a Neumann boundary condition. This model corresponds to the scattering of "vertically" polarized EM waves by one-dimensional (i.e., cylindrical) rough surface, when the magnetic field vector is directed along the generating line of this cylindrical surface. We assume that the surface roughness is small enough (in the sense of the Rayleigh parameter) and confine ourselves to the first order approximation of perturbation theory. This is equivalent to wave scattering in the Born approach, where Bragg scattering process takes place with only one resonant Fourier component of surface roughness responsible for the scattering in a given direction. But we take into account the attenuation of the incident and scattered waves due to multiple scattering processes on the way "to" and "from" the region where scattering happens. It is proved that the scattering cross section of vertically polarized radio waves by a perfectly conducting surface (Neumann boundary condition) tends to zero as a second power of grazing angle (fourth power for backscattering) at small grazing angles, due to the above-mentioned multiple scattering processes. It is shown that the angular behavior of the scattering cross section changes abruptly at grazing angles close to the pseudo Brewster angle that is connected with the effective rough surface impedance and the reflection coefficient of the coherent reflected field. For finite beam scattering the result depends on the relation between the beam width and the pseudo Brewster angle.

B/F2-2
13:40 LOW GRAZING ANGLE SCATTERING OF VERTICALLY POLARIZED WAVES BY APERIODIC SURFACES.

M. I. Charnotskii
NOAA Environmental Technology Laboratory
325 Broadway, Boulder CO, 80303 USA
E-mail mcharnotskii@etl.noaa.gov

New (Grazing Perturbation) theory for the scattering of vertically polarized waves by a periodic perfectly conducting surface was introduced in (M. I. Charnotskii, Proc. XXVI General Assembly URSI, p. 88, Toronto, 1999). This theory complements the conventional perturbation theory and predicts a nonlinear dependence of the scattering amplitudes on the roughness heights for slightly rough surface in the presence of diffraction orders propagating at low grazing angles. Grazing perturbation theory revealed the existence of the intrinsic surface impedance that strongly affects the scattering when low grazing diffraction order is present.

Here we discuss the extension of the grazing perturbation theory to the aperiodic surface. Conventionally, transition to the aperiodic case is achieved through the expansion of the surface period. This operation is intrinsically ambiguous and should be supplemented by some additional restraints.

We show that if the Fourier transform of the final aperiodic surface is required to be bounded in the transition process, the Fourier coefficients of the surface roughness are inverse proportional to the period. This implies the elimination of divergence in the conventional perturbation series at low grazing angles. The effective surface impedance of the grazing perturbation theory vanishes, and the validity domain of the grazing perturbation theory diminishes. This model corresponds to the case when roughness is confined to the finite part of the otherwise plane surface.

In the alternative case of uniform roughness the power spectrum of the roughness is bounded. This model is suitable for individual realizations of a homogeneous random surface. In this case Fourier coefficients of the surface roughness are inverse proportional to the square root of the period, and effective surface impedance attains a finite limit. This implies that grazing perturbation theory maintains a finite validity region for scattering by uniform rough surfaces.

B/F2-3
14:00

PHASE FACTORS REPRESENTATION FOR EM SCATTERING FROM ROUGH INTERFACE BETWEEN VACUUM AND PERFECT CONDUCTOR

Valerian I. Tatarskii and Viatcheslav V. Tatarskii
University of Colorado CIRES
and NOAA Environmental Technology Laboratory
325 Broadway, Boulder, CO 80303; vit@etl.noaa.gov

The problem of EM scattering from the random surface is considered in this paper. The magnetic surface (current) integral equation for plane in an average rough interface between vacuum and perfect conductor is presented in the form that contains the random elevations only in exponents. Iterations of this equation lead to the presentation of solution in powers of multiplicity of Kirchhoff scattering and contain the random elevations only in exponents. The first two terms of this expansion include as particular cases Bragg scattering, Kirchhoff approximation, small-slope approximation (see, e.g., Voronovich A. G., Berlin: Springer, 1994), tilt-invariant approximation (Charnotskii M.I. and Tatarskii V.I., 55, No 4, 361-80, 1995), and double Kirchhoff approximation (Ishimaru, A. and Chen, J. S. J. Acoust. Soc. Am1877-83, 1990).

All mean values can be expressed directly in terms of joint characteristic functions of elevations in different points of rough surface. Because modulus of any characteristic function is bounded by unity, we can expect the much better convergence of this expansion in comparison with other expansions that contain as factors statistical moments or cumulants.

We present the results of numerical calculations of back-scattering cross-sections for sea surface characterized by non-Gaussian PDF of slopes (Cox-Munk distribution) and anisotropic spectrum (Elfouhaily et al., J. Geophysical Research, 102(C7): 15,781-15,796 1997). This statistical model was developed in the NOAA Technical Memorandum ERL ETL-289 "Phenomenological Statistical Non-Gaussian Model of Sea Surface with Anisotropic Spectrum for Wave Scattering Theory" by V.I. Tatarskii and V.V. Tatarskii, (see also JEWA, 13, No 7, 899, 1999).

B/F2-4
14:20

RADAR BACK-SCATTERING FROM THE OCEAN SURFACE IN THE SMALL-SLOPE APPROXIMATION AND INFERRING SEA-ROUGHNESS SPECTRA FROM RADAR DATA

A. G. Voronovich*
NOAA/ETL
325 Broadway, Boulder, CO 80303
V. U. Zavorotny
CIRES/University of Colorado/NOAA/ETL
325 Broadway, Boulder, CO 80303

We present numerical calculations of backscattering of electromagnetic waves from a rough sea surface according to the small-slope approximation (SSA). The advantages of using the SSA rather then the two-scale (composite-surface) model are: 1) the SSA does not require an introduction of an arbitrary scale-dividing parameter and 2) a comparison between the SSA of the lowest order and the second order corrections allows us to estimate the accuracy of scattering calculations.

A comparison of experimental data regarding the zeroth- and the second azimuthal harmonic of backscattering cross-section for Ku-band (SASS-II model) and C-band (CMOD4 model) is made against theoretical results based on the empirical spectrum from (T. Elfouhaily *et al.*, *J. Geophys. Res., 102*, 15,781-15,796, 1997) and Gaussian sea-roughness statistics. It shows a good agreement for zero-order azimuthal harmonics of the VV-polarization: the average error is generally of the order of or even less then 1 dB (though it increases to about 2 dB for C-band at 5 m/s). However, the same error for the second azimuthal harmonics (VV-polarization) is larger and reaches about 4 dB. The error is most significant for small incidence angles and for low wind speeds. To fix this discrepancy a modification of the original Elfouhaily's *et al.* empirical spectrum has been suggested. The modification basically makes the long-wave part of the spectrum more isotropic, and the short-wave part of the spectrum more directional. As a result the average errors for both harmonics have been brought down to 1.5 dB or less (with a single exception of C-band at 5 m/s where average error reaches 2 dB).

For the HH-polarization the accuracy of comparisons is of the same order for small incidence angles (less then 20°), however there is a systematic underestimate of experimental data for larger incidence angles. We believe, that this bias is caused by steep, even though seldom occurring, (micro) breaking waves associated with non-Gaussianity of a sea surface.

B/F2-5
14:40

A NOVEL ACCELERATION ALGORITHM FOR THE COMPUTATION OF SCATTERING FROM TWO-DIMENSIONAL LARGE-SCALE RANDOM ROUGH SURFACES WITH THE FORWARD-BACKWARD METHOD

D. Torrungrueng* J. T. Johnson
The Ohio State University
Department of Electrical Engineering
ElectroScience Laboratory
1320 Kinnear Road
Columbus, OH 43212

The forward-backward method with a novel spectral acceleration algorithm (FB/NSA) has been shown to be an extremely efficient iterative method of moments for the computation of scattering from one-dimensional (1-D) perfect electric conducting (PEC) and impedance rough surfaces (H.-T. Chou and J. T. Johnson, *Radio Science*, **33**, 1277-1287, 1998). The NSA algorithm is employed to rapidly compute interactions between widely separated points in the conventional FB method, and is based on a spectral domain representation of source currents and the associated Green's function. For fixed surface roughness statistics, the computational cost and memory storage of the FB/NSA method is $\mathcal{O}(N)$ as the surface size increases. This makes studies of scattering from large surfaces, required in low-grazing-angle scattering problems, tractable.

In this paper, the FB/NSA method for the computation of scattering from 2-D rough surfaces will be illustrated. The NSA algorithm for this case involves a double spectral integral representation of source currents and the 3-D free space scalar Green's function. The coupling between two spectral variables makes the problem more challenging. It can be shown that the computational efficiency of the FB/NSA method for 2-D rough surfaces remains $\mathcal{O}(N)$ as one of the surface dimension increases. Comparisons of numerical results between the conventional FB method and the FB/NSA method for large-scale PEC rough surfaces shows that the latter yields identical results to the former with a great reduction of CPU time and only a slight increase in memory storage. In addition, the numerical results of FB/NSA method are in good agreement with experimental data obtained from the University of Washington (J. T. Johnson et al., *IEEE Trans. Antennas Prop.*, **44**, 748-756, 1996). The phenomenon of backscattering enhancement is observed both in the numerical predictions and experimental data.

B/F2-6
15:00

AN INNOVATIVE HIGH-ORDER METHOD FOR ELECTROMAGNETIC SCATTERING FROM ROUGH SURFACES

Oscar Bruno
Caltech
Pasadena, CA 91125
Maria Caponi
TRW
Redondo Beach, CA 90278
Alain Sei*
TRW
Redondo Beach, CA 90278

We present an innovative algorithm for the computation of electromagnetic scattering from rough surfaces, with emphasis on ocean scattering applications. Our new method couples a high-order boundary variation method with an approach based on high-order, high-frequency asymptotic expansions of singular integrals.

To solve a scattering problem on a rough surface — composed of a smooth swell of general shape underlying a rough, highly oscillatory layer — we view the roughness as perturbation of the swell. The boundary variations method, used extensively in previous studies (Sei et al., *Radio Science*, **34**, 385-411, 1999, Bruno O. and Reitich F., *J. Opt. Soc. A.*, **10**, 2551-2562, 1993), allows us to evaluate the scattered field from such rough surfaces by means of analytic continuation of an associated perturbation series of *high order* (Bruno O. and Reitich F., *Proc. R. Soc. Edinburgh. A*, **122**, 317-340, 1992).

The evaluation of each one of the coefficients in this perturbation expansion requires the solution of a scattering problem on a smooth surface with highly oscillatory boundary conditions. The solution of this notoriously difficult problem is computed efficiently and accurately by means of a new, high-order, high-frequency asymptotic expansion for the surface currents. Our high-frequency solver, which is designed to apply in the small wavelength regime — in which geometrical optics and the Kirchoff approximation are frequently used —, should be applicable to a wide range of scattering problems. Unlike the geometrical optics type expansions where amplitudes can become unbounded (at caustics), our high frequency algorithm is entirely rigorous and highly accurate.

This presentation will describe our approach to the general rough surface problem with a detailed discussion on the high-frequency solver. Numerical results in a variety of cases will be presented, demonstrating the accuracy and computational efficiency of our new methods.

B/F2-7
15:40

A FFT-MOMI FOR THE SCATTERING OF ELECTROMAGNETIC RADIATION FROM A TWO-DIMENSIONAL PERFECTLY-CONDUCTING ROUGH SURFACE

P. Tran and J. Merle Elson
Research and Technology Group
Code 4T4400D
Naval Air Warfare Center Weapons Division
China Lake, California 93555

We present an algorithm that combines the fast matrix-vector multiplication using FFT with the Method of Ordered Multiple Interaction (MOMI) to calculate the scattering of electromagnetic radiation from a two-dimensional perfectly-conducting rough surface. This hybrid algorithm has the fast scaling of the FFT and the fast convergence (as compared to a conjugate gradient solver) of the MOMI. The optimal mapping of the two-dimensional surface current to a column vector is introduced so that the fast matrix-vector multiplication can be incorporated with the MOMI. The mapping involves dividing the surface into 4 sub regions. The process is repeated for each sub region. This is carried out until the smallest sub region is of a size such that it cannot benefit from fast matrix-vector multiplication. The indexing scheme of the smallest sub regions is best illustrated in the following figure where 3 levels of division are shown. The mapping of the surface current within each sub region $\mathbf{a}_i$ is irrelevant to the algorithm with the only requirement is that it does not cause divergence of the MOMI solution. Each region is mapped sequentially to the column vector of the MOMI integral equation. We will discuss how the FFT matrix-vector multiplication is applied for this mapping. Results showing the convergence of the mapping will be presented. CPU requirements will also be discussed.

a_1	a_2	a_5	a_6	a_{17}			
a_3	a_4	a_7	a_8				
a_9	a_{10}	a_{13}	a_{14}				
a_{11}	a_{12}	a_{15}	a_{16}				
a_{33}				a_{49}			

B/F2-8
16:00

PREDICTING BISTATIC RADAR REFLECTIVITY OF THE OCEAN SURFACE

D. J. Donohue* N. Woods R. L. McDonald
Applied Physics Laboratory
Johns Hopkins Road
Laurel, MD 20723

A large-scale effort is underway at the Johns Hopkins University Applied Physics Laboratory to assemble comprehensive predictions of the bistatic radar reflectivity of the ocean surface. The predictions are based on a 2-dimensional numerical model for rough surface scattering that has been extensively tested and applied to studies in ocean remote sensing. The method of moments model is considered to be numerically "exact" for any combination of surface roughness, incident and scattering angles, surface electrical properties, and polarization state. As a result, the predictions are expected to be much more broadly applicable than existing calculations based on approximate methods such as Kirchhoff, Bragg scatter, or Barrick's (Ruck, G.T., Barrick, D.E., Stuart, W.D., and Kirchbaum, C.K., Radar Cross Section Handbook, Plenum Press, New York, 1970) quasi-specular two-scale models. The new numerical study will cover a broad range of sea states, incident angles, and wavelengths, ranging from X-band (3 cm) to W-band (3.2 mm). Given the computational intensity of method of moments models, the task will require many thousands of hours of computing time to complete. As a result, the calculations are being performed on a 64-node SGI Origin 2000 system administered by the DoD High Performance Computing Modernization Program. Given their important role in completing the task, computational performance and resource allocation issues will be addressed as part of the presentation. An early assessment of results covering the majority of the parameter space, as well as comparisons with the approximate methods will also be presented. Finally, the dependence of the bistatic reflectivity on various surface characterizations and spectra, including wind-directional versus direction independent, will also be presented.

B/F2-9
16:20

NUMERICAL COMPUTATION OF POLARIZATION DEPENDENT SCATTERING ANOMALIES FROM SIMULATED OCEAN SURFACES

Edward W. Swim* John A. DeSanto
Department of Mathematical and Computer Sciences
Colorado School of Mines
Golden CO 80401

A common feature of radar returns from ocean surfaces is the so-called sea spike. This behavior, which occurs when the radar cross section for HH polarization greatly exceeds that of VV polarization, has been observed to occur for scattering from steep wave features and breaking waves. It has recently been shown (Sei et al., *Radio Sci.*, 34, 385-411, 1999) that such results can be predicted using a modulated wave train model of the sea surface. We present computational results that confirm this theory using a periodic modulated wave train, i.e.

$$s(x) = -\frac{d}{4}[\cos(k_w(1+\delta)x) + \cos(k_w x)]. \quad (1)$$

Two methods are used to compute the amplitudes of the scattered field from the surface, one which uses sampling strictly in coordinate space, called a coordinate-coordinate or CC method, and another that utilizes both a discretization corresponding to the scattered field spectra and a spatial discretization of the surface, called a spectral-coordinate or SC method. To compute the polarization ratios, we note that for a one dimensional surface, the electromagnetic problem is equivalent to an acoustics problem and so we can treat the amplitudes as scalar quantities and hence find a ratio corresponding to each Bragg mode for a particular angle of incidence.

We present examples of surfaces that exhibit varying degrees of modulated amplitude, including capillary waves and spilling breakers. For these surfaces we have computed polarization ratios for incident angles ranging from 10° to 89°. Sea spikes at low grazing angles are illustrated for surfaces with even slight modulation in amplitude. Thus we conclude that although sea spikes can occur during events involving breaking waves and wave steepening, this is not a necessary condition for the phenomenon. For example, if we consider $s(x)$ with $\delta = 0.2$, $d = 0.025$, and $k_w = \pi$, sea spikes occur for incident angles between 60° and 90°, even though the surface does not model a wave near breaking. We measure the error of our results using the standard energy check for the incident and scattered fields.

B/F2-10
16:40

NUMERICAL SIMULATIONS OF EMISSIVITIES OF TWO-DIMENSIONAL RANDOM DIELECTRIC LOSSY ROUGH SURFACES WITH GAUSSIAN AND NON-GAUSSIAN SPECTRUMS

Qin Li and Leung Tsang*
Department of Electrical Engineering, Box 352500
University of Washington, Seattle, WA 98195
Jiancheng Shi
Institute for Computational Earth System Science
Ellison Hall 6808, University of California
Santa Barbara, CA 93106

The simulations of emissivities of a two-dimensional lossy dielectric random rough surface (three-dimensional scattering problem) with large permittivity are studied by using a numerical method. The rough surfaces are with Gaussian and non-Gaussian spectrums. A modified power-law spectrum is proposed. By choosing the order of the spectrum, the spectrum can become either a Gaussian or exponential spectrum with the rms height and correlation length unchanged. Thus it provides a method to study the wave scattering from different types of rough surfaces but with same rough surface parameters of rms height and correlation length. Using this spectrum, non-Gaussian rough surface profiles are produced to study the wave scattering from random rough surfaces.

For wave scattering from dielectric rough surfaces with large permittivity, the surfaces have to be discretized with a dense grid in order to calculate accurate results for the surface fields because the Green's function of the lower medium changes very rapidly. Accurate bistatic scattering coefficients are particularly important for the calculation of emissivities of rough surfaces which have to be accurate to within one percent for passive remote sensing applications. But a dense grid has more CPU and memory requirements. However, the physics-based two-grid method (PBTG) can give the required accuracy with only moderate increase of CPU and memory requirements. In this paper, The numerical results are calculated by using this method. The computational complexity and memory requirement of the present algorithm are O(N log(N)) and O(N), respectively, where N is the number of surface unknowns on the coarse grid. Numerical simulation results will illustrate the effects of the rough surface spectrum on the emissivity.

Session C1, 13:35 PM-Wed., Room 150

SIGNAL PROCESSING AND CHANNEL MODELLING FOR WIRELESS COMMUNICATION

Chairpersons: L. Swindlehurst, Brigham Young University (lee_swindlehurst@byu.edu)
J. Harvey, Army Research Labs (harvey@arl.mil)

C1-1
13:40 (40-min.) SPACE-TIME SYNCHRONIZATION

A. Swindlehurst*
Department of Electrical and Computer Engineering
Brigham Young University
Provo, UT 84602
G. Seco
Department of Signal Theory and Communications
Universitat Politècnica de Catalunya
08034 Barcelona, Spain
D. Astély
Research and Development Department
Nokia Telecommunications
164 22 Kista, Sweden

Synchronization is a critical aspect of virtually all communications systems. Accurate frame and symbol synchronization is especially important in time-division multiple access and packet-based systems, or with any protocol that employs training, control, or identification bits interspersed with the raw data. Multiuser detectors for code-division multiple access (CDMA) require reliable code timing information for acceptable performance in near-far environments. In addition, achieving precise synchronization is the key to obtaining location estimates with accuracies of a few meters or better in Global Positioning System (GPS) receivers.

There is a vast literature on both synchronization and time delay estimation, the majority of which focuses on the case where data is measured from a single receiver. However, the performance of single channel timing recovery methods is limited when multipath or co-channel interference (CCI) is present, such as in surveillance systems plagued by jamming and many wireless communications applications. For this reason, attention has recently shifted to the use of antenna arrays for addressing these problems. The spatial selectivity offered by an antenna array can dramatically improve performance in environments with severe interference.

A number of techniques that exploit antenna arrays for synchronization have been developed, each differing from the others in its computational load and its assumptions regarding multipath, CCI, and signal parameterization. The goal of this presentation is to compare and contrast the various techniques that have been proposed for this problem, and to provide a general mathematical framework in which these techniques can be understood. A few specific algorithms will also be described that we believe offer the best compromise between model realism and computational complexity.

C1-2
14:20 (40-min.)

ALGEBRAIC METHODS FOR DETERMINISTIC BLIND BEAMFORMING

Alle-Jan van der Veen*
Delft University of Technology
Dept. Electrical Engineering
2628 CD Delft, The Netherlands

In the context of array signal processing, beamforming is concerned with the reconstruction of source signals from the outputs of a sensor array. This can be done either by coherently adding the contributions of the desired source, or by nulling out the interfering sources. The latter is an instance of the more general problem of source separation.

Classically, beamforming requires knowledge of a look direction, which is the direction of the desired source. *Blind* beamforming tries to recover source signals without this information, relying instead on various structural properties of the problem.

The first blind beamforming techniques proposed were based on direction finding. The direction of each incoming wavefront is estimated, at the same time producing a beamformer to recover the signal from that direction. This requires at least that the antenna array is calibrated. If a source comes in via several directions (coherent multipath), then direction finding is more complicated. In some situations we also need to consider delay spread.

More recently, new types of blind beamformers have been proposed that are not based on specific channel models, but instead exploit properties of the signals. A striking example is the constant modulus algorithm (CMA), which separates sources based on the fact that their baseband representation has a constant amplitude, such as is the case for FM or phase modulated signals. A prime advantage is that these beamformers are not dependent on channel properties or array calibration. For man-made signals, such as encountered in wireless communications, signal properties are often well-known and accurate, leading to robust algorithms. Several other properties are available, for example cyclostationarity caused by the bauded nature of digital communication signals or introduced by small differences in carrier frequencies. Ultimately, sources can be separated based on their statistical independence.

The review is centered around algebraic techniques for deterministic blind beamforming. We consider two classes of algorithms: those that are based on channel properties, and others based on signal properties. Despite the fact that these properties are widely differing, the resulting algorithms show a remarkable homogeneity. All are subspace-based techniques, and end with a generalized eigenvalue problem: the beamformers are found as the eigenvectors of a simultaneous diagonalization problem in which several matrices can be diagonalized by the same (eigenvector) matrix. The message of the review is that joint diagonalization is *the* fundamental problem for source separation.

C1-3
15:00

NONCOHERENT MMSE DETECTION FOR MULTIPLE ACCESS COMMUNICATIONS

Michael L. McCloud* Louis L. Scharf
Department of Electrical and Computer Engineering
Campus Box 425
University of Colorado
Boulder, CO 80309

Orthogonal signalling is often employed to communicate over noncoherent channels. However, when multiple users share such a channel, the assignment of mutually orthogonal signal sets to each user requires a large bandwidth. Moreover, if each user employs a signal set which is orthogonal but correlated with the other users, then a low complexity receiver may produce an effective signal constellation which is no longer orthogonal for each user. For these reasons, we consider the more general case of non-orthogonal multipulse modulation (NMM) in which each user is assigned a possibly correlated signal set; from which one signal is transmitted at each signalling period. The generalized maximum likelihood (GML) detection rule has been previously investigated for detection of NMM over noncoherent channels. This detector acts to null out the interfering users' signal contribution and is consequently termed a zero-forcing detector.

In this work, we develop the minimum mean squared error multiuser detector for non-orthogonal multipulse modulation over the noncoherent additive white Gaussian noise channel. At high signal-to-noise ratios (SNRs), the MMSE detector approaches a new zero-forcing detector, termed the multipulse decorrelating (MD) detector.

In order to compare the multipulse decorrelating detector with the GML detector, we present asymptotic performance bounds for each detector. At high SNRs we find that the two detectors have different exponential dependencies. For the case of binary (two-dimensional) signaling, we find that the MD (and hence the MMSE) detector is always asymptotically superior to the GML detector but that this superiority does not generalize to larger dimensionality signal sets. Numerical results are presented which demonstrate the validity of the theoretical bounds at large SNRs.

C1-4
15:40

IMPROVED WIRELESS COMMUNICATIONS USING TRI-POLARIZED ANTENNAS

R. deCarvalho P.P. Mitra M.R. Andrews*
Bell Labs, Lucent Technologies
700 Mountain Avenue
Murray Hill, NJ 07974

We describe work to date on a wireless communications scheme that exploits the full three-dimensional vector character of radiated electromagnetic fields. Since scattering by objects in the environment can produce multiple paths between any two points, each path's transverse field polarization adds at either end to produce a resultant which can oscillate independently in all three spatial dimensions. Antennas capable of transmission and reception of such arbitrarily polarized radiation were constructed, and their use has demonstrated that the 'tri-polarization' scheme is a valuable option for future wireless communications systems. The three complex currents induced at the receiver's orthogonally polarized antenna elements, aside from noise, are linear superpositions of the three currents at the transmitter, forming a tensor. This tensor depends upon the environment, but generally was found to be rank three with good condition number under the conditions of our indoor studies. To summarize, (1) bandwidth: one can get significantly greater information-carrying capacity when using tri-polarized antennas rather than uni- or dual- polarized ones, (2) robustness: one can get immunity from fast fading because the chance of two or three field components vanishing simultaneously is negligible, and (3) compactness: in contrast to other multiple antenna schemes employing three or more antennas, the tri-polarized design is intrinsically compact (i.e., smaller than a cubic wavelength) because the elements are colocated and not arrayed. The gains in peformance should also be independent of antenna orientation, since they derive from a tensor whose properties are invariant under three-dimensional rotations. We have observed the information-carrying capacity to scale as well as can be expected, namely linearly with the number of polarizations.

C1-5
16:00

ISSUES IN SIGNAL PROCESSING AND PROPAGATION IN MOBILE COMMUNICATIONS

Brian M. Sadler
Army Research Laboratory
Adelphi, MD 20783

In this talk we discuss some of the issues associated with the multi-user mobile wireless communications problem, focusing on the ongoing and potential interplay between signal processing and propagation channel modeling.

We distinguish the semi-mobile cellular problem versus the fully mobile ad-hoc wireless problem encountered in mobile tactical military communications and elsewhere. For the fully mobile problem, alternatives to DS-CDMA (such as FH-CDMA) become attractive because they come close to inherently eliminating the power control problem. In addition, at carrier frequencies above current cellular allocations (above 3 or 4 GHz, say) fading rates become increasingly rapid, leaving little time for implementation of power control. Narrowband versus wideband issues are also viewed in this context, including multi-carrier solutions to the wideband problem. Wideband solutions come with associated tradeoffs in equalization complexity, as well as robustness to narrowband interference, and the ability to use some high resolution array processing techniques. Low antenna heights and complicated scattering environments present significant challenges for smart antenna approaches. Another important factor is the time variability (TV) of the mobile channel over each burst, with appropriate TV channel models and TV equalization techniques.

Ultra-wideband or impulsive communications have recently been advocated for overcoming frequency selective channel limitations. Due to their extreme bandwidth, such signals will simultaneously play the role of co-channel interferer and desired signal. These issues are discussed in the broader context of non-Gaussian signal processing for receivers, including interference modeling and excision. The viability of ultra-wideband for outdoor communications may be limited by propagation, e.g., forested areas produce a significant low pass propagation effect.

Issues associated with blind versus semi-blind (training based) equalization techniques are also discussed. We present some recent results on performance of blind and semi-blind spatial separation methods for co-channel interference, and consider receiver tradeoffs.

C1-6
16:20

IMPROVED COMMUNICATION OVER REALISTIC FADING MOBILE RADIO CHANNELS USING LONG RANGE PREDICTION

Shengquan Hu Alexandra Duel-Hallen*
Department of Electrical and Computer Engineering
North Carolina State University
Box 7914, Raleigh, NC 27695-7914
Hans Hallen
Physics Department
North Carolina State University
Box 8202, Raleigh, NC 27695-8202

In rapidly varying mobile radio channels, the transmitter and receiver are not usually optimized for current channel conditions, and thus fail to exploit the full potential of the fading channel. To overcome this limitation, several adaptive modulation and transmitter diversity methods were recently proposed for wireless systems. To realize these methods in practice, prediction of the channel coefficients several tens-to-hundreds of symbols ahead is essential. We describe a novel adaptive long range fading channel prediction algorithm and its utilization with adaptive transmission. This algorithm computes the linear Minimum Mean Squared Error (MMSE) estimates of future fading coefficients based on past observations. This algorithm can forecast fading signals far into the future due to its significant memory span achieved by using sufficiently low sampling rate given a fixed model order. In addition to validating our method for standard stationary fading models, we test on measured data provided by Ericsson, Inc. and on data from our novel realistic physical channel model that accounts for the variation of the amplitude, frequency and phase of each reflected component of the fading signal. The variation of these parameters is not captured by the Jakes model or the stationary random process characterization. However, the accuracy of the long-term prediction is determined by the rate of change of these parameters. Our model permits the qualitative and quantitative understanding of these variations with environmental configurations so that typical and worst case situations can be identified and tested.

C1-7
16:40

SIMULATING RADIO CHANNEL STATISTICS FOR DIFFERENT BUILDING ENVIRONMENTS

H.L. Bertoni* C. Cheon
Center for Advanced Technology in Telecommunications
Polytechnic University
Brooklyn, NY 11201

Advance radio system designs have been studied that are intended to overcome the impairments of the radio channel caused by multipath effects in urban environments. The efficient design of such systems and their evaluation requires knowledge of higher order channel statistics. For example, the design of smart antenna systems requires knowledge of the delay spread and angle spread in which the system is to function. The delay and angle spreads have been measurement in a few locations. However, it is not clear if the measured results are widely applicable to other building environments. To overcome this limitation, we have used our 3D ray tracing code, called the VPL method, to suimulate channel statistics. Our goal is to relate the variation of statistical properties to the statistics of the particular building environment, and to the geometry of the radio link.

The VPL method achieve greater computational speed as compared to conventional 3D codes by assuming the building walls to be vertical, and unrolling the cone of rays diffracted at horizontal edges into two vertical planes. In this way the ray trace can be separated into a trace in the horizontal plane, which is carried out using the pin cushion method, and an analytic construction of each ray in the vertical plane.

Simulations have been run to find the angle and delay spreads at elevated base station antennas. Results of the simulations show that both increase as the base station antenna is lowered below roof level. However, only the angle spread shows significant dependence on the separation. Simulations for three cities having different distributions of building height show that the environment effects the distribution of angle spread, but has less effect on the delay spread.

C1-8
17:00

A PHYSICS-BASED PARAMETER SIMULATION OF A COMPLEX PROPAGATION CHANNEL

Kamal Sarabandi* Il-Suek Koh
Department of Electrical Engineering and Computer Science
The University of Michigan, Ann Arbor, MI 48109-2122
James Harvey
U.S. Army Research Office
P.O. Box 12211, Research Triangle Park, North Carolina 27709
B. Sadler
U.S. Army Research Laboratory
2800 Powder Mill Rd, Adelphi, MD 20783

Accurate prediction of radio wave propagation in a communications channel is essential in the development and design of an efficient, low-cost wireless system. High fidelity models are necessary in order to treat the trade-offs between radiated power and signal processing by addressing issues such as coherency, field variations, multipath, and dispersive (path delay) effects. Current propagation or channel models are heuristic in nature and have limited applicability. A physics-based approach to the problem provides intuition and gives accurate results for the prediction of radio wave propagation. With this as a motivation a physics-based modeling approach is pursued for which advanced and efficient electromagnetic diffraction models are needed. In this paper a hybrid analytical/numerical approach is used to study the behavior of HF-UHF wave propagation in a forest environment. Forest is a very complex medium which affects the wave propagation in many different number of ways. Because of lossy nature of permittivity of vegetation particles, forest environment exhibits a relatively high attenuation rate for the direct wave. Analytical formulation for the mean-field calculation shows that the dominant source of the mean-field at the receiver comes from a ray that propagates along the interface between the air and the canopy. Analytical formulation that provides the behavior of this wave as a function of effective dielectric constant of the canopy, canopy-air roughness, distance between the transmitter and receiver, polarization, and frequency is developed. Significant multiple scattering also occurs in forest due to the existence of tree trunks. Scattering from tree trunks is the dominant source field fluctuations. Using a full-wave analysis based on the method of moments in conjunction with Monte Carlo simulations the effect of multiple scattering among a very large number of tree trunks is studied. It is shown that only scatterers near the source and the observation points contribute to the field fluctuations significantly. This result drastically simplifies the numerical complexity of the problem. Keeping about 200 tree trunks in the vicinity of the transmitter dipole and the receiver point, a Monte Carlo simulation is used to evaluate the statistics of the spatial and spectral behavior of the field at the receiver. Using a wide bandwidth simulation, the temporal behavior are also studied and the performance of antenna arrays is investigated.

C1-9
17:20

ACCURATE, EFFICIENT AND ROBUST HIGH FREQUENCY URBAN PROPAGATION MODELS

Joseph Schuster
Remcom Inc.
Calder Square Box 10023
State College, PA 16805
Raymond Luebbers*
Department of Electrical Engineering
The Pennsylvania State University
University Park, PA 16802

The prediction of the performance of radio communication channels in complex urban environments is a challenging problem for computational electromagnetics. The geometries involved are very complicated in shape. They are also very large, so that large amounts of data are needed to describe the buildings, terrain, and other features to be included in the calculations. Developments that have occurred over the past decade, and to a greater extent over the past few years, now provide the tools needed for accurate prediction of the performance of these communication channels. These developments include more accurate terrain data bases, quick availability of urban feature information, advances in computational electromagnetics, and faster computers with larger memory. Utilizing these advances, it has been demonstrated that efficient, deterministic, site-specific prediction of radio signal propagation in complex environments is possible. It is important now to take this prediction capability from the research level to a point where it can be used reliably by non-experts. In order to accomplish this, many parts of the prediction process that were accomplished by painstaking human interaction must be done instead either automatically or at least more efficiently. For example, the urban features data, which may be hundreds of buildings and thousands of building faces, must be organized and simplified so it can be used by the propagation model. For general use the propagation model must be fast, robust, and reliable. Extensive validation based on both measurements and analytical calculations is needed. Augmenting the deterministic predictions with a limited number of measurements, resulting in a hybrid deterministic/statistical approach, may increase both accuracy and reliability.

C1-10
17:40 (40-min.)

REDUCED RANK CHANNEL ESTIMATION

Yingbo Hua
Visiting Faculty
Department of Electrical and Electronic Engineering
Hong Kong University of Science and Technology
Clear Water Bay
Kowloon, Hong Kong

In applications such as wireless communications, the channel matrix between a set of transmitters and a set of receivers is often deficient in rank. For example, if all the transmitters (mobile users) are located in the same angular position with respect to an array of receivers at a base station (and there is no multi-path), then the channel matrix between the transmitters and the receivers has rank one. If the transmitters are clustered into r angular positions, then the channel matrix has rank r. For such a reduced rank channel, the conventional techniques for channel estimation have relatively poor performance.

In this talk, we show a class of optimal reduced rank channel estimators. These estimators include the one by D. Brillinger, the reduced rank Wiener filter by L. Scharf, and the reduced rank maximum likelihood estimator by P. Stoica and M. Viberg. Although these estimators were originally developed from different roots of thought, a common framework for all of these estimators is available.

The optimal reduced rank estimators can all be expressed in terms of singular value decomposition of some characteristic matrices. Direct computation of these estimators can be too costly for real-time application especially when the channel matrix has large dimensions. In this talk, we also show a very fast iterative method for computing these estimators, which is called alternating power method. The alternating power method is a generalization of the conventional power method for subspace computation. It is convergent globally and exponentially. Such a property makes the alternating power method an ideal procedure for adaptive computation of optimal estimates of reduced rank channel matrices.

This talk is based on the following papers: Y. Hua and M. Nikpour, "Computing the reduced rank Wiener filter by IQMD",*IEEE Signal Processing Letters*, Sept 1999, and Y. Hua, M. Nikpour, and P. Stoica, "Optimal reduced rank estimation and filtering", *IEEE Transactions on Signal Processing*, in review.

Session E1, 13:15 PM-Wed., Room 155
SPECTRUM UTILIZATION
Chairperson: A. Paul, NTIA (apaul@ntia.doc.gov)

E1-1
13:20

SPECTRUM MANAGEMENT RULES FOR A FLEXIBLE-USE ENVIRONMENT

Robert J. Matheson
NTIA/ITS.M
325 Broadway
Boulder, Colorado 80303

Many of the newly allocated frequency bands have been licensed by auction and have rules that permit maximum freedom to the licensees in defining the services to be offered. This freedom necessarily requires some rules to prevent interference to neighboring licensees, but these rules may be quite different from the rules that were employed for traditional frequency management. What rules are appropriate--so that interference is controlled, but flexible use is permitted to the maximum possible extent?

The principles upon which these rules are based come from three major sets of information: (1) radio wave propagation, including the ability to predict and control where radio waves travel, (2) the characteristics of electronic equipment (especially transmitters and receivers), including the ability to accept or reject particular types of radio signals, and (3) the behavior of the market-place, including the ability of people to recognize benefit and cost and to act on this knowledge.

Traditional rules typically gave permission to operate a particular transmitter at a given site to supply a specific service. If the licensee followed these rules, he was essentially guaranteed a certain level of service and protection from interference. Under the new rules, the licensee is given few guidelines for operation and no guarantees of service. Freedom from interference is not guaranteed, but is recognized to be a major factor in the details of system design. The proper role of the receiving system in interference cases is particularly ambiguous in present rules. In some bands, there is a maximum level of signal permitted to Aleak@ across a geographical or spectrum boundary; in other bands, it is merely required to Acoordinate@ system operation with neighbors in adjacent areas and frequencies. However, the bottom-line for any set of spectrum rules is the ability of each licensee to know whether a particular operation is permitted by the rules. This knowledge is needed as a legal basis for any coordination agreement and any resolution of interference. This paper will focus on identifying the problem areas that arise in flexible use spectrum rules.

E1-2 13:40 A REVIEW OF LF/MF SKY-WAVE PROPAGATION STUDIES FROM FREQUENCY MANAGEMENT POINT OF VIEW

John C. H. Wang
Office of Engineering and Technology
Federal Communications Commission
Washington, D.C. 20554

The purpose of this paper is to review the progress made in the last sixty plus years in the general field of LF/MF sky-wave propagation. All available propagation models will be presented, analyzed, discussed and compared. The most recent and largest databank has been used. This paper will help the users to select the right models for their particular applications. This paper will also help the frequency managers to achieve the most efficient utilization of this portion of the spectrum.

The earliest worldwide organized efforts to study LF/MF sky-wave propagation began in 1932. At its meeting held in Madrid, the former CCIR (now ITU-R) established a committee (B. van der Pol, Holland, Chairman) to study propagation between 150 and 2000 kHz. As a result, a sizeable amount of sky-wave data from different areas of the world have been collected. Two propagation curves known as the Cairo curves were developed. Asian countries are still using the north-south Cairo curve today.

The Federal Communications Commission of the United States, under the leadership of the late Ken Norton, also carried out a number of sky-wave field-strength measurement programs. The first campaign took place in the spring of 1935. As a result, the FCC clear-channel curves were derived. This model was adopted by the North American Broadcasting Conference in 1950 and again adopted by the 1980 Broadcasting Conference for use in ITU Region 2 (the Americas).

In anticipation of a world broadcasting conference, the former CCIR in 1963 established International Working Party 6/4 to develop a simple but accurate field strength prediction method for worldwide applications. Consequently additional measurements were carried out in many areas. A number of new methods were developed. The IWP 6/4, after careful consideration, endorsed the Udaltsov and Shlyuger method and this method became CCIR Recommendation 435.

In the 1980s, the FCC initiated two separate projects to collect data from Alaska and Puerto Rico. The latest FCC efforts were supplemented by efforts by other Region 2 administrations such as Mexico and Brazil. With the help of the latest databank, a new method was developed by staff of the FCC and became part of the Rules of the FCC.

All of these methods will be discussed in this paper. The author will attempt to recommend a single method for worldwide applications.

E1-3
14:00

INTERFERENCE AVOIDANCE METHODS FOR "UNLICENSED" SPECTRUM

David J. Cohen
University of Maryland, University College
University Blvd. at Adelphi Road
College Park, Maryland 20742

The USA Radio Regulations define two classes, licensed and unlicensed for wireless spectrum use. Licensed spectrum denotes "ownership" and users are either assigned a specific frequency channel or a data processor is utilized to dynamically assign for a given geographic area available channels (FDMA), time slots (TDMA), or pseudo random codes (CDMA). Conversely, unlicensed spectrum users make individual decisions when and where to transmit. In unlicensed spectrum there is no hierarchical control to insure interference protection among users. Regulatory rules and IEEE standards have been adopted to minimize interference for users of unlicensed spectrum. These rules and standards will be discussed.

The FCC (Part 15) Radio Regulations authorizes the use of low power unlicensed spread spectrum communication equipment in the ISM bands (902-928 MHz, 2400-2483.5 MHz, and 5725-5850 MHz.). Presently, millions`` of low-power unlicensed equipments utilize the ISM band 902-928 MHz. Examples include cordless phones, wireless LANs and the METRICOM (Ricochet) wireless Internet access system. There are no medium access rules for operation in the ISM bands. In general operations have been successful but interference problems have occurred.

The FCC allocation for the new PCS services included 20 MHz (1910-1930 MHz) for unlicensed systems. The FCC to minimize interference among equipment adopted a set of rules of operation known as "spectrum etiquette". The spectrum etiquette rules: (1) limit transmitter power, (2) limit time duration of individual transmissions and (3) require a listen before transmit protocol. Equipment utilizing this PCS unlicensed spectrum are now being deployed.

The FCC has made allocations in the 5 GHz band for unlicensed wireless devices capable of supporting 20 Mb/s data rates for multimedia communication. The FCC established power limits and antenna gains for these allocations but is awaiting industry response before establishing spectrum etiquette rules for these allocations.

E1-4
14:20

BANDWIDTH REQUIREMENTS FOR ORTHOGONAL FREQUENCY DIVISION MODULATION

Edmund A. Quincy
Institute for Telecommunication Sciences
National Telecommunication and Information Administration
325 Broadway
Boulder, CO 80303-3328

Interest by Federal Agencies and the International Telecommunication Union in specifying bandwidth requirements for orthogonal frequency division modulation (OFDM) spectrum allocation have prompted this investigation. In this analysis the power spectrum, spectral envelope, the bandwidth (BW) that contains 99% of the power, the number of dB down at the 99% BW, and the BW where the envelope is 20 dB down are calculated. Results are given as a function of the number of sub-channels N and normalized to the sub-channel spacing (1/T).

OFDM modulation has been suggested for use in cellular radio, digital audio broadcasting, and digital video broadcasting. Conceptually, blocks of N serial symbols are transmitted in parallel by employing a large number of sub-carriers. The block length (T in seconds) is chosen such that T>>rms delay spread of a channel. Thus the effects of the delay spread on the symbol rate of each sub-carrier are greatly reduced which may eliminate the need for equalization. The data symbols for each sub-carrier are often encoded by M-ary quadrature amplitude modulation (M-QAM).

The power spectrum is shown to become very rectangular and compact as N increases. An envelope is fitted to the spectral peaks using a cubic spline interpolation. The frequency where 99% of the total power is contained in that BW is shown along with the number of dB down of the envelope at that BW. This 99% BW is suggested for specifying the Occupied Bandwidth (OBW). The BW where the envelope is down 20 dB is also provided. The spectrum rolloff at the 99% BW decreases dramatically as N increases and the spectrum becomes more rectangular. For example at N=512 the spectrum is down less than 0.1 dB at the 99% BW compared with being down over 10 dB for N=32. This demonstrates the need for a guard spacing to be provided between channel allocations if the 99% BW is also employed as the Necessary Bandwidth (NBW).

The 20 dB down frequency of the spectral envelope was selected as a possible criterion for determining the NBW. Both the BW at 99% power containment and the BW where the envelope is 20 dB down are shown as N the number of sub-channels is varied. Suggested linearized BW equations are provided in terms of system parameters N and T. For N>16 the OBW and the NBW differ only by an increased offset of 16.25/T for the NBW. These provide very simple equations that could be used for specifying spectrum allocation.

E1-5
14:40

DESIGN AND APPLICATION OF A SOFTWARE HF MODEM

Christopher Behm
Institute for Telecommunication Sciences
Mail Code ITS.E
U. S. Department of Commerce
325 Broadway
Boulder, CO 80303-3328
Robert B. Stafford
Institute for Telecommunication Sciences
Mail Code ITS.P
U. S. Department of Commerce
325 Broadway
Boulder, CO 80303-3328

ALE, which stands for automatic link establishment, is a mechanism for embedding expert knowledge about the H.F. (3 - 30 MHz) communications environment within the radio system itself. An ITS project called low cost ALE replaces most of the hardware in a normal ALE system with software. The user is required to supply a radio transceiver with computer control capabilities, and a computer with a sound card. The control portion of the software, as envisioned, produces control signals to manipulate the frequency of the radio and the microphone push-to-talk switch. Protocol considerations and forward error correction encoding are also performed in software. Finally, the sound card is used as a replacement for the ALE modem, producing the 8-ary FSK tones required for transmission and decoding (through software) the tones received from other ALE stations on the network.

The low-cost ALE project breaks these requirements into three major areas. The software modem, with it's digital signal processing algorithms for tone encoding and decoding, makes up the first of these divisions. The second is comprised of the protocol handling and control code and the third is represented by a graphical user interface which controls the first two activities. This report presents the algorithms and implementation details of the first major block of the project, the software modem.

The ALE protocol uses an 8-ary frequency shift keying system. The demodulator portion of the modem is able to discriminate these eight tones at a low signal-to-noise ratio, and is also able to produce an indication of the quality of the channel for the link-quality-analysis (LQA) test. In order to achieve the dual aims of noise robustness coupled with relatively low computer processing requirements, an overlapping Goertzel algorithm is used along with a dynamic pattern recognition scheme. These aspects will be discussed in this talk along with an examination of the modulator algorithm.

E1-6
15:00

MEASURING RADAR SPURIOUS EMISSIONS FOR COMPLIANCE WITH THE NTIA RADAR SPECTRUM ENGINEERING CRITERIA (RSEC)

Frank H. Sanders
Institute for Telecommunication Sciences
Mail Code ITS.M
U.S. Department of Commerce
325 Broadway
Boulder, CO 80309

To promote efficient use of radio spectrum and minimize interference caused by radars, the National Telecommunications and Information Administration (NTIA) specifies suppression of Government radar spurious emissions in the Radar Spectrum Engineering Criteria (RSEC) (NTIA, *Manual of Regulations and Procedures for Federal Radio Frequency Management*, **Chapter 5**, 1995 ed., 1997 rev.). Guidelines for determination of RSEC compliance were published separately by NTIA fifteen years ago (J. Sell, *Measurement Procedures for the Radar Spectrum Engineering Criteria*, **NTIA Report 84-157**, 1984), but subsequent developments in radar technology have created new challenges for both radar emission spectrum measurements and application of the RSEC to such emissions. In response to these challenges, NTIA has reviewed radar emission spectrum measurement techniques and the application of the RSEC to measurements of advanced radar systems.

Major results of this review are: (1) Radar spectrum emission measurements performed inside radar waveguides are do not accurately represent the characteristics of radiated emissions and are often physically impossible to perform, especially for advanced radars. Thus, radiated measurements are preferred for determining RSEC compliance; (2) Radiated measurements can overcome multipath problems that might otherwise produce erroneous features in measured emission spectra; (3) RSEC measurement systems must generally have at least 90 dB dynamic range, with a high degree of signal rejection at the radar fundamental but high sensitivity throughout the rest of the spectrum. This necessitates a stepped-frequency, rather than swept-frequency, measurement technique, so that radio-frequency (RF) attenuation can be varied incrementally, as a function of frequency across the measured spectrum.

The only practical method identified by NTIA for performing radiated RSEC compliance measurements is through the use of custom-designed RF front-ends operated in computer-controlled measurement systems. NTIA is actively promoting the use of such measurement systems to determine RSEC compliance by radars.

Session E2, 15:35 PM-Wed., Room 155
LOW FREQUENCY NOISE ENVIRONMENT
Chairperson: E. Smith, Univ. of Colorado (ernest.smith@colorado.edu)

E2-1
15:40

OBSERVATIONS OF UNUSUAL ELECTROMAGNETIC SIGNALS IN THE 400–2000 Hz FREQUENCY RANGE

C. C. Teague* A. C. Fraser-Smith D. Porrat
STAR Laboratory
Packard EE Building, Room 314
Stanford University
Stanford, CA 94305-9505

Unusual signals recently have been observed at Stanford, California on a VLF receiver using crossed air-core loop antennas and a low-noise amplifier. They were first seen on 16 March 1999, in conjunction with an ELF generation experiment using the High Altitude Atmospheric Research Program (HAARP) transmitter in Alaska, although it appears that they have no relation to the HAARP transmitter. The signals are very weak and consist of a large number of relatively narrow lines spaced either 20 Hz or 30 Hz apart, covering a wide frequency range of roughly 400–2000 Hz. Spectrographic analysis of several of the lines over several minutes indicates a slight frequency instability confined to a range of ± 0.25 Hz at 500 Hz, with similar time signatures and increasing frequency deviation as the frequency of the line increases.

A similar spectral signature is seen on low-order harmonics of 60 Hz, suggesting that the 20 Hz comb signals are somehow coupled to the 60 Hz power line signals. Note, however, that their spacing is a *sub*harmonic of 60 Hz, and that they are not seen below about 400 Hz, although they may be masked there by an increasing background noise level. The signals were seen for about 2 hours on 16 March 1999, and during that interval they faded, reappeared with 30 Hz spacing, faded again, and reappeared with 20 Hz spacing before fading completely.

After the initial observations and analysis, an automatic recording program consisting of observations for 2.4 minutes every 30 minutes was initiated. During the period of 11 May to 31 August 1999, the 20 Hz comb signals were seen on 3 occasions: 26 June for about an hour, 6 July for one half-hour recording interval, and 8 August for about an hour. As the signals are present for only a few hours during several months, probably they are not the result of direct power line coupling to the receiving loop antennas. So far their origin is unexplained.

E2-2
16:00

VHF BACKGROUND RADIATION MAPPED BY THE FORTE SATELLITE

T. J. Fitzgerald A. D. Kipple*
Space and Atmospheric Sciences Group, MS D466
Los Alamos National Laboratory
Los Alamos, NM 87545

There is continuing interest in the VHF noise environment at low earth orbit for the design of a number of satellite based systems such as communication and radio astronomy. As a by-product of its mission to map lightning signals in the VHF, the FORTE satellite has allowed us to make extensive measurements of the noise environment from 800 km altitude looking downward towards the earth. At last year's meeting, Zeulsdorf et al. presented worldwide maps of RF background radiation for 16 different frequencies - eight sub-bands between 29 and 47 MHz and eight more spanning 121 to 139 MHz. The results indicated that the noise increased dramatically over urbanized and industrialized geographic areas. In the past year we have extended global coverage of background radiation for frequencies from 47 to 79 MHz and 242 to 295 MHz. We will present the new data along with additional analysis and an update on calibration efforts. We will also discuss public access to the data and the possibility of additional frequency acquisitions.

The FORTE (Fast On-board Recording of Transient Events) satellite was launched into an 800 km orbit on 29 August 1997. Its primary mission is the detection and characterization of electromagnetic pulses, including lightning events. The background noise data are obtained using FORTE's pair of log-periodic antennas, one aligned along the satellite's flight direction and the other positioned cross-track. Two broadband (20MHz bandwidth) receivers operate in the VHF range, with center frequencies ranging from below 30 to approximately 300 MHz. FORTE monitors eight sub-bands within the 20MHz bandwidth of each antenna. The sub-bands are spaced 2.5 MHz apart and have 1 MHz bandwidth. FORTE records the power in each of the 16 sub-bands (8 per antenna) every four seconds. (The recorded values represent the average power over 2 ms.) These data are downloaded as part of FORTE's state-of-health and are later converted into and mapped as incident electric field values.

Background radiation estimates can additionally be derived from FORTE's digitized receiver data. Background radiation levels can be estimated from these data files by calculating the power spectrum from the recorded waveform. This method produces results which are similar to the state-of-health data, with the added capability of analyzing any frequency within the 20MHz bandwidth - not just predetermined sub-bands. Geographic coverage has been concentrated over the equatorial region due to greater lightning activity there. In the past six months we have begun to acquire more general geographic coverage with the digitized receiver data.

E2-3
16:20

Electromagnetic emmisions from the fracture of concrete

N. P. Davey S. G. O'Keefe D. V. Thiel*
School of Microelectronic Engineering
Radio Science Lab
Griffith University
Nathan, Brisbane, 4111, Queensland Australia

The creation of electromagnetic (EM) signals from fracture events in rock has been previously documented (S. G. O'Keefe and D. V. Thiel, *Atmospheric and Ionospheric Electromagnetic Phenomena Associated with Earthquakes, Terra Scientific Publishing Company Tokyo* , 233-244, 1999), (S. G. O'Keefe and D. V. Thiel, *GRL*, **18 No 5**, 889-892, 1991). Previous studies have predominantly used naturally formed rock which has been fractured as a result of earthquakes, blasting or laboratory experiments. This paper presents an extension to this work which looks at the production of EM signals from the fracture of concrete.

A series of laboratory tests were conducted to investigate EM signals from the fracture of cast concrete cylinders. The concrete cylinders were incrementally loaded to failure in a uni-axial compression frame. The EM signals were received using two short dipole antennas of vertical and horizontal polarisation, a H field antenna polarised with one of the dipoles, and an audio sensor attached to the sample. All tests were conducted in an enclosed metal container to reduce interference from external noise sources.

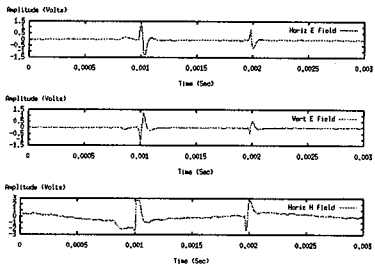

Figure: Discrete fracture event

Discrete EM events were observed during the failure phase. The figure shows a typical event. Multiple fracture events are shown here which appear with different polarity on the E field antennas and both produce strong corresponding signals on the H field antenna. Examination of the sample after the failure revealed fractured agregate in the cylinder remnants. Results presented demonstrate the correlation between recorded EM events and observed fractured agregate in the cylinder. Variations in recorded signals produced by different types of aggregate are also discussed.

Session G2, 13:35 PM-Wed., Room 245
METEOR PHYSICS AND CHEMISTRY
Chairperson: J. Mathews, Pennsylvania State University (jdmathews@psu.edu)

G2-1
13:40

OBSERVATIONS OF LONG DURATION METEOR ECHOES BY LARGE APERTURE RADARS

Q. H. Zhou
Arecibo Observatory
HC 3 Box 53995
Arecibo, PR 00612
J. D. Mathews* D. Janches D. D. Meisel
Communications and Space Sciences Laboratory
The Pennsylvania State University
Unversity Park, PA 16802

We report observations of meteor echoes by the Arecibo VHF/UHF radars (46.8/430 MHz) during the 1998 Leonids meteor shower. In the past, three types of meteors echoes had been observed by the Arecibo VHF radar (Zhou et al., Radio Sci., 1641-1654, 1998) when there was no shower present. The three types of echoes are meteor head echoes, classical diffusive trail echoes and range spread echoes, respectively. During the 1998 Leonids shower, a forth type of echo, long duration echo, was also observed. This type of echo typically lasts between several hundreds ms and several minutes and exhibits strong modulation at 50 ms to several hundreds ms. While long duration echoes have been observed in the past by other radars, strong periodicity has not been reported to our knowledge. Since the long duration echoes are closely associated with the shower activity, they are likely from shower meteors. In this report, we characterize the long duration echoes and provide an explanation for the periodicity. During the observation, the Arecibo incoherent scatter radar (ISR) was also in operation. The ISR was used to collect both the raw meteor samples as well as the time-averaged background ionosphere data. In some instances, VHF/UHF head echoes were observed to accompany the long duration echoes although no obvious enhancement was seen in the incoherent scatter signal. The long duration echoes are typically much weaker than the head echoes. Although some long lasting UHF echoes were also observed, they were not coincident with the VHF long duration echoes.

G2-2
14:00

METEOR ECHO STUDIES AT HF USING THE USU BEAR LAKE NOAA DYNASOND

C.S. Fish, F.T. Berkey
Space Dynamics Laboratory
Utah State University
Logan, Utah 84322-4145

Short-lived sporadic E (E_S) events at rates up to several per hour have been observed in ionograms recorded by the National Oceanic and Atmospheric Administration (NOAA) HF radar [R.N. Grubb, *Tech. Memo., ERL-SEL 55*, Natl. Oceanic and Atmos. Admin., Boulder, Colo., 1979] operating as dynasonde [J.W. Wright, *Proc. IEEE.*, **57**, 815-825, 1969] at the Utah State University (USU) Bear Lake Observatory (41.9EN, 111.4EW). The database from which these events were first observed is comprised of synoptic ionospheric soundings recorded in the dynasonde B-mode [J.W. Wright and M.L.V. Pitteway, *Radio Sci.*, **14**, 815-825, 1979] acquired at 5-minute intervals with each sounding lasting ~ 100 sec. The B-mode soundings sample discrete frequencies over a radio bandwidth of 1.6 to 13 MHz (10MHz) during the daytime (nighttime). While many E_S events are very short-lived and detected over a narrow frequency range, numerous events exhibiting wide radio bandwidth (4-7 MHz) have been observed between 80 and 120 km.

Since December 1998, the dynasonde has been configured to operate in IDI (imaging Doppler interferometry [Adams et al., Radio Sci., 20, 1481-1492, 1985]) mode to measure mesospheric dynamics from 50-115 km (a companion paper at this conference will discuss the results of these IDI measurements). In the IDI mode data, we frequently record underdense and overdense meteor echoes [D.W.R. McKinley, ***Meteor Science and Engineering***. McGraw-Hill, New York, 1961] between 60 to 115 km. The IDI soundings are conducted at fixed frequencies of 2.2 MHz (nighttime) and 3.8 MHz (daytime) and interspersed with the B-mode soundings. In this paper, we will present examples of typical underdense and overdense echoes as well as underdense echo height distribution, average hourly detection rate, and spatial location as a function of frequency as seen in the IDI data during the past year. We are also planning to conduct a number of special campaign soundings during Fall 1999 (particularly targeting the time of the Leonids) at number of fixed HF frequencies other than those used in IDI-mode. The soundings will occur between B- and IDI-mode soundings and will cover a height range greater than that used in the IDI-mode (~ 50-150 km).

Our long-term objective is to utilize the underdense meteor echoes to make mesospheric wind [M.A. Cervera and I.M. Reid, *Radio Sci.*, **30**, 1245-1261, 1995] measurements for comparison with the IDI wind measurements at the USU Bear Lake Observatory.

G2-3
14:20

RESONANCE LIDAR OBSERVATIONS AT THE ARECIBO OBSERVATORY DURING METEOR SHOWER AND NON-METEOR SHOWER PERIODS

J. S. Friedman*
Arecibo Observatory
HC 3 Box 53995
Arecibo, PR 00612-9400

Periodic resonance lidar observations of mesopause sodium and potassium have been carried out at the Arecibo Observatory since May 1997. Special focus was placed on observations during the 1997, 1998, and 1999 Leonid meteor shower, 1997 Perceid shower, and a 2 month campaign during the winter of 1998. Other short experiments were also carried out during the time between meteor and campaign observations. During meteor shower activity, the Na lidar operated in a short-time integration mode so that weak meteor trails might be observed. A longer integration mode was applied during non-meteor shower observations, so only strong and long- lived meteor trails were observed (B.W. Grime et al., Geophys. Res. Letters, 26, 675-678, 1999).

During the 1998 Leonids meteor shower, about 10 meteors were observed each night on the peak activity night as well as the nights before and after peak activity. Preliminary analysis does not show a notable increase in Na abundance due to the shower. These data, along with the 1997 and 1999 observations, will be discussed. Leonids observations will be compared with observations made on other dates in terms of the frequency of observation of trails and variation in column abundance.

Atomic layer enhancements are frequently observed at low latitudes. We will present data on layer enhancements observed at Arecibo, PR, along with simultaneous observations of sporadic E and meteor activity. Layers observed during the Coqui II sounding rocket campaign, February-April, 1998 (J. S. Friedman et al., Geophys. Res. Letters, in press) will also be discussed.

Observations of mesopause potassium began in August, 1999. We will present the results of recent K observations, including those from the 1999 Leonid meteor shower.

G2-4
14:40

THE RADAR MICROMETEOR SCATTERING MECHANISM AND ASSOCIATED PHYSICAL PROCESSES

J. D. Mathews* D. Janches
Communications and Space Sciences Laboratory
Penn State University
University Park, PA 16802
D. D. Meisel
Department of Physics and Astronomy
SUNY Geneseo
Geneseo, NY, 14454
Q. -H. Zhou
Arecibo Observatory
Arecibo, Puerto Rico, 00613

High-resolution V/UHF radar observations of micrometeors at Arecibo Observatory allow comparisons of the observed trajectory and Doppler velocity/deceleration information with modeling results. Of particular interest is the interaction of the meteoroid with the atmosphere, the composition of these apparently durable particles, the role of sputtering and the generation of "plasma", the radar scattering mechanism whereby the meteor is actually "seen", and the fate of the meteoroid—does it disintegrate slowly or catastrophically.

We find that the atmospheric penetration depth of these particles is consistent with their small size and refractory composition. Additionally, the only consistent radar scattering mechanism [Mathews et al., Icarus, 126, 157-169, 1997] is optically-thin, coherent scattering from an ensemble of N electrons located within about 1/4 wavelength of the meteoroid and moving at the same speed. This backscattering scattering cross-section is equal the classical electron radius and for the reasonably well calibrated 430 MHz radar yields N of the order 10^8–10^{10} electrons. Noting this instantaneous value for electron/ions near the meteoroid, we have also explored the plasma production/loss process with some success. The principal loss mechanism is apparently ion charge-exchange with atmospheric molecules yielding a one-step trail formation mechanism.

It appears that many of the meteoroids observed catastrophically destruct before—as indicated by modeling and linear decelerations—significant mass loss occurs. Indeed progressive mass loss over the observed life of the particle is undetectable in most cases. The destruction mechanism appears to be heating combined with sometimes very large deceleration stresses. Decelerations as large as $200 - 300 km/sec^2$ have been observed. Planned common-volume, time-resolved optical/IR observations of the meteor zone at Arecibo may well yield further information on these issues.

G2-5
15:00

ELECTRODYNAMICS OF METEOR TRAIL EVOLUTION IN THE E-REGION IONOSPHERE: SIMULATION AND THEORY

M. M. Oppenheim* A. F. vom Endt
Center for Space Physics
Boston University
Boston, MA 02215

Radar echoes from meteor trails are routinely used to measure wind velocities in the E-region of the ionosphere. These measurements assume that the plasma in the meteor trail largely moves with the neutral wind. Using simulations and theory we show that meteor trail plasmas become highly turbulent in the presence of even small polarization electric fields common in the E-region. This turbulence will modify the Doppler echoes from the trails.

In a meteor trail, the $\mathbf{E} \times \mathbf{B}$-drift of the electrons creates an ambipolar electric field perpendicular to the meteor trail with a horizontal component. This ambipolar electric field in turn causes a $\mathbf{E} \times \mathbf{B}$-drift of the electrons along the direction of the meteor trail, which may locally shorten the polarization field of the E-region. The relative drift velocity between electrons and ions along the trail can exceed the threshold for the Farley-Buneman instability. The long-duration, non-specular radar echoes of meteor trails observed at Jicamarca have been attributed to this instability mechanism (Chapin, E. and E. Kudeki, *Geophys. Res. Lett.* **21**, 2433-2436, 1994). Finally, they suggested that meteor trails constitute transient current paths for discharging the vertical polarization in the E-region.

We use hybrid particle-in-cell/fluid simulations to study the competing effects of diffusion and instability growth in the evolution of meteor trails in greater detail. Our results indicate three distinct stages: (1) The rise of an ambipolar field immediately after the formation of the trail, (2) a transient gradient-drift/Farley-Buneman instability and (3) a fluid convection instability not previously recognized. These instabilities also disrupt the strong electron current caused by the ambipolar field.

These simulations show the development of turbulence over a wide range of wavelengths and directions including the 3 m wavelength detected by the radar in Jicamarca. This explains the non-specular reflections and characteristic spectra observed in the presence of a vertical polarization field in the E-region.

G2-6 IONIZATION FORMED BY HYPERTHERMAL COLLISIONS
15:40 Rainer A. Dressler and Edmond Murad
(Air Force Research Laboratory, Hanscom AFB, MA 01731)

William J. McNeil
(Radex, Inc., 3 Preston Court, Bedford, MA 01730)

Meteors entering the Earth's atmosphere are heated by friction to temperatures that can reach 2000 K. At earlier stages of heating (i.e. at higher altitudes and temperatures well below the maximum attainable) metals of moderate volatility (Na and K) evaporate from the meteor with a characteristic thermal velocity characteristic of the temperature, but with a total velocity equal to the sum of the thermal and meteor velocity, i.e. $\mathbf{v} = \mathbf{v}_{meteor} \pm \mathbf{v}_{thermal}$. Since $\mathbf{v}_{meteor}$ is 11-70 km/s and since $\mathbf{v}_{thermal} \sim 1$ km/s, $\mathbf{v} \sim \mathbf{v}_{meteor}$, i.e. 11-70 km/s. We next consider what happens to Na or K atoms colliding with the atmosphere at high velocities. Simple curve-crossing models for

$$Na + O \rightleftarrows O^- + Na^+ \qquad (1)$$

indicate it to have a cross section that varies from 10^{-4} A^2 at 20 km/s to ~ 1 A^2 at 70 km/s. By contrast, collisions with O_2 are expected to yield much higher cross sections for ion-pair formation due to the more favorable coupling between a multitude of vibronic states that cross. Measurements of the Na + O_2 and K + O_2 ion pair formation cross section

$$Na + O_2 \rightleftarrows O_2^- + Na^+ \qquad (2)$$

vary by orders of magnitude. The most sophisticated, though least cited, measurements determined cross sections of ~ 2 and ~ 4 A^2 at 13 km/s for the two collision systems, respectively, with gradual increase at higher energies. Extrapolation to ~ 70 km/s suggests the cross section may be ~20 A^2. The same measurements also demonstrate that free-electron formation cross sections of alkali + O_2 collisions are sizeable, while we predict them to be negligible for the atomic system (1). The time constant for reaction (2) for Na at 100 km is ~ 2 ms for 20 km meteor and ~ 0.3 ms for a 70 km meteor. Processes such as (1) and (2) can be the source of ionization in a meteor trail, and would thus correlate the radar observations of the trails (high electron density in a narrow trail) as well as the spectroscopic observations that seem to indicate the formation of metal ions for high velocity meteor showers. In this talk we will discuss the potential chemical processes that give rise to ionization and then those processes that lead to the observation of neutral atoms in lidar studies.

G2-7
16:00

DIRECT DETERMINATION OF THE METEORIC MASS FLUX INTO THE UPPER ATMOSPHERE

J. D. Mathews* D. Janches
Communications and Space Sciences Laboratory
Penn State University
University Park, PA 16802
D. D. Meisel
Department of Physics and Astronomy
SUNY Geneseo
Geneseo, NY, 14454
Q. -H. Zhou
Arecibo Observatory
Arecibo, Puerto Rico, 00613

The advent of radar micrometeor observations at Arecibo Observatory has enabled direct estimates of the meteoric mass flux into the upper atmosphere. These observations yield on average 2200 events per day in the 300 m diameter Arecibo beam. Doppler velocity estimates are found for approximately 50% of all events and of these, approximately 10% (5% of the total) also yield measurable (nearly linear) decelerations (Janches et al., Icarus, 1999, in review). These decelerations can in turn be converted to a particle mass estimates using the meteoroid momentum equation and a model atmosphere (MSIS-90). In the case of observed decelerations and assumed spherical particles of known density (say, 3 gm/cc), meteoroid masses range from a few micrograms to nanograms. This approach yields an average mass of 0.37 microgram/particle for the 5% of all particles that manifest observable deceleration. We assume that the 45% of all particles for which velocity is determined with no detectable deceleration correspond to particle masses larger than a few micrograms. However if we assume that all observed particles average 0.37 micrograms each, we find a mass flux of about 10^{-5} kg/km^2-day over the whole Earth. This flux is strongly peaked near sunrise and is consistent with the ISR-determined metal ion production rate reported by Zhou et al. (GRL, 26, 1833-1836, 1999). Assuming a power law mass distribution matching accepted flux versus particle mass distributions for those particles for which we cannot determine mass increases our mass flux estimate by a factor of 2-3.

Many of the particles we observe show evidence of catastrophically disintegrating in the meteor zone. We thus suggest that the majority of micrometeoroid mass is deposited in the 80-110 km altitude region where ionospheric atomic metal ion layers and atmospheric manifestations such as neutral atomic metal layers are well documented. We further suggest that this "background" diurnal micrometeor mass flux maintains the mesosphere and lower thermosphere metal content and apparently dominates the mass flux from meteor showers.

G2-8
16:20

REEXAMINATION OF COSMIC DUST SMOKE PRODUCTION IN THE EARTH'S UPPER ATMOSPHERE

O. Kalashnikova* M. Horanyi G.E. Thomas O.B. Toon
Laboratory of Atmospheric and Space Physics
Campus Box 392
University of Colorado
Boulder, CO 80309

We extend earlier models of cosmic dust ablation in the Earth's atmosphere to include not only the initial size, velosity and direction but also the composition and shape of micrometeorites. In addition we now include the temperature dependence of the relevant physical parameters in the equations describing the energy and momentum exchange between the incoming dust particles and the atmosphere. Samples of cosmic dust particles collected by NASA's U2 flights show a variety of grain types ranging from simple spheres to complex fractal-like structures. NASA publication 'Cosmic Dust Catalog 15' summarizes the observation of 468 particles retrieved during a series of flights that were made during January and February 1994 (L2021) and June-July of 1994 (L2036). Based on this collection we made a simple assumption on the surface-to-volume ratio of these particles. We then used our model to examine the effects of compactness (shape) on their ablation in the atmosphere. We test the sensitivity of ablation profiles to the shape of micrometeotites by calculating the ablation rates of fractal-like particles. Fractal-like particles result in only $\sim 1\%$ contribution to the total ablated mass. We obtain input parameters from spacecraft measurements of mass, influx, velocities and positions of incoming micrometeorites. We compared ablation profiles using new spacecraft data with ablation profiles calculated with assumed velocities and angles. The use of measured velocities and realistic angular distributions results in an increase of the altitude of ablation. We investigate the latitudinal-longitudinal, altitudinal and seasonal dependence of micrometeorites entering Earth's atmosphere. Our calculations establish a more realistic deposition rate of dust than the earlier works as a function of both altitude and size in the upper atmosphere. We also apply of the our model to interstellar dust ablation and to the deposition rate of meteoric dust in the Martian atmosphere.

G2-9
16:40

THIN METALLIC ION LAYERS OVER SONDRESTROM: OBSERVATIONAL RESULTS AND UNRESOLVED ISSUES

Dr. David F. Bedey
Department of Physics
United States Military Academy
West Point, NY 10996

Dr. Brenton J. Watkins
Geophysical Institute
University of Alaska Fairbanks
Fairbanks, AK 99775

As meteoroids penetrate the Earth's atmosphere, collisional interaction between these objects and the increasingly dense neutral atmosphere causes the meteoroids to ablate resulting in the deposition of metallic atoms, a process which predominantly occurs in the upper mesosphere. Subsequently, a significant portion of these atoms undergo charge exchange with the major molecular ions, i.e., O_2^+ and NO^+, thus providing the primary source of a thick layer of metallic ions (e.g., Na^+, Fe^+, and Mg^+) that exists in the ionosphere's lower *E* region. At high latitudes, large-scale electric fields of magnetospheric origin can force this meteoric residue to accumulate into relatively dense, thin layers which generally are observed at altitudes of 95-120 km with a nominal thickness of 1-2 km and a peak density of up to 10^5-10^6 cm^{-3}. These layers constitute a form of sporadic *E*.

From August 1994 through August of 1998, we have conducted a uniquely designed observational program using the incoherent-scatter radar facility at Sondrestrom in Greenland to detect the presence of thin layers and to concurrently map the ionospheric electric field. The scientific objectives of this lengthy campaign have included an examination the correlation between layer occurrence and temporal variations in the electric field over several time scales and a study of the influence of the electric field on layer characteristics such as altitude and horizontal extent. In this paper, we summarize our previously published results relating to seasonal and diurnal periodicity in layer occurrence, review recent findings related to shorter-term effects, and present an analysis of the influence of the electric field on the structure and altitude of layers. Major findings include: (1) thin metallic ion layers occur predominantly during the summer months; (2) thin layers over Sondrestrom are most likely to occur between 2200 UT and 0100 UT; (3) layers tend to be observed at times when the electric field suddenly intensifies but then disappear despite the persistence of a favorable electric field; (4) layers tend to be "patchy" both in time and in space; and (5) layers are observed at altitudes slightly lower than predicted by the prevailing theory of layer formation. In addition to presenting and interpreting the results of our observations, we will discuss several unresolved issues, such as indications of lateral drift of layer structures.

G2-10 17:00 THE APPLICATION OF IMAGING RIOMETERS FOR DETECTION OF THIN METALLIC-ION LAYERS

B.J. Watkins
Geophysical Institute, University of Alaska Fairbanks
D.F.Bedey
US military Academy, West Point, NY
T.J.Rosenberg and A.T.Weatherwax
University of Maryland at College Park
P.Stauning
Danish Meteorological Institute, Copenhagen

The incoherent-scatter radar at Sondrestrom, Greenland has been used to study the morphology and occurrence of thin metal-ion layers that occur in the lower ionosphere at altitudes from about 90 to 110km; these result from the accumulation of metal ions that form after meteor ablation. The structures are frequently limited in spatial extent and move horizontally in response to electric fields and neutral winds. We report on efforts to use the co-located 38 MHz imaging riometer at the radar site to detect the presence, spatial extent, and motion of these metal-ion layers. The levels of cosmic noise absorption are typically about 0.05 – 0.1 dB and therefore the detection of these structures is limited to geomagnetically quiet periods in the absence of auroral ionospheric structures. Imaging riometer data in conjunction with radar-observed layer events will be presented where horizontal two-dimensional structure and layer motions are evident. For the specific data presented the radar was operated with an elevation-scan mode in the magnetic north-south meridian. Metal layer structures were detected with the radar and motions from north to south were observed. Simultaneous imaging riometer data showed a patch structure that moved north to south with a speed of approximately 170 m/s. The data evaluated to date has shown that many of the high latitude metal structures observed by radar are patches in the size range 30 - 100 km. The combination of incoherent-scatter radar plus an imaging riometer enables new insights into the dynamics of sporadic metal-ion layers. A new imaging riometer designed to operate at a lower frequency would provide greater absorption levels and enhance these studies.

G2-11
17:20

MEASUREMENTS OF THE DISTRIBUTION OF METEORIC METAL IONS AT HIGH LATITUDES

C. J. Heinselman
Radio Science and Engineering Division
SRI International
Menlo Park, CA 94025

Metal ions of meteoric origin are frequently observed as sporadic-E layers under a number of ionospheric conditions. At high latitudes, sporadic E can be formed quite efficiently through the influence of properly directed DC electric fields. This can only occur, however, if the necessary horizontal distributions and densities of metal ions are present prior to the electric field onset. While the formation mechanism has been quite firmly established both theoretically and experimentally, the distribution and horizontal extent of these altitudinally thin layers have not yet been fully explained. Most previous studies have concentrated on the vertical compression of a horizontally uniform source of ions, arguing that the nearly constant flux of meteoric material would support that source. This, however, is somewhat at odds with the sporadic nature of sporadic E as well as with the impulsive nature of measurements of meteoric ablation phenomena.

In this talk we present measurements of the horizontal extent and dynamics of sporadic-E layers as measured with the Sondrestrom Incoherent Scatter Radar. A radar operating mode was implemented which emphasizes the detection of these layers at the cost of detailed spectral information about the returns. The advantage of this approach is that it greatly reduces the minimum detectable electron density levels and allows shorter time integrations for the more intense layers. A series of measurement campaigns have been carried out for the past several years utilizing this radar mode and, more recently, they have utilized antenna scanning sequences to help separate temporal from spatial effects. This antenna motion also supports estimates of local electric field strengths and directions via measurements of F-region ion drift velocities.

The measurements to be presented cover both meteor shower times and times without major shower activity, with sporadic E present under both conditions. The data show large horizontal gradients in many of the sporadic E layers as well as significant horizontal motion. In addition, the formation and destruction of layers also appear to be observed. These measurements will be interpreted in the context of current theories.

H2-1
14:00

SPACE CHAMBER MEASUREMENTS OF TRANSVERSE ION ENERGIZATION†

D. N. Walker* W. E. Amatucci G. Ganguli J. Peñano
Plasma Physics Division
Naval Research Laboratory
Washington, DC 20375

In a collisional plasma that includes a transverse electric field, transverse ion energization can occur through the Joule heating process (e. g., Heelis and Cooley, *J. Geophys. Res.*, **93**, 7551, 1988). If the electric field is spatially localized it can cause waves, making both wave heating (Walker *et al.*, *Geophys. Res. Lett.*, **24**, 1187, 1997) and Joule heating possible. Laboratory experiments are currently being conducted in the Naval Research Laboratory's Space Physics Simulation Chamber (SPSC) to investigate ion energization by both the wave and Joule heating mechanisms in plasma conditions representative of the low-altitude ionosphere. Wave and Joule heating regimes have been isolated and a transition between the two regimes observed as the ion-neutral collision frequency, ν_{in}, was varied. The results indicate that in plasma conditions where the ion-neutral collision frequency is small enough to allow wave growth, energy dissipation through wave-particle interactions can be the dominant source of ion heating; On the other hand, at higher collision frequencies where the waves are collisionally damped, a transition to Joule heating is observed (Amatucci *et al.*, *Phys. Plasmas*, **6**, 619, 1999).

We have recently augmented our plasma parameter experimental regime by developing both new plasma sources and extending our ability to create both radially inward- and outward-directed localized electric fields. We will present ion temperature measurements made with our perpendicular ion energy analyzer (Katsumata and Okazaki, *Jpn. J. Appl. Phys.*, **6**, 123, 1967). The probe operates by utilizing the chamber's axial magnetic field to prevent electrons from reaching a current-collecting disk, which is recessed within a shielded housing by a distance greater than several electron gyroradii. The larger ion gyroradius allows all but the least energetic of these particles to reach the collector. The data presented will concentrate on the Joule heating regime where we demonstrate the coincidence of ion heating with electric field and demonstrate that this heating increases as the square of the applied field consistent with a Joule heating scenario. With a radially outward electric field we find that the plasma creates a radial density gradient in order to maintain equilibrium. This is in contrast to the case of a radially inward field which requires no gradient. Implications of field localization and direction will be covered along with conclusions related to ionospheric observations.

†Work supported by the Office of Naval Research.

H2-2
14:20

IMPEDANCE PROBES FOR SPACE PLASMA DIAGNOSTICS

C. M. Swenson* C. M. Furse C. Fish
Department of Electrical and Computer Engineering, UMC 4120
Utah State University
Logan, UT 84322
P. Nikitin
Department of Electrical and Computer Engineering
UMC 4120
Carnegie Mellon University
Pittsburgh, PA 15213-3890

The electrical impedance of an antenna exposed to the space environment is dependent upon the parameters of the space plasma in which it is immersed (electron density, collision frequencies, external magnetic field, temperature). This effect was first observed by (J. E. Jackson *J. Geophys. Res.*, 64(8), 1074-1075, 1959). Since that time probes have been built and flown to deduce parameters of the space environment based upon this effect. The technique has primarily been used to measure electron density in the Earth's ionosphere by *in situ* measurements on sounding rockets and satellites. It has a significant advantage over Langmuir methods in that it is insensitive to vehicle potential and probe surface contamination. For these reasons it has become a preferred method for determining absolute electron density in the ionosphere.

Proper data analysis requires an accurate theory for the impedance of an antenna immersed in a magnetized plasma. The problem has been solved for electrically short antennas under a quasi-static approximation. The current distribution on the surface of the antenna is assumed and the dielectric tensor for a two component fluid model of a cold plasma is used. It provides a relatively simple expression for the impedance which can be used for data analysis (K. G. Balmain *IEEE Trans. Antennas Propagat.*, AP-17(3), 389-392, 1969). A warm kinetic plasma dielectric has also been considered but expressions are only valid in non-resonant regions of the driving frequency. A good review of the theoretical work on antennas in plasmas can be found in (K. G. Balmain *Ann. Telecommun.*, 34(3-4), 273-283, 1979).

Utah State University is currently developing a new plasma impedance probe based on modern electronic devices. This instrument combines the capabilities of previous instruments build at Utah State and provides a complete antenna impedance profile. This additional information can be used to extend the diagnostics beyond simple electron density measurements. Utah State is also working on full wave computational simulations of these antennas in warm fluid plasmas. The goal is to combine improved measurement capability with improved analysis techniques to obtain electron temperature, collision frequency and other plasma parameters.

H2-3
14:40

TITANIUM NITRIDE (TiN), A NEW SURFACE COATING FOR SPACE PROBES

Bengt Holback*
Swedish Institute of Space Physics
Uppsala Division
SE-755 91 UPPSALA
Sweden

The Swedish Institute of Space Physics, Uppsala Division, has carried out many probe experiments in the earth's magnetosphere, both on sounding rockets as well as on satellites. Data from these probes, like Langmuir probes and Electric field probes, often suffer from spurious signals embedded in the real signals. Also short and long term variations of the probe properties add unwanted components to the measured signal. These false signals are difficult to sort out and extract from the measured signals causing errors in the data interpretation. A suspicion that they are, to at least some extent, caused by the surface coating material used on the probe surface, led to an investigation on the role of the coating material and a search for alternative coatings. It was found that, in most cases, Titanium Nitride (TiN) would be a better choice than the graphite coatings that has been commonly used.

For the first time in space, a Langmuir probe made of Titanium and given a TiN surface coating is flown onboard the Cassini space craft bound for Saturn. It was launched on October 1997 and after almost two years in space, data from the solar wind and from the earth "fly-by" show excellent probe performance.

Also the Swedish magnetospheric micro-satellite Astrid-2 carries two Langmuir probes and four electric field probes made of Titanium and coated with TiN. The Astrid-2 orbit is at 83 degrees inclination and 1000 km height and data are sampled at all locations of the orbit, i.e. for all geomagnetic latitudes and longitudes. Data show very good performance of the probes. Examples of data from Astrid-2 as well as from Cassini will be shown and compared to data from earlier experiments using graphite coated probes.

H2-4
15:00

LABORATORY INVESTIGATION OF SPACECRAFT SENSOR COATINGS

P. Schuck* S. P. Powell P. M. Kintner
Cornell University
W. E. Amatucci D. N. Walker
Naval Research Lab

Floating and biased Langmuir probes are simple in design and operation: a basic Langmuir probe can be constructed from a bare wire connected to a DC power supply and an ammeter and inserted into the plasma. Consequently, Langmuir probes are one of the most common plasma diagnostics carried by instrumented spacecraft investigating the earth's ionosphere and magnetosphere. The most fundamental and correctable problem degrading the performance of Langmuir probes in both laboratory and space plasmas is probe surface contamination. Contamination caused by neutral adsorbates adhering to the probe surface can result in distortions of the current-voltage characteristic, underestimates of the saturation current (electron density), and overestimates of the electron temperature. A variety of techniques have been devised to mediate the affect of surface contamination. Often spacecraft sensors are coated with carbon graphite (Aerodag) in an effort to produce a uniform "dirty" surface. Recently, *Wahlstrom et al.* (Wahlstrom et al., *Thin Solid Films*, **220**, 315-320, 1992), suggested that the performance of titanium nitride (TiN) coatings is superior to that of graphite. A probe based on this concept is incorporated in the Cassini spacecraft to monitor electron density fluctuations around Saturn.

This paper describes a laboratory (Naval Research Laboratory Space Physic Physics Simulation Chamber) investigation of the performances of several probes commonly incorporated on instrumented spacecraft that investigate the earth's ionosphere and magnetosphere. Data from spherical probes made respectively from bare aluminum, carbon graphite-coated aluminum, TiN-coated aluminum, and TiN (a duplicate of the Cassini probe) were compared to data from calibrated contamination-free NRL Langmuir probes. The "space" probes were each prepared in a manner similar to that used prior to a launch. The measured electron temperature and hysteresis of the current-voltage characteristic of each probe were used to evaluate the performance of the various coatings. All of the spacecraft sensors overestimated the electron temperature by factors of 5-10 and exhibited distinct hysteresis. Sensors affected this seriously by contamination are obviously unacceptable for quantitative space plasma physics. To mediate the affects of surface contamination, a small halogen bulb was mounted inside the TiN-coated aluminum probe and the probe was heated to 400°C by radiative transfer (Paturi et al., *Rev. Sci. Instrum.*, **69**, 3945-3947, 1997). At these temperatures, the contamination was eliminated and the measured electron temperature agreed with the calibrated NRL probe. Additionally, the hysteresis of the current voltage characteristic became indiscernible. A similar heating design may be practical for Langmuir probes carried by sounding rockets.

H2-5
15:40

FAST ELECTRON TEMPERATURE MEASUREMENT WITH LANGMUIR PROBES†

C. L. Siefring* W. E. Amatucci D. N. Walker D. Duncan
Plasma Physics Division
Naval Research Laboratory
Washington, DC 20375

Measurements of ionospheric electron temperatures with Langmuir probes are usually done with a techniques that sweeps a bias voltage to determine the current-voltage (IV) characteristic for the local plasma. We report on results in the use of a technique which is new to space experiments, but has been used in laboratory experiments. This technique should allow for faster electron temperature measurements than the typical swept probe, while imposing less disturbance to the space plasma and to other instruments. The technique uses a small ac modulation of the Langmuir probe signal at a dc bias point, and the detection of harmonics in the probe current. Analysis shows that the ratio of the fundamental and the second harmonic is dependent only on electron temperature and the amplitude of the applied ac bias.

We present results from tests of this technique in the Naval Research Laboratory's Space Physics Simulation Chamber (SPSC) and discuss the applicability for space measurements. The SPSC was designed to produce plasmas with parameters similar to those seen in the ionosphere. It appears that to make a reliable temperature measurement, it is necessary to use a two-probe system. A second probe is used to monitor the changes floating potential and provide real-time feedback for correction of the dc bias point of the active probe. The laboratory results show that it should be possible to make fast ($\sim$ 1 ms) temperature measurements using very simple electronics circuitry.

†Work supported by the Office of Naval Research.

H2-6
16:00

MESOSPHERIC DUST MEASUREMENT TECHNIQUES

L. J. Gelinas
Laboratory of Plasma Studies, Cornell University
Ithaca, NY 14853

The growing interest in mesospheric layering phenomena such as Noctic-ulent Clouds (NLC), Polar Mesospheric Summer Echoes (PMSE), and Sporadic Sodium Layers (Na_s), has reinvigorated efforts to characterize the mesospheric dust population. Dust may serve as seed nuclei for ice particles in NCL and PMSE, and may be related to the formation of Na_s. Until recently, there was little experimental evidence but strong theoretical expectations for the existence of a meteoric dust layer in the Earth's mesosphere at altitudes between 80 and 100 km. Models of this dust layer, produced by ablation of meteors in the Earth's atmosphere, predict a population of about 1000/cc nanometer-sized particles (Hunten et al., *J. Atm. Sci., 37*, 1342, 1980). These particles are difficult to detect; the altitude range of the dust layer, near 90 km, is inaccessible to both satellite observations and balloon measurements, and the ground-based scattering cross-section is small compared to the return from the neutral gas.

A mesospheric dust population usually has been inferred from lower altitude aerosol measurements (Chesworth & Hale, *GRL 1*, 347, 1974). Recent successes in in-situ characterization of the mesospheric dust population stem from measurements of the charged component of the dust population, since in the lower ionosphere the plasma density is sufficient to cause charging of the dust or ice particles. Rocket-borne mass spectrometer measurements have indicated the existence of negatively charged heavy ions ($\geq$400 amu) at altitudes over 80 km (Schulte & Arnold, *GRL, 19*, 2297, 1992). Detectors flown on sounding rockets through NLC and PMSE indicate the presence of charged ice particles with sizes as small as 20 to 30 nanometers (10^7 to 10^8 amu) (Havnes et al., *JGR, 101*, 10839, 1996), and nanometer-sized (10^4 amu), presumably meteoric, charged particles have been observed at equatorial latitudes (Gelinas et al., *GRL, 25*, 4047, 1998).

The existence of charged mesospheric dust may be also inferred from observations by sensitive ground-based instruments, such as anomalous radar backscatter (echoes) from PMSE, which may be due to a population of charged ice particles (Cho & Kelley, *Rev. Geophys., 31*, 3, 1993). Ground-based lidar systems may also be able to detect uncharged dust particles on the order of a few 10's of nanometers (von Cossart et al., *GRL, 26*, 1513, 1999).

These recent mesospheric dust measurements will be discussed, including the advantages and limitations of the various experimental techniques.

H2-7
16:20

MEASUREMENT TECHNIQUES FOR ELECTRIC CURRENTS IN SPACE PLASMAS

K. A. Lynch*
Space Science Center, Morse Hall
University of New Hampshire
Durham, NH 03824

In this paper we describe three separate techniques for measuring electric currents in space plasmas: (a) multisensor measurement of $\nabla \times \mathbf{H}$, (b) Faraday rotation in optical fibers, and (c) direct measurement of the plasma distribution function and its moments, including thermal electrons. We describe the physics behind the techniques, and the present level of technology development for each. For the multiple-magnetometer sensor method, we present recent results from multiple-payload auroral sounding rocket missions.

Research into these methods is motivated by the following ideas. 1) Direct measurements of currents are notably lacking in our data sets so far. As we move toward a quantitative understanding of our space environment, we will need quantitative measurements of the currents which connect the various parts of the Sun-Earth system. Specific work described here is directed toward the Birkeland current system, as it is the most accessible to measurement, but these techniques can – and should – be extended for use in other current systems. 2) One of the methods for direct current measurement involves the ejection of small, independent free-flyers from a main spacecraft. This simple application of the multiple-spacecraft concept will be a first step toward truly multiple-point space missions. 3) Direct observations of currents have rarely been made in the past — not because they were considered unimportant, but because the measurement is difficult. These measurements will require an infusion of new technology – miniaturization, new materials, optical systems, self-supporting miniature spacecraft – all of which will be not only useful for the missions described here, but for other future missions as well. These measurements and techniques will be useful in understanding and measuring many regions of the Sun-Earth system.

H2-8
16:40

TIME VARYING MAGNETIC FIELD MEASUREMENTS AT THE LAPD

D. Leneman* W. Gekelman S. Vincena
LAPD Plasma Lab at UCLA
1000 Veteran Avenue
Room 15-70
Los Angeles, CA 90095

At the LArge Plasma Device (LAPD) laboratory at UCLA pick-up loops are the preferred type of magnetic field probe. Many of our recent experiments have focused on the magnetic fields of waves launched by electron skin-depth size ($\sim$ 3 mm) fluctuating current filaments or waves associated with density or temperature striations. These fields often have low amplitude ($\sim$ 1 mG) and oscillate at frequencies as low as 40 kHz. This necessitates the construction of correspondingly small and sensitive loops to detect and resolve these magnetic field structures. We have built 5, 3, and 1 mm diameter loops. The 5 mm ones are composed of a pair of 56 turn loops made from 0.1 mm diameter magnet wire. The loops are paired for common mode rejection with the help of a differential amplifier. Three of these units are orthogonally assembled to measure all field components. The sensitivity of each loop pair is 0.1 V/G at 100 kHz. The 3mm diameter ones are in essentially! the same configuration but they a re composed of pairs of 8 turn loops and the sensitivity is 7×10^{-3} V/G at 100 kHz. The 1 mm diameter coils are also a triaxial arrangement of pairs of loops and have been constructed under a microscope. They are now being tested. Alternative probe schemes will also be mentioned. These include 0.1 mm diameter coils etched out of silicon wafers, Hall effect probes and optical probes which rely on polarization rotation in crystals. Several tradeoffs and difficulties with these techniques will be discussed.
Work supported by ONR and NSF.

J1-1
13:40

CYCLOTRON RESONANT HEATING OF CORONAL HOLES AND THE SOLAR WIND: WHAT CAN RADIO SCIENCE CONTRIBUTE?

J. V. Hollweg *
Space Science Center
Morse Hall
University of New Hampshire
Durham, NH 03824

For many years, the heating of the solar corona and the acceleration of the fast solar wind have been outstanding unsolved problems. Results from the Ultraviolet Coronagraph Spectrometer (UVCS) on the Solar and Heliospheric Observatory (SOHO) now suggest that coronal holes are heated by high- frequency (kHz) waves via the ion-cyclotron resonance, and that the solar wind is accelerated mainly by the pressure gradient of hot protons. The evidence is: 1. The protons and heavy ions are hotter than the electrons. 2. Heavy ions are more than mass-proportionally hotter than the protons. 3. Heavy ions, and probably the protons, are heated mainly in the direction perpendicular to the magnetic field. We will discuss in simple terms the basic kinetics of the ion-cyclotron resonance, with emphasis on how it can naturally lead to strong preferential heating of the heavy ions. However, the origin of the high- frequency waves is still unclear. In situ data, and a variety of radio data, indicate that most fluctuation power is at long periods, of the order of hours. One possibility is that the high-frequency waves are produced by a turbulent cascade up to high frequencies. There is also some evidence that the Sun launches Alfven waves with periods around 5 minutes; perhaps these are the waves that turbulently cascade to high frequencies. Alternatively, it has been conjectured that small reconnection events close to the Sun, microflares or nanoflares, generate the waves at the required frequencies; these waves must be of the order of several kHz to resonate with coronal protons. We will suggest several ways in which radio studies of the corona may be able to distinguish between these possibilities. Since the waves are magnetic, they can be detected via Faraday rotation. If the waves propagate obliquely to the magnetic field, they are compressive, and can be studied via phase or intensity scintillations. We will present a preliminary study suggesting that the conjectured directly-launched high frequency waves are not present, but can only conclude that more careful studies of this question should be undertaken.

J1-2
14:00

SOLAR WIND VELOCITY OBSERVATIONS NEAR THE SUN

W. A. Coles
Department of Electrical and Computer Engineering
Mail Code 0407
University of California
La Jolla, CA 92093-0407

Meter wavelength observations of the solar wind velocity using multistation intensity scintillations (IPS) can be made at solar distances exceeding 50 solar radii. They have been very useful in determining the structure and evolution of the fast polar streams that form during the declining and minimum phases of the solar activity cycle. They have also been used to study the distribution of turbulence in corotating interaction regions, and the structure and evolution of coronal mass ejections. IPS observations have been made closer to the Sun, using higher radio frequencies. Here they have shown that the polar solar wind accelerates much more rapidly than had been theoretically expected, reaching its final speed by 10 solar radii. However IPS observations inside of 10 solar radii show anomalies which are still not fully understood.

In this talk I will discuss IPS observations made with the VLBA at distances inside of 10 solar radii. Here we have found that it is essential to choose a frequency such that the intensity scintillations are "weak" and to choose antennas which are separated by distances several times larger than the pattern scale. This allows us to fit the auto and cross power spectra with models which can include spatial structure on the line of sight, anisotropic microstructure, and Alfvén waves. Close to the Sun we find it necessary to include additional velocity variation, but the physical mechanisms for this variation is not clear and certainly not unique. I will discuss several possiblities and the constraints that these put on the acceleration mechanism of the solar wind.

J1-3
14:20

RADIO SOUNDING OF THE SOLAR CORONA BY INTERPLANETARY SPACECRAFT: LARGE-SCALE STRUCTURE AND DETECTION OF CMEs

M. Pätzold*
Institut für Geophysik und Meteorologie, Cologne University
D-50923 Köln, Germany M.K. Bird
Radioastronomisches Institut, Universität Bonn
D-50121 Bonn, Germany

We present coronal sounding results from the solar superior conjunctions of the Ulysses (1991, 1995), NEAR (1997) and Galileo (1997) spacecraft. While Ulysses has a dual-frequency downlink at S-band and X-band, the NEAR spacecraft was transmitting an X-band radio signal only and Galileo was only capable to transmit S-band via the low gain antennas because its high antenna did not unfold early in the mission.

The Ulysses 1991 and 1995 conjunctions will be reviewed, emphasizing results for the electron density profiles and turbulence spectra in slow (streamers) and fast (coronal holes) solar wind. The transition from streamer belt to coronal holes is clearly seen in the data. In contrast to other authors, no evidence of coronal plumes could be found. Signatures of CMEs could be found in selected Ulysses tracking passes. Furthermore, a CME search was performed with data from the the NEAR and Galileo conjunctions in 1997 and compared with SOHO images. A numerical model will be presented that simulates the temporal variation in observed electron content during passage of a CME through the radio ray path. The model, adjustable for arbitrary angle between radio ray path and CME propagation direction, can be used to yield an estimate of the speed of the disturbance as well as the electron density in the front and the trailing region.

A preview will be given to future coronal sounding experiments on the Rosetta and Mars Express spacecraft. Both will be in superior solar conjunction within 40 solar radii about the solar disk (in the plane-of-sky) at the same time in 2004.

J1-4
14:40

SOHO OBSERVATIONS OF CORONAL MASS EJECTIONS

J. C. Raymond
Harvard-Smithsonian Center for Astrophysics
60 Garden St.
Cambridge, MA 02138

By combining observations made with different instruments aboard SOHO, one can derive a great deal of information about the speed, morphology, density and temperature structure of the plasma. This talk concentrates two CMEs studied by EIT, LASCO and UVCS. EIT shows the initial ejection, LASCO shows the evolving morphology and the speed, and UVCS provides doppler shifts, line widths and line intensities from which we derive the ionization state and electron and ion temperatures.

The first CME was a slow prominence eruption, and we describe the helical structure, the temperature structure and the heating requirements. For likely initial conditions, we find that the plasma did not start at coronal temperatures and that gradual heating was needed, amounting to an energy comparable to the gravitational potential energy.

The second event was a 1200 km/s CME that produced Type II radio bursts. By enormous good fortune, the radio bursts coincided with the time that the compressed gas crossed the UVCS slit. The Lyα intensity decreased by 10% due to the high velocity and increasing ionization level. The O VI lines brightened by 25% and the high temperature Si XII line doubled in brightness. We compare the densities derived from the Type II bursts with the pre-CME density estimated from the O VI doublet ratio observed by UVCS. We also discuss electron-ion and ion-ion equilibration in the collisionless shock. The very large widths of the O VI lines (900 km/s FWHM) suggests that the bulk velocities of the particles are randomized independently by the shock, and that little sharing of thermal energy among species occurs during the observation period.

J1-5
15:00

DYNAMICS OF THE SOLAR WIND DISSIPATION RANGE

Robert J. Leamon
Bartol Research Institute
University of Delaware
Newark
DE 19716

Unlike larger spatial scales of the interplanetary magnetic field fluctuation spectrum, study of the smallest scale fluctuations (comparable to the gyroradius of a thermal proton) which form the so-called dissipation range have been somewhat neglected. This is undoubtedly due, at least in part, to the large volume of data required to perform thorough studies of the high-frequency spectrum.

The dissipation range represents the final fate of magnetic energy that is transferred from the largest spatial scales via nonlinear processes until resonance with the thermal particle populations removes the energy from the spectrum and heats the background distribution. It is characterized by a steeply falling power spectrum and frequently a bias in the corresponding polarization or magnetic helicity spectrum.

Typically, the dissipation range sets in at spacecraft frame frequencies a few times higher than the proton cyclotron frequency and as such, at 1 AU sets in at a few tenths of a Hertz.

Examining the properties of dissipation range power and helicity spectra, using data from the WIND spacecraft, we deduce: (1) magnetic fluctuations are largely transverse to the mean magnetic field, but less so than is seen in the high-frequency extent of the inertial range (cf. J. W. Belcher & L. Davis, *J. Geophys. Res.*, **76**, 3533–3563, 1971); (2) a dominant fraction of the total energy is associated with wave vectors at large angles to the mean magnetic field (cf. J. W. Bieber *et al.*, *J. Geophys. Res.*, **101**, 2511–2522, 1996); (3) the aforementioned bias in polarization and helicity is significant, but not maximal, which has implications for the ion-resonant dissipation that is contributing to the magnetic spectrum. Strong plasma β effects are present in the above results.

J1-6
15:40

RADIO-WAVE SENSING IN A GLOBALLY STRUCTURED SOLAR WIND

V. J. Pizzo
Code R/E/SE
NOAA/SEC
325 Broadway
Boulder, CO 80303

In the last several years, in-situ and remote-sensing observations by the Ulysses, SOHO, YOHKOH, and other spacecraft, coupled with modern simulation capabilities, have resulted in major advances in the understanding of the large-scale 3-D structure of the solar corona and solar wind. In particular, it has become apparent that the ambient, quasi-steady solar wind structure has a significant impact upon the propagation and evolution of transient structures, such as coronal mass ejections.

We will briefly outline the state of knowledge of global solar wind structure, and then take up what this all means for the interpretation of radio observations. Two specific topics will be addressed: (1) the use of ground-based IPS observations to detect corotating and transient structures; and (2) how empirical understanding of global solar wind structure stand to be revolutionized by two-view spacecraft observations forthcoming in the NASA STEREO mission. For (1), a comparison of forward modeling results with Cambridge observations from the last solar maximum suggests corotating structures can be detected quite readily, but cadence aliasing and other effects make the observation of transients more difficult. Related observations and modeling efforts will be briefly discussed. For (2) we will sketch the mission profile and its main goals, then address how two-point radio observations, coupled with STEREO in-situ and white light observations and state-of-the-art simulation techniques will offer unprecedented opportunities for probing the structure of the solar wind on a global scale. Two-view observations of interplanetary type II and III bursts show the greatest promise in this regard, and the iterative use of these observations with simulation results will be described.

J1-7
16:00

FRACTIONAL FREQUENCY STABILITY OF RADIO LINKS THROUGH THE SOLAR WIND AND TROPOSPHERE

J. W. Armstrong
Jet Propulsion Laboratory
Mail Stop 238-725
4800 Oak Grove Drive
Pasadena, CA 91109

Radiowave phase scintillation caused by propagation through the solar wind is an important–sometimes limiting–noise process for many radio science observations. Spacecraft measurements of phase scintillation are considered here in this "scintillation-as-noise" context, rather than as a diagnostic of the interplanetary medium. The objective is to quantify this noise process for use in experiment feasibility studies and in error budget construction.

Measured S- and X-band radiowave phase scintillation on both "one-way" (spacecraft-to-earth) and "two-way" (earth-spacecraft-earth, where the spacecraft coherently transponds the uplink signal) are presented here in terms of the fractional frequency fluctuations they impose on the radio link. These Allan variance measurements are given as functions of sun-earth-spacecraft (elongation) angle. Phase noise is dominated by charged particle scintillation at S-band; observations at X-band, made sufficiently far from the sun, also have a significant contribution from the troposphere. Using X-band (Mars Observer and Mars Global Surveyor) data taken in the antisolar hemisphere, the different transfer functions of solar wind and tropospheric phase scintillations to two-way data can be used to decompose, approximately, the total phase variability into separate contributions from plasma and troposphere. The resulting plasma scintillation levels agree with independent dual-frequency spacecraft measurements and the tropospheric noise levels are consistent with those determined independently from water vapor radiometers.

The data can be modeled to predict propagation noise levels in the ecliptic for high-precision radio science and radio astronomy investigations as a function of elongation angle. As an example of a limiting case, spacecraft Doppler searches for gravitational waves are conducted when the spacecraft is near solar opposition to minimize plasma scintillation noise. The propagation noise budget for the Ka-band Cassini gravitational wave experiment will be presented. In particular, the plasma scintillation noise level for this experiment (two-way Ka-band observations at elongations greater than 160^o) will have a level $\sigma_y(\tau = 1000\ sec) \approx 9 \times 10^{-16}$.

J1-8
16:20

VLBI PHASE SCINTILLATIONS DUE TO THE SOLAR WIND

S. R. Spangler* R. L. Mutel
Department of Physics and Astronomy
University of Iowa
Iowa City, IA 52242
M. Bondi F. Mantovani
Istituto di Radioastronomia del CNR
Via Gobetti 101, 40129 Bologna, Italy

When a VLBI interferometer observes a compact radio source through the solar wind, there are phase fluctuations due to interplanetary turbulence. These phase fluctuations become larger in amplitude as the solar elongation is decreased. Using the theory of these phase scintillations, one can extract information on the spectrum of plasma density fluctuations and the speed of the solar wind. In a previous study (S. R. Spangler and T. Sakurai, *Astrophysical Journal*, **445**, 999-1016, 1995) we measured these phase scintillations and used them to determine the heliocentric distance dependence of C_N^2, the normalization constant of the interplanetary density power spectrum. Knowledge of this coefficient and the functional form of the density power spectrum allow one to predict the strength of radio wave scattering for any line of sight through the solar wind. This previous study indicated that C_N^2 varied about the mean relationship, presumably due to nonuniformity in the solar wind. In this paper we present subsequent, improved observations of VLBI phase scintillations. The observations were made with radio telescopes of the Italian Istituto di Radioastronomia at Medicina and Noto, and antennas of the European geodynamics array at Matera (Italy) and Wetzell (Germany). Observations were made in three sessions in September and October 1998. Two of the sessions involved simultaneous observations at S and X band (13 and 3.6 cm wavelength); the third session consisted of 5 GHz observations with only Medicina and Noto. Sources were observed at solar elongations ranging from 5.6 to 16 degrees, allowing the solar wind to be probed over a range of heliocentric distances. The quality of the phase scintillation data is excellent. Preliminary analyses show that the a priori model for $C_N^2(R)$, where R is the heliocentric distance, provided accurate predictions for the new observations, to at least a factor of two. This corroborates our model for radiowave scattering in the inner heliosphere, and permits us to proceed to an analysis of the variations about this mean scattering law. The existing data also permit retrieval of the solar wind speed. We will present our values for the solar wind speed as a function of heliocentric distance, and compare these wind speed measurements with those obtained by independent techniques.

J1-9
16:40

THE FREQUENCY DEPENDENCE OF VLBI PHASE SCINTILLATIONS

R. L. Mutel* S. R. Spangler
Dept. Physics & Astronomy
University of Iowa
Iowa City, IA, 52242
M. Bondi F. Mantovani
Istituto di Radioastronomia del CNR
Via Gobeti 101, 40129 Bologna Italy

A plane wave which propagates through a layer of turbulent plasma suffers phase and amplitude fluctuations caused by the changes in refractive index along the path. An interferometer can be used to measure the statistical properties of the resulting phase fluctuations, which in turn are related to the spatial spectrum of turbulent plasma fluctuations. In this paper we discuss the wavelength dependence of the phase structure function, which in standard scattering theory is expected to have a simple quadratic dependence. During September and October 1998 we used four elements of the European VLBI Network to measure the phase structure function of several compact extragalactic sources whose lines of sight passed within 15 degress of the solar disk. The sources were observed simultaneously at 13 and 3.6 cm wavelength. We applied the same delay-rate solutions for each coherence time (3 min) to the visibility data for both wavelengths. We then compared the residual phase fluctuations on short (2 sec) timescales at both wavelengths for each three minute scan.

We found that although there was a high correlation between phase fluctuations at the two wavelengths, the predicted wavelength scaling was inconsistent with theory: The 13 cm phase fluctations almost always larger than predicted based on scaling the 3.6 cm phases by the wavelength ratio. The excess phase at 13 cm has both a short timescale and a long timescale component of comparable amplitude. We will discuss this unexpected result along with some possible explanations.

J1-10
17:00

TIME SERIES ANALYSIS OF INTERPLANETARY PHYSICAL QUANTITIES FOR DISCRETE SOLAR MODES

David J. Thomson* Louis J. Lanzerotti Carol G. Maclennan
2C-360
Bell Labs
Murray Hill, NJ 07974

We report and summarize here our research related to the multitaper time series analysis of charged particle and interplanetary magnetic field data from the Ulysses and several other interplanetary spacecraft in the heliosphere beyond 1 AU. We have previously reported that a significant body of charged particle data was shown to exhibit evidence for discrete, high Q, modes that were attributed to solar acoustic (p-mode) and gravity (g-mode) mode, five minute to many hour period, oscillations (Nature, 1995). More recently, we have carried out a statistical study of interplanetary magnetic field (IMF) data from the Ulysses spacecraft at several heliosphere locations during its first orbit of the sun. Our findings include (1) the spectra of the IMF data contain many peaks that are too large to be random fluctuations; (2) the fluctuations in the spectra are unlike those expected from random data; (3) the filtering of the IMF data at the frequencies given by us in the Nature paper yield phases that are linear in time over more than a year, in the ecliptic plane and post Jupiter; (4) histograms of differences between frequencies that were estimated from IMF data over the south solar pole (Dennison and Walden, 1999) and those from our Nature paper (acquired predominantly near the ecliptic plane) have a null near zero; that is, there are fewer close matches than would be expected if the data were completely random, thus implying a systematic difference that is likely a result of real physical effects; (5) Echelle plots made from high resolution IMF data in charged particle propagation "channels" (Buttighofer, 1998) show $\sim 135\mu$Hz peak spacing, characteristic of solar p-modes (although the time duration of the channels is insufficient to allow identification of individual modes). Analysis of low-energy electrons propagating from ACE (at the L1 point) to Ulysses (at 5 AU) shows the process to be primarily linear. There have been important challenges to these conclusions, often on the basis that the interplanetary medium can be characterized as random and chaotic. We summarize and discuss in this talk our results to date, address a number of the objections to our conclusions, and discuss the implications of the results for the transfer of energy from discrete solar modes to and through the solar corona and into the heliosphere.

STAR WARS 2002: EFFECTS OF SOLAR ACTIVITY ON EM HIGH-TECH SYSTEMS AND REMEDIATIONS

William E. Gordon
Rice University
Houston, TX

There will be a war with many battles between our star, the Sun, and the engineers who defend society from the impacts of a hostile Sun. The year 2002 is just beyond the current maximum of the sunspot number and is the time when the Sun's weapons are most active. Adding to the war's intensity is the deregulation in the USA of the electric power industry which is creating longer distribution lines more susceptible to overloads by induced currents from the upper atmosphere.

The Sun nurtures us with heat, light, - all the energy we consume - and provides the beauty of a sunset or an aurora, and we think kindly of these. But the Sun also has a violent side. Solar flare radiation and coronal mass ejections impact communications, navigation, and electric power distribution grids and other long line systems. The violent activity is readily observed in x-ray, optical, magnetic, and radio observations of the Sun and its solar wind.

Remediation of the impacts requires a better understanding of the Sun and the space weather it feeds, a fully developed observing system from the ground and from satellites, models and forecasts, timely warnings, and an authority to act when a major impact is imminent

Remediation of the effects of space weather is one of the grand challenges of the next decade.

HIGH-RESOLUTION MICROWAVE RADIOMETRIC IMAGING – UNIQUE VIEWS OF THE HYDROLOGICAL STATE

Dr. Albin J. Gasiewski
NOAA Environmental Technology Laboratory
Boulder, CO

Remote sensing of geophysical processes involving water in its various phases is increasingly important to weather and climate forecasting, agriculture, and transportation. Passive microwave sensing plays a key role in hydrological observation due to the wide range of interactions of microwaves with natural media. Using appropriate microwave frequencies, measurements of ocean surface wind fields, rain cell structure, soil moisture, and vegetation cover can be made. High-resolution microwave imaging using airborne radiometers allows unique views of the hydrological state at spatial scales comparable to the natural scale of convection, specifically, at scales that are approximately a factor of 10-100 times smaller than those available using satellite microwave sensors. The use of fully polarimetric imaging techniques further facilitates the observation of hydrological features by providing additional independent data. The lecture will summarize past work in airborne passive microwave imaging at sub-mesoscale spatial resolutions, and focus on recent high-resolution conically-scanned polarimetric imagery of microwave thermal emission over severe weather, including hurricanes and maritime convection. The application of such data to the design of new passive microwave imaging sensors - both airborne and spaceborne - will be discussed.

GENETIC ALGORITHMS IN ENGINEERING ELECTRO-MAGNETICS: CONCEPT, IMPLEMENTATION AND APPLICATIONS

Yahya Rahmat-Samii
University of California, Los Angeles
Los Angeles, CA 90095-1594, U.S.A.
Tel: 310 206 3847, Fax: 310 206 8495, e-mail: rahmat@ee.ucla.edu

GA Concept: Since the last decade of the previous millennium, Evolutionary Optimization (EO) techniques have been applied with growing applications to the design of electromagnetic systems of increasing complexity. The recent popularity experienced by EO methods is not unique to the field of electromagnetics; in fact, EO techniques have been successfully applied to problems in fields ranging from engineering to economics and artificial intelligence. Among various EO's, Genetic Algorithms (GA) have attracted much attention. GA schemes are finding popularity in electromagnetics as optimization design tools and problem solvers because of their versatility and ability to optimize in complex multimodal search spaces applied to non-differentiable cost functions with discrete paramerizations.

GA Implementation: Relying on Darwin's original thoughts, it has been argued that life in this world in all its diverse and amazing forms was evolved by natural selection and natural adaptation processes controlled by the survivability of the fittest species. With this acceptance has come the temptation that perhaps one might be able to utilize nature's "selection and adaptation implementation engine" and apply it to the solution of engineering problems via the applications of Genetic Algorithms (GAs). In a few words, the machinery of Genetic Algorithms utilizes an optimization methodology which allows a global search of the cost surface via the mechanism of the statistical random processes dictated by the Darwinian evolutionary concept (Y. Rahmat-Samii and E. Michielssen, *Electromagnetic Optimization by Genetic Algorithms*, John Wiley, 1999). In this presentation, some of the key features of Genetic Algorithms are summarized in an innovative and illustrative fashion and then they are applied to facilitate the optimum design of a class of electromagnetic and antenna structures.

GA Applications: One of the aim of this plenary presentation is to provide the URSI community with an up to date body of knowledge on the application of GA techniques to the synthesis and optimization of electromagnetic systems. Specifically, this talk will focus on: (a) engineering introduction to Genetic Algorithms by reviewing simple GAs and their standard terminology and operators (populations, parents, children, chromosome, selection, crossover, and mutation), (b) demonstration of the potential application of GAs to a variety of electromagnetic engineering designs including microstrip antennas, multi-band and wideband antennas, synthesis of non-planar radar absorbing materials for RCS applications, Luneburg lens antenna design, synthesis of reflector antennas, design of photonic bandgap structures, etc, and (c) by assessing the advantages and the limitations of the technique.

Chairpersons: D.C. DeGroot, NIST (degroot@boulder.nist.gov)
P.A. Blakey, Motorola (peter.blakey@motorola.com)

A2-1
14:00

CHARACTERISATION OF FERRITE BEADS USING A COAXIAL MONOPOLE ANTENNA AND SIMULATED ANNEALLING OPTIMISATION USING PARALLELISED FDTD

S. A. Saario J. W. Lu D. V. Thiel*
Radio Science Laboratory, Faculty of Engineering,
Griffith University, Nathan Campus
Nathan QLD 4111, Australia

A novel method for characterising ferrite materials at microwave frequencies is reported. We have calculated and measured the input impedance of a monopole antenna with a ferrite bead around the outer conductor of the in-line coaxial feed cable for various positions along the cable.

The varying bead position causes an antenna impedance variation which is directly dependant on both the bead properties (including μ, ε, σ and the physical dimensions of the bead). A forward modeling optimisation technique is used to determine the material properties ($\varepsilon_r, \sigma, \mu, \sigma^*$). Initial experiments proved the concept is viable although further work is required to improve the model accuracy and program efficiency.

The simulations were based on the Finite Difference Time Domain (FDTD) method, with Perfectly Matched Layer absorbing boundary conditions. The FDTD code runs in parallel on a heterogeneous network of workstations running Linux and MPICH.

The feed cable used in the experiments is RG-402 type semi-rigid coax with an outer diameter of 3.58mm. The bead materials considered were *ECCOSORB* MF-116, MF-117 and MF-124, produced by Emerson and Cuming. The beads were machined to thicknesses of 31.5mm, 25mm and 15mm respectively. A tight fit over the cable was necessary to reduce error in the experimental results. The simulations were based on a circular cross section cable modeled with a staircase approximation. This extends the work previously reported by Saario et. al (Electronic Letters (S. A. Saario et. al., *Electronics Letters*, **33**, 1359-1360, 1997.

A comparison of the experimental and numerical optimised results demonstrate that the ferrite beads reflect the RF currents in the shield in a manner dependent on the electrical properties and mechanical size of the bead. Experimental results confirm the characteristics obtained from bead simulations and additional optimisation results will be presented.

A2-2
14:20

RADIATION EFFICIENCY OF LIQUID DIELECTRIC RESONATOR ANTENNAS

S. G. O'Keefe*
School of Microelectronic Engineering
Griffith University
Nathan
Brisbane, QLD 4111 Australia
S. P. Kingsley
Dept. of Electronic and Electrical Eng.
University of Sheffield
Mappin St.
Sheffield S1 3JD UK

Dielectric resonator antennas (DRAs) have become popular, especially at microwave frequencies, due to their high efficiency and compact size. Recently DRAs have been examined as antennas for specific applications at HF/VHF frequencies (S.P. Kingsley and S.G. O'Keefe, Beam steering and monopulse processing of probe-fed dielectric resonator antennas., IEE Proc. Radar, Sonar & Nav., 1999, 146, 3, p121). For experimentation at HF/VHF frequencies, the use of liquids as the dielectric has also been demonstrated as having certain advantages (S.G. O'Keefe & S.P. Kingsley, HF/VHF dielectric resonator antennas., Sixth Symposium on Antennas, Sydney 1999, p24). For example the interior of the DRA can be easily accessed to adjust the feeding probe, there are no airgap problems and the antenna may be tuned by adjusting the level of the dielectric. Often higher frequency scale models of the HF/VHF antennas are built and a liquid dielectric that gives moderate efficiency at the scale frequencies is required.

This paper presents measurements of the radiation efficiency of binary liquid mixtures having variable relative permittivities. One of the two liquids is chosen to be water with an Er value about 80 and the other is chosen to have a much lower Er, around 2, and to be miscible with water. By combining the two liquids in different proportions the binary mixture can quickly be arranged to have any value of Er between the two limits to suit the experimental needs. The purpose of this paper is to report on how the radiation efficiency of binary liquid varies with the mixture ratio. Two liquids were chosen for the measurements, based on their good radiation efficiency found in previous experiments, and these are TetraHydraFuran (THF) and Dioxan. Efficiency was measured by the Wheeler cap method applied to a cylindrical DRA on a ground plane in the HEM11d mode.

A2-3
14:40

MICROWAVE PERMITTIVITY MEASUREMENTS OF DIELECTRIC FILMS BY USING TDR

R. Nozaki and J. Obrzut
Polymers Division, NIST
Gaithersburg, MD 20899

We have developed a time domain reflectometry (TDR) test technique to characterize the dielectric properties of thin films. The test specimen consists of two-layer circuitry and contains thin film capacitors for termination of the 7 mm co-axial-air line as well as a number of microstrip resonators with the corresponding co-planar terminations.

Most of the difficulties in measuring the dielectric constant of thin films at higher frequencies arise because the dielectric thickness of the specimen is much smaller than the wavelength being used. Moreover, with a high value of the dielectric constant, the characteristic impedance of the specimen becomes very low, which causes the reflection coefficient to approach $\Gamma \approx 1$. For such low impedance, the usual calibration standards become unreliable.

To solve the problem, appropriate coaxial and non-coaxial terminations have been designed and built along with the test pattern. This approach allows for improvement of the dynamic range of the measurements necessary for thin film capacitors. The test specimen can be fabricated by using photolithography.

We evaluated several polymer composite films with thickness of 10μm to 50 μm and bulk dielectric constant up to 40. The materials were prepared by loading polymer resins with ferroelectric ceramics. One of the significant advantages of TDR over the frequency domain techniques is that it can cover a fairly wide spectral range using a simple compact test pattern. Unlike other techniques, TDR can provide information about the dielectric behavior from the total reflection in the presence of a large charging response. Therefore, it is our believe that TDR may have wider applications as a convenient test method for dielectric constant and loss measurements of thin dielectric films that find applications in fast electronics and microwave devices.

A2-4
15:00

EQUIVALENT CIRCUIT DESCRIPTIONS FOR OSLT VECTOR NETWORK ANALYZER CALIBRATION STANDARDS

Donald C. DeGroot, Kristopher L. Reed, and Jeffrey A. Jargon
National Institute of Standards and Technology
325 Broadway, Mail Stop 813.01, Boulder, CO 80303 USA
Tel: (303) 497-7212 | Fax: (303) 497-3970 | E-Mail: degroot@nist.gov

The majority of vector network analyzer (VNA) users rely on equivalent circuit descriptions as the sole means of defining their calibration standards. In doing so, they also rely on the instrument manufacturer's error analysis to include the measurement uncertainty due to the limitations in the equivalent circuit descriptions. Although the manufacturers provide brief descriptions and derivations of the equivalent circuit parameters, there is limited information on the complete derivation of standard descriptions.

Since we need to include a full Open-Short-Load-Thru (OSLT) calibration in our time-domain measurement software and for our nonlinear device measurement system, we derived an equivalent circuit model for OSLT calibration standards starting from a general description of waveguides and impedance transformations (R. B. Marks, *Journal of Research of the National Institute of Standards and Technology*, **97**, 533-561, 1992). We present a derivation of our model as a reference, and compare our method to the calibration of a commercial VNA. In doing so, we provide a tool for evaluating measurement uncertainty related to the approximations made in the equivalent circuit approach.

To compare our method with existing algorithms, we performed an OSLT calibration on a commercial VNA and acquired corrected data from four 2.4 mm verification artifacts. Immediately following these measurements, we collected uncorrected data for the 2.4 mm OSLT standards and the verification artifacts. We applied a software implementation of our model to compute the expected S-parameters of the standards, and then used these S-parameters and the uncorrected standard measurements to compute the error coefficients of a 12-term model (D. K. Rytting, *RF & Microwave Measurements for Wireless Applications*, ARFTG/NIST Short Course Notes, 1996.). We corrected the verification device data and compared these data to calibrated measurements made by the commercial VNA.

The figure below shows the results for the magnitude of S_{11} for a 25 Ω Beatty line. Our method agrees well with existing techniques over the 40 GHz bandwidth explored, and for our time-domain application, much better than the anticipated repeatability of our instrument.

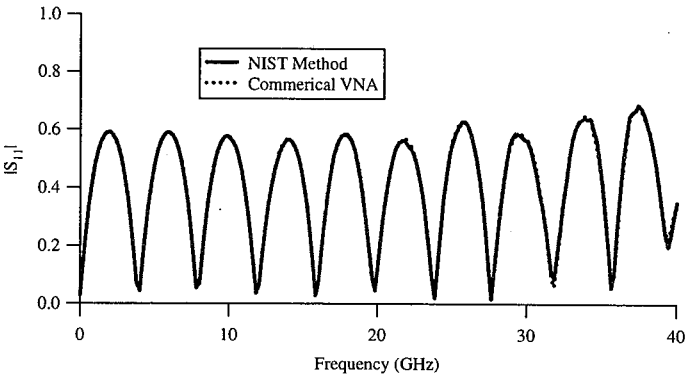

A2-5
15:40

SIX-PORT REFLECTOMETER USING MICROSTRIP THREE SECTIONS DIRECTIONAL COUPLER

E.A.Abdallah, N.A.El-Deeb, H.S.El-Henawy and A.S.Mohra
Electronics Research Institute, EL-Tahrir St., Dokki, Cairo, Egypt

Abstract

The six-port reflectometer is an alternative to the network analyzer, it is a simple device that does not need high precision components and requires only power meters in order to measure complex impedances. There are different configurations of the six-port reflectometer, one of which is that constructed from four directional couplers which was first described by Gottfreid (S.Gottfreid IEEE-IM-22, PP.325-330, 1973), but it was suitable to be built from forward couplers not backward couplers. After that some improvements were done by Hill (L.D.Hill et al , IEE, Vol.132, No.2, 1985).

The approach adopted for the six-port reflectometer design, in this paper, relies on the use of microstrip three sections backward couplers depending on the fact that their imperfections are accounted for by calibration prior to use. An analysis of this circuit was done using the coupling and transmission relations. After some derivations three equations for power ratios were obtained. To make these equations similar to that of six-port technique (G.F.Engen et al, IEEE, IM-21 PP.470-474,1972), there were three solutions which depend on the variations of the interconnection lengths between couplers and terminations at coupler terminals. The system is arranged so that it has two sliding short circuits adjusted at a certain positions, matched load and fixed short circuit at four ports of the system while the other ports are connected to the I/P, DUT and four power meters. The six-port reflectometer system was simulated by IE3D (Zeland software Inc.) and gives good agreement with the theoretical data.

The six-port reflectometer was realized on RT/Duroid ($\varepsilon_r = 6.15$ H=0.025") at 4 GHz as center frequency. The system was calibrated using a method of a matched load and three different positions of a sliding short circuits which was first described by (EL-Deeb, IEEE MTT-31, PP.509-514 1983), but this method is optimized to give the intersection points of the three circles (which represented by the three power ratios) in a simple numerical method. It was then used to measure different unknown terminations and good agreements with the results using vector network analyzer was found with an error that does not exceed 2% in magnitude and 5° in phase in the range of 2-6 GHz.

A2-6
16:00

WIDE BAND THREE SECTIONS DIRECTIONAL COUPLERS

E.A.Abdallah, N.A.El-Deeb, H.S.El-Henawy and A.S.Mohra
Electronics Research Institute, EL-Tahrir St., Dokki, Cairo-Eygpt

Abstract

The three sections coupler is a three quarter wavelength coupler with an end to end symmetry. The coupled signal travels in the direction opposite to that of the input signal and therefore, these couplers are often referred to as "backward coupler". The analysis of TEM-mode couplers of more than one section leads to long and complicated expressions. The problem is simplified somewhat when one recognizes that the TEM-mode coupler is analytically similar to the quarter-wave transformer (G.Matthaei et al, Artech house book, 1980), but the quarter wave-transformer requires a low reflection in the operating band, while the coupler requires sizable specified and nearly constant reflection coefficient across the operating band.

Here the analysis of the three sections coupler is readily carried out by taking the advantages of the four fold symmetry of the structures. We choose excitations, so that there are two symmetry planes aa and bb corresponding to an electric wall or a magnetic wall. Since the three sections coupler is symmetrical, one has to determine two-even mode and two odd-mode impedances, so that its physical dimensions and the S-parameters can be determined. The S-parameters were not uniform around the center frequency for both maximally flat or chebyshev specified ripple. So, a change of the electrical lengths of the center, and outer sections leads to a uniform performance that happened when the increase in center section length is equal to the decrease of the outer section together, but this causes a shift in the center frequency. A curve fitting process was done to obtain that shift in frequency with error not exceeding 2%. A three section coupler and single section coupler with coupling coefficient of -15 dB were design on RT/Duroid (ε_r = 6.15, H=.025") and simulated by IE3D(Zeland software Inc.) and then fabricated. The measured S-parameters for the three sections coupler give broader bandwidth and good isolation, reflection and transmission compared with that of single section coupler.

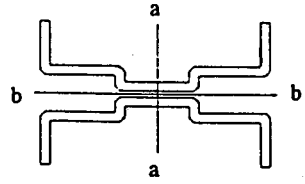

Session C2, 13:35 PM-Thurs., Room 150

SIGNAL PROCESSING FOR ESTIMATING AND EXPLOITING PROPAGATION EFFECTS

Chairpersons:D. Thomson, Lucent Technologies (djt@research.bell-labs.com)
Brian Sadler, Army Research Labs (bsadler@mail.arl.mil)

C2-1
13:40

MATCHED-FIELD SIGNAL PROCESSING FOR OVER-THE-HORIZON HF RADAR

Jeffrey L. Krolik
Department of Electrical and Computer Engineering
Box 90291
Duke University
Durham, NC 27708

Over-the-horizon radar (OTHR) employs the refractive nature of HF skywave propagation through the ionosphere to achieve wide-area surveillance of targets at megameter ranges. And although signal processing for OTHR has typically been developed assuming either single-path or resolved multi-path propagation, in fact, unresolved multipath propagation is often a dominant feature. Matched-field processing (MFP) methods use a computational propagation model which exploits unresolved multipath to improve radar performance. In this paper, two different MFP methods are discussed: (1) matched-field estimation of aircraft altitude, and (2) matched-window processing for mitigating spread-Doppler clutter. Multi-dwell matched-field altitude estimation (MFAE) works by modeling the changes in the coherent, but unresolved, direct and surface reflected target returns from dwell-to-dwell. In particular, the pattern of rapid shape changes due to aircraft motion, seen as fading of the complex radar return in delay-Doppler space, are strongly dependent on aircraft altitude. Using a raytrace multipath propagation model to predict rapid fading, and first-order Markov modeling to handle slow fluctuations due to target aspect changes and medium fluctuations, a maximum likelihood estimate of aircraft altitude is developed. Real and simulated radar data indicates an altitude accuracy of better than 3000 ft at ranges out to 2300 km can be achieved. The second problem addressed here concerns a technique for mitigating ground clutter which is spread in Doppler due to unresolved micro-multipath propagation through a disturbed and moving ionospheric layer. Since aircraft are discriminated from clutter by their non-zero Doppler, mitigating Doppler-spread clutter is critically important. In this paper, techniques for estimating the Doppler spreading sequence are discussed, including an approach which uses a thin phase-screen model for ionospheric propagation. Using these estimates, Doppler windows are designed which are matched to the aberration. Matched-window processing is shown to provide as much as a 10 dB improvement in sidelobe levels with realistically simulated radar data.

C2-2
14:00

COHERENT SIDE-BAND CANCELERS IN MULTITAPER SPECTRUM ESTIMATES

David J. Thomson*
2C-360
Bell Labs
Murray Hill, NJ 07974

While multitaper estimates of power spectra, coherences, spectrograms, etc., are now in common use, most implementations control bias by either truncation or adaptive weighting. Coherent sidelobe cancellation gives improved bias control, significantly so in some cases, and this talk describes the method and gives some performance bounds and examples. Let x_n be a finite set of N samples from a conceptually infinite sequence

$$x_t = \int e^{i2\pi ft}\, dX(f)$$

where the integral is over the Nyquist band and attempts to estimate the statistics of the spectral generator $dX(f)$. (*e.g.* the spectrum, $S(f)df$ is $\mathbf{E}\{|\mathbf{dX(f)}|^2\}$.) In multitaper analysis one chooses a bandwidth W, and computes the eigencoefficients

$$y_k(f) = \sum_{n=0}^{N-1} e^{-i2\pi fn} v_n^{(k)}(N,W) x_n$$

for $k = 0, 1, \cdots, \lfloor 2NW \rfloor$ where the $v_n^{(k)}(N,W)$ are Slepian sequences. It may be readily shown that $y_k(f)$ is a convolution of the Slepian function $V_k(f)$, the Fourier transform of $v_n^{(k)}(N,W)$, with $dX(f)$. We identify the contributions of $dX(f)$ to this convolution from frequencies further from f than the bandwidth W as exterior bias. Although the Slepian sequences have the best energy concentration properties possible in the bandwidth W, the sidebands of the higher-order functions can cause significant bias in estimated spectra. Most multitaper estimates either choose K somewhat lower than $2NW$ or use an adaptive weight, $\hat{x}_k(f) = d_k(f)\, y_k(f)$ where $d_k(f)$ is found by a process similar to Wiener filtering. In coherent sideband canceling, one estimates the spectral generator by the free-parameter expansion

$$d\hat{X}(f) = \sum_{k=0}^{K-1} \hat{x}_k(f-\xi)\, V_k(\xi)$$

for $|\xi| < W$, then estimates the exterior bias by convolving $d\hat{X}(f)$ and $V_k(f)$ *with the range* $(-W, W)$ *omitted from the convolution integral.* This estimate of then subtracted coherently from $y_k(f)$. The process is iterated, and it can be shown that the bound on the exterior bias for the order-k term is reduced from $O(1-\lambda_k)$ to $O((1-\lambda_k)^3)$. This allows considerably more accurate spectrum estimates to be formed when the range of the spectrum is large.

C2-3
14:20

MULTITAPER ESTIMATES OF POLARIZATION AND RELATED QUANTITIES

David J. Thomson*
2C-360
Bell Labs
Murray Hill, NJ 07974

Studies of propagation and advanced communications systems often require estimates of polarization and related quantities in a multipath fading environment. The procedures used to make such estimates usually are those of McPherron *et al.*, Means, and Samson, all dating from the 1970's However, in common with most statistical procedures from that era that deal with time series, they are statistically inefficient. In this talk I discuss multitaper versions of these estimates and some new estimates.

Given a set of N data vectors, or snapshots, $\vec{x}_t$, from a P-dimensional process, taken at times $t = 0, 1, \cdots, N-1$ one computes the eigencoefficients at a frequency f as

$$\vec{y}_k(f) = \sum_{t=0}^{N-1} e^{i2\pi f t} v_t^{(k)}(N, W)\vec{x}_t$$

where $v_t^{(k)}(N, W)$ is the Slepian sequence of bandwidth W and $k = 0, 1, \cdots, K-1$, where $K = \lfloor 2NW \rfloor$. The covariance matrix at frequency f may then be estimated by

$$\mathbf{C(f)} = \sum_{\mathbf{k=0}}^{\mathbf{K-1}} \vec{\mathbf{y}}_\mathbf{k}(\mathbf{f})\vec{\mathbf{y}}_\mathbf{k}^\dagger(\mathbf{f})$$

from which the usual estimates may be made. A better procedure is to view $\vec{y}_k(f)$ as a $K \times P$ matrix and compute its singular value decomposition $\mathbf{U}\sigma\mathbf{V}^\dagger$ directly for each frequency. Here the standardization of the eigenvectors given in (J.C. Samson and V. Olson, *Geophys J. R. astr. Soc.*, **61**, 115-129, 1980) so that $\Re\{V_p\}'\Im\{V_p\} = 0$ is useful because, if the states represent plane waves, $\Re\{V_p\}$ and $\Im\{V_p\}$ are the coordinates or the major and minor axes of the polarization ellipse. The p^{th} left eigenvector, $U_{k,p}$, represents via

$$z_p(t) = \sum_{k=0}^{K-1} v_t^{(k)}(N, W)\, U_{k,p}$$

the common time evolution of the state, while the corresponding right eigenvector $V_{j,p}$ gives its spatial configuration. A time-frequency-component method is also discussed and illustrated with Ulysses interplanetary magnetic field data.

C2-4
14:40

DOUBLE-FREQUENCY COHERENCE WITH APPLICATIONS TOWARDS THE DETECTION, CHARACTERIZATION, AND ENHANCEMENT OF SEISMIC SURFACE WAVES

F. L. Vernon, III*
Institute of Geophysics and Planetary Physics, 0225
University of California at San Diego
La Jolla, CA 92093

Multitaper spectral estimates combine weighted spectral estimates from a number of differently tapered versions of a given signal to yield a spectral estimate. The tapers are the prolate spheroidal series and are optimized to minimize leakage from outside the desired band. The individual tapers are orthogonal and therefore also provide statistically independent estimates of the spectra, which can be used to construct error estimates. In the double-frequency coherence technique, we calculate coherences not only between two signals, but also between different frequencies. This is a way to compare signals that had common frequency dependencies not resolvable by standard coherence estimates. If the double-frequency coherence of a single signal with itself is calculated, the result is unity where f1 = f2 but yields a value between 1 and 0 elsewhere, which shows the amount of coherence between different frequencies. For a dispersive signal, coherence between neighboring frequencies is high.

Tests of the algorithm on simple synthetic signals help to illustrate the method. The phase function of the signal can also be extracted from the complex representation of the coherence. The variance of the phase is inversely proportional to the coherence and therefore it is important to interpret the phase only where the frequencies are highly coherent. For a sweep signal, the phase difference between adjacent Nyquist frequencies is small and is straightforward to unwrap. Integration of this function yields an estimate of the phase function of the signal.

A powerful feature of the double-frequency coherence algorithm is the ability to identify relationships between different frequency components that are invisible to standard coherence estimates. In one example, results from the double frequency coherence from one signal which is frequency translated versions of the another signal as produced by a Doppler shift or a differing dispersion path will be presented.

The fundamental information which can be extracted via the double-frequency coherence algorithm is the amplitude-frequency-phase relationships of any dispersive signal. Using this information, the signal can be filtered to enhance the coherent frequencies. After calculating the coherence, we rebuild the signal keeping only the coherent frequencies and rejecting frequencies with low coherence.

C2-5
15:00

TIME-FREQUENCY ANALYSIS OF PROPAGATION IN THE MARINE SURFACE LAYER

Stephen Doss-Hammel* Carl Zeisse
D858
SPAWAR Systems Center
53560 Hull St
San Diego CA 92152

For problems in naval ship self-defense it is important to predict the nature of infrared signals propagated horizontally near the ocean surface. Over a near-surface pathlength of 20 kilometers, such a signal can be modified by three prominent processes: extinction, refraction, and scintillation. In this paper we address the measurement and prediction of scintillation effects in the marine surface layer.

The basis of this work is a set of field transmission measurements from a two week exercise in September 1998. A blackbody transmitter and a receiver were positioned at the ends of a 7 kilometer propagation path close to the ocean surface at San Diego roads (outside San Diego Bay). The beam intensity was measured at 400 Hz every 20 minutes throughout the test to capture scintillation effects for a variety of meteorological conditions.

In the analysis of this data, our emphasis is on the detection of two signature quantities: the variance of the scaled log-intensity signal, and a characteristic frequency of the variations in signal intensity that is based upon the Fresnel zone size. This Fresnel frequency is correlated with the location of the onset of the Kolmogorov power-law scaling regime.

We will show the results of an analysis of this data based upon wavelet transforms and filtering. The use of wavelet-transformed passbands makes it possible to define an observable scintillation frequency (the Fresnel frequency) which is broadband in the Fourier domain. It is also possible to predict the Fresnel frequency quite simply by measuring the path-transverse windspeed divided by the Fresnel zone size. We discuss a comparison of the observed 'Fresnel' frequency with the prediction based on data collected on a meteorological buoy positioned at mid-path.

The results support our thesis that the Fresnel frequency and the log-intensity variance might be used as signature characteristics.

C2-6
15:40

VIRTUAL REAL-TIME ENVIRONMENTAL DATA ACQUISTION SYSTEMS

F. L. Vernon, III*
Institute of Geophysics and Planetary Physics, 0225
University of California at San Diego
La Jolla, CA 92093
D. Harvey D. Quinlan
Boulder Real-Time Technologies
2045 Broadway, Suite 400
Boulder CO 80303

The most striking characteristic of the global distribution of environmental monitoring stations is it's incredibly heterogeneous nature. Many agencies from many countries support the complex infrastructure it represents. These different agencies have a range of missions from seismic monitoring to detailed hazard assessment at local levels. They are all unified, however, by the common type of data they collect. The problem of real-time data telemetry from seismic environmental stations to a primary data collection center is being solved in a variety of ways in response to each network's specific mission and based on unique hardware, communication systems, number of stations, and areal coverage requirements. While each individual network may have different missions and use different types of equipment and communications to telemeter data from their stations to the data collection center, all network data centers have one thing in common: access to the Internet. Based on this existing infrastructure we can consider the possibility of a new scale of environmental observations by a widely distributed user community through the integration of all accessible real-time data.

Starting at the end of 1998, a feasibility test was conducted for real-time data integration from multiple disparate seismic networks to create a "Virtual Seismic Network" (VSN) using the Antelope Real Time Software. In this test, data from the IRIS GSN network, the PASSCAL Broadband Array, four US regional networks (University of Alaska, UC Berkeley, UC San Diego, and University of Nevada, Reno), and the Kyrgyzstan National Broadband Network were integrated into one common data processing system. This test was quite successful, demonstrating that over 150 seismic stations from seven different primary data collection centers could be accessed through the Internet and processed in real-time. The level of processing accomplished during this test included standard real-time functions that have been performed by individual network operators for more than 20 years: data assembly, automated phase picking, event location, and display of event location and magnitude information. The concepts used in the VSN are generalized and have been used to incorporate disparate real-time data sources and other data types including infra-sonic arrays, hydroacoustic arrays, and weather data into integrated processing systems.

C2-7
16:00

LASER BEACONS FOR ON-ORBIT IR SENSOR CALIBRATIONS

F. L. Vernon, Jr.*
Photonics Technology Department, M2-246
The Aerospace Corporation
Los Angeles, CA. 90009-2957

Satellites are normally fabricated to high levels of precision and thoroughly tested in the laboratory before launch. However, after launch the satellite environment undergoes drastic changes which can vary through different parts of the orbit. This can affect the ability of the satellite instrumentation to function in the manner intended by the original design. This is particularly true for surveillance satellites whose purpose,in part,is to accurately pinpoint events which occur at or near ground level. After launch, many different functions of the satellite system can be checked. These include line-of-sight calibration, end-to-end system functional check, calibration of signal intensity, focal plane vector table accuracy, ground location resolution, diurnal variation, star sensor back-up and saturation signal levels.

The infrared laser beacon has proven to be useful as a diagnostic and calibration tool for on-orbit satellite infrared sensors. Short optical wavelengths have the inherent advantages of easily obtainable, high directivity with the consequence that relatively low power levels from the laser can be utilized to test a variety of satellite functional characteristics. However, these advantages must be weighed against the detrimental effects of the atmosphere on laser propagation. For example, scintillation effects can cause detected power fluctuations whose variance is a factor of five or more. Also, in certain parts of the atmospheric spectrum the transmission windows are very narrow and can be highly dependent upon certain atmospheric constituents (such as water vapor) in various wavelength ranges.

These issues will be discussed in the context of laser wavelength, modulation format and power requirements. This presentation will briefly cover beacon design criteria and limitations such as those imposed by the atmosphere as well as available laser sources and beam directors.

E3-1
13:40

THE HISTORY OF RADIO NOISE STUDIES AT THE DOC BOULDER LABS

Robert J. Matheson
NTIA/ITS.M
325 Broadway
Boulder, Colorado 80303

A. D. Spaulding spent his whole technical career in Noise Studies at the Boulder Labs. I spent much time there also, designing the noise measurement equipment that provided the numbers that Spaulding used in many of his studies.

The CRPL noise measurement program was aimed at providing global noise maps for frequencies between 15 kHz and 20 MHz. This data provided an estimate of radio noise received on a vertical antenna as a function of frequency, location, time of day, and season of the year. A chain of 16 noise ARN-2 noise measurement stations was directed from Boulder by a group headed by C. W. Critchlow, kicked off by an initial year of operation during the IGY. This network operated for ten years, and provided the baseline world data for CCIR Report 322 and others.

Noise measurements moved into higher frequencies (up to 250 MHz). At the higher frequencies, there was only short range propagation, and the noise came mostly from local manmade sources. An elaborate mobile measurement laboratory was developed that could move with traffic to examine noise sources like a highway full of cars or move to the site of other local sources. Geographical noise contour maps were developed for cities and military receiving sites.

Much of Spaulding's later noise work moved into a study of the uses of more detailed noise statistics like APD's and wide dynamic range tape recordings to recover more detailed statistical information. Detailed information on noise statistics was necessary to design specialized receivers that overcame much of the effect of noise. Spaulding got deeply into statistical communications theory and optimal receiver design from all sides of the topic. He was involved with testing complex receivers intended to overcome the effect of noise (e.g., for submarine communications), but also worked with using noise to protect communications from a determined interceptor (e.g., Tempest).

E3-2 14:00 DON SPAULDING'S CONTRIBUTIONS TO RADIO NOISE AND SPECTRUM OCCUPANCY MODELING

George H. Hagn, Consultant
4208 Sleepy Hollow Road, Annandale, VA 22003-2046

Dr. A. Donald (Don) Spaulding contributed greatly to the International Union of Radio Science (URSI) Commission E. He provided leadership as the first Vice Chair and the second Chair of U.S. URSI Com. E, and he gave many excellent papers on noise and interference. This paper summarizes his major modeling contributions as we honor him today.

As a summer student at the Institute for Telecommunication Sciences (ITS), Don helped Bill Crichlow scale data from the worldwide network of ARN-2 atmospheric noise measurement stations deployed during the International Geophysical Year (IGY). Thus began a career-long involvement in the study of radio noise. These data were used to create the first worldwide maps of effective antenna noise figure (Fa) in CCIR Report 322 (1964). Don developed the conversion of Vd measured in a 200-Hz bandwidth to other bandwidths of interest. He did not allow for overlapping noise impulses and thus greatly overpredicted Vd for the larger bandwidths! He later used the empirical relationship of Herman and deAngelis (1983). He also updated the worldwide noise maps of Fa for 1 MHz using data taken after the IGY for CCIR Report 322-3 (1986), now used in many LF, MF and HF system performance models.

In the late 1960s, Don became involved in studies of man-made noise with Robert Disney of ITS. They measured noise in the band 0.25-250 MHz and grouped their data into categories of business, residential and rural for modeling purposes. The parameters modeled were Fa and Vd, and the resulting model was reported in CCIR 258. This empirical model also is included in many system performance models. It currently it is under review as Don had recommended in his last ITS report. He developed a method of combining noise power from different sources to model the composite noise environment. Don also developed (with me) models for the worldwide maximum and minimum levels of noise from all sources, expressed as Fa, for the band 0.1 Hz to 100 GHz. This work became CCIR Report 670 (1982).

In the 1970s, Don began a long collaboration with Dr. David Middleton, his thesis advisor, on statistical-physical models of radio noise that were canonical (not ad hoc) with utility for predicting the performance of digital modems in non-Gaussian noise. They applied these models to optimizing the detection of signals with low signal-to-noise-ratio (SNR) by measuring the noise and characterizing it in a manner from which they could derive an optimum nonlinearity to place in the signal path before detection. The result was a locally-optimum Bayes detector. Don fitted the Class A (narrowband) and Class B (wideband) models to numerous APD data sets to deduce the model parameters required.

Don's work also involved assisting the government spectrum managers. He was tasked by the Office of Telecommunications Policy in the Executive Office of the President to review man-made noise and his report, "Man-made Noise: The Problem and Recommended Steps Toward Solution," earned him the Department of Commerce Silver Medal. He also became involved in the study of spectrum occupancy, and this led him (with me) to define occupancy as a random variable. This work became CCIR Report 825.

E3-3
14:20

ATMOSPHERIC NOISE AT ELF/VLF

A. C. Fraser-Smith
STAR Laboratory
Department of Electrical Engineering
Stanford University
Stanford, CA 94305-9515

Naturally-occurring ELF/VLF radio noise (frequencies in the range 3 Hz to 30 kHz) at most locations on the Earth is impulsive in nature, consisting of a series of impulses called 'sferics', of greatly varying amplitude, from the lightning occurring in thunderstorms around the world. Unlike the situation at higher frequencies, this ELF/VLF noise is not well modeled as a Gaussian random process, due to the contributions from nearby lightning, which produce large impulses in the noise waveform. As a result, the noise consists of a series of high amplitude impulses superimposed on a background that approximates low-level Gaussian noise.

At high latitudes two other forms of ELF/VLF noise are sometimes observed: polar chorus and auroral hiss. These two forms of noise can be very strong on occasion but they are not always present and there can be extended intervals when they are not observed at all. As a result, even at high latitudes, the general statistical properties of the noise are dominated by sferic activity, as is the case at lower latitudes.

A number of different statistical quantities are used to quantify this noise. For example, mean or median amplitudes are often used, as are amplitude probability distributions (APD's), the so-called 'voltage-deviation' (V_d), which is a convenient measure of the spikiness of the noise, and the effective antenna noise figure (Fa). The first numerical values for this latter statistical quantity at ELF/VLF frequencies were derived by A. D. Spaulding and G. H. Hagn (e.g., pp. 177–182 in *Proceedings: Effect of the Ionosphere on Space and Terrestrial Systems*, U.S. Gov. Printing Office, 1978). These were the only numerical values available for a number of years but recent measurements by the author's group at a variety of locations around the world supplement the earlier data and confirm their accuracy.

E3-4
14:40

Wideband Model of HF Atmospheric Radio Noise

John J. Lemmon
Institute for Telecommunication Sciences
U.S. Department of Commerce
325 Broadway, Boulder, CO 80303

Motivated by the application of spread spectrum technology and digital signal processing techniques to high frequency (HF) communication systems, advanced HF systems that operate over wide bandwidths (on the order of 1 MHz or more) are being developed. Since many uncertainties exist concerning the performance of such systems, it is important to have channel models for theoretical predictions of system performance and for laboratory measurements of system performance using channel simulators.

New wideband models of HF skywave propagation and of manmade noise and interference have been discussed by *Vogler* and *Hoffmeyer* [1993] and by *Lemmon* [1997], respectively. These models were developed for implementation in a channel simulator. The noise and interference models are therefore models of the noise and interference waveforms that are combined with the desired signal in a channel simulator.

This paper describes a wideband waveform model of received atmospheric noise in the HF band (3-30 MHz). Cumulative probability distributions of the noise envelope are derived and shown to be in good agreement with a large database collected from a wide range of noise environments. The model parameters are related to the voltage deviation parameter V_d (the dB difference between the rms and mean values of the noise voltage envelope) and the mean noise power measured at the terminals of a lossless, short monopole antenna, which have been specified for various geographic locations, times of day, seasons, and frequencies by *Spaulding* and *Washburn* [1985] and by the *CCIR* [1986]. These relationships therefore enable one to determine specific values of the model parameters for various environments.

The model includes correlations in the waveforms that simulate the burst structure of measured atmospheric noise. Unlike Gaussian noise, the characteristics of atmospheric noise are a function of receiver bandwidth. The bandwidth dependence of the voltage deviation parameter, which parameterizes the impulsiveness of the noise, shows behavior that is qualitatively similar to a limited amount of measured data.

E3-5
15:00

NATURAL NOISE ABOVE 50 MHZ

Ernest K. Smith
ECE Department
University of Colorado
Boulder, CO 80309-0425

My association with Don Spaulding was a little different than most. From 1958 to 1976 I was actively involved with CCIR Study Group 6 (ionospheric propagation). Report 322 (atmospheric noise below 50 MHz), in which Don Spaulding had been actively involved, held an honored position. In 1976 my attention shifted to Study Group 5 (propagation in non-ionized media) and I was immediately aware that a complementary text: "natural noise above 50 MHz" would be a useful adjunct. I set about organizing such a text for SG 5, which, in due course, became Report 720 (natural noise above 50 MHz).

Most natural noise above 50 MHz (a convenient limit for the F2 MUF) is of extraterrestrial origin up to about 2 GHz. The sun is the exception as it is a significant emitter at any frequency. Above 2 GHz noise will be primarily from thermal emission from absorbing gases in the atmosphere - by Kirchoff's law a gas emits energy in the same amount as it absorbs. Additional noise emitted from the ground or sea may be picked up by antenna sidelobes.

Obtaining noise due to gaseous absortion requires a radiative transfer program. I was at JPL at the time and Joe Waters had such a program and was willing to guide me through it. This was the source of the curves found in Report 720 (E.K. Smith, Radio Sci., **17**, 1455-1464, 1982).

For the galactic contribution I approached Richard Wielebinski, director of the Max Planck Institut fur Radioastronomie at Bonn, FRG. He agreed to provide galactic maps from the Bonn survey smoothed to 5 degrees for incorporation in Report 720.

E3-6
15:40

VHF Man-Made Radio Noise

Roger Dalke and Robert Achatz
Institute for Telecommunication Sciences
Boulder, CO 80303
(303) 497-3109
rdalke@its.bldrdoc.gov

Man-made noise is an important consideration in the design and implementation of wireless communication systems. Typical sources of man-made noise in the VHF and UHF bands include automobile ignition systems, electric motors, power systems, and a wide variety of electronic equipment such as computers, switching devices and microwave ovens. In 1974, Spaulding and Disney presented results from many years of measurements of man-made radio noise. They devised methods for estimating the noise power and noise amplitude statistics that need to be accounted for in the design of radio systems. More recently, new noise measurement methods using modern digital signal processing methods have been employed by the Institute for Telecommunication Sciences to measure man-made radio noise.

This presentation provides an overview of man-made radio noise that affects VHF space-to-earth satellite links. The noise statistics presented include recent measurements made by the Institute for Telecommunication Sciences as part of a link analysis for the broadcast of digital satellite weather images at 137 MHz. The motivation for the measurements was that published man-made noise statistics are probably outdated because they are based on measurements made more than two decades ago. Since that time, technological advances have changed man-made noise emissions. For example, automotive emissions have been reduced, while emissions from other sources such as unregulated electronic devices (e.g., computers, switching devices) and other electrical equipment such as electric motors have probably increased substantially. The measured data show that there have been significant changes in the character of man-made radio noise in the VHF band that can significantly affect space-to-earth satellite links. The conclusion being that new noise models and noise environment characterizations are required to adequately predict performance of VHF satellite links.

E3-7 16:00 A. D. SPAULDING AND F. G. STEWARTS' METHOD FOR COMBINING THE COMMON THREE SOURCES OF RADIO NOISE AT HF

David B. Sailors
Science and Technology Corporation
10 Basil Sawyer Drive
Hampton, VA 23666-1340

The technique described by Spaulding and Stewart (A. D. Spaulding and F. G. Stewart, NTIA Report 87-212, January, 1987) for combining the values of radio noise from multiple sources is described. The results calculated for each of the radio noise sources (i.e., atmospheric, galactic, and man-made) are combined assuming that each of the noise sources are log-normally distributed. The method used determines the log-normal distribution that best approximates the true distribution of the sum of the radio noise sources. For this the distribution function, the moment generating function for the *i*th radio noise source for the mean is given by the expectation value

$$\alpha_i = \mathrm{EXP}\left(\frac{\mu_i}{c} + \frac{\sigma_i^2}{2c^2}\right).$$

The corresponding moment generating function for the variance is given by

$$\beta_i = \alpha_i^2\left(\mathrm{EXP}\left\{\frac{\sigma_i^2}{c^2 - 1}\right\}\right).$$

The constant, c, is given by 4.34294; and μ_i and σ_i are the mean and standard deviation of the *i*th radio noise source. Since the three log-normally distributed processes are independent, the mean, α_T, and variance, β_T, for the combined radio noise are given by

$$\alpha_T = \sum_{i=1}^{3} \alpha_i \text{ and } \beta_T = \sum_{i=1}^{3} \beta_i .$$

The overall median value F_{am}, the upper and lower deciles, D_u, and D_l, of the radio noise are found using this process. The process begins by first determining the median value, the upper decile, the lower decile, and the prediction errors for each radio noise source. Since the standard deviation σ_i equals the decile value divided by 1.28, separate sums, α_T and β_T, are found first using the upper decile value for each source and second using the lower decile for each source. For a log-normal distribution, the mean is given by $\mu_T = c\left(\mathrm{LN}\{\alpha_T\} - \frac{1}{2}\beta_T / c^2\right)$ and the variance is given by $\sigma_T^2 = c^2\,\mathrm{LN}\left(1 + \beta_T / \alpha_T^2\right)$. The overall median value F_{am} is given by μ_T using the sums, α_T and β_T, found from the upper decile values for the noise sources. The upper decile D_u is found using the sums, α_T and β_T, found using the source upper decile values. Similarly, the lower decile, D_l, is found using the source lower decile values.

Spaulding and Stewart also modified how the radio noise prediction errors (σ_{Du}, σ_{Dl}, and σ_{Fam}) are calculated. The calculation of σ_{Fm} was simplified from earlier methods but still produces an acceptably accurate result. The new method of determination of σ_{Du} and σ_{Dl} requires the determination of six partial derivatives of each of D_u and D_l with respect to the source deciles and median values.

E3-8
16:20

Digitally Modulated Radio Link Performance in UHF Man-Made Noise

Robert J. Achatz and Roger A. Dalke
Institute for Telecommunication Sciences
Boulder, Co. 80303
www.its.bldrdoc.gov

Man-made noise measurements at UHF frequencies were recently performed by the Institute of Telecommunication Sciences (ITS). These measurements are necessary to determine the effect UHF man-made noise has on digitally modulated radio link performance. The ITS recently completed similar measurements and analysis at VHF frequencies (Achatz, Lo, Papazian, Dalke, and Hufford, NTIA Report 98-355, 1998), (Achatz and Dalke, *Proc. of 1998 RAWCON Conf.*, Colorado Springs, Co., Aug. 1998).

Noise power measurements were collected for 24 hours (or more) at 402.5- and 761.0-MHz in two residential and two urban locations during the spring and summer of 1999. Such long duration measurements allowed for correlations of noise power with cultural rhythms such as working hours. The measurement receiver noise floor was approximately 2-dB above kT_0b where k is Boltzman's constant, T_0 is 288K, and b is bandwidth. A Gaussian shaped, 30-kHz 3-dB bandwidth filter limited the measurement bandwidth prior to digitization. Independent noise power samples were digitized once every millisecond.

Several results which may impact the performance of a digitally modulated radio link were drawn from the measured data. First, the mean noise power was close to the measurement system noise floor at most locations and frequencies. The one exception to this was at one urban location at 402.5-MHz where mean noise power fluctuated on a hourly basis from 2 to 10-dB above kT_0b. Second, non-Gaussian noise was present in all urban locations and frequencies. Peak noise power was 10 and 20-dB above the peak power that would be expected for Gaussian noise with the same mean power at 402.5- and 761.0-MHz, respectively.

Third, non-Gaussian noise was absent at most residential locations and frequencies. The one exception to this was at one residential location at 402.5-MHz where the peak noise power was 15-dB above the peak power that would be expected for Gaussian noise with the same mean power. Lastly, the highest peak noise power levels were correlated with working hours in most locations and frequencies. The one exception to this was at one urban location at 402.5-MHz where the "quietest" time of day was in the afternoon during working hours.

The noise power measurement system organizes the noise power samples into histograms which represent the first order statistics of the noise random process over a 1-min. time interval. Currently ITS is using these first order statistics to investigate the effect UHF man-made noise has on the performance of a digitally modulated radio link. The results of this investigation will be discussed at the conference.

Session F2, 13:35 PM-Thurs., Room 1B-51
POLARIMETRIC REMOTE SENSING OF SURFACES
Chairperson: D. Trizna, Naval Research Lab. (triznad@ccf.nrl.navy.mil)

F2-1 13:40 **MULTIPLE POLARIZATION DOPPLER RADAR MEASUREMENTS OF COASTAL FRONTS**

Dr. Nicholas Allan and Dr. Dennis B. Trizna
Naval Research Laboratory, Code 7255
Washington, DC 20375
USA

This paper presents X-band Doppler radar observations of small-scale oceanic fronts associated with the flow of fresh water from the mouth of the Chesapeake Bay into surrounding coastal shelf waters. These measurements were made using a high-resolution radar deployed aboard the University of Delaware's R/V Cape Henlopen during the first Chesapeake Bay Outflow Plume Experiment (COPE-I) conducted by the Naval Research Laboratory in September, 1996. Coherent backscatter was obtained for the full scattering matrix (HH, VH, HV and VV) by transmitting and receiving on different ports of a dual horizontally and vertically polarized antenna configuration. The antenna was either pointed at a fixed azimuth angle to produce Range-Time-Intensity (RTI) images of the sea surface or rotated continuously to produce Plan-Position-Indicator (PPI) images. The radar has sufficiently high resolution to resolve wave profiles so that RTI images for vertical transmit – vertical receive (VV) backscatter, clearly portray the trajectory of waves as they propagate through the radar footprint. RTI images for horizontal transmit - horizontal receive (HH), however, are spiky and are indicators of wave breaking. By overlaying corresponding RTI images for both HH and VV, the regions along the wave profile that are breaking are determined. This procedure is carried out at different spatial areas across water mass boundaries to determine wave propagation parameters and degree of wave breaking. PPI images are used to determine the azimuth dependencies of the scattered signals. In addition, since the radar footprint covers a larger area as the antenna rotates, this mode is also used to map the frontal shape. These results demonstrate the utility of high resolution multiple polarization radars for remotely sensing important parameters associated with regions of wave-current interaction.

F2-2
14:00

THE DEPENDENCE OF BACKSCATTER INTENSITY ON LOOK DIRECTION AND POLARIZATION OBSERVED IN DUAL-POLARIZED, REAL-APERTURE RADAR IMAGES OF OCEANIC FRONTS

Mark A. Sletten, Elizabeth Twarog
Code 7200, Naval Research Laboratory,
4555 Overlook Ave SW, Washington DC 20375

David J. McLaughlin
University of Massachusetts, Amherst MA

In May 1997 and May 1999, the Remote Sensing Division of the Naval Research Laboratory conducted phases Two and Five of the Chesapeake Bay Outflow Plume Experiment (COPE2 and COPE5, respectively). In both experiments, an airborne, X-band, real-aperture radar was used to image the outflow plume front that forms in the mouth of the Chesapeake Bay. On an interleaved, pulse-to-pulse basis, both horizontally and vertically polarized imagery was collected. The front was generally imaged from opposite look directions (usually landward and seaward) on alternate aircraft passes, and two incidence angles, 60 and 80 degrees, were also used.

In COPE2, large changes in backscatter intensity were observed for horizontal polarization when the look direction and grazing angle were varied, with the largest across-the-front backscatter contrast occurring at an 80 degree incidence angle when a seaward look direction was used. A striking "step-function" in backscatter intensity was observed under these conditions. Significantly less variation was observed for vertical polarization, regardless of look direction. In COPE5, large contrasts were again observed for horizontal polarization, but the look dependency was in general reversed: larger contrasts were observed when a landward look direction was used. Less variation was again observed for vertical polarization.

In this presentation, these observations will be quantified and an explanation for this interesting behavior will be given. In brief, the explanation involves two main factors: the look and polarization dependencies of breaking water waves, and the generation of breaking waves through the interaction of the wind and the buoyancy-driven outflow current from the bay.

F2-3 14:20 DUAL FREQUENCY POLARIMETRIC CALIBRATIONS OF THE NAVAL ULTRAWIDEBAND SYNTHETIC APERTURE RADAR

D. B. Trizna, M. A. Sletten, N. Allan, J. Toporkov
Remote Sensing Division, Code 7255
Naval Research Laboratory
Washington, DC 20375-5351
triznad@ccf.nrl.navy.mil

Ray Harris
Metratek, Inc.
Fairfax, VA

J. West
Oklahoma State University
Stillwater, OK

A new multifrequency polarimetric ultrawideband synthetic aperture radar has been developed at the Naval Research Laboratory for use on light aircraft and UAV platforms under ONR funding. Under a Navy SBIR with Meratek, new digital technologies have been employed to allow PC based digital waveform synthesis for pulse waveform generation and high speed digital recording for radar control and data collection. Data acquisition rates of 40 MB/s are accomplished using RAID disc arrays controlled by SHARC DSP processor chips that transfer data directly from A/D converters to the storage medium. The system currently uses dual polarized wideband horns operating from 1-4 and 4-18 GHz to achieve a pulse to pulse polarimetric capability at X and L bands, and additional interleaved bands are possible using the high data acquisition rate. A series of calibration experiments were performed in the spring of 1999 using a combination of ground based dihedrals and trihedrals of different sizes and with different geometrical aspects to allow polarimetic calibration to be accomplished from flight data. As the transmitted chirped 2 μs waveform and polarization can be affected by reradiation from the aircraft components and multipath from other land scatterers using an experimental setup wit the aircraft on the ground, calibration of the system using such an arrangement are virtually impossible. Thus, overflights of the target calibration field are the only practical approach to polarimetric calibration. A new Chirp Scale SAR processor was developed for data analysis based on descriptions in the literature, including motion compensation using either differential GPS or a Litton 100G INS/GPS system. Results of overflight calibration experiments are presented, along with imagery of a number of land targets and scenes displayed in a variety of polarimetric formats.

F2-4 14:40 POLARIZATION STATE OF RADIO WAVES DIFFRACTED BY A ROUGH INTERFACE IN A LAYERED MEDIUM

I.M. Fuks and A.G. Voronovich*)
Cooperative Institute for Research in Environmental Sciences, University of Colorado/NOAA, Environmental Technology Laboratory, 325 Broadway, Boulder, CO 80303-3328, Telephone (303) 497-6879; Fax (303) 497-3577; E-mail: <ifuks@etl.noaa.gov>
*)NOAA, Environmental Technology Laboratory, 325 Broadway, Boulder, CO 80303-3328, Telephone (303) 497- 6464; Fax (303) 497-3577; E-mail: <agv@etl.noaa.gov>

The problem of radio wave reflection and scattering from the plane, stratified layer with a statistically rough boundary and interfaces is solved in the frame of the "two-scaled" model - the superposition of small scaled roughness (that assures the diffuse scattering) and large-scale smooth variations of the layer thickness. Using GPS signals for retrieval of the soil or ice parameters can be a possible application.

It is shown that the specular component of a reflected signal after its compression can be represented as a sequence of equidistant pulses that due to reflections from the layer boundaries. Those pulses have the different amplitudes and states of polarization that depend on dielectric permittivity of the layer and the bedding substrate. The multiple reflection from the layer's boundary of right- and left circular polarized incident waves is investigated and it is shown that the amplitude of the second pulse can exceed the amplitude of the first one. The polarization ellipse parameters and even the direction of electrical vector rotation in every order of specular reflection depend on the layer and substrate electrodynamic properties and the angle of incidence.

The diffuse component intensity of a scattered signal is modulated by the interference of reflected and refracted waves that propagate inside the layer. As a result the radio "brightness" of a bedding surface is an oscillation function of incident and scattering angles (or spatial coordinate on the layer upper surface for a finite distance receiver). The spatial period of these oscillations depends on the angle of incidence, the signal wavelength, the layer thickness and its dielectric permittivity. The average scattered signal power and the amplitude of its oscillations depend not only on the layer thickness and the electrodynamic parameters (dielectric permittivity and conductivity) of layer and substrate but also on the long-scale smooth variations of the layer thickness. The radio-brightness distribution maps for linear and circular polarized incident waves (scattered into co- and cross-polarized components) obtained by numerical calculations are presented. These theoretical results can be useful for interpretation of experimental radar data obtained for fresh ice or dry sand layers (the media with the small enough conductivity and decimeter radio wave absorption) subsurface remote sensing with spaceborne probing signals.

F2-5
15:00

DETERMINATION OF SOIL DIELECTRIC CONSTANT USING BISTATIC POLARIZED SCATTEROMETRY

V. U. Zavorotny*
CIRES/University of Colorado/NOAA/ETL
325 Broadway, Boulder, CO 80303
A. G. Voronovich
NOAA/ETL
325 Broadway, Boulder, CO 80303

The remote sensing of different properties of soil (for example, a moisture content) is a practically important task. The determination of soil moisture can be performed with aircraft or satellite microwave radiometry, since the soil thermal emission of the microwave wavelengths (especially at L-band) is sensitive to moisture contents. However, this technique has a relatively coarse surface resolution. Other advanced remote sensing techniques may be more accurate with this respect. Recently bistatic radar systems operating from air-borne or space-borne platforms received an interest for its advantages in remote sensing of land and ocean surfaces. One of the quantities that governs a process of forward bistatic scattering is a surface reflectivity. For obvious reason the soil reflectivity at L-band should be sensitive to moisture content as well.

Among advantages of the bistatic radar systems is a potentially higher surface resolution compared to the passive microwave radiometry. This resolution can be achieved because these systems use the highly stable carrier and coded modulation structure of the illuminating signal that allows time-delay and Doppler-frequency mapping of the surface with high enough resolution. Currently, the signal of GPS is used by NASA researchers for bistatic ocean scatterometry and wind retrieval. Among possible candidates for the sources of opportunity are communication and TV broadcast satellites.

Because a signal reflected from the land could be affected not only by the value of the soil dielectric constant, but also by the surface roughness, the mitigation of the latter factor is required. The method proposed here permits to exclude the effect of surface roughness, withholding only a factor related to the dielectric constant of the subsurface medium. It can be shown that for a rough surface with small slopes (the condition often met in practical situations) the ratio of scattering amplitudes of a plane wave for two different polarization states in the first approximation is independent of roughness. This ratio is the known function of the incidence and scattering angles and the dielectric constant of the medium (see, A. G. Voronovich, *Wave Scattering from Rough Surfaces*, 2^{nd} ed. Springer-Verlag, Berlin, 1999). The same is true for non-coherent components of scattering cross sections. It turns out that the type of polarization is not critical for calculations, so the consideration is applicable for linear as well as for circular, or any other polarization state.

Notice that, when considering cross-polarized components, the method can be applied for bistatic measurements only. Indeed, for monostatic geometry (when wave vectors of incident and backscattered waves are collinear) the scattering amplitude, $S_{VH}(\vec{k}, \vec{k}_0)$, or the non-coherent scattering cross-section, $\sigma_{VH}(\vec{k}, \vec{k}_0)$, turns into zero to the first-order accuracy in slopes. (Here $\vec{k}$ and $\vec{k}_0$ are horizontal projections of the wave vector of scattered and incident waves, correspondingly.)

F2-6
15:40

SPACEBORNE RETRIEVAL OF OCEAN SURFACE WIND VECTOR FIELDS USING MULTILOOK POLARIMETRIC RADIOMETRY: SIMULATION USING THE MAXIMUM LIKLIHOOD METHOD

A.J. Gasiewski[1] and J.R. Piepmeier[2]
[1] NOAA Environmental Technology Laboratory, Boulder, CO
[2] NASA/Goddard Space Flight Center, Greenbelt, MD

Global retrieval of ocean surface wind direction fields can be performed using spaceborne scatterometry, as shown, for example, using the NASA N-Scat and Quickscat scatterometers. Recent theoretical and experimental modeling suggest, however, that a cost-effective alternative could be based on the use of polarimetric microwave radiometry. Using the radiometric method, wind direction is associated with the direction of ocean surface waves, which in turn produce measurable anisotropic variations in the upwelling Stokes vector. Azimuthal variations of 2-3 K amplitude in the first three Stokes' parameters have been measured at incidence angles of ~53°. These variations are the result of a combination of geometrical reflection from asymmetric long-waves, resonant thermal emission from small hydrodynamically-modulated capillary waves, and asymmetrically-distributed ocean foam. Aircraft measurements of these azimuthal harmonic functions using the Polarimetric Scannning Radiometer (PSR), an airborne conically-scanning multichannel radiometer, have become the basis for an empirical mean geophysical model function (GMF) for wind-driven brightness anisotropies.

In this study we use the empirical PSR GMF along with a maximum-liklihood wind vector estimator to develop simulations of the performance of a spaceborne polarimetric wind vector sensor. Variations on the design of the sensor that are tested using the simulation include single- and two-look capability, dual-polarimetric and tri-polarimetric (three Stokes' parameter) capability, and selection of the radiometric channel set. Retrieval error performance compares favorably to the minimum possible variance obtained using the Cramer-Rao bound for a maximum liklihood estimator. Also discussed will be the effects of clouds and convection on the upwelling Stokes vector and their impact on retrieval accuracy. In particular, it is shown using aircraft imagery that the third Stokes' parameters is highly insensitive to the presence of convection.

F2-7
16:00

AIRBORNE OBSERVATION OF THE OCEAN BY A CROSS-TRACK SCANNING KA-BAND POLARIMETRIC RADIOMETER

V. Irisov* L. Fedor B. Patten
University of Colorado/Cooperative Institute for Research in Environmental Science
NOAA/Environmental Technology laboratory
325 Broadway, R/E/ET1, Boulder, CO 80303

A microwave polarimetric radiometer offers the potential for measurement of the sea surface wind vector. This explains an increasing interest on the polarimetric observations of the ocean at various frequencies, viewing angles, and environmental conditions.

The Environmental Technology Laboratory deployed a Ka-band cross-track scanning polarimeter on a Twin-Otter aircraft in the spring 1999. The radiometer measures the first three Stokes parameters which allowed us to utilize the scanning mirror mechanism. Preliminary analysis of the data obtained in the Gulf of Mexico shows important advantages of the cross-track scanning. The variation of brightness temperature as a function of viewing angle is sensitive to the gravity-capillary spectrum of the surface waves and can be used to retrieve such a spectrum. A wide range of observation angles allowed us to measure the down-welling radiation from an atmosphere along as well as the oceanic up-welling radiation. This is very important for excluding the effect of scattered atmospheric radiation from the ocean surface radiation. At the same time, angular observations of the homogeneous atmosphere give an excellent opportunity to calibrate the radiometer. These factors allowed us to achieve a high accuracy of the absolute measurement of the brightness temperature and determine the emissivity of the ocean surface.

The observations were made in near-calm conditions when the effect of the sea surface roughness on the emissivity in Ka-band is relatively small. Under such conditions an adequate model of a sea water dielectric permittivity is especially important because the uncertainty of the dielectric constant exceeds the accuracy of the radiometric measurements.

F2-8
16:20

PRELIMINARY OBSERVATIONS OF POLARIMETRIC SEA SURFACE EMISSION MEASURED FROM A PIER

F. Wang S.J. Frasier* E.J. Knapp J.R. Carswell C.T. Swift
Microwave Remote Sensing Laboratory
University of Massachusetts
Amherst, MA 01003

MIRSL deployed a Ka-band Polarimetric Radiometer operating at 36 GHz from the seaward end of a small research pier located at the UMass Center for Marine Science & Technology (CMAST) in New Bedford, MA. The pier extends approximately 50 m into Clark's Cove adjacent to New Bedford harbor. The radiometer was placed on a rotatable mount located on the seaward corner of the pier. During this deployment it was possible to observe emission at three incidence angles, 45°, 55°, and 65°, and at four azimuth angles spanning 90° in 30° increments. An X-band Doppler scatterometer was co-located with the radiometer to measure the instantaneous wave field. The purpose was to permit cross-spectral analysis of radiometric emission measurements with radar measurements of surface wave orbital velocity, similar to numerous historical measurements of the radar Modulation Transfer Function.

During this experiment we were able to measure time-series the first 3 Stokes parameters, T_H, T_V, and U, emitted from a small spot on the surface. For the U measurement, we employed a ferrite polarization switch at the throat of the horn antenna. In one state, the radiometer measured T_H and T_V, while in the other, it measured T_{+45} and T_{-45}. We performed two types of measurements: Scans and Time-series. For Scans, we made two-minute observations at 4 azimuth angles for each of the 3 incidence angles (12 positions total). For Time-series, we observed a single incidence and scan angle for 17 minutes, switching between radiometer modes at 30 second intervals.

We observed expected behavior of the mean values of T_V and T_H with incidence and scan angles. We observed opposite sensitivities to the wave field in T_{+45} and T_{-45} when scanning off the wind direction. To the left of upwind, one's modulation by waves increases while the other decreases, and vice versa to the right upwind. We also observed a large signal swing on these channels off the wind direction, likely a consequence of the short, relatively steep gravity waves. Since U is the mean value of the difference of these signals, it is relatively easy to observe how the asymmetry of the surface waves play a role in defining the U signal.

F2-9
16:40

THE ACTION OF THE OCEAN DISTURBANCES ON SHORT SURFACE WAVES

L.A. Ostrovsky[abc], J.E. Hare[ac], A.V. Smirnov[ac], R.A. Kropfli[c], K.A. Naugolnykh[ac], E.A. Skirta[d], and T.P. Stanton[e]
[a]University of Colorado, CIRES, Boulder, CO, 80303
[b]Institute of Geophysics and Planetary Physics, Los Alamos, NM
[c]NOAA Environmental Technology Laboratory, Boulder, CO, 80303
[d]Department of Mathematics, University of Toledo, Toledo, OH
[e]Dept. Oceanography, Naval Postgraduate School, Monterey, CA

New results concerning the combined *in situ* and radar observations of internal waves and swell during the Coastal Ocean Probe Experiment (COPE) are discussed jointly with theoretical models. Main focus is in the modulation of the short waves due to internal waves (IW). In particular, coastally-driven IWs are observed to modulate the spectral energy of short wind waves responsible to radar returns. These results are complemented by *in situ* measurements from wave gauges. New result is the measurement of frequency range of the damped waves.

Another issue of interest is the action of swell. Swell dynamics has not been investigated as thoroughly as that of wind waves. However, strong swell in coastal zone can play a considerable role in environmental processes such as mixing and particle transport. Due to the relatively regular character of swell remote observation can be a constructive basis for verifying models of current action on short gravity-capillary waves responsible for the radar imagery. The evidence of such interaction between swell and short waves from radar observations and a theoretical model describing the modulation are presented.

There exist numerous theories for the gravity-capillary wave modulation by long wave. The case of swell has some specific features due to its low frequency and small slopes. Two theoretical models of the effect of swell and internal waves on short surface waves are considered. They are: (i) study of the variations of surface wind stress due to the oscillating surface currents, as well as the wind profile variations by the wavy-curved surface profile; (ii) study of adiabatic variations of short waves due to the current of long wave. Neither of these models is completely satisfactory: the former is unable to explain many the data on phase of radar scattering with respect to long wave, whereas the latter works well only for large relaxation times of short wave interaction with the wind. These contradictions imply the application of a cascade model with participation of intermediate scale waves inside of a decimeter-to-meter wavelengths range.

Session G3, 13:55 PM-Thurs., Room 245
GPS AND THE IONOSPHERE
Chairperson: A. Coster, MIT (coster@ll.mit.edu)

G3-1
14:00

THE PROGRESS OF SOLAR CYCLE 23

J. Kunches
Space Environment Center
NOAA
325 Broadway
Boulder, CO 80303-3328

Solar Cycle 23 began in the latter half of 1996 and is currently in its ascending phase. The expectation was that this cycle would follow in the mold cast by the previous few cycles, and become one of the largest in the historical record. A blue-ribbon panel predicted Cycle 23 would surpass Cycle 22 in magnitude (J. A. Joselyn et al., *Eos*, Vol. 78, No. 20, 205, 1997), and as such would become one of the top 3 in the recorded history of sunspot measurements.

The practical side of this scenario meant that navigation systems, such as GPS, would be hampered periodically during the magnetic storms that accompany the strong solar activity that occurs during a large solar cycle. Scintillations and ionospheric total electron content (TEC) irregularities would affect both static and kinematic work, involving single and dual frequency GPS applications. In addition, the mere increase in TEC that occurs during all solar cycles as the EUV output of the sun intensifies, would degrade accuracy for the most precise applications, including Differential GPS.

Now that Cycle 23 is nearing what is believed to be its maximum phase, the performance of the current cycle will be discussed. Climatological data relevant to geomagnetic storms, large x-ray bursts, and energetic proton events, will be presented, with a particular emphasis on those events which are likely to be most problematic for GPS. A look at activity expected during the imminent, peak phase of Cycle 23 will be given.

G3-2 14:20 CHARACTERIZATION OF IONOSPHERIC IRREGULARITIES AT KWAJALEIN USING GPS TEC MEASUREMENTS

S. Close, A. Coster, S. Hunt
MIT Lincoln Laboratory
244 Wood Street
Lexington MA, 02173

The ARPA Long Range Tracking and Instrumentation Radar (ALTAIR) is a dual-frequency radar, operating at VHF and UHF, which supports both missile testing and satellite tracking activities. Dedicating 128 hours per week to space activities, ALTAIR provides metric and radar cross section data in support of the space surveillance mission of the US Space Command. ALTAIR is located at the Kwajalein Missile Range (KMR), which lies near the geomagnetic equator at 3°N latitude. The diverse and highly variable nature of the ionosphere at this equatorial location has, in the past, significantly impacted ALTAIR's metric accuracy and tracking abilities. As a result, the Ionospheric Error Correction Model (IECM) was developed to help alleviate ionospheric effects on tracking. The IECM is a data-driven, ionospheric range and elevation correction algorithm that consists of the Parameterized Electron Content Model (PECM) adjusted by Global Positioning System (GPS) based measurements of the Total Electron Count (TEC). GPS TEC data are used as a real-time data acquisition source to continuously scale the IECM to match actual ionospheric conditions surrounding ALTAIR.

This paper presents specific instances of ionospheric effects as measured by ALTAIR and the corresponding analysis of both the GPS TEC and the data output from the IECM model. GPS TEC data are analyzed to identify the source and location of the ionospheric effect, as well as to determine spatial and spectral characteristics.

Prepared for the Department of the Army under Air Force Contract F19628-95-C-0002. Opinions, interpretations, conclusions, and recommendations are those of the authors and are not necessarily endorsed by the United States Air Force or Army.

G3-3
14:40

DUAL-FREQUENCY GPS SCINTILLATION MEASUREMENTS FROM THULE, GREENLAND

D. S. Coco* C. Coker
Applied Research Laboratories, The University of Texas at Austin
P. Ning
Keo Associates, Hanscom AFB, MA
A. J. Mazzella, Jr.
NorthWest Research Associates, Inc., Bellevue, WA
T. Pedersen
Air Force Research Laboratory/VSBI, Hanscom AFB, MA
E. Holland
NorthWest Research Associates, Inc., Bellevue, WA
G. J. Bishop
Air Force Research Laboratory/VSBP, Hanscom AFB, MA

High-speed (20 Hz) GPS scintillation measurements have been collected from Thule, Greenland using a new GPS scintillation measurement system. This system uses a commercial off-the-shelf GPS receiver (Ashtech Z/Y-12) to collect 20 Hz phase and amplitude measurements, which are used to generate ionospheric scintillation parameters. The Real Time Monitor (RTM) system also simultaneously collects total electron content (TEC) measurements at a slower data rate (maximum 2 Hz) to characterize the background ionosphere. The high-speed measurements include carrier phase (L1, L2) and carrier-to-noise signal amplitude (L1) measurements (C/N0). In the current version of the system, these high-speed measurements are converted in postprocessing to create σ_ϕ and S4 parameters to characterize phase and amplitude scintillation, respectively. Future upgrades to the system, however, will allow this processing to be done in real-time.

This system has been used to collect scintillation parameters from the polar cap region from a station in Qaanaaq near Thule, Greenland during the recent SCOSTEP/S-RAMP International Space Weather Campaign. Scintillation parameters from the RTM system are compared with scintillation measurements from other systems, including the all sky imagers, 250 MHz scintillation receivers, and a single frequency GPS scintillation system, for system verification. One of the main objectives of this experiment was to verify the capability of the receiver to measure scintillation when operating with GPS anti-spoofing (A-S) 'ON' in codeless mode (Z mode) in an environment with strong scintillation. These scintillation data are combined with background ionosphere measurements to develop a comprehensive representation of the polar cap ionosphere during this period.

G3-4 15:00 IMPACT AND MITIGATION OF GEOMAGNETIC STORM (SUBSTORM) EFFECTS ON WADGPS IONOSPHERE MODELING

S. Skone
Department of Geomatics Engineering
University of Calgary
2500 University Dr. NW
Calgary, AB, Canada T2N 1N4

Dual frequency GPS receivers enable the estimation of absolute ionospheric delay and total electron content (TEC) along the signal path. By using a number of reference stations, each equipped with a dual frequency receiver, it is possible to estimate values of the vertical ionospheric delay at a set of designated grid points (in latitude and longitude) on an ionosphere shell. This type of ionosphere delay modeling is employed in wide area differential GPS (WADGPS) networks, where grid accuracies generally depend on the temporal and spatial correlations of TEC. These models can suffer degraded performance in high latitude auroral and equatorial regions, where large spatial gradients (and temporal variations) in TEC are present during periods of enhanced geomagnetic activity.

In this paper, the impact of several geomagnetic storm and substorm events is investigated in the auroral and equatorial regions. Periods of storm activity are identified from ground-based magnetometer data and satellite images. Data from two separate networks are used – twelve auroral and sub-auroral stations in the Natural Resources Canada network, and nine equatorial stations in the Brazilian geodetic network. Two specific issues are addressed: 1) the availability and quality of dual-frequency GPS data, within the network, in the presence of scintillation effects, and 2) the accuracy of ionospheric grid TEC values in the presence of large spatial gradients. The temporal and spatial resolutions (i.e. update intervals, station density) necessary to mitigate storm effects, and satisfy error bounds, are discussed.

G3-5
15:40

IONOSPHERIC RECONSTRUCTION USING GPS

G. H. Van Bavel* A. Brown S. Ganguly
Center for Remote Sensing, Inc
11350 Random Hills Rd, Suite 710
Fairfax, VA 22030

Total Electron Content (TEC) measurements are obtained from ground-based receivers that monitor the transmissions of the Global Positioning System (GPS) satellites. The TEC data can then be used to perform Computerized Ionospheric Tomography (CIT). Ideally, CIT requires a time-independent snapshot of the ionosphere; otherwise, temporal variations in the ionospheric structure degrade the reconstruction. Even with an observing time of one hour, GPS-based measurements typically provide information over a small fraction of any three dimensional region of interest. The geometry of the fixed ground receivers and the moving GPS transmitters produces data that is sparsest in the ionosphere's bottomside (below the F2 peak). Furthermore, the GPS orbital configuration makes the intersection of different transmitter-receiver rays unlikely. These limitations of GPS data inhibit three-dimensional CIT. We have implemented a CIT technique that removes the limitations through the assimilation of ionospheric models and direct ionosonde measurements. The result is a reconstruction scheme that uses GPS TEC data to characterize the topside ionosphere (where its data is most relevant), and ionosonde data to specify the longitudinal and latitudinal variations of the bottomside. We present some reconstructions that demonstrate the improvement in the results when GPS data are enhanced in this way. In order to establish the improvement in a quantitative manner, we first simulate ionosonde and TEC from a known source ionosphere. The simulation is setup over the continental United States. The International Reference Ionosphere is used as the source ionosphere and the actual (physical) GPS configuration is used to simulate the TEC data. A direct comparison of the recovery of the source ionosphere is then possible in the two cases. We also demonstrate the method with real TEC and ionosonde data.

G3-6
16:00

A NEW MODEL FOR RETRIEVING TEC DISTRIBUTIONS FROM GPS MEASUREMENTS

L. Sparks,* B.A. Iijima, A.J. Mannucci, X. Pi, B.D. Wilson
Jet Propulsion Laboratory
California Institute of Technology
4800 Oak Grove Drive
Pasadena, CA 91109

Measurements of the Global Positioning System (GPS) are routinely used to generate maps of the total electron content (TEC) of the ionosphere. We present a new model for retrieving distributions of vertical TEC from slant TEC measurements. Current models typically associate a given slant TEC measurement with a vertical TEC value at a specific latitude and longitude. Such models incur two distinct types of error: (1) error associated with the slant-to-vertical conversion, and (2) error arising from the neglect of horizontal gradients of the electron density along the raypath. A limitation of models that depend upon a slant-to-vertical conversion (e.g., the thin-shell model) is their reliance on a predetermined form for the unknown height variation of the electron density profile. A consequence of neglecting horizontal density gradients along the raypath is that sharply differing estimates of the same vertical TEC value can arise from simultaneous slant TEC measurements at fixed elevation angle but distinct receiver locations.

Our new model assumes that, for each measurement, the horizontal variation of the electron density at any altitude can be expressed as a power series expansion centered about the angle formed by the receiver, the center of the earth, and the point where the raypath crosses a reference height (typically 450 km). A distinctive feature of our approach is the retrieval of multiple distributions of integrated quantities simultaneously from the GPS data, not simply the vertical TEC. Instead of converting each slant TEC measurement to a single associated vertical TEC value, the simplest version of our model treats each slant TEC measurement as a linear combination of integrals of the electron density along raypaths at two or more fixed, fiducial elevation angles. A higher-order version of our model includes terms that provide first-order corrections that account for electron density gradients along the raypath.

G3-7 16:20 TOMOGRAPHIC IMAGING OF THE IONOSPHERE DURING A SOLAR ECLIPSE

L.-C. Tsai[1,2], and W. H. Tsai[2]

[1]Center for Space and Remote Sensing Research, National Central University, Chung-Li, Taiwan
[2]Graduate Institute of Space Science, National Central University, Chung-Li, Taiwan

During a solar eclipse the Moon's shadow, moving at a supersonic (~700 m/s) speed, cuts off solar heating radiation. This results in decreasing the plasma density of the ionosphere particularly in the D, E, and F1 regions. In this paper, ionospheric effects due to the transit of a solar eclipse covered almost all of Asia on 24 October 1995 have been investigated using the Global Positioning System (GPS) ground and occultation link observations.

Measuring the GPS signals from both of ground systems and a satellite receiver in low earth orbit can provide a powerful means of imaging the ionosphere. In the early study of tomographic imaging of the ionosphere, the GPS ground data can provide detailed information on the horizontal structure, but are of extremely restricted utility in sensing vertical structure. In 1993 the University Corporation for Atmospheric Research (UCAR) orbited a GPS/MET instrument (the MicroLab 1 satellite) at an altitude of ~735 km to demonstrate active limb sounding of the Earth's atmosphere and ionosphere using radio occultation techniques. Under the assumption of local spherical symmetry, the measured phases can be processed to yield ray-path bending angles through Doppler-shift analysis, which have then been used to yield profiles of refractive index via the Abel transform. Furthermore, altitude profiles of ionospheric electron density, which are sensitive to small vertical structures of approximately 1.5 km, are derived. We further have implemented a minimization functional of variance in order to regularize the inverse problem associated with three-dimensional ionospheric stochastic tomography. Such results provide considerable information on the large-scale horizontal and vertical structure to monitor the ionosphere.

Acknowledgment The authors would like to thank UCAR for permitting them to use the occultation data.

G3-8
16:40

THE IGS IONOSPHERE WORKING GROUP

J. Feltens

EDS Industrien (Deutschland) GmbH, based at Flight Dynamics Division, ESA, European Space Operations Centre, Robert-Bosch-Str. 5, D-64293 Darmstadt, Germany

Iono_WG Chairman

Abstract. The International GPS Service (IGS) was established in June 1992 as joint project by an international group of institutions. The major intent of the IGS is the provision of high quality global GPS tracking data and GPS products to general users, whereby the different institutions contribute with own tracking sites and/or serve as data centers and/or contribute with products: GPS satellite orbits and clocks, earth orientation parameters, station coordinate solutions, tropospheric models and others. Since some months, the IGS activities were also extended for GLONASS, in a first phase. At the 1998 IGS workshop in Darmstadt, Germany, decision fall to extend the IGS products palette also for the ionosphere.

At its meeting on 28 May, 1998 in Boston, the IGS Ionosphere Working Group (Iono_WG) was then formally established by the IGS Governing Board. The working group's main short-term goal is the routine provision of ionospheric TEC maps with a 2-hours resolution and of daily sets of GPS satellite differential code bias (DCB) values, based on the evaluation of GPS dual-frequency tracking data. The working group's medium- and long-term goals are the development of more sophisticated ionosphere models, also of regional and local extent, with near-real-time and real-time availability. The final target is the establishment of an independent IGS ionosphere model.

The Iono_WG started to work on 1 June 1998 with the pilot phase: IGS Analysis Centers, currently five, deliver since then routinely their ionosphere products to the CDDIS Global Data Center. A first version of a comparison/combination algorithm was worked out and coded. Based on this algorithm routine comparisons of the IGS ionosphere products are performed once per week.

However, the analysis centers use very different approaches in their processing to represent the ionosphere mathematically; this reflects also in the comparison results. Consequently the Iono_WG is now concerned with validations to assess objective values of the quality and accuracy of the individual ionosphere products, in order to achieve a reliable combination scheme. Thereafter it is planned to provide combined IGS ionosphere products to the general user community.

It is the intent of this paper to present the current status of the Iono_WG activities, to provide an overview over the progress achieved so far, and to give an outlook for the future.

G/H1-1
14:00

THE 1999 SPRITES BALLOON CAMPAIGN

E. A. Bering, III* J. R. Benbrook J. A. Garrett A. Paredes
Physics Department
University of Houston, 4800 Calhoun
Houston, TX 77204-5506
E. M. Wescott D. D. Sentman H. C. Stenbaek-Nielsen
Geophysical Institute
University of Alaska
Fairbanks, Alaska
W. A. Lyons
FMA Research, Inc., Yucca Ridge Field Station
46050 Weld County Road 13
Ft. Collins CO 80524

There are several competing models for the production of sprites, jets and elves. It has become clear it is not possible to select between these models using only ground-based data, owing to the fact that the ground shorts out the field signatures of interest. Consequently, a balloon campaign was conducted in June, July and August of 1999. The 1999 Sprite Balloon Campaign conducted three high altitude balloon flights, one from Palestine, Texas and two from Ottumwa, Iowa. Flight 1, an engineering test, was launched from Palestine at 01:14:31 UTC on 7/06/1999 and cutdown at 09:45:00 UTC on 07/06/1999. Flights 2 and 3 flew from Ottumwa at 23:57:30 UTC on 8/14/1999 to 12:35:00 UTC on 08/15/1999 and at 00:39:32 UTC on 08/21/1999 to 11:12:00 UTC on 08/21/99, respectively. The balloons floated at 32 km and drifted westward at ~30 knots. The balloon payloads were instrumented with dual three axis electric field detectors, three axis fluxgate and induction magnetometers, X-ray scintillation counter, Geiger-Mueller tube, upward looking high-speed photometer, vertical current density ammeter, conductivity measurements, and an ambient thermometer. A redundant telemetry scheme provided five orders of magnitude of dynamic range in sensitivity. An event triggered on-board memory sampled 10 quantities at a rate of 50 kHz per channel for 160 ms per event. Ground observations included low light level TV observations from three sites, WIRO, on Jelm Mtn., Wyoming, Bear Mtn. overlook fire tower, South Dakota, and Yucca Ridge, Colorado. Jelm Mountain had a fast photometer and a high speed TV imager. The 3rd flight was the most successful. During this flight, 304 events were recorded in the burst memory. At least half show waveforms that appear to be lightning related. All three ground stations had clear skies. There were two small sprite producing storms, one in eastern South Dakota and one in central Kansas. Perhaps as many as 20 transient luminous events were recorded by at least one station. At least four were recorded by two stations. Two of these were observed at three stations, one of which was observed by an independent fourth site. Multiple site observations of elves was also accomplished for the first time.

G/H1-2
14:20

OBSERVATIONS AT YUCCA RIDGE DURING THE 1999 NASA SPRITES BALLOON CAMPAIGN

W.A. Lyons* T. E. Nelson J.L Eastman
FMA Research, Yucca Ridge Field Station,
Fort Collins, CO 80524
R.A. Armstrong
Mission Research Corp.
Nashua, NH
E.R. Williams
MIT/Parsons Laboratory
Cambridge, MA
D.S. Suszcynsky
Los Alamos National Laboratory
Los Alamos, NM
M. A. Taylor
Utah State University, Logan, UT
Y. Takahashi
Department of Geophysics
Tohoku University
Sendai, Japan
J.R. Benbrook E.A. Bering
Dept. of Physics
University of Houston, Houston, TX

One component of the 1999 SPRITES Campaign was conducted at the Yucca Ridge Field Station, near Ft. Collins, CO, during the months of June, July, and August 1999. The primary emphasis was providing storm forecasting and optical sprite detection during the June and August NASA stratospheric balloon missions conducted by the University of Houston (Gar Bering). On 21 August 1999 Yucca Ridge (along with several other ground stations) observed several lightning-induced mesospheric transient luminous events above storms in South Dakota and Kansas while the NASA balloon was at 32 km over southwestern Iowa. An unusually intense elve was recorded above the Kansas Storm from several locations. VLF and ELF information were also obtained. This marks the first coordinated optical measurements by ground and balloon-borne sensors. A new record for sprites from a single storm occurred on the evening of 4-5 June 1999. At least 750 sprites were recorded using low-light imagers during a three-hour period above a large MCC in central South Dakota. Sprite frequencies as high as 15 per minute were noted. The storm, which may have been influenced from smoke from western wild fires, attained positive CG percentages as high as 80% at times. On 18 August 1999, a massive MCC formed as predicted over Colorado and moved slowly eastward into Nebraska. It produced extremely bright sprites, some of which were visible to the naked eye at 500+ km. Most sprites were recorded by several low light imagers and a 1000 fps high speed image intensified camera. Moreover, some of the sprites were also captured on monochrome and color conventional CCD cameras. This storm also produce clear evidence of a feature being termed a "troll," a distinct jet-like structure emanating from near the cloud tops and propagating upwards to about 50 km at speeds in excess of 100 km/s, apparently along the trail of a preceding sprite tendril. For a number of sprites, additional narrow band photometric measurements of first-positive, second-positive and first negative nitrogen emissions were also obtained. Detailed cloud-scale modeling of sprite-producing storms is also underway in order to learn more about the interactions of storm dynamics, microphysics and electrification.

G/H1-3
14:40

FURTHER EXAMINATION OF THE TEMPORAL ASSOCIATION BETWEEN POSITIVE CLOUD-TO-GROUND LIGHTNING STROKES AND SPRITE OCCURRENCE USING BROADBAND ELF/VLF SFERICS MEASUREMENTS

S. C. Reising*
University of Massachusetts
Amherst, MA 01003
U. S. Inan T. F. Bell
Stanford University
Stanford, CA 94305

Broadband ELF/VLF measurements of sferics at Palmer Station, Antarctica, show that the ELF "slow tails" of sprite-associated sferics have large electromagnetic energy in relation to the slow tails of non sprite-associated sferics at a range of ~12,000 km (Reising et al., *Geophys. Res. Lett. (GRL), 23*, 3639, 1996) The ELF slow tail measurements can be used to infer the moments of the cloud-to-ground (CG) charge transfer occurring on ~1-3 ms time scales (Cummer and Inan, *GRL, 24*, 1731, 1997; Bell et al., *GRL, 25*, 1285, 1998) Broadband sferics measurements at Yucca Ridge, Colorado, have shown that removal of a large amount of positive charge (~100 C) from a thundercloud results in sprite occurrence within 15 ms after the positive CG. On the other hand, removal of a smaller amount of charge (~10-50 C) from cloud to ground may lead to sprite occurrence >50 ms later (Bell et al., 1998). In the latter case, it has been suggested that subsequent horizontally extensive intracloud currents following the positive CG may be involved in sprite production (*e.g.* Lyons, *J. Geophys. Res., 101*, 29,641, 1996).

Detailed studies of over 175 sprites produced above mesoscale convective systems (MCSs) in the Great Plains during three different years examined the characteristics of those broadband ELF/VLF sferics emitted by positive cloud-to-ground lightning associated with sprite occurrence (Reising et al., 1996; Reising et al., *GRL, 26*, 987, 1999). Broadband ELF/VLF measurements show that for each of these MCSs, ~95-97% of sprites occurred within ~300 ms after a positive CG, as documented by a sferic emitted by each CG. Measurements at ~500 km range from the MCS show that a few percent of sprites occurred without a preceding CG, and instead were *followed* by a positive CG, within ~300 ms. In the present study, we analyze the sferics associated with 98 sprites measured optically above an MCS during a ~2.5-hour time period, in order to further understanding of the characteristics of the total lightning discharges leading to sprite production.

G/H1-4
15:00

LIGHTNING DISCHARGES, EARLY/FAST VLF EVENTS AND SPRITES

U. S. Inan* M. P. Johnson T. F. Bell
STAR Laboratory, Stanford University, Stanford, CA 94305

In spite of the wealth of new data that has become recently available, many aspects of the electrodynamic coupling between lightning discharges and the overlying mesosphere/lower ionosphere are not yet understood, especially in terms of the sustained effects that may accompany the luminous transient events such as sprites and elves. In particular, the physical mechanisms underlying the so-called early/fast VLF events remain in dispute, with potentially important implications concerning sustained (i.e., quiescent) ionospheric effects of thunderstorms on a global scale. The nature of the conductivity changes exhibited in early/fast events may be due entirely to elavated levels of electron temperature modulated by individual discharges or due to enhanced ionization accompanying sprites and/or elves. Although presence of channels of enhanced ionization within sprites is now evident, especially in view of recent telescopic observations, the spatial size or distribution of these columns is not consistent with the observed properties of early/fast VLF events. The resolution of some of these issues may lie in the nature of the lightning discharges that lead to early/fast VLF events and/or sprites. Lightning discharges that lead to sprites have been shown to have a particularly intense continuing current component with accompanying enhanced ELF sferics energy [Reising et al., *Geophys. Res. Lett., 26*, 987, 1999]. New evidence is now emerging [Johnson and Inan, *Geophys. Res. Lett.,* , in review, 1999] that early/fast VLF perturbations may be exclusively caused by lightning events which consist of a burst or cluster of tens of closely spaced discharges lasting from several hundred milliseconds to several seconds. In this paper, we document some of the properties of these types of causative discharges, and present new data and insights on the relationship between early/fast VLF events and sprites.

G/H1-5
15:40

NON-UNIFORM IONISATION OF UPPER-ATMOSPHERE DUE TO ELECTROMAGNETIC PULSE FROM A HORIZONTAL LIGHTNING DISCHARGE

M. Cho*
Department of Electrical Engineering
Kyushu Institute of Technology
Kitakyushu, JAPAN 804-8550
M. J. Rycroft
International Space University
Illkirch, France 67400

The effect of horizontal lightning discharge on ionisation of upper-atmosphere above thundercloud has been studied by computational simulation. The computer simulation solves Maxwell's equations via Finite Difference Time Domain method with the electronic conductivity which varies self-consistently with the time-variation of electron density due to ionisation. The simulation assumes a horizontal source current with a finite length at a given altitude between $3km$ and $10km$ and the current oscillates sinusoidally with a certain frequency from $20kHz$ to $150kHz$.

The effects of oscillating frequency, height, amplitude, duration and spatial length of the source current are studied by the simulation. The simulation results show that when the discharge current oscillates with a frequency of $30kHz$ or higher, ionisation occurs non-uniformly on the horizontal plane at the height near $80km$ with local peaks in the electron density. The non-uniformity is caused by interference of electromagnetic waves radiated by the discharge current, the wave reflected from the ground, and the wave reflected from the ionosphere. The interference also occurs by the wave radiated from different parts on the discharge path which is comparable or longer than the wavelength of interest, $< 10km$.

The local peaks in the electron density locally enhance the electrical conductivity and lowers the bottom of ionosphere as if stalactis develop downward. If the lightning discharge removes sufficiently large positive charge from thundercloud through the continuing current, quasi-static field from the remaining negative charge might induce downward streamer from the tip of the stalactis where the static electric field is geometrically enhanced. The present simulation works display the bridging mechanism between eleves and sprites which many times occur from the same parent lightning.

G/H1-6
16:00

HORIZONTAL LIGHTNING CURRENTS AND SPRITES: EVIDENCE AND PREDICTED SIGNATURES

Steven A. Cummer*
Laboratory for Extraterrestrial Physics
NASA/GSFC
Greenbelt, MD 20771
Mark Stanley
Department Physics
New Mexico Tech
Socorro, NM 87801

Sprite models are beginning to converge into agreement with many aspects of sprite observations. However, there remain observations that indicate unmodeled and unobserved large-scale lightning processes may contribute significantly to sprite generation, most notably for "dancing sprites" and sprites that are significantly delayed (>50 ms) from the apparent causative lightning discharge. Recent high speed video and electromagnetic observations suggest that horizontal lightning charge motion plays a role even in sprites delayed less than 10 ms from the causative discharge [*Cummer and Stanley, GRL*, in press, 1999]. To investigate further the possible contribution of horizontal currents to sprites, we model the relationship between lightning current and sprite current with fully electromagnetic finite difference simulations. The relationship between these quantities is understood analytically [*Pasko et al., GRL*, 3493, 1998] and limits the sprite current that can flow in response to a lightning discharge of a given magnitude. We compare the simulations to observed sprite charge moments and vertical lightning charge moments. Preliminary results indicate that for some particularly energetic sprites, the mesospheric electric field required to drive the observed sprite currents is significantly larger than would be produced by the observed vertical charge moment change, indicating that horizontal charge motion may produce a substantial fraction of the mesospheric electric field. We use the same model to investigate possible direct electromagnetic signatures of slow horizontal currents, especially at high altitudes where the Sprites99 balloon campaign made unique measurements and where horizontal electric fields are not constrained by the immediate presence of an electrically conducting ground.

G/H1-7 NEW MESOSPHERIC IONIZATION SOURCE
16:20

Leslie C. Hale, CSSL/Penn State, e-mail: LesW3LH@aol.com
Room 316 EE East, Penn State University, University Park, PA 16802

The following concepts are proposed for a source of high energy electrons in the mesosphere from above. This source is related to lightning, and is global in extent. On the millisecond time scale involved, the effective height of the ionosphere is frequently at a sharp ledge, usually at about 80 km at night and somewhat lower during daytime and disturbed conditions. The paradigmatic case of most interest to "red sprites" is a large positive lightning stroke, which deposits a negative "Wilson monopole". A quasi-static field is established between the earth and the ionosphere (left, below) on a time scale of about a millisecond (determined by round-trip propagation delay). This in turn releases free electrons into the ionosphere, where they are "one-dimensionalized" by the earth's magnetic field and bifurcate, with the upper half propelled upward into the magnetosphere by mutual repulsion. On a relatively slow time scale (milliseconds - which may be further delayed by "continuing currents"), the lower negative charge dissipates, after which the upper charge (up 100's to 1000's of km) bifurcates and half of it is accelerated downward, to energies which may be an MeV or more for large events. For sprites, the free electrons created may accelerate breakdown processes.

The establishment of the quasi-static field involves the launch of a unipolar millisecond wavelet in the earth-ionosphere waveguide. In the case of negative CG lightning the travelling wavelet releases excess electrons into the ionosphere (right, below). After the wavelet passes, this negative charge is accelerated downward for up to hundreds of km by positive charge left behind at the base of the ionosphere. Although somewhat less energetic than the previously described process, this happens on a global basis, creating a day and night source of mesospheric ionization (including positively charged aerosol) and electric fields due to charge separation.

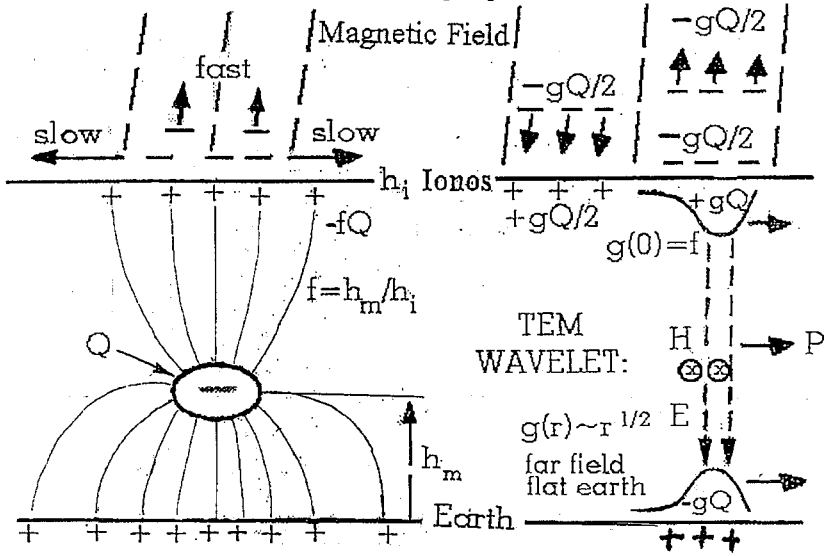

G/H1-8
16:40

UNUSUALLY INTENSE SPRITE EVENTS STUDIED WITH VIDEO, PHOTOMETRY, AND ULF/ELF/VLF RECORDINGS

C. P. Barrington-Leigh* U. S. Inan
Packard 351
350 Serra Mall
STARLab
Stanford, CA. 94305
Martin Füllekrug
Institut für Meteorologie und Geophysik
Universität Frankfurt/Main
Germany

On July 19 and August 6 1998 large nighttime mesoscale convective systems over northwestern Mexico produced numerous groups of sprites as observed from the Langmuir Laboratory's observatory at 33.98°N×107.19°W.

These events were studied with standard and telescopic video imagers, a triggered photometric array including blue and red photometers, and ULF, ELF, and VLF receivers located at several stations in North America. Several features in these recordings are notable and are discussed in terms of past observations and current theoretical models of sprites.

Sprites observed on these nights were brighter than previously reported sprite luminosities, and were brighter than those previously recorded by the authors. Several were as bright as $30 - 50$ MR (~ 1 μW/cm^2/str/s) in the wavelength range 670 nm to 780 nm, which corresponds primarily to the first positive band of N_2. Photometric signatures were also recorded in the blue range 360 nm to 470 nm and likely due to the second positive band of N_2. On July 19, many sprites were visible to the un-dark-adapted, unaided eye.

Sprite luminosities, when recorded by the photometers, generally persisted for 40 ms to 150 ms. Correlated recordings of ELF were made at Stanford (CA), and recordings of ULF, showing pulses of similar duration to the sprites, were made near Santa Cruz (CA), Socorro (NM), and Saskatoon (Saskatchewan, Canada). Sprite optical signatures often relaxed with a closely-exponential shape with time scales of $\sim$0.5 ms to a few ms.

A number of events were associated with more than one return stroke, as inferred from VLF sferics recorded with the photometer data stream. In one case, a dramatic rebrightening of a sprite occurred just before a return stroke sferic, suggesting the possibility that the intracloud rearrangement of charge can cause large mesospheric electric fields even before the charge is "removed" to ground.

The long duration of some events allows tracking of luminous regions using normal-speed video. This analysis reveals apparent propagation velocities as slow as 2-12$\times 10^3$m/s.

G/H1-9
17:00

LARGE SCALE STRUCTURE OF SPRITES

V. P. Pasko* U. S. Inan T. F. Bell
STAR Laboratory, Stanford University, Stanford, CA 94305

Sprites are spectacular luminous glows which occupy volumes in excess of thousands of cubic kilometers in clear air above thunderstorms [e.g., Sentman et al., *Geophys. Res. Lett.*, **22**, 1205, 1995]. Recent high spatial resolution telescopic imaging of this phenomena has uncovered a fascinating complex of internal sprite structure, including fine, highly branched luminous filaments with spatial scales ranging from tens to several hundreds of meters [Inan et al., *EOS Trans. AGU*, **79**, Fall Meet. Suppl., F164, 1998].

Sprites are believed to be produced by large quasi-electrostatic field transients appearing at mesospheric altitudes above thunderstorms following intense cloud to ground lightning discharges [e.g., Pasko et al., *J. Geophys. Res.*, **102**, 4529, 1997]. Recent analysis of temporal and spatial scales of the electrical breakdown at different altitudes above sprite producing thunderstorms has identified three altitude ranges with distinct differences in structure of the breakdown ionization. It was shown, in particular, that the upper extremities of sprites always appear as amorphous diffuse glows, while the lower portions exhibit a complex streamer structure [Pasko et al., *Geophys. Res. Lett.*, **25**, 2123, 1998; hereafter denoted I]. Direct large scale modeling of portions of sprites dominated by streamers is computationally not possible at present due to the extremely fine spatial resolution which is required to resolve individual streamer channels [I].

We report here results from a new model which reproduces well the general observed shapes of sprites as well as their internal structure, including the upward, downward and quasi-horizontal propagation and branching of channels of breakdown ionization. The model is based on phenomenological probabilistic approach which was proposed in [Niemeyer et al., *IEEE Trans. Electr. Insul.*, **24**, 309, 1989] for modeling of a streamer corona. We use experimentally and theoretically documented properties of positive and negative streamers in air for a realistic determination of the propagation of multiple breakdown branches in a self-consistent electric field. Model results reproduce the dynamics of a return stroke which may develop in sprites after upward propagation and attachment of streamer channels to the highly conducting lower ionosphere. Only a modest amount of thundercloud charge (<100 C) removal (by a positive cloud to ground lightning from altitude 10 km) is needed for the formation of large "jellyfish" sprites extending downward well below 40 km and having transverse extent ~50 km. Asymmetries between sprites produced by positive versus negative lightning discharges will be discussed.

Session J2, 13:35 PM-Thurs., Room 200
ADVANCES IN CRYOGENIC COOLING SYSTEMS
Chairperson: L. D'Addario, NRAO (ldaddari@nrao.edu)

J2-1
13:40 (40 min.)

MODELING AND OPTIMIZATION OF A HIGH FREQUENCY 10 K PULSE TUBE REFRIGERATOR

Ray Radebaugh* E. D. Marquardt A. O'Gallagher
National Institute of Standards and Technology
MS 838.09
325 Broadway
Boulder, CO 80303

The operation of pulse tube refrigerators at high frequencies (30 to 60 Hz) allows them to be driven with compact valveless compressors. The absence of valves leads to high efficiencies, which has been as high as 15 to 19Carnot for the most efficient pulse tube refrigerators operating at temperatures of about 80 K. As the cold-end temperature is reduced to aboutm 10 K, the performance of regenerators operating at such high frequencies in any regenerative refrigerator can deteriorate significantly unless they are carefully optimized for these conditions. Some causes for the deterioration are well known, such as the reduced heat capacity of solid matrix materials. Other possible causes and their relationship to frequency are not very well understood. We discuss some of these causes as well as approaches to minimize the effects of low matrix heat capacity. The influence of frequency is qualitatively explained by considering the regenerator thermal loss to be brought about by three processes, (a) the flow of gas through a temperature gradient, (b) pressure-driven temperature oscillations within the gas void volume, and (c) axial heat conduction. Viscous pressure drops influence the optimum hydraulic diameter, but they are not influenced much by frequency.

More exact numerical computations with a finite difference model developed at NIST, known as REGEN3.1, were used to calculate the performance of regenerators while many different parameters were varied to determine optimum operating conditions and geometry. Fixed parameters were the low temperature of 10 K and the warm temperature of 80 K. The use of Er3Co for the matrix provides for reasonably high values for the coefficient of performance, unlike that for lead. Even though parallel plates give the best COP, packed spheres still provide a useful COP of 0.022 with respect to PV input power at 80 K, and they are easier to fabricate. A comparison of one and two stages operating between 10 and 80 K is also given. The complete pulse tube refrigerator will also have a first stage operating between 80 and 300 K. The 10 K pulse tube refrigerator described here would be useful for direct cooling of sensors or for precooling helium in a Joule-Thomson stage for temperatures of 4 K or less.

J2-2
14:20

DESIGN OF A 20K PULSE TUBE COOLER

A. Kashani* B. P. M. Helvensteijn
Atlas Scientific
Sunnyvale, CA 94086
P. Kittel
NASA-ARC
Moffett Field, CA 94035

For applications requiring a cryocooler with high reliability and low vibration a pulse tube cooler (PTC) driven by a linear compressor is an attractive choice. The absence of cold moving parts in a PTC reduces wear and vibration and increases reliability. Single-stage PTCs, driven by linear compressors and with a porous, stainless steel regenerator matrix, e.g. stacked-screen, have achieved no-load temperatures below 40K. To provide cooling at lower temperatures the PTC requires additional stages with regenerators made from novel high heat capacity materials. A two-stage PTC driven by a linear compressor that achieves temperatures below 20K is being developed. The first stage (300K to 60K) will have a stainless steel regenerator matrix. The matrix for the second stage regenerator (¡60K) will be made from the compound Al-272-1 which was recently developed at Ames Laboratory, in Ames, Iowa. AL-272-1 has a heat capacity which exceeds that of all other materials, including lead, over a wide range in temperature (20K ¡ T ¡ 85K). The PTC is being designed to provide 10W of cooling at 60K and 2W at 20K. To further enhance efficiency inertance tubes will be used in each stage. The proposed PTC can be employed as the upper stage of a J-T refrigerator cooling detectors.

The paper will describe the design of the cooler. The configuration will be optimized using the PTC modeling program SAGE. Furthermore, a description will be presented of the efforts underway to establish the suitability of the new regenerator material AL-272-1 at frequencies above 40 Hz using a linear compressor.

J2-3
14:40

Measurement of Regenerator Thermal Conductivity Degradation Factors

Daniel R. Ladner
Lockheed Martin Astronautics
Denver, CO

The value of the regenerator thermal conductivity degradation factor f has been measured in situ for several pulse tube (PT) cryocoolers having various geometries and different regenerator sizes. Results of the present investigation are compared to measurements made in the National Institute of Standards and Technology (NIST) thermal conductance apparatus.

Knowledge of the degradation factor is an important consideration in the initial design of a PT or Stirling cryocooler cold head. The degradation factor provides a measure of the thermal conductance of the regenerator screen or other packing component in the presence of the GHe working fluid at the design pressure (~2 MPa). As defined here, f includes the conduction of the bulk GHe as well as the enhanced conduction through the regenerator screen stack. This definition is consistent with f as measured directly for regenerator stacks in the NIST thermal conductance apparatus. In that method the background heat leak into the regenerator component is subtracted out to determine the net heat flow attributable to the regenerator stack and bulk GHe at the design pressure.

In the present investigation the measurement approach determines f indirectly from data obtained in the as-built cryocooler. Specifically, warmup rate data and theoretically determined parasitic heat leaks are used to back out the degradation factor, which can be determined over a wide range of temperature above the coldest no-load value. In a typical measurement, the radiation heat load for the evacuated cryocooler is measured at various temperatures above ambient to determine the effective radiation coefficient. The pressurized cryocooler is then operated to attain the lowest temperature. Warmup rate versus heater power data are plotted to obtain the total parasitic heat leak at various temperatures. The degradation factor can then be determined as a function of temperature by subtracting out the theoretical radiation leak and conductance leaks of the PT and regenerator components. Although the NIST measurement method is in principle a more direct one, a relatively large unknown background heat leak from all sources must be assumed constant under vacuum and pressurized conditions to obtain the net heat flow across the regenerator under test. In the method employed here, the total parasitic heat load is very well determined from the warmup data, but the radiation and conduction contributions must be separately calculated. The radiation contribution is the more difficult one to estimate, and it is relatively more important in smaller PT cryocoolers. Results of the two methods are compared and the effects of temperature, regenerator size, and cryocooler geometry are discussed.

J2-4
15:00

LONG TERM PERFORMANCE OF 4 K GIFFORD-McMAHON CRYOCOOLERS ON THE BIMA ARRAY

R.L. Plambeck*
Radio Astronomy Lab
University of California
Berkeley, CA 94720

SIS mixers on the BIMA array are cooled to 4 K with 3-stage Gifford-McMahon refrigerators. We constructed these refrigerators ourselves by welding 15 cm long × 1.27 cm ID third stages onto standard CTI model 1020 cryocoolers. Approximately 60 grams of Er_3Ni spheres are used as the third stage regenerator. A key difference from most cryocoolers is that we use a continuous seal on the third stage, clamped to the warm end of the cylinder, rather than a split seal mounted on the displacer. We find that this gives more stable performance at low temperatures.

Our refrigerators cool the BIMA receivers from room temperature to 4 K in 5 hours. The heat loads on the refrigerators' first, second, and third stages are estimated to be 6 watts (from the 50 K radiation shield), 0.5 watt (from the 12 K inner radiation shield and IF amplifiers), and 15 milliwatts (from conduction losses and SIS bias circuits), respectively.

We operate the refrigerators at a cycle frequency of 31 rpm. The temperature at the tip of the third stage cycles by 0.2 K with each stroke of the refrigerator. Thermal resistance damps this temperature swing to 20 mK at the SIS mixer, which still is sufficient to cause receiver gain fluctuations of a few percent. When observing, we choose integration times which are an integral number of 1.92 sec refrigerator cycles in order to average out these gain fluctuations. Over longer time periods the SIS mixer temperatures (averaged over the refrigerator cycle) are stabilized to 2 mK r.m.s. with heater resistors.

Nine 4 K refrigerators are installed on the BIMA array. One has been in use since February 1994. The median third stage temperature over the past 3 years ($\sim$ 25 refrigerator-years operation) is 3.5 K. Generally the third stage temperatures are stable to $\pm$ 0.1 K for days or weeks, even while the refrigerators are tipped from 0 to 90 degrees as the telescopes track radio sources. Sometimes the temperatures creep upward, possibly due to accumulation of contaminants in the cold head, then snap back to their original values following a power interruption or a 10-minute 'defrost' cycle.

Maintenance consists of cleaning out the cold heads every 1–2 years and replacing the third stage seals when needed, typically every 2–4 years. Although we experience occasional helium compressor failures, no cold head has failed in the past 5 years.

J2-3
14:40

Measurement of Regenerator Thermal Conductivity Degradation Factors

Daniel R. Ladner
Lockheed Martin Astronautics
Denver, CO

The value of the regenerator thermal conductivity degradation factor f has been measured in situ for several pulse tube (PT) cryocoolers having various geometries and different regenerator sizes. Results of the present investigation are compared to measurements made in the National Institute of Standards and Technology (NIST) thermal conductance apparatus.

Knowledge of the degradation factor is an important consideration in the initial design of a PT or Stirling cryocooler cold head. The degradation factor provides a measure of the thermal conductance of the regenerator screen or other packing component in the presence of the GHe working fluid at the design pressure (~2 MPa). As defined here, f includes the conduction of the bulk GHe as well as the enhanced conduction through the regenerator screen stack. This definition is consistent with f as measured directly for regenerator stacks in the NIST thermal conductance apparatus. In that method the background heat leak into the regenerator component is subtracted out to determine the net heat flow attributable to the regenerator stack and bulk GHe at the design pressure.

In the present investigation the measurement approach determines f indirectly from data obtained in the as-built cryocooler. Specifically, warmup rate data and theoretically determined parasitic heat leaks are used to back out the degradation factor, which can be determined over a wide range of temperature above the coldest no-load value. In a typical measurement, the radiation heat load for the evacuated cryocooler is measured at various temperatures above ambient to determine the effective radiation coefficient. The pressurized cryocooler is then operated to attain the lowest temperature. Warmup rate versus heater power data are plotted to obtain the total parasitic heat leak at various temperatures. The degradation factor can then be determined as a function of temperature by subtracting out the theoretical radiation leak and conductance leaks of the PT and regenerator components. Although the NIST measurement method is in principle a more direct one, a relatively large unknown background heat leak from all sources must be assumed constant under vacuum and pressurized conditions to obtain the net heat flow across the regenerator under test. In the method employed here, the total parasitic heat load is very well determined from the warmup data, but the radiation and conduction contributions must be separately calculated. The radiation contribution is the more difficult one to estimate, and it is relatively more important in smaller PT cryocoolers. Results of the two methods are compared and the effects of temperature, regenerator size, and cryocooler geometry are discussed.

J2-4
15:00

LONG TERM PERFORMANCE OF 4 K GIFFORD-McMAHON CRYOCOOLERS ON THE BIMA ARRAY

R.L. Plambeck*
Radio Astronomy Lab
University of California
Berkeley, CA 94720

SIS mixers on the BIMA array are cooled to 4 K with 3-stage Gifford-McMahon refrigerators. We constructed these refrigerators ourselves by welding 15 cm long × 1.27 cm ID third stages onto standard CTI model 1020 cryocoolers. Approximately 60 grams of Er_3Ni spheres are used as the third stage regenerator. A key difference from most cryocoolers is that we use a continuous seal on the third stage, clamped to the warm end of the cylinder, rather than a split seal mounted on the displacer. We find that this gives more stable performance at low temperatures.

Our refrigerators cool the BIMA receivers from room temperature to 4 K in 5 hours. The heat loads on the refrigerators' first, second, and third stages are estimated to be 6 watts (from the 50 K radiation shield), 0.5 watt (from the 12 K inner radiation shield and IF amplifiers), and 15 milliwatts (from conduction losses and SIS bias circuits), respectively.

We operate the refrigerators at a cycle frequency of 31 rpm. The temperature at the tip of the third stage cycles by 0.2 K with each stroke of the refrigerator. Thermal resistance damps this temperature swing to 20 mK at the SIS mixer, which still is sufficient to cause receiver gain fluctuations of a few percent. When observing, we choose integration times which are an integral number of 1.92 sec refrigerator cycles in order to average out these gain fluctuations. Over longer time periods the SIS mixer temperatures (averaged over the refrigerator cycle) are stabilized to 2 mK r.m.s. with heater resistors.

Nine 4 K refrigerators are installed on the BIMA array. One has been in use since February 1994. The median third stage temperature over the past 3 years ($\sim$ 25 refrigerator-years operation) is 3.5 K. Generally the third stage temperatures are stable to $\pm$ 0.1 K for days or weeks, even while the refrigerators are tipped from 0 to 90 degrees as the telescopes track radio sources. Sometimes the temperatures creep upward, possibly due to accumulation of contaminants in the cold head, then snap back to their original values following a power interruption or a 10-minute 'defrost' cycle.

Maintenance consists of cleaning out the cold heads every 1–2 years and replacing the third stage seals when needed, typically every 2–4 years. Although we experience occasional helium compressor failures, no cold head has failed in the past 5 years.

J2-5
15:40

BOLOCAM: A BOLOMETRIC RECEIVER WITH AN INNOVATIVE 280 mK TRIPLE-STAGE HELIUM REFRIGERATOR

Jason Glenn* James J. Bock Samantha F. Edgington
Andrew E. Lange Amanda Mainzer
Department of Physics, Math, and Astronomy
Caltech, MC 59-33
1200 E. California Blvd.
Pasadena, CA 91125
Eyal Gerecht Phil M. Mauskopf Brooks Rownd Lunming Yuen
FCRAO, Department of Astronomy
University of Massachusetts
Amherst, MA 01003
Simon T. Chase
Chase Research
35 Wostenholm Rd.
Sheffield S7 1LB
UK

We describe a liquid cryogenic system using an innovative triple-stage, closed-cycle helium sorption refrigerator for cooling an array of detectors to 280 mK. The array of 144 semiconducting bolometers is the heart of Bolocam, a broadband millimeter-wave camera. Bolocam will be used for making astrophysical observations from the Caltech Submillimeter Observatory and the Large Millimeter Telescope (J. Glenn et al., *Proceeding of SPIE*, **3357**, 326-334, 1998). A liquid ^{4}He bath vented to atmospheric pressure and backed by liquid nitrogen in a standard dewar precools the closed-cycle refrigerator to 4.2 K. The first stage of the refrigerator condenses ^{4}He into a reservoir which is pumped through a small diameter pump tube by activated charcoal to achieve a temperature < 2.5 K. At this temperature ^{3}He is condensed into two reservoirs, an intercooler and a cold head, which are also pumped by charcoal pumps. The intercooler intercepts the 60 μW heat load from the suspension system and 288 detector wires (which terminate at 4 K) and equilibrates at 500 mK. The cold head provides a heat lift of 3 μW for the detector focal plane, equilibrating at 280 mK. During observing runs, the pumps are automatically cycled daily by running current through resistive electrical elements to evaporate helium from the charcoal pumps and condense it in the reservoirs. Operation is simplified substantially compared to conventional helium sorption systems that require pumping on the helium bath and mechanical valves. As with single-stage sorption refrigerators, the heat lifts and hold times can be adjusted by tuning the pump tube diameters and the number of STP liters of helium in the refrigerator. Because the refrigerator operation is simple and it can be run from an unpumped helium bath, this design is being incorporated in several other millimeter-wave instruments with bolometers.

J2-6
16:00

THE POLATRON: INTEGRATION OF A MECHANICAL COOLER AND A 250 mK TRIPLE-STAGE HELIUM REFRIGERATOR FOR A BOLOMETRIC COSMIC MICROWAVE BACKGROUND POLARIMETER

Jason Glenn* Ravinder Bhatia Andrew E. Lange Peter Mason
Byron J. Philhour
Department of Physics, Math, and Astronomy
Caltech, MC 59-33
1200 E. California Blvd.
Pasadena, CA 91125
Sarah E. Church
Department of Physics
Stanford University
Stanford, CA 94305
Simon T. Chase
Chase Research
35 Wostenholm Rd.
Sheffield S7 1LB
UK

We describe a hybrid cryogenic system coupling a mechanical cryocooler[a] to an innovative triple-stage, closed-cycle 250 mK helium sorption refrigerator. This system provides the low temperature bath for bolometric detectors in the Polatron, a millimeter-wave cosmic microwave background polarimeter used to make observations from the Caltech Owens Valley Radio Observatory. Observations are made remotely for several weeks at a time, requiring the autonomy afforded by a mechanical cryocooler and a closed-cycle sorption refrigerator. The cryocooler precools the sorption refrigerator to 3.5 K. Glenn et al. in another paper in these conference proceedings describe a sorption refrigerator in detail that differs from this only in that it is tuned to achieve 280 mK. ^{4}He is condensed in the first stage at 4.2 K, then pumped by an activated charcoal bath to achieve a liquid helium temperature < 2.5 K. At this temperature, ^{3}He is condensed into reservoirs in the intercooler and cold head. The intercooler intercepts the 60 μW heat load from the focal plane suspension system and detector wires, which terminate at 4 K. The cold head provides a heat lift of 4 μW at 250 mK for the bolometers. Each day the refrigerator is automatically cycled by evaporating the helium from the charcoal pumps with electrical heaters and condensing it into the reservoirs. High impedance (~ 3 MΩ) bolometers are susceptible to electrical interference and microphonic noise generated by variable capacitive coupling to electrical ground by vibrating signal wires. Both of these types of noise are generated by the mechanical cryocooler. We use flexible couplings and a vibration isolator to decouple the cryocooler cold tip from the detector wires, and a sapphire insulator to electrically isolate the detectors from the cryocooler.

[a] APD Cryogenics, Inc. Model HS-4

J2-7
16:20

A COMPACT, LONG-HOLDTIME ^{3}He/^{4}He EVAPORATION REFRIGERATOR

J.L. Puchalla M.J. Devlin* H. Eberhart J. Klein
Department of Physics and Astronomy
209 So. 33rd St.
University of Pennsylvania
Philadelphia, PA 19104

We have developed a compact, low-cost ^{3}He-^{4}He refrigerator with a single cycle hold-time greater than 5 days at a base temperature of 260 mK with no load. Temperatures below 300 mK can be maintained with up to 50 μW of loading. The closed-cycle ^{3}He system uses a 1 Kelvin heat exchanger produced by an externally pumped ^{4}He reservoir to both extend the ^{3}He pot life and allow for ^{3}He condensation during recycling. The heat exchanger reservoir is filled from a large unpumped tank through a tuned impedance and operates indefinitely with up to 15 mW of cooling power. However, its reservoir is large enough to allow short term but large heat loads and a rapid (1 hour) recycle of the ^{3}He system. Cryogens can be added to a cryostat without interupting ongoing tests. The system has no moving parts and can be remotely cycled via a computer-controlled thermometry/heater box.

The refrigerator was developed to cool bolometric detectors on the Mobile Anisotropy Telescope (MAT). MAT observes at a site near the proposed Millimeter Array site on Cerro Toco in Chile. The long holdtime and ease of use of our refrigerator are a great advantage when operating in remote locations. In addition, the externally pumped ^{4}He reservoir allows the refrigerator to be cycled without pumping on the main ^{4}He bath (as is the case with most ^{3}He systems). Since the cost of liquid helium at the site is $\geq$4 times the cost in the US, this reduction in the liquid helium usage results in a substantial savings.

Two previous observation were made using a Gifford-McMahon closed-cycle refrigerator to cool HEMT amplifiers to 40 K and SIS detectors to 4 K.

J2-8
16:40

CRYOGENICS FOR THE ALMA TELESCOPE

Larry R. D'Addario
National Radio Astronomy Observatory
949 N Cherry Ave, Campus Bldg 65
Tucson, AZ 85721

The Atacama Large Millimeter Array (ALMA) is expected to include about 64 parabolic antennas of 12 m diameter for operation as a synthesis array at frequencies up to 950 GHz. It will be located in the Atacama desert of northern Chile at an elevation of 5000 m. The array will be constructed by an international partnership, some details of which are still under discussion. Design and development work has been funded in the U.S. and Europe, and is actively under way. Large scale construction is expected to begin in 2003.

Each antenna will include up to 10 cryogenic receivers in order to cover all accessible mm and sub-mm bands. Most receivers will use SIS mixers operating at 4K. This paper describes the present design for the required cryocoolers and the thermal design of the receiver package, along with test results on some components. The large number of cryogenic systems and the difficulty of working at the high and remote site demand that the reliability be much greater than is usually achieved on telescopes.

The two or three lowest-frequency receivers will be based on HFET amplifiers for which cooling to 20K is sufficient. The remaining receivers require cooling to 4K. In addition, cooling to around 80K is required for IF amplifiers and local oscillator electronics, as well as for intercepting heat due to radiation (shields) and conduction (wires and waveguides) from outside. The loads have been analyzed based on an assumed optical configuration in which each receiver uses a separate window or waveguide for its signal input. The dominant load on all stages is from infrared radiation. To ensure confidence in knowledge of the actual loads, a "thermal mockup" is being constructed; it will accurately reproduce the radiation, conduction, and dissipation loads of the ALMA receiver and be instrumented to measure actual heat flows.

A three-stage cryocooler common to all receivers has been tentatively selected. A Joule-Thompson (JT) expander was chosen for the 4K stage in order to avoid the temperature modulation that is inherent in cyclic coolers such as Gifford-McMahon (GM) or pulse tube (PT). An existing JT design has been experimentally characterized in order to establish parameters for the new system. Several innovations to improve reliability are planned, including use of oilless compressors.

The first two cooling stages will use either GM or PT refrigerators, with the pulse tube preferred because of its expected higher reliability. A suitable PT refrigerator is under development at NIST (see paper by R. Radebaugh, this conference).

J2-9
17:00

HYDROGEN SORPTION CRYOCOOLER DEVELOPMENT FOR THE PLANCK SURVEYOR AND ARISE MISSIONS

G. Morgante[1], P. Bhandari[2], R. C. Bowman[2], D. Crumb[3], C. A. Lindensmith[2], T. Loc[2], C. Paine[2], M. Prina[4], D. Rapp[2], R. Sugimura[2], L. A. Wade[2].

[1]Te.S.R.E.-CNR, Bologna, Italy
[2]California Institute of Technology, Jet Propulsion Laboratory
Pasadena, CA 91109, USA
[3]Swales Aerospace, Pasadena, CA 91107, USA
[4]Politecnico di Milano, Milano, Italy

The first decade of the next millennium will strongly advance our knowledge of the Universe in the radio bands. Among other projects, two space missions will provide a decisive contribution to this effort: Planck and ARISE.
Planck is an ESA (European Space Agency) mission with the target of mapping the Cosmic Background Radiation (CBR). Planck will carry two instruments: the High Frequency Instruments (HFI), based on an array of bolometers, and the Low Frequency Instruments (LFI) utilizing an array of InP HEMT amplifier radiometers.
ARISE (Advanced Radio Interferometry between Space and Earth) is a space Very Long Baseline Interferometry (VLBI) mission consisting of one (or possibly two) 25-meter radio telescope(s) in a high elliptic Earth orbit. The telescope(s) will observe in conjunction with a large number of ground-based radio telescopes to obtain very high resolution images of the most energetic astronomical phenomena.
In both missions the radiometric detectors will be cooled to the operative temperature by sorption cryocoolers based on metal-hydrides. These systems work in continuous operation by thermally cycling a metal-hydride to absorb and desorb hydrogen gas, which is used as the working fluid in a Joule-Thomson refrigerator. Without any moving part they are truly vibration-free and can be easily scaled to perform over a wide range of cooling powers.
The sorption coolers for the Planck and ARISE missions will be able to reach and mantain a temperature of 20 K even in presence of large thermal loads (approximately 1.5 W for Planck), with an input electric power of about 500 W, rejecting heat at 270 K.
We will present the conceptual design of these coolers and their operating conditions along with their predicted performance compared to the missions requirements.
JPL is operated by California Institute of Technology under a contract with NASA.

Session K1, 13:35 PM-Thurs., Room 155
ELECTROMAGNETIC FIELDS AND BIOLOGY
Chairperson: F. Barnes, Univ. of Colorado (barnes@boulder.colorado.edu)

K1-1 13:40 EXPOSURES TO MAGNETIC FIELDS AND HIGH LEVELS OF AIR POLLUTION IN COMBINATION MAY SUBSTANTIALY RAISE CANCER RISKS IN CHILDREN

Howard Wachtel, University of Colorado, Dept. of Electrical Engr., Boulder, CO 80309-0425, Bob Pearson, Radian Corporation, Denver, CO 80202

Certain chemical agents can act in combination to be far more carcinogenic than either one alone. Often this is due to one acting as a cancer initiator while the other acts as a promoter. Reports of combined carcinogenic effects of chemical pollutants with physical agents such as electromagnetic fields are rarer, but this may be due to the usual segregation of study approaches for the two categories.

We had been separately exploring associations of mobile source air pollution and electromagnetic fields (derived from power lines) with the occurrence of leukemia and other childhood cancers in the Denver, Colorado, metropolitan area. We have recently looked at risks of exposures to these combined agents.

Distance weighted traffic density (DWTD) is used as a representative metric for air pollution while the "wiring configuration" of nearby power lines is taken as an indicator of the time-averaged exposure of 60 Hz magnetic fields. Odds ratios (O.R.) for childhood cancer risk were determined for high levels of DWTD, high "wire code" categories and for high exposures to both factors in combination. There is a substantial elevation of childhood cancer risk for the cases exposed to both high traffic and high wire code. For example, the odds ratios based on city wide controls for highest wire code and DWTD above 20,000 vehicles per day referenced to homes with buried wiring and less than 20,000 vehicles per day is 3.24 (95% CI 1.57-6.69). These odds ratios are much higher than those for wire code 1.03 (95% CI 0.62-1.71) or traffic 1.44 (95% CI 0.95-2.16) alone.

These results imply that mobile source air pollution (surrogated by DWTD) and EM fields (surrogated by wire codes) could be acting as co-carcinogens in children exposed to both factors. There is a plausible biophysical basis for this since vehicular exhaust contains volatile organic compounds, such as benzene, which are known to be leukemia initiators, while low frequency EM fields have been linked to cancer promotion mechanisms. The degree to which there is concurrent exposure to high levels of traffic exhaust and to EM fields is likely to vary greatly from city to city since it depends very much on how the street and wiring patterns intermesh. This could explain why the apparent risk of childhood cancer in association with traffic exhaust or with EM fields may differ in various locales.

K1-2
14:00

REDUCED BIOHAZARD ANTENNA FOR HANDHELD RADIOS

Seong-Youp Suh, Warren L. Stutzman, and William A. Davis
Antenna Group
Bradley Department of Electrical and Computer Engineering
Virginia Polytechnic Institute and State University
Blacksburg, VA 24061-0111
www.ee.vt.edu/antenna

There is considerable public concern about the possible harmful effects of handheld wireless transceivers on humans. Reduction of the interaction between an antenna and the human head is the main topic of interest.

This paper presents results from simulations of an antenna for use with a handheld radio called Safetenna. The antenna is designed for low power deposition into the human head and reduced interaction between the antenna and a human head. The basic concept of the Safetenna is to elevate a balanced antenna above the human head. The Safetenna in an extended position was modeled using a sleeve dipole antenna elevated 14cm above the handset. The antennas reported in (W.L.Stutzman and J.Randall Nealy, *US Patent No 5,541,609,* July 30, 1996.) and (H.E.King and J.L.Wong, *IEEE Trans. On Antennas and Propagation*, pp. 376-379, May 1977) were modeled for PCS and AMPS bands using the commercial Finite Difference Time Domain numerical code, Fidelity.

A simple box head model containing a homogeneous liquid similar to human tissue (ε_r=43.5, μ_r=1, σ_r=0.9) and a handset were modeled to investigate the interaction between the antenna, the handset, and the human head. In this work, the operator's hand is not included because of its minimal effect on antenna performance. Material loading was explored by placing dielectric at several locations on the sleeve dipole antenna in an attempt to reduce the size of antenna. Size reduction of the antenna is achieved by loading with a dielectric material at the top of the antenna.

The VSWR, antenna pattern, and SAR (Specific Absorption Rate) of the antenna (Safetenna) are compared with those of a conventional sleeve antenna for both AMPS and PCS bands. The simulation results indicate that Safetenna has significantly less antenna pattern distortion and less head absorption than conventional antennas for both the AMPS and PCS bands. The antenna patterns of the Safetenna are close to the patterns in free space. The SAR distributions of the Safetenna indicate that there is a relatively small amount of power absorption into head compared to a conventional antenna. Another finding reveals that the VSWR of the Safetenna is affected less by the handset than with a conventional antenna.

The results of this study demonstrate that the Safetenna provides an excellent alternative to typical handset antenna and has improved patterns and SAR.

K1-3
14:20

SOURCE LOCALIZATION IN A 3-LAYER SPHERICAL MODEL OF THE HEAD WITH COMBINED FORWARD INVERSE COMPUTATIONAL METHODS

C. Ramon[1], A. Ishimaru[1], S. Jaruwatandilok[1], J. Haueisen[2], Y. Kuga[1], K. Maravilla[3], G. Dawson[4]

Departments of [1]Electrical Engineering, [3]Radiology and [4]Psychology, University of Washington, Seattle, WA 98195, U.S.A.
[2]Biomagnetics Center, F. S. University, Jena, Germany

A 3-layered spherical model of the head was used to test a combined forward-inverse modeling technique to localize the sources of the electrical activity in the head. It was found that the dipolar sources could be localized successfully with 2-3 image pixel-size resolution. In the model the first layer represents the scalp, the second layer represents the bone and the third layer represents the gray matter of the brain. Using finite element methods, the potentials on the scalp were simulated for a given source in the gray matter. These potentials were then used to solve for the inverse problem. An initial image of the sources was reconstructed by use of the weighted minimum norm technique. The background noise was reduced by thresholding the reconstructed image at 20% of the peak value. This image of the source was then used to predict the potentials on the surface of the skin. The error between the simulated and predicted potentials was reduced by using iterative optimization techniques. In each iteration the position and the intensity of the dipole was changed in gradual steps based on L2 norm of the error. The iterations were stopped when a preset error limit (~ 1%) was achieved. The original position and the intensity of the dipole were compared with the reconstructed values and it was found that the original dipole was successfully identified. We did find the ghost images in the reconstructed image, but these can be removed by use of the image filtering techniques. The combined forward-inverse modeling technique provides an accurate accounting of the volume currents in the conducting medium and improves the localization of the deeper sources. The biomedical applications of this technology will be in localizing the sources deep inside the brain or heart which are difficult to do accurately at the present moment.

K1-4
14:40

MULTI-LAYERED REPRESENTATION OF fMRI DATA

Francois G. Meyer
Department of Electrical and Computer Engineering
Campus Box 425
University of Colorado
Boulder, CO 80309

Functional magnetic resonance imaging (fMRI) of brain activity can detect and quantify hemodynamic changes induced by brain activation and neuronal activity. In this work we address the problem of detecting, and removing from the fMRI signal, contaminants, and physiological noise, in order to isolate stimuli induced transients.

Implicit in almost all existing fMRI analysis methods is the assumption that changes in the fMRI signal are only due to the presence of an hemodynamic response to a stimulus. In reality there are many contaminants to the stimuli induced response that create some fluctuation in the signal. We assume that the fMRI time series at a given voxel in the brain is a complicated mixture of signals:

1. a signal induced by neuronal activation, that only exists if the voxel is inside a functionally activated brain area.
2. a periodic physiological noise due to cardiac and respiratory aliasing.
3. a non periodic noise with an $1/f$ spectrum due to longterm physiological drifts, and instrumental instability.
4. a white noise caused by thermal and quantum noise

In this setting we advocate that the actual analysis of the data could be most efficiently carried out by organizing the fMRI time series as a superposition (or a mixture) of several appropriate waveforms. This adaptive representation of the fMRI data will increase the sensitivity and the detectability by shrinking the noise to zero, while keeping the activated regions untouched.

This work is supported by a biomedical engineering research grant from The Whitaker Foundation.

K1-5
15:00

THE EFFECTS OF STATIC MAGNETIC FIELDS ON THE OXYGEN SATURATION LEVEL IN BLOOD

Ted D. Kutrumbos, Frank S. Barnes
Department of Electrical and Computer Engineering
Campus Box 425
University of Colorado
Boulder, CO 80309

Static magnetic fields have been shown to have effects on blood flow, leukocyte count, and hemoglobin. The purpose of this study was to determine if static magnetic fields ranging between 0.1T and 1.0T have an effect on the oxygen saturation (SpO2) level in blood. Since oxyhemoglobin is diamagnetic it should be repelled by the magnetic field and since deoxyhemoglobin is paramagnetic it should be attracted by the magnetic field. From these magnetic properties, it could be hypothesized that the magnetic field will repel the oxygenated hemoglobin and the SpO2 level will be lowered.

Using pulse oximetry, a preliminary study was conducted in which the SpO2 level in the human index finger was measured before, during and after exposure to a static magnetic field. The SpO2 level was also recorded on the subjects' opposite index finger and used as a base line. The trials were run for seven test subjects. Each subject was exposed to two different static magnetic field configurations: dipole and quadrupole. From the preliminary study, it was found that the quadrupole configuration showed little effect on the SpO2 level. The dipole trials showed that there was a change in the SpO2 level, but this change could not be attributed only to the magnetic field. The dipole combination exerted pressure on the subjects' index finger. This pressure could have interfered with the SpO2 level.

This paper presents the results of a more controlled study of the static magnetic field interactions on the SpO2 level in the index finger. A protective ring has been added to prevent the dipole magnet configuration from exerting pressure on the index finger. The results from a stronger quadrupole configuration will also be presented.

C3-1
08:40

LIMITATIONS ON DETECTION AND CLASSIFICATION FROM COMPRESSED IMAGES

Robby Gupta Alfred O. Hero III*
Department of Electrical and Engineering and Computer Science
University of Michigan
Ann Arbor, MI 48109-2122

Data rate reduction is often a requirement for high throughput imaging sensors in remote sensing, dynamic tomography, and non-destructive testing. Such reduction can be acheived through image compression via cell averaging, wavelet thresholding, vector quantization, and other types of image coding. As image compression necessarily entails a loss of information, it is important to characterize the impact of compression on the accurate classification, detection, or estimation of image features from the compressed image. In this paper we will present results which establish lower bounds on decision errors for detection and also characterize the optimal compression schemes that acheive these lower bounds. This is specified by the optimal vector quantizer which minimizes a bound on the probability of decision error. A representation for the asymptotically optimal cell density and cell shape per unit volume is obtained. This representation indicates that the number of cells (number of bits of coding) in a given volume should be proportional to the difference between the Fisher information under the null and alternative hypotheses. The cell shapes of the optimal vector quantizer for detection are no longer Voronoi regions unlike the case of compression for minimizing mean square reconstruction error. Using these results it is possible to determine the minimum required number of bit planes (multi-resolution levels) which should be retained in a multi-resolution decomposition of natural images. This work is pertinent to target detection in SAR/IR imaging, data mining, medical image archiving (storage and retreival), and other high data rate applications. This work is supported in part by the Air Force Office of Scientific Research (AFOSR) under the AASERT program, contract No. F49620-98-1-0370.

C3-2
09:00

MULTISCALE PROBABILITY MODELS FOR INVERSE PROBLEMS IN IMAGING

R. D. Nowak
Department of Electrical and Computer Engineering
Rice University MS-380
PO Box 1892
Houston, TX 77251-1892

Probabilistic multiscale image models often yield very powerful image processing and analysis algorithms requiring minimal computational resources. However, in many (perhaps most) applications of interest, the object we wish to recover is subjected to a transformation or distortion during data acquisition (e.g., tomographic projections, atmospheric distortions, blurring). In such cases, image recovery requires the solution of an *inverse problem.* Multiscale image models have proved to be tremendously useful in image denoising, segmentation, and texture synthesis, but less is understood about their utility in solving inverse problems in imaging. The goal of this work is to propose a unified multiscale framework for image reconstruction and restoration problems involving transformed or distorted data, treating both Gaussian and Poisson observation models. The new framework described here is based on earlier work in the Gaussian setting (Y. Wan and R. Nowak, *Proceedings of SPIE*, Conf. **3813**, 1999) and the Poisson case (R. Nowak and E. Kolaczyk, *Proc. 32nd Asilomar Conference on Signals, Systems and Computers, 1682-1686, 1998*).

The new framework for inverse problems is based on Bayesian multiscale image modeling and iterative optimization algorithms (e.g., EM and related Alternating-Maximization algorithms). The framework is founded on a novel hierarchical Bayesian modeling approach beginning with a multiscale "state" model representing a latent image "primitive" followed by successive modeling stages representing the image formation, transformation/distortion, and observation processes. A key feature of our hierarchical models is that they admit iterative training and optimization algorithms which inherit the desirable features of classical multiscale analysis such as low computational complexity, simple processing strategies, and straightforward interpretation and adaptation. Moreover, in combination the models and optimization strategies allow us to solve problems in which the object of interest is indirectly observed, undergoing a known linear transformation. In addition to providing a unifying multiscale framework for inverse imaging problems, the hierarchical modeling approach pursued here also serves as a theoretical paradigm for studying natural image modeling.

Applications of the new approach are many, ranging from image restoration and deblurring to tomographic image reconstruction.

C3-3
09:20

RECURSIVE SEGMENTATION OF POISSON FIELDS

Mario A. T. Figueiredo*
Instituto Superior Tecnico, and
Instituto de Telecomunicacoes
1049-001 Lisboa PORTUGAL

Photon-limited images are formed by detecting and counting individual photon events. This type of data, which is governed by Poisson statistics, appears in several imaging techniques; examples include gamma-ray astronomy and several medical imaging modalities. Segmenting these images into regions that are well modelled as having homogeneous Poisson intensity is an important problem. We describe novel methods for estimating piecewise homogeneous Poisson fields based on Rissanen's *minimum description length* (MDL) criteria. By adopting a coding-theoretic model selection approach, our methods are able to adapt to the the observed field in an unsupervised manner; that is, it is able to select the best level of segmentation (number of regions) supported by the data. ¿From an algorithmic point of view, we present a parsing scheme based on fixed multiscale trees (binary trees, for 1D data, quad-trees, for 2D image) and an adaptive recursive partitioning algorithm, both guided by the MDL criteria. From a coding-theoretical perspective, the proposed schemes can be seen as predictive techniques operating in scale, from coarse to fine. One of the interesting aspects of our proposal is that, since the Poisson data (counts) are integer-valued, we are able to derive MDL criteria without asymptotic approximations. In contrast, most previous applications of MDL in imaging contexts involve Gaussian statistics (which are real-valued) and require asymptotic arguments. Hence, our application of MDL here is especially simple and well motivated. The experiments reported testify for the good performance of our approach and show that the recursive scheme outperforms the fixed tree approaches.

C3-4
09:40

STATISTICAL IMAGE MODELING USING WAVELET DOMAIN HIDDEN MARKOV TREES

Richard Baraniuk
Department of Electrical and Computer Engineering
Rice University MS-380
PO Box 1892
Houston, TX 77251-1892

The wavelet domain provides a natural setting for the statistical analysis and processing of images, especially those rich in *singularities* (edges, ridges, textures, and other transients). Since wavelets form a basis, they can reproduce arbitrary functions, from highly structured real-world images to completely unstructured noise. In linguistic terms, the wavelet *vocabulary* can be too expressive. To realistically model real-world images, we must narrow this vocabulary's scope by imposing a set of constraints — a *grammar* — that captures the salient structures of singularities. While much research has concentrated on developing new wavelet vocabularies, the current challenges to wavelet-based image processing lie in grammatical modeling.

We have developed a class of tree-structured probabilistic image models that capture the dependencies and nonGaussian statistics encountered in real-world wavelet transforms. Based on a hidden Markov model framework, with its fast training and likelihood computation algorithms, our *hidden Markov tree* (HMT) models are particularly well suited to images containing singularities and textures.

When employed as a prior distribution in a Bayesian image processing setup, the HMT enables simple yet and computationally efficient schemes for image estimation, detection and classification, segmentation, and synthesis. We illustrate with a new image segmentation algorithm that fuses HMT-based likelihood calculations into a reliable final segmentation. A useful feature of this algorithm is its ability to work directly on wavelet-compressed images, without the need for decompression.

For more information, see H. Choi and R. Baraniuk, "Multiscale Texture Segmentation using Wavelet-domain Hidden Markov Models" (submitted to *IEEE Trans. Image Proc.*, 1999) and M. Crouse, R. Nowak, and R. Baraniuk, "Wavelet-based Statistical Signal Processing using Hidden Markov Models," (in *IEEE Trans. Signal Proc.*, vol. 46, pp. 886–902, April 1998), both available from the Rice DSP web site at www.dsp.rice.edu.

C3-5
10:00

APPLICATION OF AN EXPECTATION-MAXIMIZATION ALGORITHM FOR STRUCTURED COVARIANCE ESTIMATION TO RADIO ASTRONOMY

Aaron D. Lanterman
Coordinated Science Laboratory
Univ. of Illinois
1308 W. Main
Urbana, IL 61801

Image restoration in radio astronomy is often posed as a problem of reconstructing a nonnegative function from sparse samples of its Fourier transform. We explore an alternative approach which reformulates the problem in terms of estimating the entries of a diagonal covariance matrix from Gaussian data. The received data is modeled as $r(t) = \Gamma^\dagger c(t) + w(t)$, where $c(t)$ is zero-mean complex Gaussian with diagonal covariance Σ, Γ is a matrix of complex exponentials associated with the phase delays of the various detector elements, $w(t)$ is i.i.d. complex Gaussian receiver noise with variance N_0, and the snapshots are independent from one time sample to the next. For each t, $r(t)$ is zero-mean complex Gaussian with covariance $\Gamma^\dagger \Sigma \Gamma + N_0 I$. The maximum-likelihood estimate of Σ cannot be readily computed analytically; hence we explore an iterative expectation-maximization algorithm proposed by Snyder, O'Sullivan, and Miller (*IEEE Trans. on Info. Theory*, **35**, 536-548, 1989) in the context of radar imaging. The computations for one step of this EM algorithm may be written as: 1) $K = \Gamma^\dagger \Sigma^{old} \Gamma + N_0 I$, 2) $\Xi = \Sigma^{old} \Gamma K^{-1}$, and 3) $\Sigma^{new} \stackrel{d}{=} \Xi(\frac{1}{N} \sum_{t=1}^{N} r(t) r(t)^\dagger - K) \Xi^\dagger$, where $\stackrel{d}{=}$ indicates that only the elements along the diagonal are assigned; the remainder are set to zero. Such EM iterations are guaranteed to enjoy increasing likelihood.

One of the advantages of maximum entropy in traditional radio astronomy formulations is that the entropy functional ensures nonnegative estimates. Nonnegativity is similarly guaranteed by the EM iterations. The main practical difficulty in implementing the EM algorithm is the matrix inverse in step (2); we will discuss approaches to overcoming this hurdle.

The resulting maximum-likelihood estimates tend to be unacceptably rough due to the ill-posed nature of maximum-likelihood estimation of functions from limited data, so some kind of regularization is needed. We will explore penalized likelihoods based on entropy functionals, a roughness penalty proposed by Silverman (*The Annals of Statistics*, **10**, 795-810, 1982), and an information-theoretic formulation of Good's roughness penalty crafted by O'Sullivan (*IEEE Trans. on Image Proc.*, **4**, 1258-1268, 1995).

C3-6
10:40

ACCELERATED MAXIMUM LIKELIHOOD RECONSTRUCTION VIA PROXIMAL POINT ITERATIONS WITH KULLBACK PENALTY

Alfred O. Hero III* Stephane Chretien, Robinson Piramuthu
Department of Electrical and Engineering and Computer Science
University of Michigan
Ann Arbor, MI 48109-2122

Iterative maximum likelihood (ML) algorithms are important for nonlinear estimation problems when no closed form ML solution exists or when high dimensionality makes analytical methods impractical. In this paper we present a new class of fast and stable iterative ML algorithms which generalize the expectation-maximization (EM) algorithm. These iterative methods can handle penalties which are non-convex and non-differentiable, arising in channel equalization, non-destructive testing, tomography, and edge preserving image restoration applications. Our method is based on a *proximal point algorithm* implemented with a Kullback-type penalty function. The Kullback penalty is a measure of distance between the incomplete data log likelihood and the complete data log likelihood functions. When the proximal regularization parameter is set to unity one obtains the classical expectation maximization (EM) algorithm. For other values of the regularization parameter, relaxed versions of EM are obtained which can have much faster convergence. By smoothly varying the regularization parameter from one to zero we obtain a hybrid EM algorithm which benefits from the stability of EM in the initial iterations and benefits from the superlinear convergence of Newton's method in the final iterations. A full analysis of convergence has been performed for the case of smooth differentiable likelihood functions. We present an implementation of the algorithm using Moré's *trust region* update strategy. For illustration the method is applied to a non-quadratic signal restoration problem arising in quantum photo-detection and positron emission tomography (PET).

C3-7
11:00

NOISE REMOVAL AND SEGMENTATION USING DIFFUSION EQUATIONS

Ilya Pollak
Brown University, Division of Applied Math
182 George St., Box F, Providence, RI 02912

Image processing based on partial differential equations (PDEs) of evolution has lately been a very active and rapidly developing field of research. The general premise is to treat the image to be processed as the initial condition of a PDE evolving in time. Then the output is the solution to the PDE at some positive time instant. For example, if the PDE is the linear heat equation, then the procedure is equivalent to linear low-pass filtering, since the solution of the heat equation at time t is the convolution of the initial data with a Gaussian function whose variance is $2t$. Even though high-frequency noise gets removed by this procedure, its utility for extracting information from images is limited, since important image features are lost in the process. For example, low-pass filtering tends to blur, displace, and remove edges, corners, and T-junctions, thereby distorting boundaries of objects, merging distinct objects which are close to each other, and removing small objects.

An elegant idea proposed by D. Gabor in the 1960s (D. Gabor, *Laboratory Investigation*, **14**, 801-807, 1965) and resurrected by many researchers during the last decade allows to retain noise suppression yet reduce or even avoid blurring by replacing the linear heat equation with a nonlinear evolution whose diffusion strength and/or direction depends on the image gradient. Some examples of these include shock filters (S. Osher, L.I. Rudin, *SIAM J. Num. Analy.*, **27**, 919-949, 1990), the anisotropic diffusion (P. Perona, J. Malik, *IEEE Transactions on Pattern Analysis and Machine Intelligence*, **12**, 629-639, 1990), and descent equations for the total variation (C. Bouman, K. Sauer, *Proc. of the Conference on Information Science and Systems*, 383-387, Baltimore, MD, March 1991; K. Sauer, C. Bouman, *IEEE Transactions on Nuclear Science* **39**(4), August 1992; L.I. Rudin, S. Osher, E. Fatemi, *Physica D*, **60**, 259-268, 1992). After reviewing these evolutions, we introduce stabilized inverse diffusion equations (SIDEs), which automatically produce a fine-to-coarse family of segmentations of the input image. Like some of the previous frameworks, SIDEs can be generalized to vector-valued (e.g., color) images and orientation images (i.e., images whose pixels take values on a half-circle). What radically sets SIDEs apart, however, is their robustness to both blurring and pervasive non-Gaussian noise, as well as their computational efficiency—which we demonstrate through many examples. We refer to other literature for theoretical results concerning many important properties of SIDEs, including their well-posedness, stability, and robustness (I. Pollak, A.S. Willsky, H. Krim, *IEEE Transactions on Image Processing*, 1999, to appear), as well as their interpretation as the optimal maximum-likelihood edge detector for certain 1-D problems (I. Pollak, A.S. Willsky, H. Krim, *Proc. Intl. Conf. on Acoustics, Speech, and Signal Processing*, Phoenix, AZ, 1999).

C3-8
11:20

A PROBABILISTIC AND SPATIAL MODEL FOR MESO-SCALE CLOUDS BASED ON A WAVELET DECOMPOSITION

P. Naveau
Geophysical Statistics Project
P.O. Box 3000
National Center for Atmospheric Research
Boulder, CO 80307

To model the atmospheric characteristics of mesoscale clouds system in the Western Pacific, a variety of simulated numerical models has been generated and studied in the past. Because of the very large size of these data sets, the statistical analysis of such simulated outputs can be very complex, and classical statistical tools are not always possible to implement. A key aspect in this study is that clouds present different spatial structures at different scales. Hence, we choose to base our model on a wavelet decomposition which can capture the inter-scale dependencies.

Different constraints on our data exist. The algorithm has to be fast, to take into account the double-periodicity of our images, and to give results that have a physical interpretation. Also, each snapshot of the data belongs to one of the three cloud system regimes: squall-lines, non-squall clusters and scattered convection. Our model has to reproduce these three kinds of regimes since they reflect distinct physical and atmospherical phenomena. We will present a stochastic model based on the discrete wavelet transforms that satisfies all these required conditions. In particular, the distribution of wavelet coefficients of the total water condensate will be identify and used to model the three cloud regimes. The wavelet domain will be decompose into two primary components, based on the rate of change of vertical wind. This mathematical decomposition will allow us to separate two different scales of motions (convective and mesoscale) that are important in terms of statistical properties and in terms of physical interpretation. This type of approaches lends itself to a number of different applications in the processing of geophysical data. Various examples will illustrate the proposed technique.

C3-9
11:40

BAYESIAN IMAGE ANALYSIS IN SCANNING MAGNETORESISTANCE MICROSCOPY

D. M. Higdon*
Duke University
Durham, NC 27708-0251
S. Y. Yamamoto
Phase Metrics, Inc.
San Diego CA, 92121

We apply Bayesian image analysis techniques to a problem in a newly developed scanned probe technology which uses commercial magnetoresistive (MR) record/playback heads as probes to sense magnetic fields. This technology can be used both for magnetic imaging, and for evaluating playback and record processes in magnetic recording. In MR microscopy, an MR head is raster-scanned while in physical contact with a magnetic sample (e.g., hard disk media, tape, or fine magnetic particles). By plotting the MR resistance as a function of position, a very high resolution (on the order of $.1 \times 1.0$ μm) magnetic image of the sample is constructed.

This case study focuses on characterizing the head sensitivity function (HSF), which depends on the physical dimensions and the magnetic properties of the MR head. These sensitivity functions are of great practical interest since they ultimately relate to the head's performance in a high density data storage environment. Properties in the MR head make it difficult to specify the HSF from purely physical (theoretical) models, so we take a Bayesian approach to model and estimate the HSF.

On the surface, the HSF estimation is a deconvolution problem. However there are a number of features in this application that make this problem challenging:

- the scanned image contains a substantial amount of correlated noise, much of which results from microfluctuations in temperature during the scan;
- the actual magnetic field, which is treated as known in standard deconvolution problems, has a fair bit of uncertainty attached to it. We need to account for this in our estimation;
- the MR head shows some "head asymmetry" which must also be accounted for;
- characterizing uncertainty in the HSF estimate is required so that we can assess whether features in a point estimate appear to be genuine.

We take a Bayesian modeling approach which relies on Markov random field models and accounts for the features described above. The resulting posterior distribution is explored using Markov chain Monte Carlo.

C3-10
12:00

PARAMETRIC ESTIMATION FOR GRANULOMETRY PROBLEMS

Alfred O. Hero III
Department of Electrical and Engineering and Computer Science
University of Michigan
Ann Arbor, MI 48109-2122

We consider estimation of parameters of the shape distribution of a population of i.i.d. shapes, or grains, in 2D and 3D images. This problem is important in diverse applications such bio-assay, microscopy, balistics, and numerical taxonomy. We adopt a Boolean random coverage model with Poisson spatial statistics and random shapes arising from a probability distribution of known functional form. The image formation processes introduces mutual occlusion, spatial blurring and background noise for which a multidimensional filtered-Poisson/Gaussian process model is proposed. We use a information theoretic transmission channel paradigm to derive an approximate expectation-maximization (EM) type estimation algorithm and a lower bound on minimum attainable estimation error. For illustration we consider a geometric coverage process consisting of a random number of spheres having random radii and positions. For this problem analytical expressions for the error bound and the M step of the EM algorithm are obtained. The lower bound characterizes optimal shape estimator performance as a function of the underlying parameters such as: Poisson rate, background noise level, point-spread-function standard width, and shape distribution. The bound establishes existence of two operating regimes: a Poisson-limited regime where performance is expected to be close to that obtainable with perfect image formation (no blurring and no noise), and a Gaussian limited regime where the spatial blurring and noise dominate the estimator's performance.

Session D/J1, 10:55 AM-Fri., Room 200
NEW TECHNOLOGY FOR ARRAY TELESCOPES
Chairpersons: J. Dreher, SETI Inst. (dreher@seti.org)
Z. Popovich, Univ of Colorado (zoya.popovic@colorado.edu)

D/J1-1
11:00

A LOW FREQUENCY ARRAY FOR THE NEXT DECADE

N. E. Kassim
Code 7213
Remote Sensing Division
Naval Research Laboratory
Washington, DC 20375

Low frequency ($\leq$ 150 MHz) arrays of the past and present, even those with formidable collecting area, have been blind to many important imaging investigations. This is because the ionosphere has limited baseline lengths ($<$ 5 km) and restricted the angular resolution, in turn severely limiting the sensitivity due to confusion. The new 74 MHz VLA system now routinely demonstrates that self-calibration can remove ionospheric distortions over long baselines (N. E. Kassim et al., *Astronomical Journal*, **106**, 2218-2228, 1993). This offers the opportunity of opening a new window on the electromagnetic spectrum at low frequencies with a suitably designed large, Low Frequency Array (LOFAR). While radio astronomy was discovered by Jansky near 20 MHz, the quest for ever higher angular resolution and the ionospheric limitation have ironically left this region among the most poorly explored in the entire spectrum. LOFAR applications exist across virtually all areas of astrophysics (N. E. Kassim and W.C. Erickson, *SPIE*, **3357**, 740-754, 1998), and the two to three orders of magnitude improvement in imaging power it will provide over past low frequency arrays favors new discoveries.

LOFAR is inspired by the success of a narrow band 74 MHz VLA system of modest collecting area ($< 5 \times 10^3\ m^2$) and limited, albeit unprecedented, angular resolution ($\sim 20''$). This opens the way to developing a much larger (longest baselines $\sim$500 km, collecting area $\sim 1 \times 10^6\ m^2$) and more versatile, broad-band ($\sim$ 3-300 MHz) instrument. A completely electronic LOFAR could explore these low frequencies at high sensitivity (mJy) and high angular resolution (arc-second), and will provide multiple, independently tunable and steerable IFs which will define a new approach to observing. A ground-based LOFAR with intrinsically modest bandwidths and relatively cheap hardware can be developed at a fraction of the cost of higher frequency ground or space-based systems of comparable size or sophistication.

In addition to astrophysical applications, LOFAR's innovative use of active dipole receptors and digital signal processing provides a technological stepping stone to the SKA. There is also interest in its use as a radar receiver. Solar radar could detect Earth-directed Coronal Mass Ejections for geomagnetic storm prediction, while terrestrial ionospheric and magnetospheric investigations are also possible. Finally, if sited in New Mexico, synergistic coordination with the VLA expansion could allow mutual sharing of infrastructure and development costs. These joint interests have spurred formation of a NRL-NFRA-NRAO consortium to build LOFAR in the next decade.

D/J1-2 ELECTROMAGNETIC WAVE PROPAGATION ON A THIN WIRE ABOVE EARTH:
R.G. Olson, J.L. Young, D.C. Chang, School of EEOS, Washington State Univ.

D/J1-3
12:00

VLBI ARRAYS, PRESENT AND FUTURE

J. S. Ulvestad
National Radio Astronomy Observatory
P.O. Box O
Socorro, NM 87801

In the 1990s, Very Long Baseline Interferometry (VLBI) techniques have advanced because of a number of new arrays, new telescopes, and new features added to existing telescopes. The Very Long Baseline Array of the U.S. National Radio Astronomy Observatory, formally dedicated in 1993, is the first full-time VLBI array. The long-standing European VLBI Network has consolidated many of its operations in the Joint Institute for VLBI in Europe, which incorporates a new 16-station VLBI correlator. The Australia Pacific Telescope has combined existing antennas with the new Australia Telescope to provide better coverage for imaging southern radio sources. The first dedicated Space VLBI satellite, HALCA, was launched in 1997 to work with all three of these sets of telescopes, providing the first VLBI images on baselines longer than Earth's diameter. Finally, the Coordinated Millimeter VLBI Array was formed in recent years to provide logistical and technical support for the drive to VLBI wavelengths of 3 mm and shorter.

Key technologies used in the current generation of VLBI arrays include (1) several new wideband recording systems (VLBA, Mark 4, S-2, and VSOP), with instantaneous data rates ranging from 128 Mbit/sec to (ultimately) 1 Gbit/sec; (2) a new generation of correlators associated with the new recording systems; (3) low-noise amplifiers with performance within a factor of a few of the quantum limit; and (4) a variety of technologies (e.g., ground-to-space time transfer) associated with Space VLBI.

A number of advanced technologies are under study or development for the next generation of VLBI observatories. A key requirement for the future is the need for much more sensitivity in VLBI. Larger apertures and increased bandwidths (hence higher data rates) are the primary routes to this enhanced sensitivity. Several means of achieving large apertures are being studied in conjunction with the Square Kilometer Array, which is likely to have at least some VLBI elements. Data rates of many Gbit/sec will require either new recording technologies or, more likely, development of real-time "VLBI" systems making use of fiber-optic data transmission. The move to higher observing frequencies in VLBI will make use of a new generation of ground telescopes, such as the Large Millimeter Telescope and the phased Atacama Large Millimeter Array; the latter array also will require the high-bandwidth fiber-optic transmission. Future Space VLBI missions may downlink their data by means of optical transmission from space to ground, and large inflatable apertures are being explored as a means of providing space antennas having sensitivities similar to those on the ground.

Session E/J1, 08:35 AM-Fri., Room 200
SPECTRUM MANAGEMENT AND RFI MITIGATION
Chairpersons: M. McKinnon, NRAO (mmkinno@gb.nrao.edu)
J. Murray, ASR World (jmurray@ASRWorld.com)

E/J1-1 08:20 CURRENT ISSUES IN SPECTRUM MANAGEMENT AFFECTING RADIO ASTRONOMY AND REMOTE SENSING

P. G. Steffes
School of Electrical and Computer Engineering
Georgia Institute of Technology
Atlanta, GA 30332-0250

The National Research Council Committee on Radio Frequencies (NRC/CORF) serves to coordinate and define the U.S. research community's needs for passive radio frequency allocations and assignments in research areas such as space science, radio astronomy, meteorology, oceanography, agriculture, and remote sensing. Over the past year, CORF has considered a number of frequency allocation issues which involve potential interference to the passive services, including proposals by the FCC to allocate frequencies adjacent to the 10.6-10.7 GHz radio astronomy and passive sensing bands for satellite downlinks, both from geostationary and non-geostationary satellites. Since such allocations are immediately adjacent to the passive bands, the potential for harmful interference is great from even the most minute out-of-band emissions from these spaceborne transmitters.

Another source of concern is interference to radio astronomical observation from a growing number of hand-held satellite uplink transmitters in the 1610-1660 MHz band. While potential interference from uplink transmissions from ground stations to satellites can usually be mitigated by coordinating operations around radio observatories so as to limit emissions and establish protection zones, the coordination of potentially large numbers of hand-held transmitters is especially challenging. CORF has urged the FCC to require such coordination and out-of-band emission protection as part of the implementation of the Global Mobile Personal Communications by Satellite (GMPCS) Memorandum of Understanding.

While some potential spectrum allocations present substantial risks to passive services, others, by nature of their fixed terrestrial implementations and well-controlled emission levels, present better alternatives for adjacent frequency allocation, or even shared allocations, with the passive services. The concept of allocating high-priority, low-interference services (e.g. in-hospital medical telemetry) adjacent to the passive bands may present a useful paradigm for future allocations in the fast-filling microwave spectrum.

Results of these studies will be presented, in addition to a general discussion of topics of concern to scientific users of passive allocations.

E/J1-2
08:40

RADIO ASTRONOMY ISSUES AT WRC-2000

Tomas E. Gergely
National Science Foundation
4201 Wilson Blvd.
Arlington, VA 22230

World Radiocommunication Conferences (WRCs) are held regularly, at 2-3 year intervals. Items that relate directly or indirectly to radio astronomy can be found on the Agendas the Conferences with increasing frequency and the next one (WRC-00), to be held in Istanbul, Turkey in May-June, 2000 is no exception.

One WRC-00 agenda item of great interest to radio astronomers is the revision of the International Table of Allocations between 71 and 275 GHz, with the specific goal of allocating additional spectrum to radio astronomy and remote sensing. Radio astronomy at millimeter wavelengths is one of the fastest growing areas of astronomy, and several large telescopes are in the design phase or under construction, that will to operate in this range. Interest in commercial uses of the millimeter spectrum is also increasing, and a revision of frequency allocations is timely, before the use of these bands increases substantially. Since mm-telescopes observe up to at least 1000 GHz, astronomers would also like to secure access to the spectrum above 275 GHz, which is not allocated currently. WRC-00 will elaborate the preliminary Agenda for WRC-03 and representatives of the radio astronomy and remote sensing communities intend to propose that WRC-03 should consider allocations between 275 and 1000 GHz.

Other agenda items of interest deal with radio astronomy sharing in the neighborhood of the 42.5 GHz astronomy band with satellite downlinks and high altitude platforms intended to provide broad band data services, with satellite downlinks at 15.4 GHz, which are also adjacent to a radio astronomy band, and with unwanted emissions from space stations.

I discuss the proposals put forward by the radio astronomy community on, the status of the relevant U.S. proposals and the possible outcome of these issues at the WRC.

E/J1-3
09:00

ADJACENT BAND INTERFERENCE

Gerald F. Hurt
NTIA, U.S. Department of Commerce
Room 6725
1401 Constitution Ave., N.W.
Washington, DC 20230 U.S.A.
Tele: 202-482-4107 Fax: 202-482-4595
e-mail: ghurt@ntia.doc.gov

Extensive radio regulations have been developed, both nationally and internationally, to help assure that the various radio services can operate compatibly in the same environment without unacceptable levels of interference. These regulations are primarily focused on radio systems sharing the same allocated bands of frequencies. Recent years have seen a dramatic increase in the number of instances/concerns of adjacent band interference, i.e., interference from a transmitter in one band causing interference to a receiver in an adjacent allocated band. Examples include: emissions from mobile satellite space stations into GPS and radio astronomy receivers, radar emissions into digital fixed and fixed-satellite service receivers, emissions from high powered Government systems into commercial systems in bands reallocated by Congressional mandate, and spurious emissions from unlicensed (Part 15) radio frequency devices. These types of problems are expected to increase due several fundamental factors, including: continuing increases in overall spectrum use, conversion from analog to advanced digital modulations, marketplace pressures for inexpensive radio equipment, loss of previously available Aguardbands,@ and manufacturer's lack of awareness regarding radio equipment operating in adjacent bands.

This presentation will describe a comprehensive program to investigate all aspects of adjacent band interference to identify the steps that might be taken to lessen these problems in the future. Included in the review are: documenting and reviewing case histories of adjacent band interference, the role of transmitter and receiver spectrum standards, measurement techniques, analysis methods (including factors such as propagation, building attenuation, aggregate effects, etc.), and interference mitigation techniques.

One of the key outputs of the program will be the development of a comprehensive data base of information characterizing Federal use of the spectrum in bands adjacent to bands used for commercial, consumer, public safety, and research activities. This data base, to be available on the web, should provide radio equipment designers, manufacturers, operators and regulators with a common baseline from which to make more informed decisions and better overall management of the radio spectrum.

E/J1-4
09:20

COMMERCIAL SATELLITE COMMUNICATION SYSTEMS: THE DEMAND FOR NEW SPECTRUM

John V. Evans
COMSAT Corporation
6560 Rock Spring Drive
Bethesda, MD 20817

Commercial satellite communications systems (e.g. INTELSAT) were first developed to provide *fixed* services at C-and Ku-band from geostationary satellites. These systems provided point-to-point connectivity for voice, video and data. Later, satellites were employed for broadcasting television first to cable head ends, and more recently direct to the home. Services to *mobile* users have been introduced at L-band, also employing geostationary satellites (e.g. Inmarsat). All of these systems have so far co-existed with other services (e.g. radio astronomy) without notable instances of interference.

In recent years there has been a demand for additional RF spectrum for new satellite systems (e.g. Iridium) to provide *mobile* services in the L-and S-bands and for *fixed* satellite services delivering multimedia at Ku, Ka and Q/V-band. The paper reviews the mobile systems that have received FCC licenses and the multimedia system that have been filed for at the FCC. Of the mobile systems Iridium, Globalstar and ICO are either already in service or will be shortly. These systems employ non-geostationary satellites to achieve global coverage, while other systems (e.g. ACeS) employing geostationary satellites will provide regional coverage. Systems to provide homes and small offices with data services (e.g. Internet access and delivery of broadband information) have been proposed that would employ non-geostationary satellites in the existing Ku-band as well as geostationary and non-geostationary satellites at Ka and Q/V bands. None of the multimedia systems is expected to be in service prior to 2003, and the first entrants are expected to be the Hughes' "Spaceway" and Lockheed Martin "Astrolink" geostationary Ka-band systems with others likely to follow. The paper concludes with observations about the likely commercial viability of these systems, and the belief that this will greatly limit the number that are actually built.

E/J1-5 09:40 EFFECTS OF IRIDIUM SATELLITES ON OBSERVATIONS WITH THE ARECIBO RADIO TELESCOPE

Michael M. Davis
National Astronomy and Ionosphere Center
Arecibo Observatory, Arecibo, Puerto Rico

The Arecibo Observatory 305-m reflector is the largest filled-aperture radio telescope in the world. A major upgrade has recently been completed (P.F. Goldsmith, "The Second Arecibo Upgrade", *IEEE Potentials*, *15*, No. 3, Aug./Sept. 1996). Both before and after the upgrade, its sensitivity has provided a unique facility for the study of atomic and molecular spectra, including the OH line at 1612 MHz.

New Mobile Satellite systems have been developed during this decade to provide communication capabilities to customers anywhere on the earth's surface. IRIDIUM is such a system, with 66 active satellites in low earth orbit. The IRIDIUM downlink band, 1621.35-1626.5 MHz, used to transmit to hand-held units and other terminals on the ground lies just above the 1610.6-1613.8 MHz band allocated to Radio Astronomy. Close spacing of frequency bands for use by sensitive radio telescopes and powerful satellite transmitters is generally undesirable. Successful operation by both parties requires very close coordination.

The International Telecommunications Union recognizes both Radio Astronomy and Mobile Satellites as Services, and provides Recommendations to adhering countries. Within the United States, the NTIA and the FCC implement these Recommendations. In particular, the FCC set the following as one of the licensing requirements for proposed Mobile Satellite Systems (FCC Report and Order 94-261, Oct. 1994):

> *Mobile-Satellite Service space stations transmitting in the 1613.8-1626.5 MHz band shall take whatever steps necessary to avoid causing harmful interference to the radio astronomy facilities in subparagraphs (a)(1)(i)-(ii) of this section* [including Arecibo] *during periods of observation.*

and a complementary requirement for use of the 1612 MHz band by the Radio Astronomy Service in the US:

> *The Radioastronomy Service shall avoid scheduling radio astronomy observations during peak MSS/RDSS traffic periods to the greatest extent practicable.*

NAIC and IRIDIUM signed a formal Coordination Agreement in March 1998, prior to start of operation of the IRIDIUM system in November 1998. The Coordination Agreement spells out practical details, including notification of scheduled 1612 MHz observations a minimum of 30 days in advance and a requirement that IRIDIUM emissions shall not exceed –238 dBW/m^2/Hz in the RAS band during such scheduled observations.

We have now had many months of practical experience under the Coordination Agreement. This talk will describe how it is working.

E/J1-6
10:20

MONITORING IRIDIUM SATELLITE SIGNALS NEAR THE 1612 MHz OH-BAND

John Galt
Dominion Radio Astrophysical Observatory
Box 248 Penticton BC
Canada V2A 6K3

Astronomical observations in the 1610.6 to 1613.8 MHz band where the Radio Astronomy Service has primary allocation have been contaminated for several years by Russian GLONASS navigation satellites. Recently some progress was made in persuading Russian engineers to redesign any new satellites and to operate the offending satellites in a way which would lessen interference to radio astronomy and other services. Shortly thereafter, astronomers learned that an American company, Iridium LLC, intended to use the 1616.0 to 1626.5 MHz band for downlinks from satellites in a manner which, with high traffic levels, might generate strong intermodulation signals in the nearby radio astronomy band.

In late 1997 very little was known about the proposed IRIDIUM transmissions. I therefore assembled monitoring apparatus to study the spectral and temporal behaviour of these signals to determine whether they were in compliance with the ITU's Radio Regulations, how they might affect astronomical observations and what steps might be taken to ameliorate detrimental effects.

The apparatus uses a pyramidal horn with a beamwidth of 29° and an aperture of $0.153m^2$. Although the antenna points to the zenith, its sidelobes pick up IRIDIUM signals from whatever satellites are above the local horizon as would a large parabaloid pointing to an astronomical radio source. The horn feeds a preamplifier followed by a 40 MHz-wide filter passing both the 1612 MHz radio astronomy band and the adjacent satellite bands. After three stages of mixing and amplification signals are applied to a 128 channel digital autocorrelation spectrometer. Frequency switching can be used to observe an 8 MHz-wide band and load-switching or similar methods can be used to observe a 4 MHz-wide band. Spectra and histograms show that IRIDIUM signals are mostly confined to discrete channels spaced 0.333 MHz apart.

To study the pulse structure of the transmissions the spectrometer automatically tunes a communications receiver to a single active IRIDIUM channel. This receiver's 5.8 kHz-wide output is detected, sent to an A/D converter and recorded. Pulses occur at intervals of 180 ms and are typically 10 ms wide.

E/J1-7
10:40

BLANKING OF TEMA INTERFERENCE AND ITS EFFECT ON RADIO-ASTRONOMICAL CORRELATION MEASUREMENTS: EXPERIMENTAL RESULTS

Amir Leshem Alle-Jan van der Veen*
Delft University of Technology
Dept. Electrical Engineering
2628 CD Delft, The Netherlands

The fast growth of the wireless communication industry poses severe limitations on radio astronomical observations. Two such examples are the Iridium system which will probably cause problems within bands reserved to radio astronomy and the GSM system which became ubiquitous and thus prevents observation in its band. These developments cause an increasing interest in detection and suppression of man-made signals in radio astronomy.

Several methods have been proposed for single dish radio telescopes. Among these we find detection of change in the mean power (P. Friedman, Proc. IEEE SSAP workshop 1996, 264-266), Weber's detector implemented in Nançay (Weber et-al. AA Supp.126, 161-167 1997) and adaptive filtering (C. Barnbaum and R.F. Bradely, AJ 115,2598-2614,1998) . The main drawback of such single channel detectors is that they cannot exploit spatial properties of the interference. In synthesis radio telescopes the desired astronomical signals as well as the interference are received by large sensor arrays. In this situation we can perform combined spectral-temporal and spatial processing to detect and remove only those narrow-band slices for periods and in directions in which the interference is present. This type of solution is very well suited to improve radio astronomical observations in the presence of TDMA communication systems such as GSM and Iridium.

In this paper we propose a simple spatio-spectral detection scheme which enables the blanking of narrow-band interference. Our approach is based on subbband decomposition of the data so as to maintain narrow-band assumption, and detection based on the eigenstructure of the data covariance matrix. We have tested a likelihood ratio test and a test based on the MDL principle. A more extensive overview of these ideas is descried in (A. Leshem et.al Proc. IEEE SPAWC 1999) and (A. Leshem and A-J. van der Veen (Proc. IEEE HOS 99, 25-29).

We will also describe a system built for recording RFI on-line. The effectiveness of the space-time detection and blanking process is also demonstrated by applying the algorithms to data measured at the WSRT radio-telescope using the on-line recording system.

Keywords: Interference rejection, signal detection, synthesis imaging, radio-astronomical receivers.

Session F3, 08:35 AM-Fri., Room 1B-51
PROPAGATION MODELING AND MEASUREMENTS
Chairperson: G.D. Dockery, Johns Hopkins University (dan.dockery@jhualp.edu)

F3-1
08:40

EVAPORATION DUCT ASSESSMENT FROM BUOYS

Herbert V. Hitney
Propagation Division
Space and Naval Warfare Systems Center
49170 Propagation Path
San Diego, CA 92152-7385
Email: herb@spawar.navy.mil

The evaporation duct is usually assessed using measurements of sea surface temperature and, at a convenient reference height, bulk meteorological measurements of air temperature, moisture, and wind speed. One such method is described by R.A. Paulus, "Practical application of an evaporation duct model," *Radio Science*, vol. 20, no. 4, 1985. Using this method in conjunction with various propagation models to assess propagation loss on microwave over-the-horizon paths has generally given very good long-term statistical results. Median modeled loss is often within a few dB of the median observed loss (H.V. Hitney and R. Vieth, "Statistical Assessment of Evaporation Duct Propagation," *IEEE Trans. Antennas & Propagat.*, vol. 38, no. 6, 1990 and R.A. Paulus, "Propagation in the Evaporation Duct," NRaD Tech. Report 1644, March 1994). However, time series comparisons of modeled and observed losses have shown much more variation, presumably from the less-than-ideal meteorological measurements, which were typically made at or near coastlines and may be influenced by land effects not representative of the propagation paths involved (L.T. Rogers and R.A. Paulus, "Measured Performance of Evaporation Duct Models," 1996 Battlespace Atmospherics Conference, NRaD TD 2938, December 1996).

Evaporation duct assessments based on high-quality meteorological measurements made on oceanographic buoys will be presented. The 10-meter diameter buoys are operated by the Scripps Institution of Oceanography and are known as the SIO Marine Observatory (see http://tenby.ucsd.edu/default.htm). The buoys are located just west of Point La Jolla and San Clemente Island in California, and separated by a distance of about 128 km. Data have been collected on both buoys since May 1998. Comparisons of propagation assessments at the two buoy locations will be presented. Also, comparisons between modeled loss and observed loss for a 2.4 GHz link between the Point La Jolla buoy and Point Loma in April 1999 will be presented. This link was implemented using low cost, license free, spread-spectrum digital transceivers. The terminal heights were 7 and 21.5 m above sea level and the path length was 18 km.

F3-2
09:00

ANALYSIS AND VALIDATION OF AN OPERATIONAL BULK SURFACE- LAYER (EVAPORATION DUCT) MODEL

P. A. Frederickson and K. L. Davidson
Department of Meteorology
589 Dyer Rd., Room 254
Naval Postgraduate School
Monterey, CA 93943-5114

A. K. Goroch
Naval Research Laboratory
Marine Meteorology Division
7 Grace Hopper Avenue
Monterey, CA 93943-5502

The US Navy has a major design/acquisition program (MORIAH) underway to replace/upgrade the meteorological and oceanographic (METOC) measurement systems on over 225 ships. MORIAH will consist of shipboard environmental sensors and an automated data acquisition and processing system. The processing system will estimate EM propagation conditions based on measured quantities. In this study, the planned MORIAH bulk model for estimating surface layer refraction profiles and evaporation duct height over the ocean from mean environmental measurements is described and analyzed in detail. The model is based upon Monin-Obukhov similarity (MOS) and surface renewal theories and incorporates results from the recent over-water TOGA-COARE experiment (Fairall et. al, *J. Geophys. Res.*, vol. 101, 3747-3764, 1996). The sensitivity of the duct height estimates upon the model input parameters (wind speed, air and sea temperature, humidity and pressure) is demonstrated for different stability conditions and errors associated with measurement uncertainties are discussed. These analyses demonstrate that in certain stable conditions the bulk evaporation duct estimates become highly uncertain.

A critical issue is the choice of dimensionless profile functions used in the model. The empirical functions currently used for scalar (temperature and humidity) profiles have been largely influenced by over land experiments. Little is known at present on scalar profile variations that may occur over ocean waves. The type of profile functions used has a dramatic impact on the resulting evaporation duct estimates, and upon whether a model solution can be obtained at all. In stable conditions with light winds the bulk model may fail to converge to a solution depending upon which profile functions are used. When the model does converge in stable condition, the final solution is very sensitive to small differences in any of the measured parameters

Bulk model evaporation duct estimates are compared with rocketsonde measured refractivity profiles, duct height estimates from radar sea clutter returns, and profile predicted field strengths obtained during a recent propagation experiment. The bulk model performance is evaluated according to the surface-layer scaling regime (bulk Richardson number) and coastal meso-scale regimes.

F3-3
09:20

USE OF MEASURED PROPAGATION LOSS TO EVALUATE EVAPORATION DUCT HEIGHT MODEL PERFORMANCE

Janet Stapleton
NSWCDD / T44
17320 Dahlgren Road
Dahlgren, VA 22448

In the spring of 1998 a series of propagation loss measurements were made at Wallops Island VA using a calibrated transmit/receive link operating across the 2 to 18 GHz band. These transmission measurements were made over water with the receive tower on shore at the high water mark and the transmit array onboard a boat moving radially outbound from shore between about 5 and 35 nmi. A variety of meteorological sensors on separate platforms including buoys, boats, and a helicopter were operated simultaneously. These meteorological measurements provided the basis for evaporation duct height estimation. These evaporation duct refractivity profiles were then used in conjunction with the helicopter measurements of refractivity above the evaporation duct to generate a set of range varying composite refractivity profiles suitable for use with propagation models such as the Johns Hopkins University Applied Physics Laboratory Tropospheric Electromagnetic Parabolic Equation Routine (TEMPER) (Kuttler J., Dockery G.D., 1991: *Radio Science,* 26 (2), 381-393.). The TEMPER model's resulting propagation factor values versus range and altitude were compared with the directly measured propagation factor levels obtained from the transmission link. A number of statistical parameters evaluating the comparisons were then used to determine the best estimate of the evaporation duct. These results will be presented.

The evaporation duct height models covered by the analysis include the Liu, Katsaros, and Businger (LKB) model (Liu, W.T., K. B. Katsaros, and J. A. Businger, 1979: *J. of the Atmos. Sci.* 36, 1722-1735.), the Constant Virtual Temperature (CVT) model and the Surface Measurement Model (SMM) (Rowland J.R., 1995: *Proceedings of the Electromagnetic Propagation Workshop, NRaD Technical Document 2891,* 233-240.), the Paulus model (Paulus, R. A., 1985: *Radio Science,* 20(4), 887-896.), and the neutrally stable model. These evaporation duct height estimates were merged with the helicopter-measured profiles to create a composite refractivity profile before use with the TEMPER model. In the case of the Paulus and LKB models, the duct "shape" as well as duct height is produced. This shape was used in generating the composite refractivity profiles for these models. For all other evaporation duct height models, the neutrally stable profile shape was used. The evaporation duct estimates were also evaluated without the helicopter data, assuming a standard atmosphere above the evaporation duct. These results were analyzed to evaluate the importance of the inclusion of upper air profiles.

F3-4
09:40

MESOSCALE MODELING OF COASTAL REFRACTIVITY CONDITIONS

T. Haack* S.D. Burk
Naval Research Laboratory
Marine Meteorology Division
7 Grace Hopper Ave, Stop #2
Monterey, CA 93943-5502

The June/July 1996 Coastal Waves field experiment (CW96) was conducted along the California coast to characterize the marine layer in the littoral region. These observations suggest that the summertime marine boundary layer (MBL), typically bounded above by a strong temperature inversion and laterally by the coastal topography, may behave as supercritical, channeled flow. Supercritical regimes are defined by dimensionless Froude Numbers greater than unity whereby the background flow velocity is greater than the phase speed of internal gravity waves. Consequently, perturbations are swept downstream and result in abrupt and dramatic changes in the marine layer as it interacts with changes in coastal orientation. Reduced MBL heights and accelerated velocities are characteristic of supercritical flow leeward of topographic capes and points while the blocked flow upwind of these topographic features often becomes subcritical, favoring elevated MBL depths and reduced velocities.

The height of electromagnetic trapping layers, which tend to occur at the base of the MBL inversion, can also be influenced by changes in the coastline and correlated to changes in flow criticality. In this study we examine the sensitivity of the refractivity field to variations in flow criticality. The electromagnetic ducting properties of various summertime coastal flow regimes are investigated with the aid of a high-resolution, non-hydrostatic mesoscale model, the Navy's Coupled Ocean/Atmosphere Mesoscale Prediction System (COAMPS), along with the CW96 observations. COAMPS skill in producing microwave refractivity forecasts previously has been evaluated using the VOCAR (Variability of Coastal Atmospheric Refractivity) dataset for which 425 radiosonde at eight observing stations in the California bight were released during August/September 1993. Statistics of model forecast duct base, strength, and thickness as compared to the verifying VOCAR radiosondes will be presented at the conference. Our current modeling study indicates that preferential regions of surface based ducting frequently occur in the enhanced supercritical flow downwind of convex coastal bends such as south of Cape Blanco, Oregon and Cape Mendocino, California. The same dynamics altering the refractivity field also often produce pronounced changes to the coastal stratus that can be identified by satellite imagery.

F3-5 10:00 EQUIVALENT IMPEDANCE OF ROUGH SURFACE AT LOW GRAZING ANGLES

R. Janaswamy
Code EC/Js, Department of Electrical & Computer Engineering
Naval Postgraduate School, Monterey, CA 9394
Email: janaswam@ece.nps.navy.mil,

Parabolic equation method has been widely used to study forward propagation in a half-space in inhomogeneous atmosphere, over terrain undulations, and over rough ocean surfaces (G. D. Dockery and J. R. Kuttler, *IEEE Trans. Antennas Propagat.*, 44 (15), 1592-1599, 1996). In the split-step algorithm of solving the parabolic equation the effects of boundary interactions and inhomogeneous atmosphere over a small range step are separately accounted for and applied in succession. The boundary interactions are accounted for by choosing appropriate eigen-functions for the vertical operator. In a Cartesian coordinate system, the eigen-function expansion can be carried out exactly only for flat surfaces and, for this reason, modelers have been using some kind of flat equivalence for a rough surface, such as using the Miller-Brown roughness reduction factor (A. R. Miller, R. M. Brown and E. Vegh, *IEE Proc.*, pt. H, 131 (2), 114-116, 1984), and defining an equivalent impedance. Unfortunately, such an impedance becomes dependent on the grazing angle and it is not straightforward to include angle dependent impedance surfaces rigorously within the framework of the split-step algorithm.

In the present work we study the problem of forward propagation over a random rough surface by means of a Volterra integral equation of the second kind under the standard parabolic equation approximation. By comparing the normalized field at a fixed distance from the transmitter to the normalized field over a flat surface we extract an equivalent impedance that is valid at low grazing angles. In contrast to the small perturbation approach, which yields an equivalent impedance from small roughness at all grazing angles (T. B. A. Senior, *Appl. Sci. Res., 8-B*, 437-462, 1960), our approach gives an equivalent impedance for large scale roughness, but for low grazing angles only. We show that the limiting value of the impedance at zero grazing angle can itself be used to predict low grazing angle propagation over a rough surface.

F3-6
10:40

CALCULATION OF THE SURFACE INCIDENT FIELD USING TEMPER FOR IMPROVED LAND AND SEA CLUTTER MODELING

G. C. Konstanzer and J. Z. Gehman
The Johns Hopkins University Applied Physics Laboratory
11100 Johns Hopkins Road
Laurel, MD 20723-6099

The Johns Hopkins University/Applied Physics Laboratory's Reflectivity with Propagation Model (REPROP) accounts for effects of arbitrary propagation conditions (ex. ducting, subrefraction) on modeled average clutter cross section. REPROP results are typically used to model radar clutter returns for realistic environmental conditions. This technique is currently used at JHU/APL and several other organizations and results have been compared favorably to measured data for several strong ducting cases. REPROP's current approach for modeling surface clutter cross section, however, contains an approximation to the surface incident field as the total field at a certain height above the surface, where the total field is obtained from the TEMPER propagation program. For sea clutter, this height is dependent on the wave height and grazing angle; for land clutter it is the first point above the surface. This paper describes a new algorithm for computing the incident field on the surface from the total field. In regions that are directly illuminated by a transmitting source (ex. interference region), this algorithm applies the Fresnel reflection coefficient to extract the incident field from the total field. In other regions (ex. diffraction region), the algorithm switches to an approach that varies with range like the total field. The algorithm is shown to work well with the Miller-Brown rough surface modification to the reflection coefficient and is applicable at frequencies from 500MHz to 20GHz. Examples are provided to demonstrate the approach's effectiveness for standard atmosphere and complicated ducting cases, where the incident field solution transitions from the interference region, through skip zones and hot spots.

F3-7 11:00 MODELING PROPAGATION OVER IRREGULAR TERRAIN VIA THE METHOD OF UNSYMMETRICAL FINITE DIFFERENCES

Ra'id S. Awadallah, James R. Kuttler & Denis J. Donohue
The Johns Hopkins University Applied Physics Laboratory
11100 Johns Hopkins Rd.
Laurel, MD 20723

Forward propagation of electromagnetic waves over irregular terrain is invariably modeled using the one-way parabolic wave equation (PWE) which can be solved by forwardly marching the field over range increments using either the split-step Fourier method (SSFM) or the implicit finite difference method (IFDM). The solution is subjected to the terrain boundary condition in addition to a non-reflecting boundary condition at the upper boundary of the propagation domain. For a non-perfectly conducting terrain, an approximate impedance boundary condition (IBC) is usually assumed.

For a 2-D atmosphere with x representing range and z altitude, the IFDM discretizes the PWE on a grid with rectangular subintervals of width equal to the range increment (Δx) and height equal to altitude increment (Δz). This is accomplished by replacing the x and z derivatives in the PWE by their central finite difference approximations on a stencil of width Δx and height $2\Delta z = \Delta z + \Delta z$. The IBC equation is similarly discretized and used at each range increment to relate the field at the point immediately below the terrain (sometimes called a virtual point) to the fields at the terrain point and the point immediately above it. This whole process results in an efficiently solvable tri-diagonal system of equations relating the field at a certain range to that at the previous range. For the tridiagonal structure to be preserved the IBC equation must not contain any range derivatives, i.e. its discrete finite difference form must only relate fields at a specific range. For a flat terrain, this is obviously the case and the above procedure is straightforward. The above procedure can be easily extended to the case of irregular terrain if the governing PWE is of the narrow-angle form, where the range derivative can be eliminated from the IBC equation by simultaneously solving it with the governing PWE. On the other hand, for the different versions of the wide-angle PWE, which is used to accurately model propagation scenarios involving large angles from the horizontal, the above procedure can only be carried out on the expense of destroying the efficient tri-diagonal structure of the resulting system of equations.

This paper presents a method for mitigating the above difficulty is presented. The method represents both the governing PWE and the IBC in the neighborhood of the terrain by finite difference formulas based on the unsymmetrical stencil formed by the two grid subintervals containing the terrain at each range increment. This stencil has a width of Δx and a height of $2\Delta z = \Delta z_1 + \Delta z_2$, where Δz_1 and Δz_2 are functions of the terrain location within each range increment. This technique facilitates the application of a procedure to eliminate virtual points and, at the same time, preserves the tri-diagonal structure of the resulting system of equations. Numerical results based on this method will be presented and some of these results will be compared with those obtained using the SSFM.

F3-8
11:20

K-FACTOR STATISTICS FOR SUBREFRACTION IN THE MID-ATLANTIC COAST OF THE UNITED STATES

Julius Goldhirsh, G. Daniel Dockery
The Johns Hopkins University Applied Physics Laboratory
11100 Johns Hopkins Road, Laurel MD 20723-6099
julius_goldhirsh@jhuapl.edu

The bending effects of propagating rays may be partially accounted for by replacing the earth's radius "a" by an effective radius "Ka" where K is a constant which may be smaller or greater than 1. This concept, first introduced by Schelling et al. (Proc. IRE, vol. 21, p 427, March 1933), was expanded by Lagrone (Proc. IRE, Vol. 48, pp. 1009-1015, 1960) who showed five year averages of "K-factor" isopleths for the winter and summer months throughout the United States. These contours were derived from radiosonde measurements over the first 300 meters from the surface. The use of a K-factor, such as K = 4/3 referred to as a "standard propagation condition," implies the rate of change of refractivity with height is constant from the surface upwards and the troposphere is laterally homogeneous. Its use, therefore, should be applied with extreme caution since refractivity may be highly variable in space and time. Nevertheless, K-factors are used by the systems community to calculate "quick look" assessments of propagation conditions at locations where little or no real time refractivity data are available.

In this effort, we show statistics of "equivalent K-factor" associated with subrefraction using three years of near continuous line-of-sight link signal measurements at 4.7 GHz in the mid-Atlantic coast of the United. The original measurements were expressed in the form of cumulative distributions of propagation factor and duration of fading (Goldhirsh et al., Radio Science, Vol. 29, No. 6, pp. 1421-1431, 1994). Knowledge of the link geometry provides estimations of signal fades for different K factors that are smaller than unity. These fade values were related to probabilities using the original database. The "equivalent K-factor" is here defined as one in which the corresponding fading has a duration that exceeds two hours. This is a somewhat arbitrary definition and other durations may be selected. Unlike previous descriptions of K-factor, the present analysis assigns a probability to each value of K. Of course, there are associated caveats that accompany this definition as well. Preliminary results show K factor values are less than 0.9, 0.8, 0.7 and 0.6 for approximately 6, 4, 2, and 0.2 % of the time, respectively, during the period November through July. Subrefractive events tend to be rare during the period August through October.

F3-9 11:40 PARABOLIC EQUATION AND CLUTTER MODELING METHODS FOR SITE-SPECIFIC RADAR SYSTEM PERFORMANCE ANALYSIS

Dr. Michael H. Newkirk
The Johns Hopkins University
Applied Physics Laboratory
Laurel, MD 20723-6099

Recent attention has been focused on using radar system modeling techniques in a way that provides more realistic and stressing environments to a radar system designer. This approach has the advantage of judging the performance of a candidate radar system in a realistic environment without having to perform expensive field tests with high risk developmental systems. The designer can also perform system trade-off studies in a controlled, reproducible manner before committing resources to hardware design and construction. In order to provide the required fidelity for this type of modeling, parabolic equation based propagation models, such as TEMPER or APM, as well as detailed models for sea, land, rain and discrete clutter must be carefully used.

This presentation will outline some of the more recent advances to the TEMPER propagation model that pertain to this subject. These improvements include more accurate and efficient methods to determine grazing angles over terrain, a new procedure that allows one to initialize a TEMPER run with data from a previous case and a methodology to facilitate making numerous TEMPER runs, e.g. one run per bearing for a sector of interest.

In addition, some of the ways that a modeler can use the TEMPER data will be demonstrated. Terrain data for a specific region is extracted from the DTED database and prepared in an efficient manner specifically for use with the TEMPER program. The main TEMPER output products of propagation factor and grazing angle are then used in recently updated sea, land, rain and discrete clutter models. These clutter sources can then used along with the propagation factor data in a given radar system model to assess the effects of the atmosphere and various clutter sources on system performance against specific threats. Example cases for specific regions and environments will be shown to demonstrate this concept. Finally, some discussion on the future work on this effort will be provided.

F3-10 12:00 AN ENERGY-CONSERVING AND RECIPROCAL PARABOLIC APPROXIMATION IN THREE-DIMENSIONAL PROPAGATION PROBLEMS

Oleg A. Godin
NOAA/ERL/ETL, Mail Code R/E/ET1, 325 Broadway, Boulder, CO 80303

We consider continuous wave propagation in 3-D inhomogeneous media with time-independent parameters. Wave fields are modeled as solutions to the scalar reduced wave equation. It is assumed that material parameters vary weakly or gradually along one Cartesian coordinate and are arbitrary functions of the other two coordinates. Then, neglecting backscattering, mathematical modeling of the wave field can be reduced to solving certain one-way (or parabolic) wave equation. Solving one-way wave equation instead of the full, two-way wave equation radically decreases requirements to computational resources. Whether solutions to a one-way wave equation inherit physical properties of solutions to the full wave equation (such as energy conservation and reciprocity) depends, though, on the choice of the one-way wave equation. The paper reports an extension to 3-D propagation problems of an energy-conserving and reciprocal 2-D parabolic approximation described in a recent article [Godin O. A., Wave Motion **29** (2), 175-194 (1999)].

A class of 3-D one-way wave equations is proposed such that each member of the class ensures fulfillment of the fundamental symmetries of the wave field as expressed by the energy conservation law and the reciprocity principle. Within the class, higher-order parabolic equations provide wider-angle capability and higher accuracy in reproducing solutions to the full wave equation.

Boundary conditions are derived that are consistent with the parabolic equations and, together with the equations, ensure energy-conservation and reciprocity of the wave field in media with piece-wise continuous parameters. Unlike the two-way formulation, within the parabolic approximation the boundary conditions and the very number of the boundary conditions to be imposed depends on the parabolic equation considered and orientation of the boundary with respect to the preferred propagation direction.

Normal-mode and ray approaches are applied to study asymptotic accuracy of the energy-conserving and reciprocal parabolic approximation. It is demonstrated that using the energy-conserving parabolic wave equations instead of traditional parabolic equations enables one to drastically reduce asymptotic errors in modeling field amplitude without any loss in the accuracy of phase modeling.

Memorial Session 1, 08:35 AM-Fri., Room 265
MEMORIAL SESSION FOR JAMES R. WAIT
Chairperson: D. Hill, NIST (dhill@boulder.nist.gov)

W1-1
08:40

JAMES R. WAIT - REMARKABLE SCIENTIST

Ernest K. Smith
ECE Department
University of Colorado
Boulder, CO 80309-0425

This talk will be on the life of James R. Wait with special attention to his research as reflected by his publications. While one tends to think of Jim as an independent sort of person, in fact he may hold the record for number of different co-authors: 90. Jim authored over 830 publications in archival journals and eight books but he drew more satisfaction from his publications which became Citation Classics than the sheer numbers.

His life divides conveniently into three periods: The Canadian 1924-1955, the Colorado 1955-1980, and the Arizona 1980-1998.

Jim was born in Ottawa on January 23, 1924. His father, George Enoch Wait, was Canada's first Air Vice Marshall, the top rank in the Royal Canadian Air Force at that time. Jim joined the Canadian Army in 1942 and spent the war years as a radar technician (S/Sgt). At the end of WWII he enrolled in the University of Toronto. He received his B.A.Sc. in 1948, his M.A.Sc. in 1949 and then became Prof. George Sinclair's first Ph.D. in 1951. He worked from 1948-1952 at Newmont Exploration Co. in Jerome, Arizona where he met Gertrude Laura Harriet Norman, his future wife. He returned to Canada in 1952 to join the Defense Research Telecommunications Establishment (DRTE) in Ottawa.

Jim joined the NBS Central Radio Propagation Laboratory (CRPL) in Boulder, Colorado in 1955 and remained until 1980. Skiing was certainly a major attraction. These were enormously productive years for Jim who became an instant hero of the Boulder Laboratories and a major asset to the electromagnetics program at the University of Colorado. The sixties saw great reorganization for the Boulder Labs and Jim successfully navigated the transition from NBS into ESSA and thence into NOAA. He consistently rejected administrative entanglements.

In 1980 Jim retired from NOAA and accepted a joint professorship in Electrical Engineering and Geosciences at the University of Arizona, Tuscon where he became Regents Professor in 1988. In 1990 he retired from the University to become a private consultant. He died in Tuscon of brain cancer on October 1, 1998.

Jim founded the journal Radio Science in 1959 and was its editor from 1959 to 1968. He was co-editor of the International series of Monographs on Electromagnetic Waves, Pergamon Press from 1961 to 1973, Associate Editor URSI Radio Science Bulletin 1995 to 1998.

His honors included membership in the National Academy of Engineering, Fellow of the IEEE, IEE(UK), and the AAAS, Dept. of Commerce Gold Medal (1958) , Samuel Wesley Stratton Award (NBS) 1962, Van der Pol Gold Medal (URSI) 1978 and the Heinrich Hertz Medal (IEEE) 1992.

W1-2
09:00

INVESTIGATION OF RADIO WAVE PROPAGATION IN IRREGULAR STRUCTURES USING LABORATORY SCALED-DUAL MODELS

Ezekiel Bahar
Electrical Engineering Department and the
Center for Electro-Optics
University of Nebraska-Lincoln
Lincoln, NE 68588-0511

A laboratory model first conceived by J.R. Wait to investigate radio wave propagation in the perturbed environment of the earth-ionosphere waveguide is described here. The construction of the laboratory model involves the exploitation of the following fundamental invariant properties of Maxwell's equations and the ability to physically simulate the appropriate boundary conditions including the earth's curvature. (a)Invariance of Maxwell's equations to size-wavelength transformations permits the scaling down in size of the earth-ionosphere waveguide. (b) Duality relationships between the electric and magnetic fields, permits the representation of the azimuthally independent $TM_{n,o}$ modes excited by vertical dipoles in the earth ionosphere waveguide by the $TE_{n,o}$ modes in rectangular waveguides. (c) A perfectly conducting magnetic wall (where the tangential component of the magnetic field vanishes) is simulated through the use of imaging techniques. (d) To account for dissipation in the ionosphere an equivalent surface impedance boundary is simulated using a wall loading material with a specific complex permittivety. (e) To simulate the earth's curvature in the rectangular waveguide, an especially fabricated dielectric material with a prescribed permittivity height profile is used as the medium of propagation in the interior of the waveguide.

One or a combination of the above five artifices can be employed by researchers today to construct laboratory models from which controlled experimental data can be obtained to validate analytical and numerical solutions as well as to provide insights for novel approaches to solve difficult propagation problems.

The specific objective of this paper is to describe the development of electromagnetic models. It is shown here how they are applied to the investigation of propagation in the earth ionosphere waveguide for cases in which the effective height of the ionosphere and or its physical parameters (characterized by a surface impedance) change along the path of propagation. These will be used not only to prove or disprove the validity of approximate mathematical solutions already available, but will also be used to provide insight on the derivation of novel solutions to these problems by gaining direct information as to the effects upon propagation of boundary perturbations.

W1-3
09:20

ROUGH SURFACE SCATTERING QUANDARIES AT GRAZING RESOLVED VIA THE SURFACE IMPEDANCE

Donald E. Barrick
CODAR Ocean Sensors
1000 Fremont Ave., Suite K
Los Altos, CA 94024

Wait was perhaps the first to recognize the link between near-grazing scatter and radiation/propagation above a rough surface. Based on perturbation theory for vertical diipole radiation over an irregular spherical earth interface, his results show the attenuation rate to be increased because the surface impedance is modified by the roughness spectrum (Wait, J.R., *Electromagnetic Probing in Geophysics,* Golem Press, P. Beckmann, ed., 370-381, 1971). What remained a quandary up to the present is the fact that perturbation-predicted scatter from a perfectly conducting slightly rough boundary appears to remain constant as grazing is approached, even though any non-zero impedance demands that power decrease with grazing angle to the fourth power. Yet HF ground-wave radars at grazing incidence see ample sea echo.

This quandary has recently been reconciled. We have found exact expressions -- for plane wave incidence on surfaces with arbitrary roughness scales -- that separate into factors accounting for propagation and scatter. The propagation factors include the direct and specular waves, the latter reflected from a surface having the roughness-modified impedance. These combined propagation factors convey the grazing-angle to the fourth dependence. The scattered power factor is then independent of angle as grazing is approached. Closed-form expressions for this are derived in the slightly rough limit from perturbation theory, while general but exact modal field solutions are solved for propagation and scatter for one-dimensional rough surfaces of arbitrary height.

W1-4
09:40

TIME DOMAIN RESPONSE OF A CONDUCTING PERMEABLE DISC EMBEDDED IN A LOSSY MEDIUM

Samir F. Mahmoud
ECE Dept. Kuwait University, P.O.Box 5969
Safat 13060, Kuwait Fax: (965) 4817451,
e-mail: samir@eng.kuniv.edu.kw

Scattering of electromagnetic waves from nearby conductive and/or permeable anomalies within the earth has been of interest for many years. The problem of a cylindrical disc anomaly has been recently considered by Mahmoud and Wait (URSI Symposium, Thessaloniki, Greece, May 25-28 1998) where frequency domain analysis has been pursued.

In this paper we wish to extend the previous work to the time domain. Thus, a buried anomaly with a disc shape is assumed to be excited by a nearby current loop with a step function current. For ease of analysis, it is assumed that the disc, while having an arbitrary conductivity for the azimuthal currents, has a zero conductivity in the radial direction. This allows the modeling of the disc by a number of concentric noncontacting rings since no radial currents are supported. The currents are then derived in terms of the incident electric field on the rings and their self and mutual impedances. At low frequencies, such that all relevant dimensions are less than say a quarter of a wavelength, all self and mutual impedances are derived in simple closed forms.

It is shown that the late time (or low frequency) response of the conductive permeable disc is dominated by the scattering from an equivalent vertical magnetic dipole plus an equivalent horizontal electric dipole representing the induced ring currents. With a step current in the source loop, the time domain behavior of the two induced equivalent dipoles is obtained. Both display a peak value at a time which is close to $\mu_0 \sigma_e R^2$ where R is the distance between the source and the center of the disc , and μ_e and σ_e are the permeability and conductivity of the earth. The value of the peak increases with the contrast between the parameters of the disc and the host medium. Plots of the scattered fields such as the vertical magnetic and vertical electric fields versus time will be presented and their diagnostic features indicated.

W1-5
10:00

PETROPHYSICS OF MAGNETIC DIPOLE FIELDS IN AN ANISOTROPIC EARTH

A. Q. Howard, Jr.,
TERRAGRAF
Logan, Utah 84341
e-mail: terragraf@aol.com

Measurement-while-drilling (MWD) resistivity log data are often acquired in highly deviated or horizontal holes. The conductivity of the earth in the vertical direction σ_v and horizontal direction σ_h are almost always different. In directional drilling, the concept of geo-steering uses many pre-computed resistivity simulated logs at various dip angles. When an MWD resistivity tool enters a new bed, the response is compared with the pre-computed logs to aid in the determination of the location of the drill bit. Therefore comparison of wireline logs in vertical holes, with nearby MWD highly deviated holes is important. The MWD tool response however is sensitive to resistivity anisotropy. Classic references on resistivity anisotropy include (J.H. Morgan and S. Gianzero, Geophysics, 26, 1979, 1266-1286), and the book (J.R. Wait, **Geo-Electromagnetism**, Academic Press, New York, 1982). More recently Hagiwara has published several papers on the interpretation of wireline and MWD logs in anisotropic layered media. An example containing other references is (T. Hagiwara, SPE Formation Evaluation, Society of Petroleum Engineers, SPE paper 28426, 211-216, 1996).

The earth's conductivity is anisotropic because gravity differentiates the direction normal to the earth's surface. Sedimentary sequences under vertical stress produce as a consequence pore space geometries and often vertical fractures that differentiate horizontal and vertical permeability. An interpretation of thinly laminated pay zones is (J.D. Klein, P.R. Martin and D.F. Allen, 1995, SPWLA 36^{th} Annual Logging Symposium). Considered as a bulk medium, such zones are anisotropic. In particular, they show that water wet oil-saturated formations with large variability in grain size can be highly anisotropic. Thus significant anisotropy in porous sediments is an indicator of hydrocarbon.

An alternative method is used to derive analytical expressions for the Sommerfeld type integrals. Numerical results give typical MWD tool response as a function of the inclination angle θ the tool makes with respect to the axes of anisotopy, and also as a function of the anisotopy index $\kappa = (\sigma_h/\sigma_v)^{1/2}$.

W1-6
10:40

Impedance-Type Boundary Conditions for a Periodic Interface Between a Dielectric and a Highly Conducting Medium

Christopher L. Holloway[1] and Edward F. Kuester*[2]
[1]Institute for Telecommunication Sciences/U.S. Dept. of Commerce
325 Broadway, Boulder, CO 80303, 303-497-6184
[2]University of Colorado, Boulder, CO

The method of homogenization is applied to the derivation of the equivalent (or "averaged") generalized impedance type boundary conditions for a two-dimensional, periodic, highly conducting rough interface. If the level of detail at which information about the field is needed is significantly larger than the fine scale (the period of the roughness), we can discard the information about microscopic field variation, and use only the macroscopic (on the scale of the wavelength or other dimension much larger than the roughness period) variation of the field, to which alone the equivalent boundary condition will apply. In other words, as long as the critical dimensions of the roughness are small compared to the wavelength of interest, as well as to the size of any "measuring device" we might employ, the use of the equivalent boundary condition will be enough, without the need to study the fine structure of the field.

In a large class of electromagnetic problems (i.e., scattering and reflection) we are only interested in the effective field (the global field behavior). By separating the boundary-layer field from the effective field, it is possible to derive an equivalent boundary condition for the effective field. Hence, the scattering from a rough periodic interface can be approximated by applying the effective boundary condition to a smooth surface. This effective boundary condition along with Maxwell's equations are all that are needed to determine scattering and reflection from a rough interface.

We further show that the coefficients in this equivalent boundary condition can be interpreted as electric and magnetic polarizability densities. The effective boundary condition at a reference plane ($y = 0$) above the roughness profile has the form:

$$\begin{aligned} \mathbf{a}_y \times \mathbf{E}(\mathbf{r}_o) &= j\omega p[\mathbf{a}_x \alpha_{mx} B_x(\mathbf{r}_o) + \mathbf{a}_z \alpha_{mz} B_z(\mathbf{r}_o)] \\ &\quad -p\alpha_{ey}\mathbf{a}_y \times \nabla_r E_y(\mathbf{r}_o) \end{aligned}$$

where $r_o = (x, 0, z)$, p is the period, and α_{ey}, α_{mx}, and α_{mz} are the electric and magnetic polarizability densities respectively associated with the profile of the rough interface. The electric polarizability is that of a perfectly conducting surface, while the magnetic polarizabilities are complex, and account for the eddy currents flowing in the conductor. It can be shown that this form of boundary condition can be deduced from one given by *Biot* [1957] and *Wait* [1959]. Results for various geometries will be presented.

W1-7
11:00

NATURAL PROPAGATION AND RADIATING CABLE TECHNIQUES FOR MINE COMMUNICATIONS

Martine Lienard and Pierre Degauque
University of Lille, Electronics Dept., Bldg P3
59 655 Villeneuve d'Ascq Cedex, France

During the past twenty years, considerable attention has been devoted for the development of different techniques which can be used for mobile communications in mines. A first workshop, held in Boulder in 1978, was organized by James R. Wait, to review research in electromagnetic guided waves that was relevant to mine communication (J.R. Wait, Ed., *CIRES Pub*, 1978). At this time, the emphasis was on employing either an auxiliary axial conductor already present in the mine such as a trolley wire or an especially designed cable, usually called « leaky feeder », to permit transmission to distances on the order of 1 km. Typically, the transmitting frequency was on the order of few hundred of kHz up to few tens of MHz and one of the most reliable and less expensive support for the waves appeared to be the braided coaxial cable which has thus been extensively studied by J.R. Wait and his colleagues, for example (J.R.Wait and D.A. Hill, *IEEE Trans on MTT*, 23, 401-405, 1975). In mine galleries, this structure gives good results and is quite appropriate to this environment since the transverse distance between the mobile set and the cable is not important, on the order of few meters, allowing a low coupling loss between the energy propagating in the coaxial cable and the received power. On the contrary, if the exploitation of the mine is made with a room and pillars technique, it is out of question to implement a network of leaky cables in the rooms. High frequency techniques have thus been proposed so that the natural propagation does not suffer an important attenuation, the propagation in rectangular straight tunnels being studied through either a modal approach or a ray theory (J.R.Wait, *Radio Sci.*,9, 567-572, 1974).

However, it appears that a unique sytem working in the 400 MHz-1000 MHz frequency range and allowing to use either a radiating cable or the natural propagation, depending on the environment, is now cost-effective. The objective of this contribution is to present an overview of the last research in this field. The first part deals with the theoretical and experimental approach of the radiating cable. It is assumed that the radiation is ensured by periodic inclined slots behaving as an array of equivalent magnetic dipoles. After recalling the basic principles leading to the definition of the cable bandwidth, the effects of the tunnel walls on the radio link characteristics and on the radiation pattern of the cable are pointed out. Indeed, if the longitudinal radiation is significant, one can expect to get a beating between the waves due to the radiation of the slot array situated nearly in front of the mobile receiver and those which have been excited in the gallery which acts as an oversized waveguide. The theoretical approach is based on the summation of the radiation of each slot and of its images on the tunnel walls. Theoretical and experimental results are first described for the carrier frequency, i.e for a narrow band analysis, and show the influence of the slot spacing on the field variation when the cable is installed in tunnel. For a digital communication, another parameter of interest is the complex impulse response of the propagation channel. This is achieved by applying a Fourier transform on the channel transfer function and experimentally by calculating the intercorrelation between a transmitted pseudo-random sequence and the received one. The direction of arrival of the waves at the receiving point is also determined.

The natural propagation of the waves, excited typically by a half-wave antenna, is then presented. First, the propagation in a mine entry is considered and both the field average attenuation, versus distance and frequency, and the amplitude distribution along a regression line are determined and compared to the performance of a radiating cable. Then the field distribution in a room and pillars, the impulse response and the direction of arrival of the rays are determined experimentally for predicting the performance of a radio link.

W1-8
11:20

ELECTROMAGNETIC WAVE PROPAGATION ON A THIN WIRE ABOVE EARTH

R.G. Olsen
School of EECS
Washington State University
Pullman, WA 99164-2752

J.L. Young
MRC Institute
University of Idaho
Moscow, ID 83844-1024

D.C. Chang
Polytechnic University
Brooklyn, NY 11201

The electromagnetic properties of a current on a thin horizontal wire above a flat lossy earth are reviewed. Attention is given to the historical development of the topic, starting with the seminal work of Carson and followed by Kikuchi's important extensions to Carson's work. Particularly, the importance of Professor Wait's contribution to the initial understanding of the modal and radiative behaviors of the current, as described in his influential paper in Radio Science (J.R. Wait, *Radio Sci.*, 7, 675-679, 1972) is discussed in detail. A description of Wait's full wave analysis is provided to show how it justified many of the assumptions embedded in Carson's and Kikuchi's results and also how it reduces to the simple complex image theory for wires above earth at low frequencies developed in the 1960's. Waits' full wave analysis also led to a fuller understanding of spatial spectrum of the current that was shown to include three sets of continuous modes and two discrete modes. Although no rigorous proof is known to exist with respect to the completeness of this spectrum, a necessary conditions for completeness is offered; the basis for this condition is the measurable input conductance of the wire. Following this, attention is paid to the physical interpretation of the terms in this spectrum. The paper is concluded with a short discussion on the various extensions of Wait's classic work that have been provided over the last two decades. These include extensions to multiple wires above a layered earth, applications to the prediction of electromagnetic interference from power lines as well as application to the analysis of microstrip propagation.

W1-9
11:40

GROUND WAVE OF AN IDEALIZED LIGHTNING RETURN STROKE

James R. Wait
Deceased
David A. Hill
Radio Frequency Technology Division
National Institute of Standards and Technology
Boulder, CO 80303

Usually in analyzing the electromagnetic fields produced by lightning (J.R. Wait, *IEEE Trans. Electromag. Compat., 40,* 180-181, 1998), it is assumed that the ground is perfectly conducting. This assumption provides an adequate prediction of the space wave except at very low angles where the space wave vanishes and the ground wave is the dominant field. The purpose of this paper is to derive an expression for the ground wave of a lightning return stroke which accounts for the finite conductivity of the earth. The results have application to remote sensing of lightning from ground-based observations.

Our idealized model consists of a traveling-wave current which propagates upward from the air-earth interface. The earth is modeled as an imperfectly conducting half space, and the analysis is performed in the frequency domain to allow for frequency dependence of earth conductivity and permittivity. The height dependence of the lightning current is taken to be an exponential with a complex propagation constant to allow for phase shift and attenuation. The Sommerfeld integral analysis is similar to that of a vertical electric dipole except that the source is distributed in height. The height integration can be done analytically, and the remaining integral over radial wavenumber can be split into two integrals. The first integral is the classic Sommerfeld integral result for a vertical electric dipole whose moment depends on the traveling-wave current parameters. It can be evaluated numerically or asymptotically to obtain the classic Sommerfeld attenuation function for large radial distance. The second integral has a similar asymptotic expansion in inverse powers of distance.

The asymptotic expansions of the two integrals for the fields can be combined to obtain a simple height-gain interpretation. The height-gain function for an elevated vertical electric dipole is well known (J.R. Wait, *Radio Sci., 2,* 747-750, 1967), but in this case the effective height is complex because of the complex propagation constant of the traveling-wave current. For most cases of interest, we find that the height-gain function does not differ greatly from one.

Friday Afternoon, January 7, 2000
Session D/J2, 13:35 PM-Fri., Room 200
NEW TECHNOLOGY FOR ARRAY TELESCOPES
Chairpersons: J. Dreher, SETI Inst. (dreher@seti.org)
Z. Popovich, Univ. of Colorado (zoya.popovic@colorado.edu)

D/J2-1
13:40 (40-min.)

THE MILLIMETER ARRAYS

Wm. J. Welch*
Radio Astronomy Laboratory
University of California
Berkeley, CA 94720

Observations of the universe at both millimeter and sub-millimeter wavelengths have proved to be so important in so many sub-fields of astronomy, that there are now major efforts in the development of arrays at these wavelengths to enable imaging with high sensitivity, angular resolution, and field of view. Instruments now operating at these wavelengths include four small arrays designed primarily for these short wavelengths (the Iram, Owens Valley, BIMA, and Nobeyama Millimeter Arrays), one interferometer pair (the CSO/JCMT), and the VLA operating at 7mm. In addition, the SubMillimeter Array will soon go into operation in Hawaii, and the Australia Telescope Compact Array will shortly be equipped with receivers for wavelengths as short as 3mm. Very Long Baseline observations are also carried out at these wavelengths. For the future, we anticipate the major Atacama Large Millimeter Array, a comparably large array by the Japanese, and the amalgamation of the OVRO and BIMA arrays into the CARMA Array. The fields of astronomy touched by these instruments are the structure of the universe, the formation and evolution of galaxies, the formation and early evolution of stars and planets, the late stages of stellar evolution, the structure and composition of the dense interstellar medium, the S un, and the composition of the solar system. The principal technical problem areas faced by these instruments are Low Noise Receivers, Antennas, the Field of View, Image Distortion by Atmospheric Phase Fluctuations, and the Calibration of Visibility Amplitude and Phase. We wll review the properties of the operating and planned arrays and discuss the various schemes employed for dealing with problems in the above areas, unsolved problems, and plans for the future.

D/J2-2
14:20

METHOD OF MOMENT SIMULATIONS OF A ROTATIONALLY SYMMETRIC, SELF-COMPLEMENTARY FEED STRUCTURE FOR A f/0.7 RADIO TELESCOPE

G. Engargiola* W. J. Welch
Radio Astronomy Lab
Campbell Hall
University of California
Berkeley, CA 94720

We have investigated the feasibility of constructing a low loss, broadband constant impedance antenna structure with 12 dB gain, which can be matched to a cooled MMIC amplifier from 1 - 10 GHz. This requires designing a self-complementary, log-periodic, three dimensional antenna structure which allows positioning of the MMIC, input leads, and associated cryogenics close enough to the balanced input of the antenna to keep transmission line losses and disruption of the frequency independent feed pattern to a minimum.

A commercial electromagnetic simulation package, Zeland Software's IE3D, was used to calculate the feed pattern and impedance of several potential designs. IE3D is a full-wave method of moment simulator which solves for the current distributions on a metal structure of entirely general shape. Its flexible automatic meshing scheme fits a combination of rectangular and triangular cells of varying sizes to the shape of the antenna trace. This yields accurate results for currents across the regular regions and irregular boundaries comprising the antenna trace, while keeping the number of unknowns which need to be solved for to a minumum. The program can be run efficiently on available PCs with upgraded memory, provided certain simplifying assumptions are made about the design problem.

Of particular interest are self-similar, self-complementary shapes which can be fabricated on flat circuit board panels. One particularly promising antenna structure consists of four proportionally spaced, triangular teeth type arrays, fabricated on the surfaces of a truncated square pyramid. Inside is a metallic pyramidal shield of smaller opening angle which surrounds the cryogenic insert containing the MMIC amplifier. This four terminal antenna design can receive two independent polarization modes, depending on the phases of the terminals. The far-field feed pattern as well as the VSWR of the antenna/balun combination are calculated. Noise contributions from ohmic losses and the "even mode" excitation of the antenna structure are estimated.

D/J2-3
14:40

ULTRA-LOW-NOISE, InP FIELD EFFECT TRANSISTOR RADIO ASTRONOMY RECEIVERS: STATE-OF-THE-ART

Marian W. Pospieszalski
National Radio Astronomy Observatory*
2015 Ivy Road, Ste. 219
Charlottesville, VA 22903

Edward J. Wollack
NASA Goddard Space Flight Center
Greenbelt, MD 20771

Recent developments in ultra-low-noise AlInAs/GaInAs/ InP heterostructure field-effect transistor receiver technology for frequencies up to W-band are discussed. The following main topics are covered:

- noise and signal properties of heterostructure field-effect transistors (HFET's), also known as high-electron mobility transistors (HEMT's), at cryogenic temperatures,
- design and examples of the realization of wideband low-noise, cryogenically-coolable HFET amplifiers in the 12 to 115 GHz range,
- examples of realization of receivers for interferometric arrays,
- examples of realization of very broadband continuum radiometers, and
- a comparison of HFET receivers with SIS mixer/HFET IF amplifier receivers, shown in the figure below:

NRAO SIS MIXER AND InP AMPLIFIER RECEIVER PERFORMANCE

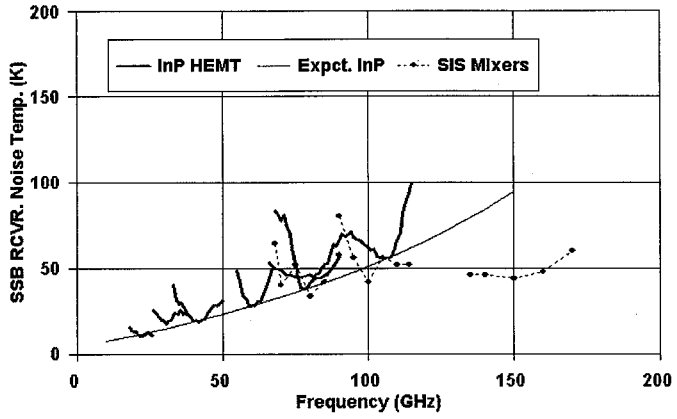

*The National Radio Astronomy Observatory is a facility of the National Science Foundation operated under cooperative agreement by Associated Universities, Inc.

D/J2-4
15:00

INTEGRATION FOR SKA AND THE 1HT FRONTENDS

J G Bij de Vaate
NFRA
P.O Box 2
7990 AA Dwingeloo
The Netherlands

The advantages for a phased array concept for the Square Kilometer Array (SKA) with many small receiving elements are clear; flexible, multiple beams and adaptive beam forming possibilities for suppression of Radio Frequency Interference. That this concept will take 30-100 million receivers brings up a new requirement for the designer of radio astronomy equipment, besides a very good performance a very low cost per element is necessary. Another example is the one-hectare antenna (1hT) SETI concept, where a very broad band instantaneous bandwidth and 1000 antenna dishes drives the need for 10.000 receivers.

For SKA and the 1hT, an introduction will be given on the integration aspects. Integration in monolithic Integrated Circuits (IC) will be addressed, but a very, possible more, important (cost) aspect is the packaging of the ICs and passive components.

The packaging of Radio Frequency (RF) and Intermediate Frequency (IF) Components is a crucial part in the performance and in the cost of the receiver. Packaging materials and methods drive the assembly costs, the testing costs, the size and the overall yield. The receiver performance requirements combined with the limits of todays (and future) integrated circuit technology makes a fully single chip receiver solution impossible in most cases. Therefore, a combination of ICs and off chip components, like filters or resonators, but also more basic elements as resistors and capacitors, will be necessary. And selecting the most cost effective packaging method has to be done early in the design process.

This paper will give an outline how complex RF and IF designs can be integrated, starting with the ICs, where already has to be anticipated that the highest integration level in a low cost IC process does not necessary lead to the best overall solution. Followed by the packaging concepts, where a differentiation will be made between the packaging of dies, with e.g. SMD, flip-chip or Ball Grid Array technology and the assembly of the complete circuits. For complete circuits, a high integration level and low cost combined with a high performance, creates a need for (ceramic) multi layers. An introduction will be given on the advantages and disadvantages of Low Temperature Cofired Ceramic (LTCC) packages, High Temperature Cofired Ceramic (HTCC) Packages, Multi Chip Modules (MCM) and PCBs.

D/J2-5
15:40

THE DESIGN AND PERFORMANCE OF LARGE-N RADIO ASTRONOMICAL ARRAYS

Colin J. Lonsdale* Roger J. Cappallo Alan R. Whitney
MIT Haystack Observatory
Westford, MA 01886 Jacqueline N. Hewitt
Department of Physics
MIT
Cambridge MA

A new generation of radio telescopes is on the drawing board, ranging from the One Hectare Telescope of the SETI Institute and UC Berkeley, to the LOFAR telescope planned for the New Mexico desert surrounding the VLA, to the ambitious international Square Kilometer Array project. In an era of unprecedented signal processing capability, it is possible to contemplate building these instruments using hundreds or thousands of small antennas, and cross-correlating millions of signal pairs in order to synthesize a filled aperture with much greater fidelity than in the past. The benefits of such an approach go beyond such aperture-filling properties, however, and enable whole new families of data processing techniques. These include (u,v) crossing point analyses for calibration and interference excision, wavefront curvature analysis for interference and astronomical transient detection, atmospheric phase screen modelling for precision astrometric measurements, and others.

Extensive studies of the benefits of such "large-N" arrays, and the techniques that will be required to achieve them, are underway at Haystack Observatory, and the progress to date will be reviewed. Architectural issues for a large-N signal distribution and correlation subsystem will also be discussed. Particular emphasis will be placed on various aspects of array configuration, including the physical layout of antenna stations and the interconnection topology. It is not possible to predict the performance of array configurations without realistically simulating datasets, subject to a variety of corrupting influences, and passing them through data reduction algorithms designed to take advantage of the unique properties of large-N datasets. This implies the need for an extensive preliminary design phase for such instruments involving powerful new software tools. Plans for the design and development of such tools will be described. Important cost and performance drivers are identified, and current thinking on the optimum approach is summarized.

D/J2-6
16:00

A PARAMETRIC APPROACH TO RFI SUPPRESSION

S. W. Ellingson*
The Ohio State University ElectroScience Laboratory
Columbus, OH 43212

Active suppression of radio frequency interference (RFI) is desired for the next generation of large radio telescopes. RFI suppression systems should have (1) large rejection ratio, perhaps on the order of 70 dB; (2) insignificant distortion to desired signals as a result of suppression processing; (3) algorithms practical for implementation given the available computing power; and (4) preferably "canceling" (RFI estimation/subtraction) algorithms as opposed to "excision" (e.g., blanking) algorithms, allowing telescopes to "look through" RFI. In this context, much attention has been paid to adaptive filtering techniques. Several recent investigations using this class of techniques have shown promise. However, it has also become clear that there are some difficult challenges in making this approach useful for Radio Astronomy.

This presentation addresses an alternative approach to RFI suppression based on parametric modeling. RFI waveforms are represented using simple models with just a few parameters. For example, an FM radio signal can be modeled as a complex sinusoid $Ae^{j(\omega t+\phi)}$ whose parameters are magnitude A, frequency ω, and phase ϕ. This turns out to be an excellent approximation if the telescope output can be broken up into blocks of sufficiently short duration so that the modulation is not apparent. In this case, simple algorithms exist for estimating the model parameters on a block-by-block basis. "Clean" RFI waveforms can then be synthesized using the estimated parameters, and subtracted from the telescope output to achieve suppression. Analogous space-domain (antenna array) and joint space-time algorithms exist.

The parametric approach has some attractive properties, and a few drawbacks. An important advantage is that this approach introduces only deterministic signals into the telescope output and thus avoids the problem of reference channel noise injection. Simple procedures exist for detecting when the algorithm has failed, allowing corrective action to be taken. In addition, the parameter estimates are useful side information which can be used to characterize RFI. Disadvantages include: degraded performance with decreasing interferer-to-noise power ratio (a trait common to many RFI suppression techniques), increased complexity with respect to adaptive filtering (although not necessarily increased computational requirements), and limited effectiveness against signal behaviors which are unforeseen or difficult to model; for example, power-up transients.

D/J2-7
16:20

RF-PHOTONIC ADAPTIVE-ARRAY PROCESSING

Kelvin H. Wagner* Gregory R. Kriehn Paulo E. X. Silveira
Optoelectronic Computing Systems Center
University of Colorado
Boulder, CO 80309-0525

Broadband RF arrays with 10^3-10^5 antennas are envisioned for radio astronomy and defense applications, but require adaptive time-delay-and-sum processing of each antenna element to eliminate unwanted interference and achieve optimum performance. Such signal processing of GHz bandwidth signals requires thousands of broadband A-to-D converters and requires in excess of 10^{15} multiplications per second—well beyond the projected capabilities of even supercomputers. We show here how to use photorefractive crystals (PRC) as holographic adaptive weights in a time-delay-and-sum adaptive array processing system which enables the full utilization of arbitrarily large arrays.

Our new BEAMTAP (Broadband and Efficient Adaptive Method for Time-delay-and-sum Array Processing) algorithm decreases the number of tapped-delay-lines (TDLs) required to process an N-element broadband phased array antenna from N to only 2. The adaptive weights are calculated using least mean square (LMS) error driven adaptation and are implemented as holographic gratings in a photorefractive crystal, with each resolvable holographic grating acting as an interferometric time integrating multiplier (G. Kriehn et al, submitted to *Applied Optics*, 1999).

In the optical BEAMTAP system a single laser illuminates an array of electrooptic (EO) modulators that convert the incident RF wavefront on each antenna into a modulation of the optical field. The resulting optical fields are launched by the fiber feed into a PRC. Diffraction by the grating in the PRC is detected and the output is subtracted from a desired waveform $d(t)$ and applied to the feedback acousto-optic delay line. The interference of the array signals with the feedback builds up dynamic gratings throughout the crystal volume which are Bragg matched to the signal of interest. Jammers arriving from a different angle will be Bragg mismatched, while the desired signal is diffracted toward the scrolling output detector, interferometrically detected, and time integrated using a velocity matched photoconductive traveling fringes detector (TFD). Simulations of the BEAMTAP architecture in Fig. 1 show a strong squint-free receptivity pattern in the direction of a desired chirp signal and squint-free nulls pointed towards any jammers which may be present.

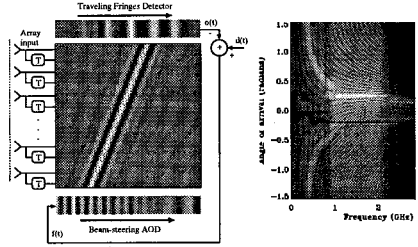

Figure 1: BEAMTAP algorithm schematic and simulated receptivity pattern of a 64 element array after 300μs of adaptation.

We acknowledge the support by Dr. William Miceli of ONR and the Office of the Secretary of Defense through the MURI program grant no. N00014-97-1-1006.

D/J2-8
16:40

HIGH SPEED INTERCONNECT TECHNOLOGIES FOR DIGITAL SYSTEMS

Howard L. Davidson
Sun Microsystems
901 San Antonio Road, M/S MTV29-235
Palo Alto, CA 94303

The problem of interconnecting the processing resources in a large correlator for a radio-telescope array is very similar to that of connecting the processors, memories, and I/O adapters in a large parallel computer. The correlator problem is slightly relaxed because many signal processing algorithms are amenable to deep pipelining, and relatively long link latencies, as might be imposed by serializing across wide words, can be tolerated.

Two technologies are becoming appropriate for this class of interconnect, high speed wire, and various forms of fiber optics. The PC and computer industry is driving a number of new standards that have the potential to significantly reduce the cost of these new technologies by driving them down the learning curve.

At the moment it appears that CMOS ASIC I/O cells at 2.5 Gbit/sec per pin will become commodity items in the next couple of years. Early versions are already already on the market, as are SER/DES chipsets that gang up to four channels.

In fiber optics 1 Gbit/sec serial links are already commodity parts. The emerging Gbit Ethernet standard will drive the cost of these components under $30 for a link. The 2.5 Gbit/sec parts will follow closely. In addition to the single line parts it is now possible to obtain fiber ribbon transceivers that deliver 12 X 1.25 Gbit/sec.

In a large system both types of technology will be necessary. For any interconnect between cabinets the single fiber and fiber ribbon components already compete in cost with electrical signaling on differential pairs. When the relative size of connectors is examined the fiber components are clearly preferable in terms of bandwidth per unit panel area.

Inside of a cabinet it is possible to make a case for both electrical and optical backplanes. At the moment electrical has a cost advantage. In an interconnect rich topology the space advantage of the fiber devices may be decisive.

On cards within the cabinet electrical connections should dominate for the near future. By using the best electrical interconnect technology at least 24" runs can be attained at 2.5 Gbit/sec in PWB trace. Using transmitter equalization this could be extended to 4 Gbit/sec.

Examples of these technologies will be presented, along with some crystal ball gazing about price and availability.

D/J2-9
17:00

THE RAPID PROTOTYPE ARRAY FOR THE ONE HECTARE TELESCOPE

D. R. DeBoer*
School of Electrical and Computer Engineering
Georgia Institute of Technology, Atlanta, GA
J. W. Dreher
SETI Institute, Mountain View, CA
W. J. Welch
Radio Astronomy Lab
University of California
Berkeley, CA

A seven element array composed of 3.6-m dishes in a hexagonal arrangement with baselines approximately 6.4-m long is currently under development as an instrument to research aspects of the upcoming One Hectare Telescope (1hT). This array, dubbed the Rapid Prototype Array (RPA), will serve as a test-bed primarily for the back-end and data processing (e.g. high-speed data management, beam forming, RFI excision, GPS calibration), as well as a learning tool and fixture to investigate the overall 1hT architecture (including embedded controllers, communication protocols, fiber links and software architecture). Development of this test array involves personnel from the SETI Institute, UC Berkeley, Sun Microsystems, and the Georgia Institute of Technology, and has served as an effective springboard for discussions and progress on the 1hT, which is a formal collaboration between the SETI Institute and the UC Berkeley Radio Astronomy Laboratory (RAL). The array will most likely be sited at a Sun Microsystems facility in Palo Alto, CA, and will largely be completed in early 2000.

The antennas are standard 3.6-m Orbitron TVRO mesh antennas (f/D 0.36) with dual linear actuators that will be supported in a freestanding modular structure on a rooftop, making this array reasonably transportable. Control will be achieved utilizing a low-cost Peripheral Interface Controller (PIC) embedded RISC controller at each antenna which will drive both actuators, monitor positional feedback and communicate with the control computer via fiber. Control and communications are being designed in collaboration with Sun Microsystems for seamless connectivity via the internet.

In order to utilize GPS for calibration and Iridium for RFI studies, as well as observe in the protected (*sic*) band at 1420 MHz, the operational frequency band will be 1400-1630 MHz and is set by an RF band-pass filter. The dual linear polarization feeds have better than 40 dB cross-polarization isolation and 15-20 dB return loss. An Ortel L-band fiber-optic analog link will transport the RF bandwidth to a central location for real-time processing. The desired instantaneous processing bandwidth is 10 MHz, requiring approximately 1 Gbit/second/channel of data handling for 14 channels, with 12 bit complex samples and 2x oversampling.

D/J2-10
17:20

THE ALMA CORRELATOR 4 GHz BANDWIDTH FIR DIGITAL FILTER

R. P. Escoffier, J. C. Webber, L. R. D'Addario, and C. M. Broadwell
National Radio Astronomy Observatory*
2015 Ivy Road, Ste. 219
Charlottesville, VA 22903

The FIR digital filter being developed by the National Radio Astronomy Observatory (NRAO) for the Atacama Large Millimeter Array (ALMA) radio astronomy array correlator is presented here. This filter, designed with FPGA ICs, is designed to have an equivalent clock rate of 4 GHz and can do low pass, high pass, or bandpass filter operations.

The NRAO, in cooperation with several European scientific agencies, is presently developing the ALMA radio astronomy array. This array consists of up to 64 twelve-meter diameter antennas to be used for observing astronomical sources at millimeter and submillimeter wavelengths. Each antenna is to have an aggregate bandwidth of 16 GHz (typically 8 GHz per polarization), organized as 8 channels of 2 GHz each.

Each ALMA correlator filter card must take the output of a single 4-Gsamp/s digitizer and perform full band, 1/2 band, ..., through 1/32 band filtering. The input to the filter card is in the form of 32 parallel 4-bit samples at the correlator system clock rate of 125 MHz. The filter output is in the form of 32, 16, 8, ..., or 1 two-bit, four-level samples depending on the filter configuration.

When configured as a 1/2 band filter, the filter operates with 128 taps. With each factor of two reduction in bandwidth, the number of taps available goes up by a factor of 2 to the limit of the 1/32 band filter (62.5 MHz bandwidth), in which case the card operates with 2048 taps. Even narrower bandpasses are possible, but the number of taps cannot increase past 2048.

Multiplication of sample values by tap weights is accomplished with 4-bit address look-up tables implemented in RAM, and tap weight summation is done with 10-bit precision. Conversion of the final card output to the 2-bit digitization level required by the correlator is done with RAM look-up tables. The filter configuration is changed by loading new tap weight values into the RAM look-up tables and reprogramming the adder tree.

We present here some design details, simulation results, and prototype test results.

*The National Radio Astronomy Observatory is a facility of the National Science Foundation operated under cooperative agreement by Associated Universities, Inc.

D/J2-11 THE ALMA CORRELATOR

17:40 R. P. Escoffier, C. M. Broadwell, J. Greenberg, and J. C. Webber
National Radio Astronomy Observatory*
2015 Ivy Road, Ste. 219
Charlottesville, VA 22903

The correlator being designed by the National Radio Astronomy Observatory (NRAO) for the Atacama Large Millimeter Array (ALMA) radio astronomy array is presented here. This correlator will process the output of the planned 64 antennas of the ALMA array with a bandwidth of 16 GHz per antenna. When built, the ALMA correlator will dwarf in size all other correlators presently being used in radio astronomy, performing 5×10^{16} operations per second.

The NRAO, in cooperation with several European scientific agencies, is presently developing the ALMA radio astronomy array. This array consists of up to 64 twelve-meter diameter antennas to be used for observing astronomical sources at millimeter and submillimeter wavelengths.

A lag (XF) architecture has been selected for the ALMA correlator, working at a system clock rate of 125 MHz. Antenna-based electronics in the correlator include 4-Gsamp/s digitizers, digital FIR filters for bandwidth selection working at an equivalent 4 GHz clock rate, delay lines, and signal conditioning logic to packetize the output of the high-speed digitizers in order to drive lower speed correlator circuits.

Cross- and auto-correlation will be performed in custom ASICs with 4096 lags per IC including 16-bit integration and secondary storage registers. Increasing the integration level of the ALMA correlator chip to provide 8192 lag circuits is being considered. The system will include circuitry to provide a wideband digital or analog-phased array output.

At present, the design and prototyping of all station-based logic cards (with the exception of the digitizer) have been completed and prototype testing has begun. Detailed design of the correlator chip, the correlator card, and the long-term accumulator is in progress. We present here some design details and test results.

*The National Radio Astronomy Observatory is a facility of the National Science Foundation operated under cooperative agreement by Associated Universities, Inc.

E4-1
13:40

DOUBLE-RIDGE TEM ANTENNA DESIGN FOR A HIGH-POWER GPR SYSTEM

John F. Aurand
ITT Industries, Systems Division
6400 Uptown Blvd. NE, Suite 300E
Albuquerque, NM 87110
(Work Performed at the University of New Mexico, EECE Dept.)

As part of a high-power VHF/UHF ground-penetrating radar project at Sandia National Laboratories, we recently developed a new transverse electromagnetic (TEM) antenna for use in a bistatic configuration. This presentation describes the design of the scale-model double-ridge TEM antenna developed during this work, along with experimental data.

The double-ridge TEM antenna was designed to satisfy several criteria: 1) clean time-domain radiation performance for use in a wideband time-domain radar system; 2) minimum physical size with acceptable gain at VHF/UHF frequencies; 3) input matching to a high-voltage transient pulser with parallel-plate transmission-line geometry; 4) sufficiently minimized antenna ringdown; and 5) well-behaved main-beam characteristics (comparable E-plane and H-plane beamwidths).

The resulting endfire TEM antenna configuration consists of a pair of flared ridge conductors which have a quarter-section elliptical profile, lossy-foam aperture loading, and an input transition to either parallel-plate line (for the transmit antenna) or to transverse-fed coaxial line (for the receive antenna). The ridge conductor geometry is specifically designed to impart the beneficial main-beam pattern characteristics of tapered slot antennas (also called coplanar finline, exponentially-tapered slot, or Vivaldi) to a TEM antenna which mates in a straightforward manner to the typical parallel-plate line geometry of high-power pulsers. An elliptical curve was chosen for the longitudinal profile of each ridge to provide the most compact structure with efficient radiation over moderate bandwidth (several octaves). And aperture loading is employed to attenuate the ringing antenna currents, as well as to improve the input match at very low frequencies.

A pair of scale-model antennas were built, with 1-4 GHz primary band operation, and extensive measurements were made of input match, bistatic transmit/receive performance, and bistatic isolation optimization. By physical scaling, a comparable antenna set was designed for high-power use in the VHF/UHF band.

E4-2 14:00 COLLAPSIBLE IMPULSE RADIATING ANTENNAS

Leland H. Bowen, Everett G. Farr
Farr Research Inc.
614 Paseo Del Mar NE
Albuquerque, NM, 87123

A reflector Impulse Radiating Antenna (IRA) consists of a parabolic reflector with a TEM feed. This antenna has a beamwidth which is too narrow for some applications. To broaden the beam, the Multifunction IRA, or MIRA was introduced in (E. G. Farr, C. E. Baum, and W. D. Prather, Multifunction Impulse Radiating Antennas: Theory and Experiment, Sensor and Simulation Note 413, 1997). The current paper describes the development of a man portable MIRA. The approach selected by Farr Research utilizes an umbrella like design, with a reflector sewn from conductive fabric. Two versions of the antenna were constructed. The first antenna did not have multifunction capability and, therefore, was described as a Collapsible IRA, or CIRA. The second had expansion seams in the reflector to allow the surface curvature to be adjustable. This antenna was described as a Collapsible MIRA, or CMIRA. Both antennas had parabolic reflectors and feed arms constructed from conductive rip-stop nylon. The reflectors were 1.22 m (48 in) in diameter with a focal length of 0.488 m (F/D = 0.4). The multifunction capability of the CMIRA was achieved by flattening the dish somewhat by opening 4 seams in the reflector surface. For the focused case, these seams are held closed by conductive Velcro.

The characteristics of the antennas were measured using time domain techniques to obtain the normalized impulse response as described in (E. G. Farr and C. E. Baum, Time Domain Characterization of Antennas with TEM Feeds, Sensor and Simulation Note 426, 1998). The data processing includes conversion to IEEE standard gain in the frequency domain.

This class of antenna is compact, lightweight and man-portable and provides very good RF characteristics. For the CIRA, the FWHM of the normalized impulse response is 100 ps. This antenna is usable from below 50 MHz to above 8 GHz based on the IEEE standard gain on boresight.

E4-3
14:20

SELECTION OF ANGLES BETWEEN PLANES OF TEM FEED ARMS OF AN IRA

Carl E. Baum
Air Force Research Laboratory DEHP
3550 Aberdeen Ave. SE
Kirtland AFB, NM 87117-5776

In [C.E. Baum, Sensor and Simulation Note 327, 1991] various choices of feed-arm configurations for an impulse-radiating antenna (IRA) were discussed. Among these was a set of two arms of nominally 400Ω. There was also a set of four arms with one pair rotated by 90° with respect to the other so as not to interact significantly with the other pair (by symmetry) giving a 200Ω feed when appropriate arms are connected together. The arms can be circular cones or flat-plate cones, although the latter have the advantage that they can be oriented to minimize the aperture blockage in the case of a reflector IRA. Such feed structures have accurately calculable characteristic impedances, accomplished by a combination of stereographic and conformal transformation [E.G. Farr and C.E. Baum, Sensor and Simulation Note 337, 1992]. There it is also shown that, when appropriately used with a paraboloidal reflector, the spherical TEM wave on the feed exactly transforms to a planar TEM wave (before other scattering can reach the observer) according to the above stereographic transformation. This allows us to consider the two-dimensional form of the transmission-line feed in the calculations.

Symmetry considerations have led to feed-arm structures for an impulse-radiating antenna lying on perpendicular planes (also perpendicular to the aperture plane). This paper extends these considerations to other constant-ϕ planes for the feed arms. Based on an approximation of thin conductors of circular cross section, analytic formulae are obtained. Retaining horizontal and vertical symmetry planes, the position of the first feed-arm plane can be increased from a ϕ_0 of 45° (previous, noninteracting case) to somewhat larger values with some potential improvement in performance, depending on various factors. An interesting case has a ϕ_0 of 60° leading to a symmetrical 6-arm case with appropriate combinations of four arms giving various polarizations.

E4-4 14:40 GENERALIZED E AND H MODES IN DIFFERENTIAL-GEOMETRIC LENS DESIGN

Carl E. Baum
Air Force Research Laboratory
Directed Energy Directorate
3550 Aberdeen Ave SE
Kirtland AFB, NM 87117-5776

Alexander P. Stone
Department of Mathematics
University of New Mexico
Albuquerque, NM 87131-1141

Recent results concerning generalized inhomogeneous TEM plane waves were specialized to the case of unipolarized waves in formal coordinates (u_1, u_2, u_3). The formal fields are functions of u_1 and u_2 and propagation is in the u_3 direction. This assumption resulted in an additional degree of freedom in specifying acceptable coordinate systems which then imply lens designs. Several examples were found in the case of purely dielectric lenses (permittivity dependent on position and constant permeability).

In this paper we consider the case of TE (or TM) waves propagating in the u_3 direction in a generalized orthogonal curvilinear coordinate system (u_1, u_2, u_3) for comparison to the TEM case. Such waves might also propagate in our transient (TEM, dispersionless) lenses, depending on excitation at appropriate boundaries. We seek conditions on the media parameters which, in the formal parameters in general (u_1, u_2, u_3) orthogonal curvilinear coordinates, allow such modes to exist.

This is a first step toward finding what orthogonal curvilinear coordinates are possible by the method of differential geometric scaling. The basic idea in the scaling method in the creation of a class of electromagnetic problems, each having a complicated geometry and medium, which are equivalent under the scaling to an electromagnetic problem with a simple geometry and medium. Solutions to Maxwell's equations can then be used in specifying various types of EM lenses. This case, for the TE or TM modes, can then be compared to those appropriate for TEM modes.

E4-5
15:00

DETERMINATION OF COMPLEX PERMITTIVITY BY IMPULSE PROPAGATION MEASUREMENTS

W. Scott Bigelow* Everett G. Farr
Farr Research, Inc.
614 Paseo Del Mar, NE
Albuquerque, NM 87123

We describe here a TEM transmission line method for determination of the complex permittivity of dielectric materials over a wide frequency range using impulse propagation measurements. The procedure is based on comparison of the propagation of fast impulses through short and long samples of material embedded in a coaxial test fixture. Signal processing to extract the permittivity involves calculation of the frequency domain ratio of time domain short and long sample measurements. This approach eliminates any need to account explicitly for the Fresnel losses that arise from the impedance discontinuities at entrance and exit planes of the dielectric samples. Multiple reflections are time-gated out of the measurements. The propagation delay through the dielectric is related to the real part of the permittivity; the alteration in shape of the transmitted impulse is related to the imaginary part. Use of a fast impulse leads to a response bandwidth of approximately 20 GHz.

This procedure was originally established and used for measurements of annular samples of water, sand, and concrete in a coaxial test fixture with axially symmetric cross section (E. G. Farr and C. A. Frost, *Measurement Notes*, **49**, 1996, and **52**, 1997). Here we measure and report the complex permittivity of several polymeric resins, employing a new test fixture, having rectangular outer conductor cross section and center conductor strip with fully rounded edges. The fixture permits two dielectric sample halves, molded or machined externally, to be inserted from opposite sides and compressed against the center conductor by a pair of cover plates. This design approach helps to exclude air from around the center conductor, an important consideration, since the electric field there is high.

We measured polyethylene, polystyrene loaded with titanium dioxide, and several polyurethane formulations, some with varying degrees of titanium dioxide loading. We were successful in measuring the complex permittivity of the polyurethanes with a bandwidth extending from below 1 GHz to more than 10 GHz. Although we were able to measure the real part of the permittivity of the polyethylene and polystyrene, their loss factors were below the sensitivity of our measurements. Longer sample propagation lengths would improve measurement sensitivity.

E4-6
15:40

GEOMETRIC CONSIDERATIONS FOR ULTRAFAST HIGH POWER SPARK GAP SWITCHING

Jane M. Lehr and Carl E. Baum
Air Force Research Laboratory
Directed Energy Directorate
3550 Aberdeen Ave SE
Kirtland AFB, NM 87117-5776

Juan M. Elizondo
Allied Signal, FM & T/NM
Kirtland AFB, NM 87196

In general, spark-gap design is dominated by features that enhance the switch initiation mechanism and affect performance, such as over-voltages, gap inductance, delay time and switch jitter. As achievable risetimes approach the picosecond timescale, the geometry of the spark gap itself influences its performance.

For timescales exceeding sub-microsecond duration, many of the geometry dependent parameters, such as capacitance, can be ignored. In particular, as the risetime of the charging waveform decreases, the capacitance of the spark gap may determine the effective switching time, thus affecting switch performance. Moreover, in the post-breakdown switch, the capacitance of the spark gap combines with the inductance of the spark channel to determine the transmitted wave. A circuit model of the spark gap is introduced for an analytical solution, and bounds are placed on the circuit parameters that reflect the physical geometry of the spark gaps. A full circuit synthesis has been performed on a spark gap that is both fed and terminated in a transmission line. The transmitted waveforms are calculated from the model, and related back to the physical geometry of the system. The critical damping condition resolves to a simple function of the equivalent circuit model components. Moreover, the treatment allows an estimation of time regime in which an equivalent circuit may be used to model the high power switch behavior. Thus, the timescale for which a full electromagnetic treatment is required has also been determined. The simple circuit model of the high-power spark gap is validated by correlating its spectrum with the measured waveform of the radiated power.

E4-7
16:00

HIGH CURRENT CATHODES WITH CONTROLLED A-K GAP CLOSURE

Juan M. Elizondo
Allied Signal, FM & T/NM
Kirtland AFB, NM 87196

Jane M. Lehr
Air Force Research Laboratory
Directed Energy Directorate
3550 Aberdeen Ave SE
Kirtland AFB, NM 8717-5776

Materials presently used for high current, electron beam diodes are typically carbon felt and velvet cloth for single pulse operation. These materials have a relatively long life and low degradation. When used in repetitive mode, heating and explosive vaporization of the fibers yield an excess molecular density that effectively increases the pressure in the gap. The limiting factor for high current electron beam sources has been the space charge, and for long conduction times, gap closure. Space charge is a fundamental limitation that may not be overcome unless electron-positron sources are developed. The gap closure is a limitation associated with the emission of ionic species from the electrode surfaces forming an expanding plasma that eventually fills the gap. The gap closure phenomenon has been investigated from the point of view of long pulses and high perveance emission. A key feature for using ferroelectric materials as electron emitters is that surface charge deposited on the electrode surface of ferroelectric materials can be released by flipping the polarization of the applied field and the switching fields are low enough that ionic species are not extracted from the cathode surface.

Electron emission is achieved applying a high voltage pulse to the ferroelectric material. The fast change in the polarizaton vector within the material results in a transition that liberates the polarization surface charge, resulting in a current pulse limited only by the transition time. Charge transfer in excess of 100 μC have been demonstrated. This translates into a current density in excess of 100 A/cm^2 for surfaces of 10 cm^2 and of 1 kA/cm2 for a 1 cm^2 surface. In general the results far exceeded expectations. Charge densities of 20 μC/ cm^2 correspond to current densities well in excess of 200 A/cm2. For the sample size tested. A second unexpected result is that there is control of the pulse length, with high current amplitudes corresponding to short pulses, 50-100 ns, and low amplitude corresponding to long pulse at 100-500 ns.

E4-8 16:20 MODELING AND EXPERIMENTAL INVESTIGATIONS OF HIGH SPEED GAS DISCHARGE SWITCHING FOR WIDEBAND AND ULTRA-WIDEBAND APPLICATIONS

Ron Pate, Doug Riley, Larry Rinehart, and Paull Patterson
Sandia National Laboratories
Albuquerque, NM

Erich Kunhardt
Stevens Institute of Technology
Hoboken, NJ

Tom Hussey
Air Force Research Laboratory
Kirtland AFB, NM

Scott MacGregor and Andrew Dick
University of Strathclyde
Glasgow, Scotland, UK

High-voltage gas discharge switching has performed successfully over the years as a key component in many high power electromagnetic pulse generator systems. Recently there has been increasing interest in improving the performance and expanding the applications of pulsed high power microwave (HPM), wideband (WB), and ultra-wideband (UWB) source technologies. Despite gas switch limitations and the great advances being made in solid-state and other competing switch technologies, high-voltage gas discharge switching often remains the best option for various high-power pulsed electromagnetic applications.

High-power WB and UWB applications, in particular, require switching relatively low-energy (tens of Joules or less), short duration (on the order of nanoseconds or less) pulses with sub-nanosecond rise-times within relatively low-impedance circuits (on the order of ten ohms or less) operating at high voltages (tens to hundreds of kilovolts). Switch turn-on speed and energy loss behavior become critical system design and performance issues within this demanding hard-discharge regime of operation. Currently, gas discharge switch modeling and performance prediction as a function of detailed switch configuration, gas type, gas pressure, and drive circuit parameters is not well developed for this operating regime.

The authors are currently engaged in a coordinated analytical, experimental, and computer modeling investigation involving the integration of powerful time-domain circuit and electromagnetic modeling & simulation tools with improved codes for treating the physics of the gas discharge streamer formation, channel heating, and rapid channel expansion phases that characterize the switch turn-on and associated early-time energy loss behavior within the discharge circuit. Experimental results provide data for comparison and feedback to the modeling and analysis. The effort is directed toward the development of improved design and engineering modeling capabilities for simulating and predicting the functional performance of gas switching, as a function of switch parameters, operating within high-power, low-impedance circuit configurations (i.e., the hard-discharge regime). This presentation will describe the work accomplished, the results obtained, and future directions.

E4-9
16:40

MODELING OF THE PROPAGATION OF LIGHTNING CURRENTS BELOW 400 M

R. L. Gardner
Spectral Synthesis Lab
6152 Manchester Park Cir.
Alexandria, VA 22310

A lightning channel begins when leaders join, often near the ground, and the return stroke currents start to flow. As currents flow through the channels the air is heated so that the air glows and expands. The hot air acts as a resistor for additional current flow. While the current and brightness are not linear, they are monotonic so that regions of high brightness indicate regions of large current. Further, the resistance of the channel is dependent on the current that has flowed through it. That resistance then governs the current flowing through the channel and the whole process in nonlinear. Gardner described such a system using a nonlinear, nonuniform transmission line model (R. L. Gardner, *A Model of the Lightning Return Stroke*, Thesis, University of Colorado, 1980). That model used assumed inductance and capacitance to provide initial velocities similar to observed values and calculated the resistance of the channel from the plasma parameters. We expect the current waveform of such a model to show a softening as the waveform propagates along the resistive channel.

The velocity of a current waveform traveling along the channel must be defined with care since the waveform itself is changing with propagation along the channel. If we pick a particular value of the waveform (as would be required for a given signal to noise) then the velocity will appear to decrease with propagation distance. The leading edge of the current waveform (the high frequency limit), however, will continue on a transmission line at the velocity governed by the inductance and capacitance.

Wang, Takagi and Watanabe (*J. Geophys. Res.*, **104**, No. D12, 14,369-14,376, June 27,1999) have recently published optical data on the behavior of the first 400 m of a lightning channel. The observed waveforms show, qualitatively, the described behavior. In this paper, we will compare and contrast the model and the published observations.

E4-10 17:00 GENERATION OF RF RADIATION BY ABSORPTION OF MODULATED LASER LIGHT IN SEMICONDUCTORS

William Page
Air Force Research Laboratory DEHP
3550 Aberdeen Ave. SE
Kirtland AFB, New Mexico 87117-5776

Laser light absorbed in semiconductors can produce or effect charge distributed in the medium. If the light intensity is modulated, and it is absorbed by non linear processes, mixing will allow the generation of RF energy. The volume dipole moment in the medium will include both the induced (non linear part) as well as that due to polarization of the medium. The resulting fields can be calculated from the total dipole moment density P. The far field is given by

$$\vec{E}_F(\vec{R},t) = (1/4\pi\varepsilon_0)\int_V (1/c^2 r)\ddot{\vec{P}}(t-\vec{r}/c)\{(\vec{r}.\vec{z})\vec{r}-\vec{z}\}dV$$

, and the near and intermediate fields by corresponding equations in P/r^3 and P'/r^2. The polarization and geometrical factors involved in determining the total fields for typical laboratory measurements can be complicated. The non linear part of the dipole moment produced by various processes may be estimated to gauge their effectiveness in producing RF fields.

Three mechanisms will be discussed to illustrate these phenomena in a semiconductor such as silicon or germanium. (1) The surface volume of a typical semiconductor has an intrinsic charge layer due to incomplete crystal bonding at the surface interface. The value of this intrinsic surface field is about ½ of the band gap of the semiconductor. The absorption of laser light in the material can create free charges which will move to relax this field. The temporal behavior will depend on the rate of charge generation and motion on the modulation of the incident laser beam. (2) The light absorbed can produce charge carrier pairs (electrons and holes) in the bulk of the semiconductor material. The electrons and holes will tend to diffuse to a state of space charge neutrality and will have typically different diffusion constants or drift velocities. An electric field will be produced, associated with the charge density gradient. This process, known as the Dember effect, can be modulated at RF frequencies. (3) Non linear process at high laser intensities often involve the Pondermotive force acting on charges existing or generated in the material. This force acting on free or bound charges in the material pushes the charge to regions of lower field energy density. The general analysis of this effect in real materials becomes very complex. In simple cases however (i.e. plane waves and free charge carriers) the basic mechanism can be understood in terms of average values resulting from the application of the Lorenz forces to the individual charge carriers.

The three types of phenomena outlined above will be discussed in terms of pulsed laser light absorbed in silicon or germanium. Some estimates of the RF production will be given showing that, though energy conversion efficiencies are typically small, they may be sources of noise or signal in some cases.

E4-11
17:20

PERFORMANCE MEASURES OF INFORMATION SYSTEMS IN THE PRESENCE OF RF AND HPM INTERFERENCE

I.Kohlberg
Kohlberg Associates, Inc.
P.O. Box 23077
Alexandria, VA 22304

Modern information systems are characterized as complex computer and telecommunication networks. The information path structure combined with the interior environmental electromagnetic field produced by RF and/or HPM interference determines in many cases the information errors in the systems. Implementation of Electromagnetic Compatibility (EMC) techniques can often reduce the information errors by lowering the levels of the unwanted interior environmental electromagnetic field. Application of these methods may, however, be costly. This paper describes a method for minimizing the hardening cost by coupling the minimization algorithm to constraints provided by performance measures appropriate to RF and HPM interference. It is assumed that the information system is characterized by *M* control functions. Each control function is associated with an input/output pair of nodes. Information will flow between these pairs through a network containing numerous common intermediate nodes and relays. That is to say there is redundancy in part of the network. The *required* performance level of each pair is defined by a specific allowable character error rate, CER, appropriate to the function.

The performance of the entire information system is evaluated in terms of a set of functions: $F_\mu(x,t)$ = probability the CER transmitted between the μ th pair is less than or equal to x at t seconds after the onset of the interference. We shown that $F_\mu(x,t)$ is of the form

$$F_\mu(x,t) = \sum_l G_l(x,t) + \sum_m G_m(x,t)G_n(x,t) + \ldots \sum_q \sum_r \sum_s \qquad (1)$$

The *G's* are functions of the nodal response to the unwanted field; and the *x*'s are functions of the character error rates produced at each node through which information passes in support of the μ th control function. The sums are over all the paths connecting the μ th pair. The system performance measure is established by requiring that the following inequality is satisfied for each μ:

$F_\mu(x,t) \geq H_\mu$ = specified probability (a number) for each μ: $\mu = 1,2,\ldots.M$.

We show that the minimum cost to harden the system is the sum $\sum_i C_i(x_i)$ subject to the *M* constraints. $C_i(x_i)$ is the cost that is required to harden the i^{th} node so that the CER passing through it is less than or equal to x_i. Theoretical details and examples are given.

E4-12
17:40

ELECTRICAL DESIGN PARAMETERS OF ALL-DIELECTRIC-SELF SUPPORTING FIBER OPTIC CABLES ON HIGH VOLTAGE TRANSMISSION LINES

M.W. Tuominen
U.S. Department of Energy
Bonneville Power Administration
Portland, OR 97208

R.G. Olsen
School of EECS
Washington State University
Pullman, WA 99164-2752

All-dielectric self-supporting (ADSS) optical fiber cable located on high voltage transmission line structures is exposed to electric fields of sufficient strength to cause corona, microsparking and dry band arcing (G. Carleton et. al., *Power Engineering Journal*, 9, 7-14, 1995) Recent studies of corona and microsparking indicate that these can be controlled with electric field grading devices (G.G. Karady et. al., *IEEE T and D.Conf.*, 2,734-738, 1999). Dry band arcing occurs when contamination on the cable becomes wet and hence conducting. As a result, substantial currents are induced on the cable. When the cable dries, small dry areas called dry bands occur which have much higher resistance than the rest of the cable. Arcing across these bands has caused a number of ADSS cables to fail. To study dry band arcing, a model for induced voltages and currents on ADSS cable near high voltage transmission lines is needed. A new lumped circuit model to do this has been developed and shown to be equivalent to a recent model based on reciprocity theory (R.G. Olsen *IEEE Trans. on EMC*, 41, 180-192,1999). The new model allows for the study of differential sag between transmission line conductors and ADSS cables and for non-uniform contamination levels along the ADSS cable. Studies using the model show that contamination levels, tower attachment points relative ADSS and conductor sag and electrical phasing of the transmission line conductors are important parameters and must be considered in calculations for determining the possibility of dry band arcs which could lead to cable damage. One interesting result is that conditions have been found for which phase matching can occur and substantially increase the induced currents and possibility of cable failure.

Session F4, 13:35-Fri., Room 1B-51
SATELLITE AND TERRESTRIAL PROPAGATION

Chairpersons: J. Goldhirsch, Johns Hopkins University (julius.goldhirsch@jhuapl.edu)
W. Vogel, Univ. of Texas (wolf_vogel@mail.utexas.edu)

F4-1
13:40

SHORT BASELINE KA-BAND DIVERSITY MEASUREMNTS IN FLORIDA

Henry Helmken
Florida Atlantic University
777 W. Glades Road
Boca Raton, Florida, 33431
J. Duval and R. Henning
University of South Florida
Tampa Florida

The Advanced Communication Technology satellite (ACTS) Ka-band propagation measurements program has entered its sixth year of data collection. The high occurrence of deep fades has underlined the necessity of developing fade mitigation techniques suitable for tropical areas. Even though ACTS is now in inclined orbit, the basic propagation data measurements have been extended to include some site diversity measurements. Florida, because of its sub-tropical summer climate is very suitable to test the effectiveness of spatial site diversity in order to improve system performance. Earlier diversity work at long baseline separations (30 km) was performed with the COMSTAR satellite in the Tampa area. This current work seeks to extend these measurements to very short baselines (< 5 km) which may be more attractive to commercial implementation.

A second transportable terminal, similar to the ACTS propagation terminal has been in operation for over one year. This terminal collects data at only one frequency, namely 20.185 GHz. A second ACTS terminal, modified for inclined orbit operation, has been obtained from NASA and has been collecting spatial diversity data since July 24. It is currently at 1.2 km baseline separation and plans are to move it to a second location with a baseline separation of 5 km. Preliminary data suggest that up to 5 dB improvement at the 0.1% exceedence level can be obtained at these short base lines. At the conference, the analysis techniques and results obtained at the two baseline separations at 20 GHz and 27 GHz will be presented and compared to the 6 years of ACTS data.

F4-2
14:00

AN OVERVIEW OF PROPAGATION MEASURMENT DATA NEAR 30 GHz FOR LMDS

Peter Papazian
National Telecommunications Information Administration
Institute For Telecommunication Sciences
Boulder, Colorado
papazian@its.bldrdoc.gov

High frequency wireless data transmission systems are being deployed in the United States and Canada as well as in overseas markets where reliable fiber and wire line communication links are unavailable. The initial market strategy is to first target point to point business markets where fiber is unavailable or too expensive. A secondary but ultimate objective is to deploy systems in a point to multi-point broadcast mode where the mass consumer and residential market can be tapped. Critical propagation issues are signal attenuation by rain, vegetation and buildings, signal depolarization, multipath, and cell to cell interference in the broadcasting mode. Published radio propagation data at these frequencies is very limited. This paper summarizes the results of propagation measurements made at ITS which address these issues. Rain measurements made in 16 US cities illustrate the geographic variability of attenuation due to rain. A set of suburban measurements made in Boulder, CO summarizes path loss and multipath using a 130 ft high transmitter. Vegetation loss measurements made in orchards, catalog signal attenuation due to trees of different species with and without leaves. A point to multi-point broadcast experiment in suburban neighborhoods in California and Colorado answers question concerning area coverage, multipath and signal depolarization. A long term measurement made through vegetation in Boulder, CO quantifies seasonal signal variability and provides data on signal variability due to wind. These efforts are quantified and compared at either 28.8 or 30 GHz. Area coverage results for San Jose CA using 40 ft and 80 ft transmitters are compared. Here the area coverage probability is plotted versus basic transmission loss for a 99% grade of service. The computational methods used to generate these graphs will be discussed. Scatter plots of attenuation versus distance and signal depolarization also from San Jose are presented. Attenuation due to a deciduous tree with and without leaves are given for orchards in Texas and Washington State. The seasonal variability due to leaves versus no leaves is measured in Colorado. The variability of a signal propagating through vegetation due to wind is plotted on Rayleigh paper with the distributions associated Rician k factor.

F4-3
14:20

MEDIUM FREQUENCY PROPAGATION PREDICTION TECHNIQUES AND ANTENNA MODELING FOR BROADCAST APPLICATIONS

Nicholas DeMinco
Institute for Telecommunication Sciences
Boulder, CO 80303
(303) 497-3660
ndeminco@its.bldrdoc.gov

This paper discusses the basic aspects of radio-wave propagation and antenna modeling in the medium frequency (MF) band. This band covers the frequencies of 300 to 3000 kHz. More specifically, we are concerned with the ground wave and the sky wave in the 300 kHz to 1705 kHz band. The sky wave models described in this paper are valid from 150 kHz to 1705 kHz. The ground wave models described in this paper are valid from 10 kHz to 30 MHZ. The AM Broadcast band of 535 to 1605 kHz is in this band and is planned to be used in the Advanced Traveler Information Systems (ATIS) of Intelligent Transportation Systems (ITS) for rural travelers. This system would provide information like road conditions, road hazards, weather, and incident reporting. The 285 kHz to 325 kHz band is presently being used for a differential correction signal in another application of ITS called the Differential Global Positioning System (DGPS) that will be used for precision location of vehicles. The propagation of radio waves in this band depends on both a ground wave and a sky wave and is quite different from propagation at any other frequency. Antenna modeling in this band is also quite unlike that in other bands. This paper describes radio wave propagation together with antenna modeling in this frequency band so that a better understanding of the phenomena can be obtained for use in design and application of ITS subsystems. The models described here can be used for designing systems and making performance predictions for both of these ITS applications and any other systems that operate in this band. The paper contains descriptions of both sky-wave and ground-wave propagation models in addition to the methodology used to analyze antennas that operate in this band. A method of calculating and normalizing antenna gain for MFsystems computations is also discussed. Some comparisons of measured and predicted data are also contained in the descriptions.

F4-4
14:40

PROPAGATION MODELS FOR TERRESTRIAL LAND MOBILE SERVICES

Alakananda Paul and Frederick Najmy
NTIA, U.S. Department of Commerce
Room 6725, 1401 Constitution Ave. Washington, D.C. 20230

There is a need to calculate the signal strength and propagation loss in built-up areas for terrestrial land mobile services at VHF and UHF frequency bands. The median signal strength is determined by the shadowing of buildings, channeling of radio waves along streets, scattering of radio waves from fixed and moving objects, foliage effects etc. Since there are so many variables in mobile services, there is no single universally accepted method. The accuracy of any method will depend on the estimates of the input parameters of the model that best describe the given area. Empirical formulas based on measured data are mostly used for prediction of path loss and field strength for land mobile services in VHF and UHF bands. The empirical models, accepted by ITU and many other organizations, are based on extensive propagation measurements done by Okumura and others in Japan. (Y.Okumura et al, *Rev. Elec. Comm. Lab, 16,* 825-873, 1968). Hata has given empirical formulas derived from Okumura's measured data for limited ranges of input parameters and different environments. (M. Hata, *IEEE Trans. Veh. Tech, VT-29,* 317-325, 1980). Hata's equation for urban environment has been modified by a working committee (231) of European Cooperative for Scientific and Technical Research (COST) to extend the frequency range to 2 GHz. Hata's urban formula has also been modified to extend the range of validity from 20 to 100 km. (ITU-R P. 529-2, 1997). Telecommunications Industries Association (TIA) has adopted a modification by Davidson to extend Hata's formulas to full ranges of Okumura's data and beyond, distances to 300 km and base station antenna heights to 2500 m.

Expressions from the sources mentioned above have been combined, modified and integrated such that they can share the same input parameters and can be easily updated for different input parameters from graphic display dialog boxes. Path loss and field strength can be computed for different models and compared in graphical form. The measured data may be superimposed for validation, if necessary. Since the models discussed above are sometimes valid for overlapping ranges of input parameters, a validation check was done to compare the computed results with measured data, using Okumura's data and ITU-R Rec. P. 370 VHF and UHF data. Results of the comparison will be presented.

Finally, variability issues for mobile services are different from that of fixed services or broadcasting. Also, for interference calculations required for spectrum management, one needs the field strength which will be exceeded or path loss which will not be exceeded even for a small percentage of cases. The variability issues for mobile services will be addressed.

F4-5
15:00

PCS BAND CHANNEL SOUNDING MEASUREMENTS IN A SUBURBAN AREA

Perry Wilson and Peter Papazian
NTIA/ITS
325 Broadway
Boulder CO, 80303

The radio link channel characteristics are key to the performance of wireless communication systems. Thus, both modeling and measurement are extensively used to predict and quantify channel parameters for system design and evaluation. One technique that has been used extensively at the Institute for Telecommunication Sciences (ITS) is the use of a psuedo-noise (PN) signal for broadband channel characterization. The PN signal is transmitted through the channel and then cross correlated with itself yielding an impulse like channel response. The impulse response can then be used to determine various channel parameters such as path loss (signal attenuation) which affects range and coverage, delay statistics (impulse spreading and multipath echoes) which impact digital signal bit error rates, and fast fading statistics which affect link reliability. Additional parameters of interest when multiple antennas and adaptive arrays are used, are diversity gain and angle of arrival.

This paper will report on the latest upgrade of the ITS channel sounding system and give representative measured examples of the above channel parameters. In particular, PCS band (1920 MHz) measurements were made using a 511 bit PN word at 10 Mb/s. The theoretical impulse signal power to correlation noise power level is 54 dB for the 511 bit PN sequence. Multipath signals separated by 100 ns can be resolved to a maximum delay of 51 μs using this configuration. The nominal nul to null bandwidth was 20 MHz. Table 1 summarizes the data acquisition parameters used for the measurements to be reported, as well as the range of permissible values for the ITS channel sounding system.

Table 1. Data Acquisition and RF Parameters used for Diversity Tests

Configurable System Parameters		
Parameter	PCS Band Tests	ATB System
Receiver Channels	4	1-8
Carrier Frequency	1.92 GHz	.45 – 6 GHz
Bit Rate	10 Mb/s	.1 – 50 Mb/s
Resolution	100 ns	10 μs – 20 ns
Code Type	Maximal Length	Programmable
Code Length	511 bits	Programmable
Acquisition Mode	Burst	Continuous or Burst
Positioning	GPS/Dead Reckoning	GPS/Dead Reckoning
Transmitters	1	Multiple
Data Processing	Post	Post or Real Time

Session F5, 15:35-Fri., Room 1B-51
OPTICAL & IR MEDIA EFFECTS
Chairpersons: A. Barrios, SPAWARSYSCEN (barrios@spawar.navy.mil)
J. Gozani, CIRES (gozani@stripe.colorado.edu)

F5-1 15:40 RECENT DEVELOPMENTS IN HIGH-DATA-RATE OPTICAL COMMUNICATIONS AT JPL

Keith E. Wilson
Jet Propulsion Laboratory
California Institute of Technology
4800 Oak Grove Dr. MS 161-135
Pasadena CA 91109-8099
(818) 354-9387

Optical communications is a telecommunications technology that meets the demand for high-data-rate, long-range free-space links using small, low-mass, low-power-consumption subsystems. To better understand the performance of this technology, a series of turn-of-the–century demonstrations that follow up on the successes of the early and mid-1990s have been planned both in the U.S. and abroad. This paper will report on planned key developments in the NASA/JPL optical communications program in the first decade of the next millenium that will pave the way for future high-data-rate, free-space optical communications.

We shall describe progress in the construction of NASA/JPL's first optical communications ground terminal, the Optical Communications Telescope Laboratory (OCTL). Construction of this 200 square meter laboratory at TMF (Table Mountain Facility, Wrightwood, CA) is scheduled to be completed in October 1999. The contract for the telescope, its pier, and the dome was awarded to Contraves-Brashear, Pittsburgh, PA in September 1999. First light at the telescope is scheduled for the first quarter of 2001. An R&D station, OCTL will serve as NASA/JPL's primary ground station for its optical communications demonstrations. In addition, it will be used as an experimental laboratory for evaluating the performance of optical receivers for the future deep space and near-Earth optical ground station networks. It will also be used to develop laser-beam-propagation strategies for beacon and data uplinks to satellites and spacecraft.

Developments at the TMF and AMOS (Air Force Maui Optical Station, HI) ground stations for the (Space Technology Research Vehicle) STRV-2 demonstration will be reported. This LEO (Low-Earth-orbit)-to-ground demonstration is scheduled for early 2000, and it will support unidirectional and bi-directional links from the STRV-2 satellite. Downlink data rates are up to 1 Gbps, at ranges out to 3300 km.

The high-data-rate optical communications demonstration from the International Space Station (ISS) to the OCTL will be discussed. This demonstration is scheduled for 2003 and will use the optical communications demonstrator (OCD) terminal currently under development at JPL. A key objective of the demonstration is to assess the performance of a 2.5 Gbps space-to-ground link. In addition, the OCD will provide a high rate capability to the ISS transmitting data to the OCTL at up to OC-3 (155 Mbps) data rates.

LEO-to-GEO (geostationary orbiter) optical crosslinks can facilitate the recovery of the large volumes of data from spacecraft instruments such as hyperspectral imagers and Fourier transform spectrometers. We shall describe the design of a second-generation OCD terminal to support a crosslink for recovering such data from a typical polar orbiting satellite.

The research described in this paper was performed at the Jet Propulsion Laboratory, California Institute of Technology, under contract with the National Aeronautics and Space Administration.

F5-2
16:00

OROGRAPHY-INDUCED EFFECTS ON LASER SCINTILLATION

J. Gozani
Cooperative Institute for Research in Environmental Sciences
Campus Box 449
University of Colorado
Boulder, CO 80309

A notable validation of the theory of the scintillation of waves propagating through random media was achieved in 1993, when the comparison of numerical simulations and experiments agreed to within 20% (S. M. Flatté, G. Y. Wang, and J. M. Martin, *J. Opt. Soc. Am.*, **A 10**, 2363 1993) and (A. Consortini, F. Cochetti., J. H. Churnside, and R. J. Hill, *J. Opt. Soc. Am.*, **A 10**, 2354 1993). The comparison applies to any fully developed turbulence, i.e., a locally homogeneously random isotropic medium. To avoid inhomogeneity, one of the requirements is to choose a flat terrain. However, in many practical cases the propagation is over irregular terrain, and the question is how large an effect it has on the scintillations.

In this report I analyze data of an experiment administered in 1993 by the Environmental Technology Laboratory/ ERL/ NOAA at the Table Mountain facility north of Boulder, Colorado. The experiment composed of laser beams propagating from the West to the East along the southern edge of a vast plateau bordering on the south a valley 50 meters deep with a slope of about 15 degrees. Anemometers, which were used to monitor the cross wind, indicated whether turbulent eddies were transported from the plateau or from the valley across the propagation path.

Preliminary results reveal a strong dependency of the root mean square scintillation index on the winds. This variability is beyond the one expected by the estimation error. Moreover, it is quite easy to verify that the scintillation index does not depend directly on winds. Thus we hypothesize that this variability is due to the variability of the strength and the inner scale of the turbulence. Because the scale of this effect is much larger than the outer scale of the turbulence, it is characterized as global intermittency.

The analyzed results show a strong sensitivity of the parameters of turbulence to the direction of the wind, thereby confirming the hypothesis that the turbulence produced in the valley and dragged across the ridge is inhomogeneous, whereas the one produce over the plateau is homogeneous.

Since we have chosen a specific situation, where the propagation path runs along the ridge, our experiment is only indicative of the problems anticipated in more complicated terrain. Moreover, since our long-time average exhibited a variability, short-time observations are bound to be highly sensitive to winds. These limitations should be borne in mind when designing real-time systems.

F5-3
16:20

REFRACTIVE EFFECTS IN INFRARED TRANSMISSION

Dr. Carl Zeisse, Amalia Barrios, Dr. Stephen Doss-Hammel
SPAWARSYSCEN SAN DIEGO D858
49170 Propagation Path
San Diego, CA 92152-7385

Optical transmission along low altitude paths is governed by extinction (absorption and scattering) due to molecules and aerosol particles, and by refraction. Of these effects, refraction is currently the least understood, due to the fact that refractive effects have generally been overlooked at infrared (IR) frequencies. Transmission paths for most IR applications have been far from the surface and at relatively steep angles, where refractive effects could be ignored. Recent interest is now focused on low angle, low altitude transmission paths where refraction plays an important role.

Atmospheric transmission data were obtained in the long wave (30 THz) and mid wave (100 THz) infrared bands along 7 and 15 km paths within a few meters from the ocean surface at Zuniga Shoals during a 13 day period in November 1996. A Santa Ana weather condition occurred during the experiment, with offshore winds and air-sea temperature differences reaching +10 C°. Refractive events were evident in transmission values that exceeded 100% (free-space) for short times (a minute) on the short path and long times (an hour) on the long path.

Buoys anchored at mid-path provided meteorological data that were used to continually assess the molecular extinction via the transmittance code MODTRAN. Approximately 150 measurements of aerosol particle size distribution were made using an aerosol spectrometer, which was located on a boat that moved along the path. Mie theory was used to derive aerosol particle extinction from these boat measurements.

Analysis of these data, with particular attention to those time periods where IR transmission exceeded 100%, will be presented. Two approaches were used to determine refractive effects along the path, ray optics and the parabolic equation (PE) method. Obstacles in the analysis of these data will be discussed. These include the application of the PE method at IR frequencies and failure of the LKB method to converge to a solution for the vertical profile of modified optical refractivity (for stable conditions).

F5-4
16:40

IR CHARACTERIZATION OF TURBULENT ATMOSPHERIC INDUCED OPTICAL DISTORTION BY PASSIVE PHASE DIVERSITY TECHNIQUE

Lewis DeSandre, Albert Ogloza, Randy Dewees, Peter Gillis
Naval Air Warfare Center Weapons Division
Research Department, Physics Division
China Lake, CA 93555

Adaptive optics systems require the use of a wavefront sensor to sample the aberrated wavefront and to provide appropriate error signals to the actuator system so that the wavefront aberrations can be removed. Typical wavefront measurements by Shearing or Shack-Hartmann sensors require a guide-star or point source reference. Phase diversity techniques have advantages over conventional wavefront sensors. Firstly, the method is scene insensitive in that images do not need be of a point source but of any image. Secondly, phase diversity can detect piston error directly thus potentially offering robust evaluation of turbulence in highly scintillation atmosphere. Finally phase diversity uses the image scene directly in order to evaluate the turbulent field.

Basically, the phase diversity technique can be viewed as a wavefront sensor that detects phase aberrations in a volume. It works by collecting two or more images separated by a few waves of aberration. The first image is the typical focal plane image computed by an unknown amount of aberration. Inducing a known amount of aberration such as spherical forms the second image of the same object. The key is that the induced aberration is precisely known and requires precise calibration of the focal volume of a telescope.

The Naval Air Warfare Center Weapons Division, China Lake, CA is developing a mid-wave infrared phase diversity camera. The camera will be tested in a laboratory setting to explore phase diversity techniques, wavefront measurement, and algorithms. In the future this instrument will be used to characterize atmospheric turbulence of horizontal path imaging and to explore the limitations of the phase diversity techniques in terms of signal to noise ratio, turbulence strength, and atmospheric scintillation.

F5-5
17:00

APPLYING THE PARABOLIC EQUATION METHOD TO MODEL REFRACTIVE EFFECTS ON INFRARED TRANSMISSION

Amalia Barrios, Carl Zeisse
SPAWARSYSCEN SAN DIEGO D883
Propagation Division
49170 Propagation Path
San Diego, CA 92152-7385

It is well understood that electromagnetic (EM) radiation in the communications and radar frequency spectrum is drastically affected by atmospheric refraction along the propagation path, particularly when ducting conditions are present. What is often overlooked is the effect refraction may have at electro-optical frequencies. Aerosol extinction and molecular absorption have always been considered to be the dominant mechanisms by which the transmission of electro-optical radiation is reduced. In the past, propagation paths for infrared (IR) transmission have been somewhat short and relatively far from the surface; therefore, effects from atmospheric refraction along the path could be neglected as a useful first order approximation. In most cases, this first order assumption has worked well. However, due to a convergence of interest in optical paths very close to (within several meters of) the ocean surface in response to the sea skimming missile threat, the most recent measurements have indicated that refractive effects on these paths can no longer be ignored (C. Zeisse, et. al., *SPAWAR TD 2989*, pp. 589-599, 1998).

Current research on the effects of refraction on IR transmission are based on ray tracing and/or ray optics methods. There are inherent limitations to these techniques, primarily in regions of caustics, for which the ray method breaks down. Propagation models based on the PE algorithm have already been shown to be valuable assets to the communications and radar community. The method is now extended to infrared frequencies. Problems in applying and modeling an infrared source, along with questions regarding spatial and temporal coherence, will be addressed. Comparisons between ray optics and PE results will also be shown.

Session G/H2, 13:15-Fri.
IONOSPHERIC MODIFICATION
Chairperson: P. Bernhardt, Naval Research Laboratory (bern@ppdu.nrl.navy.mil)

G/H2-1 13:20 THE STATUS OF THE HF IONOSPHERIC MODIFICATION FACILITY AT ARECIBO

M. P. Sulzer*
Arecibo Observatory, Arecibo, PR 00612

We describe the current status of the Arecibo HF facility and our plans for the future. Problems for the facility began when the government-operated pumps which keep the area dry temporarily failed, resulting in the cancellation of scientific operations until operation could be restored. The area, known as Cano Tiburones, has been pumped dry since about 1950, primarily to allow the land to be used for agricultural purposes. Two environmental groups sued the Puerto Rican Land Authority, claiming that restoring the pumps would result in the illegal destruction of a wetland. Later the Governor of Puerto Rico declared part of the Cano Tiburones a nature preserve. The part occupied by the HF facility is not part of this preserve, but it is almost surrounded by it, and it appeared that we would eventually have to leave the site when pumping ceased, probably in several years following the completion of studies concerning the restoration of the wetland.

In late September, 1998 hurricane Georges struck Puerto Rico. The HF facility was severely damaged. After determining the cost of repairs, consulting the National Science Foundation, and considering the temporary status of the facility, it was decided to close the site. The pumps have operated sporadically at partial capacity since the Hurricane and we have not been able to remove our equipment. We have been negotiating an agreement with the Land Authority and the Department of Natural Resources concerning the closing of the site, but the suit from the environmental groups has caused delays. On September2, 1999 a hearing was held in the Centro Judicial of Arecibo, and an agreement was reached and confirmed by the judge stating that the government will pump the cano to three feet below sea level by January 10, 2000 and hold it there for a period of six months, allowing removal of our equipment.

In the spring of 1999 the National Science Foundation funded professor James Breakall of the Pennsylvania State University to conduct a feasibility study for the construction of a high power HF feed over the main Arecibo dish. This option was selected among other possibilities as the one most likely to succeed for financial and political reasons. Prof. Breakall's report shows that it is practical to construct a feed meeting performance and reliability requirements. We are now studying the details of his results.

G/H2-2
13:40

HF IONOSPHERIC HEATING AT ARECIBO FOR THE STUDY OF WHISTLER WAVE INTERACTIONS WITH SPACE PLASMAS

M.C. Lee* M.J. Starks R.J. Riddolls A.X. Zhang
Plasma Science and Fusion Center
Massachusetts Institute of Technology
Cambridge, MA 02139 W.J. Burke
Air Force Research Laboratory
Hanscom AFB, MA 01731 S.P. Kuo
Polytechnic University
Farmingdale, NY 11735 M.P. Sulzer
Arecibo Observatory
Arecibo, PR 00612

Ionospheric HF plasma heating experiments were conducted at Arecibo to demonstrate that signals at 28.5 kHz, emitted from the Naval (NAU) transmitter in Puerto Rico, effectively interact with large-scale sheet-like ionospheric irregularities induced/enhanced by the HF heater, allowing them to propagate as whistlers to the conjugate hemisphere. Subsequent interactions of the ducted 28.5 kHz whistler waves with energetic electrons trapped in the radiation belts may have caused some to precipitate into the atmosphere over Arecibo. Here presented are the suspected radar detections of whistler-triggered electron precipitation events. NAU generated whistlers have intensities sufficient to parametrically excite lower hybrid waves and field-aligned zero-frequency plasma density irregularities in the ionosphere over Arecibo [Lee and Kuo, 1984]. The excited ionospheric density irregularities have scale sizes of 10 meters that align with the geomagnetic field lines to form filaments. The lower hybrid waves can accelerate electrons and ions along and across the geomagnetic field respectively, generating non-Maxwellian distribution functions. The subsequent heating of electrons and ions by the lower hybrid waves yield a chain of ionospheric plasma effects, such as airglow, short-scale density depletion, and plasma line enhancements in a range of altitudes which far exceed that caused by the HF heater. However, it is puzzling why 15 m scale plasma depletions should be detected in patches above and below the heater wave's reflection height and well removed from the region of intense wave-plasma interactions [Kelley et al., 1995]. Backscatter radar echoes from HF heater wave-enhanced Langmuir waves (plasma lines) occurred over a broad range of altitudes. They extended from 250 km to nearly 450 km, well away from the heater reflection height of 285 km [Carlson et al., 1982]. We suggest that disturbances in the ionosphere above NAU by whistlers can significantly affect heater-induced perturbations and produce apparent discrepancies in results reported from Arecibo and other heater sites.

G/H2-3 14:00 OPTICAL IMAGES OF SPORADIC-E LAYERS ILLUMINATED BY HIGH POWER RADIO WAVES

P.A. Bernhardt[1], F.T. Djuth[2], C.A. Tepley[3], M.P. Sulzer[3], L.M. Kagan[4], M.C. Kelley[5], Francisco Garcia[5], J.A. Gardner[6], A.L. Broadfoot[7]
[1]Plasma Physics Division, Naval Research Laboratory, Washington, DC 20375
[2]Geospace Research Corporation, El Segundo, CA 90245
[3]Arecibo Observatory, Arecibo, PR 00613
[4]Radiophysical Research Institute, N. Novgorod 603600, Russia
[5]Dept. of Electrical Engineering, Cornell University, Ithaca, NY 14853
[6]Air Force Research Laboratory, VSBI, Hanscom AFB, MA 01731
[7]University of Arizona, Lunar and Planetary laboratory, Tucson, AZ 85721

Two-dimensional images of Sporadic-E layers have been produced using a new technique which makes them glow when being stimulated by high power radio waves. Normally sporadic-E layers to not radiate visible emissions. Experiments on January 1998 at Arecibo Observatory in Puerto Rico have shown that the layers can be made to glow at 557.7 nm and other wavelengths by illuminating them with radio waves at 3.175 MHz with effective radiated powers of 80 megawatts. The regions of the sporadic-E layers that have electron densities greater than the critical density for reflection of the radio waves emit electrons that collide with and excite atmospheric atomic oxygen and molecular nitrogen. A charge-coupled-device (CCD) imager located on the ground is used to capture images of the glowing E-region structures. The camera exposure times were in the range of 15 to 45 seconds. The images obtained using this technique show a wide variety of structures in the sporadic-E layers. Some layers cover the 15 x 30 km region illuminated by the radio wave beam. Other layers show strong modulation of the E-region by gravity waves. Finally, other layer structures show random features that drift across the illuminated region. Consecutive images using this technique can provide (1) measurements of the lifetime of the individual sporadic-E patches, (2) the zonal and meridional components of the drift velocities in the E-region, and (3) the temporal evolution of the spatial features. Future research should use this technique of Artificial Radiowave Induced Airglow (ARIA) for studies of sporadic-E and intermediate layer structures along with complementary radar techniques of incoherent and coherent backscatter. The ARIA technique yields a large area description of the sporadic-E layer structures and the radars provide the altitudes and densities of the layers along the radar lines of sight.

G/H2-4 14:20

Na LAYER CHANGES BY 70MW RF HEATER

R.F.Wuerker* A.Y.Wong P.Kidd
UCLA Plasma Physics Laboratory
Los Angeles, CA 90095-1547

The 90-100 km high arctic sodium layer at 64 degrees 52-1/3' N lattitude, 146 degrees 50-1/2' W longitude, was monitored with a resonant lidar while the ionosphere was being modified by the 2.85 MHz or 4.85 MHz - 200 Hz square wave modulated - 70 MW peak ERP-RF "heater" also at the HIPAS Observatory. The 20 Hz - 20 ns duration laser pulses were emitted during the RF modulation off period, so that the Na layer scattered photons arrived back at the lidar site while the transmitters were quiescent (eliminating any RF induced false photon counts). The transmitter ran a 5 minute on - off pattern throughout the night. When the plasma critical layer frequency equals the plasma frequency energy is RF energy is absorbed by the ionospheric plasma. When the altitude of the critical layer coincided with the sodium layer, the sodium density dropped approximately 10%, presumably due to ionization of Na neutrals. When the critical layer was above the sodium layer, the Na density increased presumably due to liberation of sodium from compounds-particulate.

A sodum lidar system at HIPAS operated during the March 1999 campaign, was electronically timed so that the resonant 20 Hz YAG pumped dye laser "fired" during an off period of the square-wave modulation patter of the HIPAS, 70 MW (ERP) HF transmitter. The timing arrangement avoided any effects by either the ground-wave (from the 0.5 kilometer distant array), or even 100-600 km distant sky-wave on the lidar's photoelectron counting and data processing system.

Preliminary data indicated tat the sodium layer decreased whenever the heater was on and recovered whenever it was turned off. HF ionograms taken at Poker Flat showed E layer absorption at 2.8 MHz, at an altitude of 100 km, wihtin the normal sodium layer. The experiment indicates that the sodium layer is affected by HF heating when the critical plasmafrequency matches the location of the layer.

G/H2-5
14:40

COMPUTATIONS OF THE ARTIFICIAL OPTICAL EMISSIONS INDUCED BY SUPRATHERMAL ELECTRONS DUE TO HF-HEATING

A. V. Gurevich[1], G. Milikh[2], A. V. Lukyanov[1] and K.A. Zybin[1]
[1]P. N. Lebedev Institute of Physics
Moscow 117924, Russia
[2]Department of Astronomy
University of Maryland, College Park, MD 20742

Numerous optical [Haslett and Megill, *Radio Sci., 9,* 1005–1012, 1974; Bernhardt et al., *J. Geophys. Res., 94,* 9071–9092, 1989] and plasma line observations Carlson et al., [*J. Atmos. Terr. Phys., 44,* 1089–1100, 1982] indicate generation of suprathermal electrons by the powerful HF radio waves near the reflection point. Existing theories rely on the electron acceleration by Langmuir waves in the radio wave reflection region. However, recent observations of the green-line artificial emission made at lower altitude associated with the HF reflection from E_s layer [Djuth et al., *Geophys. Res. Lett., 26,* 1557–1560, 1999] hardly can be explained by existing models. In order to describe the artificial emissions we apply modified model of generation of suprathermal electrons by Gurevich et al. [*J. Atm. Terr. Phys., 47,* 1057–1070, 1985]. In this model the electrons are accelerated due to the formation of density wells /cavitons/ filled with local blobs of electric field, near the HF reflection height. Each time when the electron crosses the caviton it gains the energy. Since the thickness of the acceleration layer is less than the electron mean free path, the electrons can return to the layer due to the collision scattering, re-increasing the energy. Thus the suprathermal electrons are produced. Current modifications of the model include effects due to anomalous absorption of the powerful radiowave, along with the losses of the electron energy caused by the electron transport. The objective of the work is to discuss a generation of the suprathermal electrons due to the ionospheric HF-heating near the reflection region. We obtain first the electron distribution function of the suprathermal electrons, and assess then the intensity of the artificial optical emissions caused by the suprathermal electrons.

We compute first intensities of red- and green-line oxygen emissions which correspond to the electronic transitions $O(^1D) \rightarrow O(^3P)$ and $O(^1S) \rightarrow O(^3P)$ respectively. Compare then the computed intensities with those observed in the F-layer [Bernhardt et al., *J. Geophys. Res., 94,* 9071–9092, 1989] we estimate the effective temperature of suprathermal electrons along with the value of anomalous absorption. Recently artificial green-line oxygen emission has been observed for the first time from the sporadic E, or E_s layer using the Arecibo facility as the ionospheric HF-heater [Djuth et al., *Geophys. Res. Lett., 26,* 1557–1560, 1999]. Simultaneously the artificial N_2 first positive emissions were observed. We compute brightness of green-line and $N_2(1P)$ emissions generated by the Arecibo HF-heater in the E_s layer, and estimated then the effective temperature of suprathermal electrons along with the value of anomalous absorption. Notice, that generation of the suprathermal electrons is much more effective in the E_s layer than in the F layer due to lesser divergency of the radio beam. Finally we consider characteristics of cavitons required to generate suprathermal electrons.

G/H2-6
15:00

COMPUTERIZED IONOSPHERIC TOMOGRAPHY (CIT) IMAGING OF AN HF-HEATED IONOSPHERIC VOLUME

C. A. Selcher* P. Bernhardt
Naval Research Laboratory
Washington, DC 20375
G. Bust T. Gaussiran J. Holmes S. White
Applied Research Laboratory
Austin, TX 78713
F. Djuth
Geospace Research, Inc.
El Segundo, CA 90245
C. Tepley M. Sulzer
Arecibo Observatory
Arecibo, PR 00614

Tomographic techniques use line integral measurements to reconstruct local values of the measured parameter. These techniques have recently been applied to the ionosphere by using radio transmissions to measure the integral of electron density between a satellite and a chain of ground-based receiving stations. The resultant reconstructions form a 2-dimensional map of the electron density in the plane of the satellite / receiver chain (Jeffrey R. Austen, et al, *Radio Science*, **23**, 299-307, 1988). These reconstructions are nonunique due to limited angle considerations or possible nonoptimal receiver placement which may be required by geographic constraints. The limited angle problem can be alleviated by making use of alternative data sources which provide information on the electron density vertical structure, such as incoherent scatter radars (ISR). The nonoptimal receiver placement problem can be resolved through the use of sophisticated reconstruction algorithms (Paul A. Bernhardt, et al., *Phys. Plasmas*, **5**, 2010-2021, 1998).

During the January 1998 Arecibo heating campaign, an array of CIT receivers was deployed on the island of Puerto Rico, forming a three by three matrix. This arrangement allows for three reconstruction planes and provides information on the evolution of the HF heater induced density cavities. Measurements of Total Electron Content (TEC) using the differential Doppler technique were made, during both heater on and heater off periods. To supplement this closely-spaced data set, the Applied Research Lab (ARL) of the University of Texas at Austin made available the data from a chain of CIT receivers deployed throughout the Caribbean region. Vertical electron density profiles were obtained by use of the ISR at Arecibo Observatory, and were used to form empirical initial conditions for the reconstructions. Reconstructions generated using code developed at the Naval Research Laboratory (NRL) will be presented, and will demonstrate the applicability of CIT to the imaging of HF heated volumes.

G/H2-7
15:40

THEORETICAL AND NUMERICAL SIMULATION INVESTIGATION OF PARAMETRIC PROCESSES ASSOCIATED WITH UP-SHIFTED IONOSPHERIC STIMULATED RADIATION

H. Xi* W. A. Scales
Bradley Department of Electrical and Computer Engineering
Virginia Polytechnic Institute and State University
Blacksburg, VA 24061-0111 USA

Stimulated Electromagnetic Emission SEE produced by heating the earth's ionosphere with high powered radiowaves is currently a topic of significant interest in ionospheric modification physics. SEE is also a fundamental nonlinear process in plasma physics that is not currently well understood on a theoretical basis and it has tremendous potential as an ionospheric diagnostic tool. SEE is believed to be produced by nonlinear wave-wave interactions involving the electromagnetic and electrostatic plasma waves in the altitude region where the pump wave frequency is near the upper hybrid resonance frequency. The most prominent up-shifted feature in the SEE spectrum is the broad up-shifted maximum BUM. From characteristics of this feature, a four-wave parametric decay process has been proposed as a viable mechanism for its production. The object of this work is to (1) investigate the development of the four-wave decay instability by using theoretical and numerical simulation models and (2) access its possible role in the production of the BUM spectral feature.

The theoretical model (J. Huang, and S. P. Kuo, *J. Geophys. Res.*, **99**, 19569-19576, 1994) is first described as it applies to the production of the BUM. This model assumes a second harmonic oscillation associated with the long wavelength heater wave parametrically decays into a frequency down-shifted electron Bernstein wave, a frequency up-shifted upper hybrid wave along with a low frequency oscillation near the lower hybrid resonance frequency ω_{lh}. Important parametric dependences of this four-wave instability are described by considering growth rate calculations. A one dimensional magnetized particle-in-cell PIC simulation model is used to provide the first investigation of the nonlinear evolution of the four-wave decay instability (A. A. Hussein *et al.*, *Geophys. Res. Lett.*, **25**, 955-958, 1998).

Preliminary results of this investigation show that there is good agreement between predictions of the proposed theoretical model and the numerical simulation experiments. Detailed comparisons have been made for various harmonic numbers, frequency separations, and propagation angles. The simulation frequency spectrum exhibits many of the important features of the experimental observations. The numerical results show that consideration of the full nonlinear development of the four-wave parametric instability may provide insight into the asymmetric nature of the wave frequency spectrum observed during the experiments.

G/H2-8
16:00

LANGMUIR TURBULENCE IN LARGE-SCALE ARTIFICIAL IONOSPHERIC IRREGULARITIES

J. P. Sheerin*
Department of Physics and Astronomy
303 Strong Hall
Eastern Michigan University
Ypsilanti, MI 48197

Irradiation of the overdense F-region of the ionosphere with HF radiowaves has been long been known to produce artificial irregularities over a wide range of length scales, from large-scale (10's of km's) down to small-scales (cm's), and timescales, from minutes down to milliseconds and below. Simulations of Strong Langmuir Turbulence (SLT) have successfully modeled and predicted many of the features of the small-scale, early-time behavior of the plasma line backscatter observed in experiments performed in a quiescent, unmodified ionosphere at mid-latitudes (Arecibo Observatory), (D. F. DuBois, *Proc. of IVth URSI Suzdal Symposium on Artificial Modification of the Ionosphere*, URSI, Uppsala, Sweden, 1994). Applications over a wider range of experimental conditions and parameters, however, require investigations of SLT in sometimes highly-modified ionospheric plasmas, replete with large-scale irregularities. These investigations must incorporate phenomena as may occur over a wide range (up to five decades or more) of spatial and temporal scales.

We report results of numerical simulations of SLT within a background of large-scale artificial ionospheric irregularities as often occur in typical HF experiments. Use is made of short-scale averaging techniques to achieve an efficient model of the SLT. Large-scale ionospheric irregularities are modeled using fully nonlinear ion hydrodynamics. Results of these simulations are then compared to experiments we have performed at Arecibo. The temporal evolution of the plasma line is shown to have comparable features in simulation and experiments. The spatial localization of the SLT found in simulations may also be compared with available experimental data. Of particular interest, are the couplings of longitudinal electrostatic modes within the artificial irregularities, to transverse modes near the HF pump frequency, which may be detected by ground-based receivers. The results of these investigations may afford an improved understanding of HF ionospheric experiments as performed under a much wider range of conditions and parameters.

G/H2-9 THE HAARP FACILITY
16:20

Robert A. Jacobsen
APTI
1250 24th St NW Suite 850
Washington DC 20037

The HAARP Facility is now fully operational. The intent of this talk is to provide the listener with an overview of the systems features and capabilities to assist in guiding experimental planning utilizing the HAARP Array.

The HAARP Array is a 48 element (6x8) phased array constructed of novel wide band crossed dipoles operating in the frequency band of 2.8 to 8.5 MHz. Each crossed dipole is powered by a dual 10 kW transmitter, providing 20 kW per element for a total array radiated power of 960 kW. The antenna directivity of 23.8 dB on broadside provides an ERP of 82.5 dBW at 8 MHz.

Arbitrary polarization is provided since each transmitter is individually controlled in amplitude and phase. The beam can be scanned to 30 degrees from zenith in any azimuth and can be rapid scanned +/-15 degrees. The fundamental RF signal can be both FM and AM modulated from DC to 30 kHz as well as operated in pulse modulation mode. The beam-width being 18 degrees.

The HAARP Facility has been constructed in the environmentally sensitive marginal permafrost sub-arctic near Gakona Alaska. This has required the incorporation of modern arctic engineering in the design of the array, the 10,000 sq ft operations center and the diesel generator power-plant. The severe environment has placed stringent requirements on the design of all the RF power electronics and array support systems to allow experimental operation from -40 to +90 F, with damage free survival of all the equipment down to -60 F.

The overall system, its controls, transmitters, environmental shelters, antenna and the antenna matching units will be described as will its experimental operation and performance.

G/H2-10
16:40

TRANSHEMISPHERIC PROPAGATION OF VLF EMISSIONS MEASURED BY MATCHED FILTER IN THE PRESENCE OF IONOSPHERIC HF HEATING

M.J. Starks*
Air Force Research Laboratory
29 Randolph Rd VSBS
Hanscom AFB, MA 01731

M.C. Lee, P. Jastrzebski
Massachusetts Institute of Technology
77 Massachusetts Avenue NW16-240
Cambridge, MA 02139

The application of matched filtering to the problem of very low frequency (VLF) radio signals ducted between magnetically conjugate points on the Earth by ionospheric plasma structures has been examined theoretically and implemented in recent field experiments. These experiments, carried out at the Arecibo Observatory in Puerto Rico and the magnetic conjugate location in Argentina, have demonstrated a significant connection between the prevalence and intensity of the transhemispheric propagation of man-made VLF emissions and HF heating of the ionosphere.

With accurate knowledge of the source VLF emissions, the subionospheric component of a waveform received at the conjugate location can be effectively removed and the characteristics of any remaining transionospheric signal accurately estimated. Although the technique has been shown not to produce strictly consistent estimates of the subionospheric and ducted signal amplitudes, it is able to efficiently recover the transit delays and amplitudes of ducted man-made whistler-mode emissions for reasonable values of the relevant signal to noise ratios. This is substantiated by the use of matched filtering to analyze data collected by radio receivers placed at the conjugate ends of a magnetic field line in field experiments, thereby recovering the amplitudes and transit delays of ducted signals with time-resolution as small as 30 seconds.

These measurements suggest that the O-mode CW heater appears to encourage the coupling of VLF emissions into the affected region of plasma. These signals then enter plasmaspheric ducts more efficiently and typically lead to conjugate measurements of relatively high amplitude. No such effects are seen with pulsed or X-mode heating. Short time resolution measurements of fading transmissions also demonstrate that transit delays and amplitudes remain nearly constant as the frequency of transhemispheric propagation diminishes, consistent with a plasmaspheric duct complemented by favorable plasma properties extending well into the F region but producing the majority of the total transit delay at plasmaspheric altitudes. It is also suggested that weak long-delay receptions are most probably mixed-path ducted/non-ducted modes that have interacted significantly with the plasma and which represent an omni-present contaminant in ducted VLF experiments of all types.

G/H2-11
17:00

GENERATION AND PROPAGATION OF LOW FREQUENCY WAVES IN STRONGLY NONUNIFORM IONOSPHERE

L. I. Rudakov[1,2], G. Milikh[1] and K. Papadopoulos[1,2]
[1]Departments of Physics and Astronomy
University of Maryland, College Park, MD 20742
[2]Advanced Power Technology, Inc.,
1250 24–th Street, Washington, DC 20037

Generation of VLF/ELF emission by using modulated HF-heating of the lower ionosphere was first reported more than two decades ago. It is expected that the efficiency of ELF generation will be increased by using new HAARP facility which besides having high effective radiated power (ERP) is able to change continuously frequency and polarization of the radiating radiowave. However, in order to reach maximum VLF/ELF generation efficiency a proper choice of the HF-frequency and polarization has to be made. It is based on models of VLF/ELF generation, however the existing models still have some unresolved issues despite a significant progress. Early models suggested that the ionospheric VLF/ELF source could be modeled as an equivalent horizontal electric dipole (HED) [Barr and Stubbe, 1984; Papadopoulos et al., 1989]. This, however, led to inconsistencies between the model and ground observation, since the model significantly overestimates the conversion efficiency. As mentioned by Zhou et al. (*Phys. Plasmas, 3,* 1484–1494, 1996) currents induced by the HF-heating should be closed in the ionospheric plasma. The current closure implies that contrary to previous suggestions the dominant radiating moment of VLF/ELF ionospheric source is an equivalent horizontal magnetic dipole. This model, however, did not take into consideration nonuniformity of the ionospheric plasma, which plays an important role in the HF into VLF/ELF conversion. Existing numerical models of VLF/ELF generation are based on some simplifications, such as totally reflecting boundary conditions (H.L. Rowland, *J. Geophys. Res., 104A,* 4317–4327, 1999) which need to be justified. The objective of this work is to present an analytical model of the plasma response to the current induced by the HF-heating in strongly nonuniform lower ionosphere. This model could be later used in conjunction with existing numerical codes to guide experimental campaigns and interpret the obtained data.

Two different methods are applied to the problem. One is quasi-classical approach which is valid when the wave vector k exceeds the scale height of the electron density gradient in the ionosphere H. Within the scope of this approximation the quasi-classical helicons attenuate due to the ion dissipation. The second method is an abrupt approximation valid for $k < H$. In order to answer questions regarding the efficiency of excitation of TEM mode propagating along the ground one need to know the effective size of the current loop caused by closure of the current induced in the ionosphere by the HF-heating. The apparent answer is that the current loop is vertical, which corresponds to horizontal magnetic dipole. Its vertical size which depends on the VLF/ELF frequency range is evaluated. Some experimental verifications of the theory are suggested. In fact, the horizontal magnetic field component B_y measured at the ground is dominant. Besides, the B_z component measured at the ground reaches its maximum beneath the center of the HF-heated region in the ionosphere, while the B_x component peaks beneath the antenna edge. This fact is related to the existence of the drift term in the dispersion relation for VLF/ELF.

G/H2-12
17:20

GENERATION OF DENSITY IRREGULARITIES AND WHISTLER WAVES BY AMPLITUDE MODULATED HF WAVES IN THE POLAR ELECTROJET

S.P. Kuo*
Polytechnic University,
Department of Electrical Engineering,
Farmingdale, NY 11735
E. Koretzky
TRW Electronics Systems & Technology Division
Redondo Beach, CA 90278
M.C. Lee
Plasma Science and Fusion Center,
Massachusetts Institute of Technology
Cambridge, MA 02139

Using amplitude-modulated powerful HF waves to generate spatially periodic temperature and density irregularities together with whistler waves in the E-region electrojet of the polar ionosphere is investigated. It is shown that a thermal instability is first excited by the HF wave. This instability leads to a significant electron temperature enhancement, but is quickly stablized by the nonlinear damping of inelastic electron collisions with N2 and O2. Simultaneously, the thermal diffusion of electrons also causes the temperature perturbation to develop nonlinearly into spatially periodic irregularities along the geomagnetic field. The recombination rates of electrons with NO+ and O2+ ions decrease as the electron temperature increases. Thus the background plasma density in the presence of ionization sources, such as UV radiations during the daytime and precipitated energetic particles at night, varies in a similar form as the temperature perturbation. The spatial period of the irregularities varies with the HF wave power and frequency in the range between 400 m and 1.6 Km. Moreover, a distributed mode current of whistler waves at the modulation frequency of the HF wave is also induced through the coupling between the generated density irregularities and the HF wave-modulated electrojet current. This current produces whistler waves directly without going through a low efficiency antenna radiation process. This direct excitation mechanism also helps to reduce the harmonic components of the excited whistler wave, which has a frequency between 3 and 27 KHz depending on the polarization, frequency, and power of the HF wave and the modulation scheme.

G/H2-13
17:40

STIMULATED THERMAL INSTABILITY FOR ELF AND VLF WAVE GENERATION IN THE POLAR ELECTROJET

S.P. Kuo*
Polytechnic University,
Department of Electrical Engineering,
Farmingdale, NY 11735
M.C. Lee
Plasma Science and Fusion Center,
Massachusetts Institute of Technology
Cambridge, MA 02139
P.A. Kossey K.M. Groves J.L. Heckscher
Air Force Research Laboratory,
Hanscom AFB, MA 01731

Generation of ELF and VLF waves in the HF heating wave modulated polar electrojet is studied. Through the Ohmic heating by the amplitude-modulated HF heating wave, the conductivity and thus the current of the electrojet is modulated to set up the ionospheric antenna current. However, it is shown that a stimulated thermal instability is also excited by the amplitude-modulated HF heating wave. This instability produces electron temperature modulation in addition to the modulation produced directly by the Ohmic heating mechanism. The result shows that this instability is, in fact, a dominant process of electron temperature modulation before it is stablized by the nonlinear damping of inelastic collisions. Therefore, this study suggests an alternative approach to improve the modulation efficiency by introducing ways to reduce inelastic collisions of electrons with neutral particles, so that the instability can grow to a higher level. The other approach to be presented for the improvement of the modulation efficiency is to employ a proper amplitude-modulation method on HF heating waves. Thus four periodic modulation schemes: (1) rectangular wave, (2) beat wave, (3) half-wave rectified wave, and (4) triangular wave, have been studied and compared. From the results of a defined efficiency factor ?1 and the nth harmonic noise factor Nn for each modulation scheme, we will show that the beat wave scheme generates the best quality signal which has the lowest harmonic content, the half-wave rectified wave modulation scheme is the most efficient one to generate signal at the modulation frequency, and the symmetric triangular wave modulation scheme provides a compromise between generation efficiency and signal quality.

G/H2-14 18:00 ULF GENERATION BY ELECTROJET MODULATION USING HAARP

C-L. Chang
Applied Physics Operation
MS 2-6-9
1710 Goodridge Drive
SAIC
McLean, VA 22102

Feasibility study has been conducted on the excitation of ULF waves using HF heater at HAARP. Physical model includes local ionospheric profiles derived from IRI90, plasma density modification due to HF interactions, electrojet modulation at ULF frequencies, and ULF excitation and propagation in the earth-ionosphere environment. There are two issues to be addressed by this study. The first issue is to explore the physical mechanisms and the efficiency of ULF generation using HAARP. The second issue is to model the actual ULF measurements in support of HAARP experimental campaigns.

Typical ULF waves stimulated by ionospheric modification consists of two basic wave modes: the magnetosonic waves and the shear Alfven waves. These two wave modes have very distinct excitation and propagation characteristics. It is found that by modifying electron density of the E region the magnetosonic modes are easier to generate than the shear Alfven waves. The magnetosonic waves propagate mainly along the meridian plane in a ULF duct centered around the F peak. However, such propagation is not possible below a cut-off frequency defined mainly by the conductivity profiles of both earth and ionosphere. The shear Alfven waves, on the other hand, propagate mainly along the ambient magnetic field line and has no such cut-off. In the E region modification, ground level ULF signals is mainly due to the conversion from magnetosonic modes to the shear Alfven modes in the E layer.

Several other important findings can be summarized as follows. First, the efficiency of ULF generation is proportional to the electron density in the lower ionosphere. Therefore, excitation under day time condition is preferred. Second, HF modification near F peak results in substantial enhancement of direct shear Alfven excitation. This is a useful technique if the emphasis is to send artificial ULF waves into the magnetosphere. Finally, ULF signals measured at ground level depend on the coupling and the combination of both magnetosonic and shear Alfven waves. A detailed study on ionospheric conditions, propagation properties, and excitation mechanisms will be required in order to fully understand the empirical results such as polarization and temporal variations of the ULF amplitudes.

Memorial Session 2, 13:35-Fri., Room 265

GEOELECTROMAGNETICS — A TOPIC OF LIFELONG INTEREST TO JAMES R. WAIT

Chairperson: G. Hagn (ghagn@erols.com)

W2-1
13:40

METHODS OF MEASURING THE ELECTROMAGNETIC PROPERTIES OF EARTH MEDIA-A NEW IEEE GUIDE DEDICATED TO PROFESSOR JAMES R. WAIT

George H. Hagn* David V. Thiel*
Wave Propagation Standards Committee
IEEE Antennas and Propagation Society
Institute of Electrical and Electronics Engineers

This paper has two goals: a) to recognize the profound contributions Professor Wait made to the field of geoelectromagnetics; and, b) to highlight significant advances made in the field of measurements of the earth's conductivity and relative dielectric constant since 1974.

Professor Wait's major contributions to geoelectromagnetics - including his many talks, lectures, papers and books - all have in common his expert use of advanced mathematics to analyze complex problems involving lossy earth media, including layered media. His interests covered the frequency range from DC (for probing deeply into the Earth) to light (where he was interested in solitons). His practical grounding in the field of electromagnetic geophysics began when he served from 1949-52 as an exploration geophysicist for Newmont Exploration in Jerome, AZ. He also contributed to improving communications to and from underground miners, and he maintained a large interest beyond the mathematics to the applications of electromagnetics to practical problems.

Prof. Wait was one of three members of the IEEE Wave Propagation Standards Committee (WPSC) which produced the first "IEEE Guide for Radio Methods of Measuring Earth Conductivity," IEEE Std 356-1974. He was an active member of the WPSC subcommittee preparing the completely rewritten second IEEE Std 356-1999: "IEEE Guide for Measurement of Electromagnetic Properties of Earth Media." He was not only a major contributor but also a mentor to the rest of the subcommittee, which has dedicated the new standard to his memory.

IEEE Std 356-1999 reflects the application of much higher frequencies in both communications systems and remote sensing. It has therefore become more important to address the questions associated with measuring the effect of EM sources on earth planes that are not predominantly conductive. Thus the new IEEE standard describes remote sensing tools at frequencies above 1 GHz where the earth's surface is predominantly a good dielectric, in addition to more traditional measurement techniques for lossy dielectric earth materials, such as ice-covered regions and permafrost. Another development has been the use of numerical modeling techniques. These techniques are almost all "forward modeling", i.e. if one knows the earth's structure, one can calculate the response. With greater computing power, automated optimization can be used to address the "inverse" problem. The validation of electromagnetic geophysical techniques using laboratory measurements is also addressed.

W2-2 TIME-DOMAIN PROPERTIES OF THE ELECTROMAGNETIC PROPERTIES OF SOILS:
14:00 R. Stafford, NIST

W2-3
14:20

ON MEASURING ELECTROMAGNETIC SURFACE IMPEDANCE - DISCUSSIONS WITH PROFESSOR JAMES R. WAIT.

David V. Thiel
Radio Science Laboratory
Griffith University - Nathan
Australia 4111

Electromagnetic surface impedance, defined as the ratio of the horizontal electric field component measured in the plane of incidence of a distant radio source, to the horizontal magnetic field component perpendicular to the plane of incidence, has been used in geophysics since the early 1950's for subsurface earth mapping. Traditionally the electric field component has been measured using a staked voltage probe. In 1989 Wu & Thiel (*IEEE Trans. Geosci. Remote Sensing), (27), (1), pp. 24-27*) suggested that an insulated wire dipole without the stakes was a more reliable measurement technique. In 1997, Thiel and Mittra (*IEEE Trans. Geosci. Remote Sensing), (35), (5), pp. 1357-1362*) explored the problem using finite-difference time-domain numerical (FDTD) modeling. Professor Wait responded to both of these papers, and the discussion continued in the literature until his last comments were published in 1999.

The major arguments centered on which is the more reliable method of detecting the horizontal electric field component for surface impedance measurements, and focussed on the following inter-related questions:

Is the staked voltage probe an electric field probe or a loop antenna?

Does a staked voltage probe respond to both the magnetic field and electric field components, and if so, are they additive?

Does the effect of the very strong vertical electric field component on an insulated antenna make this type of measurement unreliable?

What is the effect of the receiver input impedance on the measurements?

Is the stake length an/or stake contact area important in measurements?

What happens to the performance of the staked probe when the top layer of the earth is highly resistive?

In this presentation, these major points are discussed, the answers to these questions are presented, and the final arguments summarized. The major conclusion reached is that either technique can be used provided caution is exercised. The successful practical field implementation of both types of field probes supports this conclusion. It must be noted however, that at higher frequencies, some of the uncertainties which are insignificant at lower frequencies, are exacerbated.

W2-4
14:40 MOISTURE EFFECTS ON THE DIELECTRIC PROPERTIES OF SOILS

John O. Curtis
U.S. Army Engineer Research and Development Center
3909 Halls Ferry Road
Vicksburg, MS 39180
e-mail: curtisj@wes.army.mil
voice: 601-634-2855 FAX: 601-634-2732

Laboratory-measured dielectric property data and related electromagnetic wave propagation parameters are reported for a broad range of soil textures. A network analyzer-based measurement system operating within the 45 MHz to 26.5 GHz frequency range was used for all data collection. Coaxial sample holders varied in length from 1.5 cm to 10 cm and had a diameter of about 0.75 cm

The dielectric permittivity and phase velocity are shown to be very strong functions of volumetric soil moisture at single frequencies. Polynomial moisture prediction models are presented for several frequencies. Data collected in this study validate another moisture-permittivity model that is widely accepted within the geophysics community (G. C. Topp, et al *Water Resources Research*, Vol. 16, No. 3, June 1980, pp. 574-582) as long as soil moisture values are within a normal range and as long as the frequency of measurement is on the order of 100 MHz.

The data indicate that there is no simple relationship between soil moisture and apparent conductivity. Any attempts to model this phenomenon would have to take into account the parameters that should be important to the dominant conduction mechanism, including pore-size distribution, mineral content (which gives an indication of how water might bind with the soil particles), specific surface area, etc.

Data are also presented as properties vs frequency at constant moisture contents. In this form it is possible to easily visualize the dominant loss mechanisms; namely, ionic conductivity and free water dipole relaxation.

Some discussion is offered for the effects of sample density on the dielectric response of the soils. The data indicate that for a single soil sample, dielectric permittivity is a weak function of density, but that for data representing a broad range of soil textures, there is no clear relationship between sample density and dielectric properties.

W2-5
15:00 ELECTROMAGNETIC PARAMETERS OF SURFACE SOIL AND ROCKS FOR ANTENNA AND PROPAGATION MODELING

George H. Hagn
Consultant
4208 Sleepy Hollow Road
Annandale, VA 22003-2046
Ghagn@erols.com

The electromagnetic properties of surface soils and rocks are required for input data for various antenna and propagation models. Measured values of the soil conductivity and relative dielectric constant at the frequencies of interest are rarely available, with the exception of calibration and model validation efforts. Therefore, there is a need for best-estimate values in order to run the models such as the Numerical Electromagnetics Code (NEC) for antennas over real ground, and the Sommerfeld-integral-based groundwave propagation models for predicting field strength for broadcast station coverage, etc.

In this paper the various available input data sources are discussed, from the standard handbook values (e.g., Terman, 1943; ITT, 1990) for different soil categories (where only one valued is provided per category) to the International Telecommunication Union-Radiocommunications Sector (ITU-R) Recommendation 527-3 (where there is dispersion in the frequency domain). Other models in the literature that predict the complex relative permittivity given certain known quantities such as the volumetric soil mositure content also are discussed. A strategy is suggested for how to make the best estimates when all of the desired soil or rock information is not available.

Problems with these various sources of "ground constants" data are discussed, and a new set of curves are provided for possible inclusion in a future version of ITU-R 527-3 that are more representative of measured data in the MF, HF and VHF bands than the current curves.

W2-6
15:40

PROPAGATION AND SCATTERING OF VLF WAVES IN THE EARTH-IONOSPHERE WAVEGUIDE

U. S. Inan* T. F. Bell
STAR Laboratory, Stanford University, Stanford, CA 94305

One of the important legacies of Jim Wait's prolific career originates from his early work on the propagation and scattering of very low frequency (VLF) waves in the earth-ionosphere waveguide. Built upon by R. Pappert and others, this early work led to the development of the extensively utilized Long Wave Propagation Capability (LWPC), and later to development of new methods for remote sensing of transient and localized ionospheric disturbances, such as those produced by lightning. The problem that Wait faced in the late 1950's and early 1960's was one of daunting complexity, involving electromagnetic propagation in a 'waveguide' with both boundaries being lossy, inhomogeneous, and one of them also being anisotropic. Unlike metallic waveguides which can be designed to preclude the propagation of all but few modes, VLF propagation in the earth-ionosphere waveguide involves multiple (typically ~20 or mode) modes, each with different attenuation rates, which couple into one another at the various boundaries, such as land-sea interfaces. Wait's early work [Wait and Spies, *NBS Tech Note No. 300*, 1964] in characterizing the lower ionospheric boundary of this waveguide remains the standard reference in defining the nighttime D region, both for propagation and scattering applications. Wait's work [Wait, 1961; 1964] on diffraction of VLF waves from a localized disturbance (e.g., as produced by an atomic explosion) formed the basis for recent extensions of the LWPC code for application to three dimensional problems, involving localized ionospheric disturbances produced by lightning discharges, and high altitude luminous glows such as sprites. In fact, Jim Wait himself became quite interested in tackling problems involving ionospheric effects of lightning discharges, authoring a number of papers in this area well after his retirement and during the last two years of his career. In this paper, we review the state of the art in subionospheric very low frequency remote sensing, with particular attention to connections with Wait's early work, and the use of current VLF propagation and scattering models for interpretation of experimental data.

W2-7
16:00

MODELING ELECTROMAGNETIC PROPAGATION IN THE EARTH-IONOSPHERE WAVEGUIDE

Steven A. Cummer*
Laboratory for Extraterrestrial Physics
NASA/GSFC
Greenbelt, MD 20771

The ionosphere plays a role in radio propagation which varies strongly with frequency. At extremely low frequency (ELF, 3–3000 Hz) and very low frequency (VLF, 3–30 kHz), both the ground and the ionosphere are good electrical conductors and form an spherical Earth-ionosphere (E-I) waveguide. Many giants of the electromagnetics community worked on ELF-VLF propagation in the E-I waveguide, which was critically important for long range communication and navigation systems. James R. Wait was undoubtedly the most prolific publisher in this field, starting in the 1950's and continuing well into the 1990's. He solved many fundamental propagation problems both analytically and numerically, and also produced fundamental formulations for scattering from large- and small-scale E-I waveguide inhomogeneities.

Although it is an old problem, there are new scientific and practical applications that rely on accurate modeling of ELF-VLF propagation, including ionospheric remote sensing, lightning remote sensing, global climate monitoring, and even earthquake precursor detection (although this assertion remains controversial). While the theory of ELF-VLF propagation in the E-I waveguide is mature, there remain many ways of actually performing propagation calculations. Most techniques are based on waveguide mode theory, with either numerical or approximate analytical formulations, but direct finite difference time domain (FDTD) modeling is now also feasible. Furthermore, in either mode theory or FDTD, the ionospheric upper boundary can be treated with varying degrees of approximation. While these approximations are understood in a qualitative sense, it is difficult to assess a priori their applicability to a given propagation problem. With a series of mode theory and FDTD simulations of propagation from lightning radiation in the E-I waveguide, we investigate the accuracy of these approximations. The calculations show that mode theory is practical even for propagation paths as short as 100 km. However, fields from the zero frequency excitation implicit in the lightning source become important at the lowest frequencies over short distances. These fields are not easily modeled with mode theory but are inherent in the FDTD formulation of the problem. While mode theory calculations can be much faster than FDTD over long propagation distances, the simplicity of FDTD propagation modeling and ever-increasing computer power probably make FDTD the technique of the future. However, the physical insight provided by Wait's and others' mode theory is indispensible for understanding the propagation problem and interpreting purely numerical simulations.

W2-8
16:20

MODAL PHENOMENA IN THE NATURAL ELECTROMAGNETIC SPECTRUM BELOW 5 kHz

D. Porrat* A. C. Fraser-Smith C. C. Teague
STAR Laboratory
Department of Electrical Engineering
Stanford University
Stanford, CA 94305-9515

This paper presents new measurements of the natural magnetic field in the ELF range and their comparison with modal propagation theory as described by J. R. Wait in his book *Electromagnetic Waves in Stratified Media*, Pergamon Press, 1972. The nightly spectrum below 5 kHz often contains a sharp increase in spectral level at the cutoff frequency of the TM_1 mode ($\sim$1700 Hz), and a distinct variation of the spectral behavior at the cutoff frequency of the TM_2 mode ($\sim$3400 Hz), where the indicated cutoff frequencies are calculated for perfectly conducting earth and ionosphere, with the ionosphere 88 km above the earth. We attribute these features to the enhanced levels of the TM_1 and TM_2 modes at night, which makes their level comparable to the TEM mode contribution to the spectrum. All these features disappear during the day.

Another spectral feature, which also prevails during the night, is semi–periodic fluctuations of the spectrum between the cutoff frequencies of the TM_1 and TM_2 modes, with a short period (about 60 Hz) at the low end of the band, and a gradual increase of the period as frequency increases (up to about 600 Hz at the high end of the band). The same semi–periodic fluctuation is apparent above the cutoff frequency of the TM_2 mode up to the limit of the measured band at 5 kHz.

These semi–periodic fluctuations of the spectrum are related to the modal nature of the electromagnetic wave propagation. We show the similarity of the spectrum of vertical lightning in the earth–ionosphere waveguide, calculated theoretically, with the measured spectra. The semi–periodic fluctuations of the spectrum are produced when the lower modes of propagation are summed.

The differences between the daytime and the nighttime measured spectra are explained by the diurnal change in attenuation factors of the different modes. Calculations of the attenuation factors during the day and at night show that the TM_1 and TM_2 modes propagate much better (with lower attenuation) at night, which explains why the modal features of the spectrum are apparent during the night but are not significant during the day.

B1-1 08:40 GEOMETRICAL OPTICS-MOMENT METHOD HYBRID FORMULATION OF A SCATTERING PROBLEM

Kaveh Heidary
Department of Electrical Engineering
Alabama A&M University, Normal AL 35762

The problem of electromagnetic scattering by a PEC cylinder clad partially with layers of simple matter has been formulated. Equivalence principle and GO based dyadic Green's functions are applied to cast the scattering problem into that of an integral equation for EM fields inside the coating. Moment method is then applied to solve the integral equation. Exact Green's functions, obtained by applying the reciprocity principle, are utilized to formulate the scattered EM fields and other parameters of interest.

Pertinent Green's functions are related to EM fields of elementary sources radiating in the presence of the PEC cylinder in unbounded free space. Field vectors (near field region) associated with a Hertzian dipole source (electric or magnetic) radiating in the presence of the conductor are derived using the geometrical optics (GO) approximations. For each source the entire space is divided into shadow and lit regions by two planar surfaces passing through the source point and tangent to the cylinder. For field points within the lit region, EM fields are expressed as the superposition of direct and reflected fields. For field pints inside the shadow region, on the other hand, EM fields are assumed to be zero.

The above GO approximation neglects the effect of diffracted fields. These fields, which are due to the creeping rays (surface waves) propagating around the conductor, are severely attenuated in close proximity of the conducting body. It is for this reason that the GO approximation is valid only for electrically thin coatings, with increasing error for thicker coatings. The dyadic Green's functions pertaining to the problem are obtained from the above GO fields. For observation points situated inside an elementary source region (self terms), quasi-static approximations are utilized to formulate the problem.

The coating is partitioned into a set of electrically small cells. The internal fields are expressed in terms of a set of orthogonal basis functions. Delta weighting functions are utilized to cast the integral equations into systems of linear equations, which are then solved for the internal fields.

Computed results based on this formulation are compared to published data based on the exact modal formulation.

B1-2
09:00

ANALYSIS OF LOSS IN IRIS COUPLING TO A CAVITY

W.A. Davis*
Department of Electrical and Computer Engineering
340 Whittemore Hall
Virginia Tech
Blacksburg, VA24061-0111
J.R. Thomas, Jr B. McConnell
Department of Electrical and Computer Engineering
3114 Randolph Hall
Virginia Tech
Blacksburg, VA24061-0238

Microwave cavities are being developed for the improved heating of thermal runaway materials. To study the heating process and improve the cavity design, numerical modeling of the thermal and electromagnetic problems are being coupled and compared to experimental results. Experimental work has demonstrated that as much as fifty percent of the absorbed energy is dissipated in the iris structure (John M. Curtis, Jr., "Experimental Verification for Microwave Processing of Materials in a Single Mode Rectangular Resonant Cavity", MS Thesis, Virginia Polytechnic Institute & State University, 1999). The initial electromagnetic model was not designed to analyze the loss mechanisms in the iris walls, only the waveguide walls. This paper reports on the numerical study of loss in the iris. Ultimately the iris may be modeled by a simple set of S-parameters for the fundamental mode of the guide, but the solution in the vicinity of the iris requires a higher order mode expansion to obtain the correct solution for the fundamental mode - a standard mode-matching problem. The loss is added to the mode-matching solution with an impedance boundary condition at the metal interface of the iris.

To extend the concept of the loss, the lossy mode-matching solution is compared to a perturbed solution of the no-loss case with an perturbation estimate of the loss on each side of the iris. This estimate uses the no-loss magnetic field at the iris surface to predict the loss current and resultant resistive loss in the iris walls. Results are also compared to the classic incident-field approximation to the fields in the aperture with related perturbation. Finally, results for the lossy mode-matching solution are compared to the measured S-parameters of the iris. With this final comparison, confidence in the computational algorithms is demonstrated, allowing for further refinement of the cavity design without extensive and costly experimental trials.

B1-3
09:20

HIGHER ORDER MODELING IN THE BEM/FEM HYBRID FORMULATION

P. W. Fink
NASA-JSC
Houston, TX 77058

D. R. Wilton
University of Houston
Houston, TX 77204-4793

Hybrid formulations using low order curl-conforming bases to represent the total electric field within a finite element region and low order divergence-conforming bases to represent equivalent electric and magnetic currents on the boundary are well known (J. Volakis, et al., *Finite Element Method for Electromagnetics*, IEEE Press, 1998). However, higher-order divergence and curl-conforming bases have been shown to provide significant benefits in convergence rates and accuracy when employed in strictly integral equation and strictly finite element formulations (D. Wilton, et al., ICEAA, Torino, Italy, Sept. 1999). In this paper, a hybrid electric field formulation employing higher order bases is presented. The paper addresses benefits and issues associated with using higher order divergence- and curl-conforming bases in the hybrid finite element/boundary element electric field formulation.

The method of singularity subtraction may be used to compute the self terms of the boundary integral when the bases are of low order. But this method becomes laborious and requires great care when the divergence-conforming bases are of higher order. In order to handle these singularities simply and accurately, a generalized Gaussian quadrature method is employed in which the expansion functions account for the singularity (J. Ma, et al., *SIAM J. Num. Anal.*, 33, 971-996, 1996).

In preliminary tests of the higher order hybrid formulation, the equivalent electric current induced by scattering of a plane wave from a square dielectric cylinder is examined. Accurate results are obtained using only a two-triangle mesh when the current basis is of order 4 or 5. Additional results are presented comparing the error obtained using higher order bases to that obtained using lower order bases when the number of unknowns is approximately equal. Also, convergence rates obtained with higher order bases are compared to those obtained with lower order bases for selected sample problems.

B1-4
09:40

MEASUREMENTS AND MODELING OF DIFFERENT NON-IDEAL RETURN PATH STRUCTURES

Andrew Byers* Pelle Fornberg Melinda Piket-May John Dunn
Department of Electrical and Computer Engineering
Campus Box 425
University of Colorado
Boulder, CO 80309
Stephen H. Hall Zale Schoenborn
Intel Corp.
2111 NE 25th Avenue, MS JF2-54
Hillsboro, OR 97124

As system bus and clock speeds continue to increase, previously subtle effects on signal integrity (SI) and electromagnetic emissions (EMC) start to have more of a significant impact. One good example of a structure that has such an effect is a non-ideal return current path. A non-ideal return current path occurs whenever a return current is forced to diverge from the path of least inductance, which is usually located directly under the signal trace. These paths can occur in several different forms, including slots in reference planes, level transitions within a printed circuit board, or package-to-board interfaces. An awareness of these non-ideal structures is necessary for a packaging engineer to avoid the potential SI and EMC repurcussions of not providing a good return path for a signal trace. The first step is to identify the non-ideal return paths that pose the largest threat and quantify the effect through measurement. After this has been done, lumped and distributed element models can be developed to include the effects of the specific non-ideal return path structure in the established design methodology.

Several different types of non-ideal return path structures were measured on a test board. Microstrips completely changing reference layers, microstrip-to-stripline transitions, and microstrips passing over ground plane slots were measured in both time and frequency domains. Signal integrity problems such as driver noise, overshoot/undershoot, and timing pushouts will be shown. EMC issues that arise from increased current loops will also be identified. The effects of both coupled and single lines interacting with these non-ideal return paths are included. Systematic line length and decoupling capacitor placement variations were made to draw correlations between the physical board parameters and the resulting waveform characteristics. These correlations are useful in understanding which physical layout parameters can by tranferred to lumped element models, and ultimately how to generalize the lumped element model to cover a wider range of non-ideal return path structures. The measurements, combined with full-wave FDTD simulations, are used to verify different lumped and distributed modeling techniques. Measurements, FDTD simulations, and modeling results will all be presented.

B1-5
10:00

DIGITAL FILTERING TECHNIQUES USED TO INCLUDE MULTIPORT DEVICES IN FDTD SIMULATIONS

Ian Rumsey
Asa Holley
Melinda Piket-May
University of Colorado at Boulder
Department of Electrical and Computer Engineering
Campus Box 425 Boulder, CO 803039
mjp@boulder.colorado.edu

Microwave and digital circuits are achieving ever-increasing speeds and physical complexity, and as a result the need for system-level simulation of electromagnetic effects has also increased. The Finite-Difference Time-Domain (FDTD) technique is well-suited to this task because it can model arbitrary geometries and material properties, as well as modeling time-domain signal properties such as rise time and propagation delay. While this technique is powerful, it is also too computationally intensive to perform practical system-level electromagnetic simulations.

This presentation will show the development of a method for approximating the time and frequency-domain behavior of multiport devices and subsystems with digital filters (I.Rumsey, Master's Thesis, University of Colorado 1999). By approximating the terminal behavior of transmission line networks and lumped devices with an equivalent digital filter, the physical size and aspect ratio of system-level FDTD models can be reduced to provide practical simulation times for microwave circuit and printed circuit board design. These approximate filter models can be constructed from frequency response data, or from previous FDTD simulation of the subsystem. This method is based on the equivalent source method (J. Mix, USNC/URSI National Radio Science Meeting, 1998 Digest, Atlanta GA, pp.75) which allows for FDTD transmission line voltages and currents to be utilized in lumped circuit calculations without direct alteration of the standard FDTD update equations. These line voltages and currents are used in calculating reflection and transmission at each port of the subsystem to all other subsystem ports. The digital filter approximation allows for recursive convolution in the time domain (T.J. Brazil, IEEE Trans. Microwave Theory and Techniques, vol. 43, no. 2, pp. 315-323) as the simulation is running. The basic principles of this method, as well as implementation issues will be discussed.

B1-6
10:40

POLARIZATION EFFECT OF THE TRANSMITTED WAVE THROUGH A LOSSY CHIRAL SLAB FOR NORMAL INCIDENT PLANE WAVES

Y.C. Huang and K.H. Lin
Department of Electrical Engineering
National Sun Yat-sen University
Kaoshiung, 80424
Taiwan

In this paper we used the propagating eigenmodes (S. He and I. V. Lindell, *IEEE AP, 41,* 1659-1664, 1993) and fit the boundary conditions to derive the wavefields in an anisotropic slab situated in the simple medium when the wave incidents normally from the simple medium to the slab. In particular, the theory can be applied to a lossy chiral slab. Here, the transmitted wave was interested. The polarization ratio was employed to investigate changes in polarization states of the transmitted wave.

The case of a chiral slab was thoroughly studied, including the lossy effect. The chiral medium is a bi-isotropic medium. In general there are two elliptically polarized waves in a homogeneous lossless bi-isotropic medium. When the medium is lossy, the two characteristic waves are usually attenuated differently (I. V. Lindell et al., *Artech House,* 1994). Specifically, chiral parameters given by F. Mariotte et al. (*IEEE AP Magazine, 38, 2,* 22-32, 1996) were used to perform the computations. The field inside the slab and the transmitted field were investigated. The polarization state and the power loss of the transmitted wave were computed for various slab thickness.

If the slab is thick enough, the multiple reflected waves inside the slab are negligible. In this case the field can be described using two orthogonal circularly polarized waves. Since the two waves are attenuated differently, the transmitted wave will eventually become LHCP or RHCP, depending on their relative attenuation, for an arbitrary incident polarization. For the lossless case, if the incident wave is linear polarization, the transmitted wave polarization is linear too. In this case the tilt angle will be rotated in a manner similar to that in ionospheric propagation.

One particular result showed that the polarization state changed to LHCP eventually when the slab thickness was increased. On the other hand, the transmitted power decayed quickly with the slab width increased. As a result, there is a trade-off between the transmitted power and the desired polarization state. If the medium parameters were varied according to the passive condition, $\kappa_{im}^2 < \mu_{im}\varepsilon_{im}\ \mu_o\varepsilon_o$ (I. V. Lindell et al., *Artech House,* 1994), such that $\eta_{im} \approx 0$ where the subscript im means the imaginary part. In this case, only one eigenfield decayed quickly with the slab thickness. The relation between medium parameters and the polarization state of the transmitted wave as well as the power loss are discussed and summarized.

B1-7
11:00

A BEAM-SPLITTING REFLECTION GRATING

P. L. E. Uslenghi
Department of Electrical Engineering and Computer Science
University of Illinois at Chicago
851 South Morgan Street, Chicago, IL 60607-7053

A metallic grating with identical triangular grooves parallel to the z-axis is considered. The cross-section of each groove is an isosceles triangle with the two equal sides forming 30-degree angles with the plane x=0 of the grating. The triangular grooves are filled with a penetrable material characterized by a scalar electric permittivity and a scalar magnetic permeability, and the half-space in front of the grating is filled with air. The grating with filled grooves presents a smooth planar surface to the incoming primary field.

A plane wave propagating in the +x direction is normally incident on the interface x=0 between air and grating. The incident electric field is perpendicular to the grooves and is, therefore, parallel to the y-axis. The incident wave is partly reflected and partly transmitted across the frontal planar interface of the grating. The transmitted wave is reflected at the slanted perfectly conducting surfaces of each groove, and after reflection propagates in a direction parallel to the other face of the groove with the electric field perpendicular to that face, so that the boundary conditions on the second face are satisfied. Additional reflections and transmissions occur when this reflected wave impinges on the planar surface x=0, and so on. When the infinite number of reflected and transmitted waves are added, one obtains three geometric series, representing the backreflected plane wave and two plane waves obliquely reflected in directions perpendicular to the z-axis of the grooves and at symmetric angles with respect to the incident direction, provided that the contributions of all grooves to the obliquely reflected waves add in phase. This last requirement means that for a discrete set of frequencies, the incident plane wave splits, upon reflection, into three plane waves, one backreflected and two symmetrically directed with respect to the direction of incidence. In particular, it is found that a necessary and sufficient condition for the backreflected field to be zero is that the material filling the grooves be isorefractive to air.

B1-8
11:20

On the Use of a Hybrid MFIE/FDTD Method for the Analysis of Electromagnetic Scattering and Coupling Problems

Maria Sabrina Sarto[1] and Christopher L. Holloway*[2]
[1]Dept. of Electrical Eng., Univ. of Rome "La Sapienza"
via Eudossiana 18, 00184, Rome, Italy
[2]Institute for Telecommunication Sciences/U.S. Dept. of Commerce
325 Broadway, Boulder, CO 80303, 303-497-6184

There has been a great amount of attention paid in recent year on the use of the finite-difference time-domain (FDTD) technique for solving large electromagnetic problems. Two of the difficulties in the FDTD approach are: first, the need to spatially resolve (or grid) large regions of space around the problem of interest; secondly, the need to use absorbing boundary conditions to truncate the computational volume. In this talk, we present a hybrid technique, combining the magnetic field integral equation (MFIE) and the FDTD methods, for the elimination of both of these difficulties. The MFIE is applied to the treatment of region surrounding the computational volume and the FDTD approach is applied to the inner fields in the computational volume. The MFIE is used as an absorbing boundary condition and/or as a means of coupling the incident field into the problem space.

In this approach, the computational volume is truncated with magnetic field nodes. The boundary condition for these external magnetic fields are obtained by imposing the MFIE on the boundary. For a two-dimensional problem and in the case of a TM_x polarized wave, the MFIE reduces to

$$H_z(\mathbf{r},t) = 2H_z^i(\mathbf{r},t) - 2\epsilon_o \int_{S_o} \frac{\partial E_y(\mathbf{r},t)}{\partial t} * g(\mathbf{r},\mathbf{r}',t)\ ds'$$

where H_z^i is the z-component of the incident field, E_y and H_z are the tangential components of the electric and magnetic fields on the plane boundary surface S_o, orthogonal to the x-axis, and g is the time-domain free-space Green's function given by

$$g(\mathbf{r},\mathbf{r}',t) = \frac{\delta\left(t - c_o^{-1}|\mathbf{r}-\mathbf{r}'|\right)}{4\pi\ |\mathbf{r}-\mathbf{r}'|}$$

where δ is the Dirac's delta function. The magnetic and electric fields in the FDTD computational volume are offset by half a spatial cell size ($\Delta h/2$), while the integral equation requires the H and E fields to be at the same location. This discrepancy can result in reflections from the integral equation boundary. We discuss methods for reducing these unwanted reflections from the integral equation boundary. Results for various geometries will be given.

B1-9
11:40

Absorbing Boundary Condition for both Propagating and Evanescent Modes in FDTD Simulations of Waveguide Structures

Yaowu Liu*
Dept of Electronic Engineering, City University of Hong Kong, Kowloon, Hong Kong

Zhiyuan Yu
Institute of Applied Physics, University of Electronic Science and Technology of China, Chengdu, Sichuan, China

When finite-difference time-domain (FDTD) method is used in simulations of waveguide structures, the main cost of CPU time and memory requirement will pay how to handle the evanescent modes which are triggered either by a wide-band exciting source or stirred by waveguide discontinuities. Although the evanescent wave triggered by the wide-band source can be eliminated by a band-pass source (Z. Yu, Microwave and Optical Technology Letter, 32-133, Feb. 5 1998), the evanescent modes stirred by the discontinuities can not be filtered out. In order to attenuate the evanescent modes to negligible level, a longer distance from the discontinuities needs to be added. This is the reason why a large computation domain should be used in the waveguide structures. Therefore, both the CPU time and the memory requirement have to be increased. In order to solve this problem, a lot of efforts have been made. For examples, an absorbing boundary condition for both propagating and evanescent waves in microstrip structures is presented (V. Betz et. al., IEEE Microwave and Guided Wave Letters, 82-184, June 1993), but it is not suitable for the waveguide structures where much stronger wave dispersion exists. A technique of decomposing the wave into a set of orthogonal modes is proposed for absorbing both evanescent and the propagating modes (M. Mrozowski, et. al., Electronics Letters, 109-1110, June 1996). Finally, perfectly matched layer (PML) technique is used for absorbing the propagating and evanescent waves in the waveguides (J. P. Berenger, IEEE Microwave and Guided Wave Letters, 188-190, May 1998), but the additional layers required by the PML increase the computation space. In this paper, a new ABC for absorbing both propagating and evanescent modes in the waveguide structures is proposed. This new technique allows us to put a truncated boundary much closer to the waveguide discontinuities than the conventional ABC. The efficiency of the new technique is demonstrated by 70% computation space saving for finding S parameters of a Ka band rectangular waveguide with a symmetrical inductive iris.

Session F6, 08:35-Sat., Room 1B-51
RADAR REMOTE SENSING OF THE ENVIRONMENT
Chairpersons: D. Zrnic, NOAA/NSSL (zrnic@nssl.noaa.gov)
R.A. Kropfli, NOAA/ETL (rkropfli@etl.noaa.gov)

F6-1
08:40

RAIN DROP SIZE DISTRIBUTION DEDUCED FROM UHF AND S-BAND PROFILERS USED IN SUPPORT OF GROUND VALIDATION OF THE TRMM SATELLITE

Christopher R. Williams, Paul E. Johnston and Warner L. Ecklund
Cooperative Institute for Research in Environmental Sciences (CIRES)
University of Colorado, Boulder, CO, USA

Kenneth S. Gage and David A. Carter
National Oceanic and Atmospheric Administration (NOAA)
Aeronomy Laboratory, Boulder, CO, USA

The use of vertical pointing Doppler profilers in recent years has provided a new opportunity to sample the characteristics of precipitating clouds nearly continuously. The high vertical resolution of these profilers enables the vertical structure of the precipitation to be studied in great detail. We are evaluating established techniques as well as developing new techniques to estimate the rain drop size distribution of the precipitation from the high resolution Doppler velocity spectra. The retrievals are performed from observations a couple hundred meters above the surface to just below the melting level in stratiform rain. One goal is to estimate the vertical structure and evolution of the drop size distribution to better understand the four dimensional structure of latent heating in the atmosphere.

The NOAA Aeronomy Laboratory has configured two collocated profilers operating at 915 MHz (UHF) and 2835 MHz (S-band) in support of the Tropical Rainfall Measuring Mission (TRMM). The profiler pair has been deployed at the TRMM Ground validation sites in south Texas (April-May 1998), in central Florida (July-September 1998), and in the Amazonia region of Brazil (January-February 1999). The profiler pair will operate in the western tropical Pacific on Kwajalein Atoll, Marshall Islands, for an extended period of time (July 1999-July 2001). Disdrometers collocated at the profiler site record the drop size distributions reaching the surface. These surface observations provide independent reflectivity calibration values for the profilers as well as drop size distribution estimates to corroborate the profiler retrievals. Results from estimating the drop size distribution using the UHF/S-band profiler pair and the surface disdrometers from the Florida campaign will be presented at the conference.

F6-2
09:00

S-BAND POLARIMETRIC RADAR OBSERVATIONS OF TROPICAL RAINFALL DURING THE TRMM-LBA EXPERIMENT.

Lawrence D. Carey
Department of Atmospheric Science
Colorado State University
Fort Collins, CO 80523

From 10 Jan - 28 Feb 99, the NCAR S-POL radar (10.7 cm, linearly polarized) took continuous observations of tropical convection over Rondonia, Brazil as part of the Tropical Rainfall Measurement Mission - Large Scale Biosphere Atmosphere (TRMM-LBA) Experiment. The S-POL radar will be utilized to characterize the structure of convection and to provide unprecedented estimates of rainfall over the Amazon.

In order to provide a statistical framework for the S-POL observations, joint probability density functions (PDF) of Z_{dr}, K_{dp}, LDR, and ρ_{hv} versus Z_h were created as a function of height. Since ice rarely survives unmelted more than 2 to 3 km below the height of the 0° C level in the tropics (4.5 to 5 km), joint PDF's below 1 km provide uncorrupted polarimetric radar characteristics of tropical rainfall. Since many of the original S-band polarimetric radar observations of rainfall were taken beneath midlatitude hailstorms, it is interesting to compare those results to the TRMM-LBA observations.

In Fig. 1, the Z_{dr} versus Z_h joint PDF in rainfall is summarized. Comparison with midlatitude observations (e.g., Aydin et al., *J. Clim. Appl. Meteor., 25*, 1475-1484, 1986; Sachidananda and Zrnic, *J. Atmos. Oceanic. Tech., 4*, 588-598, 1987) suggests that tropical Z_{dr} is significantly lower for a given Z_h. For Z_h = 40 dBZ, Z_{dr} has a mode of 0.75 dB and ranges from 0.25 - 2.2 dB when removing 5% of the data at the lower and upper extremes. For the midlatitude observations at Z_h= 40 dBZ, Z_{dr} typically ranged from 1.25 to 3 dB with a mode of 2 dB. A similar downward bias in the tropical Z_{dr} exists at all $Z_h \leq 50$ dBZ. This bias may be the result of differences in the drop shape versus size relationship for tropical versus midlatitude rainfall. For example, rainfall beneath midlatitude hailstorms may contain ice cores that stabilize the drops and mitigate the effect of oscillations on the drop shape. These differences have important implications for hydrometeor identification.

Fig. 1. Range of S-POL Z_h-Z_{dr} pairs in rainfall below 1 km. Each pair of lines represents

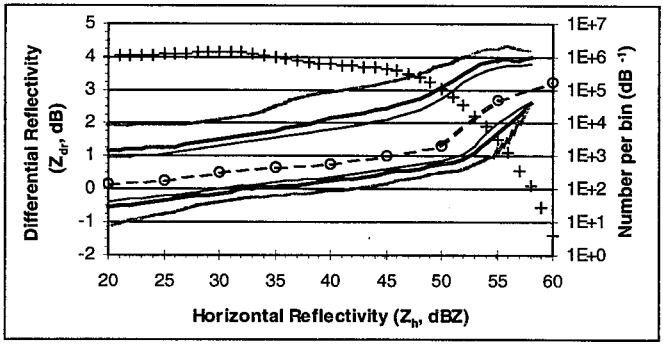

the range of Z_{dr} with the lower and upper extrema removed [gray: 1% extrema removed (98% retained); thick solid: 5% (90%); thin solid: 10% (80%)]. The dashed line represents the mode of the observed Z_h-Z_{dr} pairs. Approximately 83 hours of radar data over 12 days were analyzed. The '+' symbols indicate the number of samples per Z_h bin.

F6-3
09:20

SLANT-LINEAR POLARIZATION FOR DISTINGUISHING AMONG QUASI-SPHERICAL TYPES OF HYDROMETEORS

R. F. Reinking*
NOAA Environmental Technology Laboratory
Boulder, CO 80303
S. Y. Matrosov
University of Colorado - CIRES
and NOAA Environmental Technology Laboratory
Boulder, CO 80303

Dual-polarization radar can be used to identify hydrometeors according to their shapes and related parameters. First, it is demonstrated that depolarization ratios can uniquely separate the "regular", pristine planar ice crystals, columnar ice crystals, and drizzle drops from one another. The next questions are: (1) Can drizzle, which if supercooled is an icing hazard to aircraft, be separated from the more spherical types of ice particles, such as blocky columns, graupel, snow pellets, and aggregates? And (2) Can these types of ice particles be differentiated among themselves?

For the Ka-band (? = 8.66 mm) radar that is used in the Environmental Technology Laboratory, most particles in non-precipitating to moderately precipitating clouds satisfy the conditions of Rayleigh scattering theory, so this wavelength is optimal for drizzle detection. Deviations from this theory due to larger particles (> 2mm) are generally not too large; therefore, the depolarizations are recognizable extrapolations from smaller particles of the same kinds. Such measurements are presented and examined for hydrometeor identification.

Which polarization state is optimal for this task of distinguishing among hydrometeors? Our most recent experiments, reported here, have tried the 45 degree slant-linear state as one of a few good options being tested, because (1) slant-linear polarization is the closest relative to horizontal (linear) polarization, the state most explored and commonly used, (2) slant-linear can be simply implemented and is a state considered for the dual-polarization of the WSR-88D radars, (3) generally, a cross-channel return greater than that for horizontal polarization is achieved, thus allowing a potential for surveillance of weaker clouds such as those containing drizzle-sized drops, and (3) the use of slant-linear produces a greater dynamic range for the measured depolarization ratios than that achieved with elliptical polarizations, thus enhancing the separation of the signatures of various hydrometeor types.

F6-4 09:40 THE EFFCTS OF DROP SIZE DIESTIBUTION ON POLARIMETRIC MEASUREMENTS OF RAINFALL

D.S. Zrnic[(1)], A.V. Ryzhkov [(2)]
(1) National Severe Storms Laboratory, USA
(2) Cooperative Institute for Mesoscale Meteorological Studies, University of Oklahoma, USA

Evidence, including measurements with a 2 D video disdrometer, suggests that in the US Great Plains the drop sized distribution (DSD) variability might be the dominant cause of discrepancy between rain gauges and radar estimates at distances less than 100 km. Moreover, literature search reveals that very little is known about the DSD at sizes larger than about 5 mm which is the limit imposed by impact type disdrometers. At the 10 cm wavelength the uncertainty in largest size concentrations is of secondary importance because these are within the Rayleigh regime of scattering. Yet, for the 5 cm wavelength and at sizes between 5 and 7 mm, polarimetric variables exhibit a strong resonance effect which can confuse interpretation; this is because the real part of the dielectric constant is about twice the imaginary part hence energy stored in the reactance is about twice the one dissipated. The resonance is subdued at the 3 cm wavelength because there the real part of the dielectric constant is about equal to the imaginary part. Comparisons with rain gauge measurements has brought out the fact that the fixed polarimetric rain rate relations (for the 10 cm wavelength) occasionally produce outliers. That is, there is considerable bias in total rainfall accumulation compared to the dense raingauge network. Moreover, we have observed several times that, although the total storm accumulations of rainfall from gauges and radar agree, the time evolutions of hourly totals can be vastly different. This type of error has no effect on climatological studies but it might be devastating for hydrologic models or flash flood forecasts, both of which require a correct forcing function (i.e. rainfall over short periods of time). An adaptive estimation of rain rate is proposed (relying exclusively on polarimetric data) which we believe might vastly improve polarimetric rainfall measurements. Its essence is in using polarimetric variables to match rain rate relations for a specific rain type.

F6-5
10:00

MEASUREMENTS OF POLARIZATION COVARIANCE MATRIX FOR HYDROMETEORS

A. Ryzhkov[1,2], D. Zrnic[1], E. Brandes[3], J. Vivekanandan[3]

(1) National Severe Storms Laboratory, Norman, Oklahoma
(2) Cooperative Institute for Mesoscale Meteorological Studies, University of Oklahoma, Norman, Oklahoma
(3) National Center for Atmospheric Research, Boulder, Colorado

First measurements of all elements of the covariance scattering matrix for clouds and precipitation have been performed using NCAR S-POL dual-polarization radar during the TEFLUN experiment in Florida in 1998 and the TRMM-LBA campaign in Brazil in 1999. The radar operates at S band and utilizes horizontal and vertical polarizations. In the "full-polarization" mode of operation the radar transmits alternately horizontally / vertically polarized waves and receives co-polar and cross-polar components of reflected signal using dual-channel receiver system. Seven independent radar variables were measured directly, namely, radar reflectivity at horizontal polarization Z_h, differential reflectivity Z_{dr}, linear depolarization ratio L_{dr}, differential phase Φ_{dp}, the magnitude of the co-polar correlation coefficient $|\rho_{hv}|$, and two complex co-cross-polar correlation coefficients ρ_h and ρ_v. Specific differential phase K_{dp} was obtained as a radial derivative of Φ_{dp}, and correction for differential attenuation based on Φ_{dp} was made for Z_{dr}, L_{dr}, and the phases of ρ_h and ρ_v.

Two cases from the Florida data set and four rain events from the Brazil data have been studied in more detail. The major emphasis was on examination of the complex correlation coefficients ρ_h and ρ_v that haven't been explored before for polarimetric radars operating in linear polarization basis.

As predicted by theory, the magnitudes of ρ_h and ρ_v decrease as the width of canting angle distribution increases, i.e., atmospheric particles become more randomly oriented. This fact is fully confirmed by the observational data. The lowest values of $|\rho_h|$ and $|\rho_v|$ are observed within the melting layer. Both parameters are lower in convective rain compared to stratiform precipitation. The highest values of $|\rho_h|$ and $|\rho_v|$(sometimes exceeding 0.9) are detected near the tops of convective cells. These signatures are consistent with negative K_{dp}s that are often observed in the same areas. This is an indication of tilted crystals with high degree of common alignment that is neither horizontal or vertical. This unusual orientation of crystals is likely caused by strong electric fields in electrically charged regions of the cloud. Another confirmation of this crystal habit is very "flat" behavior of the phases of ρ_h and ρ_v. The phases slightly fluctuate around zero in these regions, whereas elsewhere spatial fluctuations are much stronger due to changes of the sign of the mean canting angle from one spatial domain to another. The arguments of ρ_h and ρ_v also exhibit well pronounced drop in the melting layer that indicates, according to theory, the presence of scatterers with sizes within the range between 7 and 10 mm.

Multiparameter data analysis shows that each measured variable represents quite independent and complementary piece of information that makes a polarimetric radar indispensable tool for hydrometeor identification.

F6-6
10:40

HYDROMETEOR CLASSIFICATION USING FULL POLARIMETRIC RADAR COVARIANCE MATRIX

A. Ryzhkov[1,2] and D. Zrnic[1]

(1) National Severe Storms Laboratory, Norman, Oklahoma
(2) Cooperative Institute for Mesoscale Meteorological Studies, University of Oklahoma, Norman, Oklahoma

Modern polarimetric weather radar allows to measure all components of the covariance scattering matrix $<|s_{hh}|^2>$, $<|s_{vv}|^2>$, $<|s_{hv}|^2>$, $<s_{hh}^* s_{vv}>$, $<s_{hh}^* s_{hv}>$, $<s_{vv}^* s_{hv}>$, where s_{ij} denote complex scattering amplitudes of individual scatterer if the wave with i^{th} polarization is transmitted and the wave with j^{th} polarization is received, brackets indicate ensemble averaging, and indices h and v stand for horizontal and vertical polarization if measurements are made in the horizontal / vertical linear basis. Recently, various schemes for automatic hydrometeor classification have been developed based on the first four listed covariances (Vivekanandan et al., *Bull. Amer. Met. Soc., 80*, 381-388, 1999, and D. Zrnic and A. Ryzhkov, *Bull. Amer. Met. Soc., 80,* 389-406, 1999). The last two covariances that are proportional to the co-cross-polar correlation coefficients ρ_h and ρ_v, haven't been explored for linearly polarized radar for which majority of weather observations are being done and which is suggested as forthcoming upgrade of the existing operational network of the WSR-88D radars. The focus of this paper is to examine information content of the coefficients ρ_h and ρ_v and their possible use for hydrometeor identification.

Theoretical analysis shows that the magnitudes of the coefficients ρ_h and ρ_v are roughly proportional to the ratio of sin $2<\psi>$ and σ_ψ, where $<\psi>$ is the mean canting angle of atmospheric scatterers and σ_ψ is the width of canting angle distribution. It is important that the magnitudes of both coefficients are almost entirely determined by orientation of particles and do not depend on particle sizes and shapes. Knowledge of the orientation of atmospheric particles is essential for reliable hydrometeor classification and discrimination between liquid and frozen hydrometeors.

The phases of ρ_h and ρ_v or half of their sum $\delta_{cr} = ½ (\arg \rho_h + \arg \rho_v)$ are also very informative. For scatterers small enough compared to radar wavelength (Rayleigh regime of scattering), δ_{cr} is either 0 or π depending on the sign of the mean canting angle. However, for larger scatterers in the Mie domain, the phase δ_{cr} is different from 0 or π. The magnitude of this difference depends primarily on particle equivolume diameter, its dielectric constant, and radar wavelength. Remarkably, it is not affected by hydrometeor orientation and its oblateness (provided that the particle has some nonsphericity and, thus, depolarized component of the radar signal is not zero). This "non-Rayleigh" addition to the phase δ_{cr} is much larger than the co-polar backscatter differential phase, that is, the phase of the covariance $<s_{hh}^* s_{vv}>$, and, therefore, might be very attractive for gauging size of melting hailstones and discriminating between wet and dry snow.

The conclusions are illustrated by results of computations for S-, C-, and X-band radar frequencies. Estimation of propagation effects and their influence on the magnitudes and phases of the coefficients ρ_h and ρ_v is also made.

F6-7
11:00

ANALYSIS OF COMBINED AIRBORNE AND GROUND-BASED MILLIMETER-WAVE RADAR MEASUREMENTS OF HIGH CLOUDS

Lihua Li* Stephen M. Sekelsky Steven C. Reising
Microwave Remote Sensing Laboratory
Knowles 101, University of Massachusetts at Amherst
Amherst, MA 01003
Gregory A. Sadowy Steven L. Durden Steven J. Dindaro
Fuk K. Li
Jet Propulsion Laboratory
4800 Oak Grove Drive
Pasadena, CA 91109
Arlie Huffman Graeme Stephens
Department of Atmospheric Science
Colorado State University
Fort Collins, CO 80523

Cloud measurements at millimeter-wave (MMW) frequencies are attenuated by atmospheric gases, clouds and precipitation. Estimation of the true equivalent radar reflectivity, Z_e, is complicated because the extinction and Mie scattering coefficients are not well characterized at these short wavelengths. Although attenuation is an unwanted effect, it does provide valuable information about cloud properties. In order to better understand the attenuation characteristics of clouds and precipitation and to intercompare the calibrations of millimeter-wave cloud radars, two 95 GHz (W-band) radars and a 33 GHz (Ka-band) radar were deployed in the field during the summer of 1998. The dual frequency Cloud Profiling Radar System (CPRS) from University of Massachusetts (UMass) was operated as a ground-based system. The 95 GHz Airborne Cloud Radar (ACR), jointly developed by UMass and NASA's JPL, was installed in a nadir-viewing configuration on NASA's DC-8 research aircraft.

This abstract presents simultaneous measurements collected by CPRS and ACR in New Iberia, Louisiana. By using the upward-looking CPRS and the downward-looking ACR, radar data for the same cloud and precipitation volume was obtained from opposite viewing angles. These measurements have unique advantages for studying the properties of the clouds between the aircraft and the ground surface, because *a priori* knowledge of attenuation from clouds, the atmosphere and precipitation is not required. True radar reflectivity can be recovered by combining upward-looking and downward-looking calibrated profiles. This reduces the uncertainty in radar reflectivity estimation since we do not have to make any assumptions about the microphysical properties of the hydrometeors.

F6-8
11:20

A DUAL-WAVELENGTH RADAR TECHNIQUE FOR MEASURING THE TURBULENCE ENERGY DISSIPATION RATE ε

T. E. VanZandt[1], W. L. Clark[1], C. R. Williams[1,2], W. L. Ecklund[1,2], and K. S. Gage[2]

[1] NOAA Aeronomy Laboratory, 325 Broadway, Boulder CO 80303

[2] CIRES, Campus Box 216, University of Colorado, Boulder CO 80309

We have used wind-profiling radars with wavelengths of 11 and 33 cm (2835 and 920 MHz, S- and UHF-band) in summer during the MCTEX campaign at the Tiwi Islands near Darwin, Northern Territories, Australia, and in fall/winter at the Flatland Atmospheric Observatory in Illinois.

Theoretically, the ratio of the radar reflectivities equals the ratio of Hill's (1978) model spectra of turbulent fluctuations of the radio refractive index for the two wavelengths. When the S-band radar observes in the viscous subrange of turbulence, the theoretical ratio is a strong function of ε. Thus, a measurement of the ratio determines the corresponding value of ε in the observed volume. The present pair of radars can determine ε between about 10^{-4} and 10^{-6} m^2/s^3 in the lower troposphere. Other ranges of ε and/or other altitudes can be studied with different pairs of wavelengths.

In the boundary layer during MCTEX we observed ε's an order of magnitude smaller than those observed by other techniques, with a day/night ratio of the order of 10 and a slow decrease with altitude.

The dual-wavelength technique has several advantages over other radar techniques. First, most contaminating non-turbulent echoes, especially particulate echoes, are filtered out. Other than such filtering, no corrections to the data need to be made. Second, the similarity of the shapes of the scatter plot of the observed ratios and Hill's model ratio confirms that the observed ratios are due to turbulence. Third, the technique relies on the relative rather than the absolute calibration of the two radars.

F6-9 11:40 SIMULATION OF SUBSURFACE TIME-DOMAIN ELECTROMAGNETICS

*Anatoliy Boryssenko, Gennadiy Kokorin**

Scientific Research Company Diascarb
P.O. Box 148, Kyiv, Ukraine, 02222
Tel./Fax +(380) - 44-515-3414
E-mail:diascarb@public.ua.net

Detection and discrimination by subsurface high-resolution radars of objects hidden in opaque media are important for scientific and engineering practice as valuable technology of remote sensing and nondestructive testing. This technology is based on registration and processing of electromagnetic pulsed fields scattered by internal heterogeneity of a medium under investigation. Practical application of subsurface radars is often limited due to complexity of interpretation of scattered fields.

This paper is devoted to obtain simple general model with clear physical picture of events and some ability to estimate problem qualitatively from parametric point of view. There are the three parameters of problem, i.e. (1)-transmitting (Tx) and receiving (Rx) impulse antennas, (2)-subsurface media and (3)-hidden objects. The problem is considered in time domain (TD) that is more preferable and adequate due its inherent physics in contrast to frequently domain because the transformation of signal waveform of transient nature is key moment of subsurface radar operation.

A general 2-D geometry of problem is presented in Fig. 1 where bistatic antennas of radar are located on the interface between the upper air medium and the lower opaque one with hidden object in it. Results presented below in Fig. 2-3 were being computed with simulator for several structures of subsurface finite-sized objects. The left side of each pictures shows image of an original geometry of problems under investigation, while the right side is its simulated radar image.

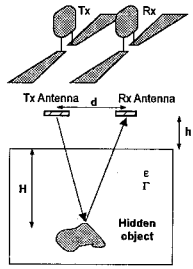

Fig. 1.

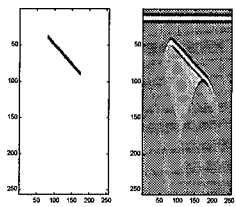

Fig. 2.

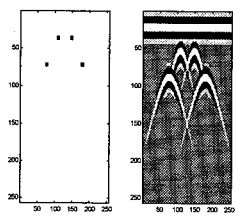

Fig. 3.

F6-10
12:00

NATURAL PULSED ELECTROMAGNETIC FIELDS USED FOR EARTH'S NEAR-SURFACE PASSIVE PROBING

A.Boryssenko, G. Kokorin, V.Polishchuk*

Scientific Research Company Diascarb
P.O. Box 148, 02222 Kyiv, Ukraine
Tel./Fax +(380) – 44 - 515-3414
E-mail: diascarb@public.ua.net

It was estimated experimentally that numerous natural and man-made processes in the Earth interiors cause electromagnetic radiation in the frequency band of the 100 Hz - 10 MHz. A registered electromagnetic emission can be called as the natural Earth's pulsed electromagnetic field (NEPEMF). Local geodynamics events cause statistical variations of the NEPEMF registered on the Earth's surface also. Objects of these studies are localization of subsurface underground hidden objects of artificial origin by monitoring disturbances of pulsed electromagnetic background.

A measurement of signals of the NEPEMF and their following statistical processing allow and mapping of subsurface artificial local hidden objects. To do this we use a magnetic inductor device with electronic registration of the magnetic flux density speed. Fixed on the Earth surface an electromagnetic pulsed radiation is a mixture of the NEPEMF and interference signals. But those components have different statistical features and can be separated by corresponding statistical processing. A perspective object to study by the NEPEMF technique is illustrated in Fig. 1.

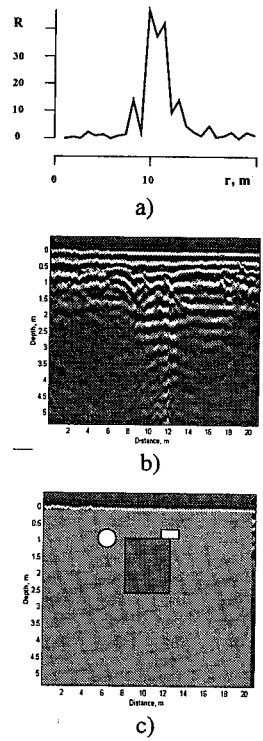

Fig. 1. Detection of old script accomplished by combined remote sensing techniques: (a) NEPEMF approach, (b) subsurface radar, (c) schematic reconstruction of script.

Session G4, 08:55-Sat., Room 245
IONOSPHERIC PROPAGATION
Chairperson: J. Foster, MIT (jcf@haystack.mit.edu)

G4-1
09:00

THE EFFECT OF ELECTRON COULOMB COLLISIONS ON THE JICAMARCA INCOHERENT SCATTER SPECTRUM: REVIEW OF THEORY AND COMPARISONS WITH EXPERIMENTAL DATA

M. P. Sulzer*
Arecibo Observatory, Arecibo, PR 00612
S. González
Arecibo Observatory, Arecibo, PR 00612

The physics describing the effect of electron Coulomb collisions on the incoherent backscatter spectrum looking nearly perpendicular to the magnetic field has been recently described (M. P. Sulzer and S. A. González, JGR, in press). This paper attributes problems with modeling the width of the spectrum as well as the electron and ion temperatures to the effects of these collisions. The fact that the effects electron Coulomb collisions need to be included is now generally accepted. However, there is some controversy over our detailed predictions. In particular, we predict a relatively slow reduction of the collisional effect as the the aspect angle moves further from perpendicular, as the electron density decreases, and as the electron temperature increases. These results, which are unexpected from experience with the predictions of simpler collisional models such as Brownian motion (Langevin's equation) and the BGK approximation, have been questioned.

The variations with these parameters are the result of the specific characteristics of Coulomb collisions, in particular the variation of the magnitudes of the diffusion coefficients with electron speed, the fact that electron-ion collisions modify the momentum strongly without significantly affecting the energy, and the fact that the electron-electron collisions affect the energy relatively slowly. We present a comparison between an analytic calculation for Brownian motion and a numerical calculation for Coulomb collisions, showing how the surprising parameter variation comes about.

As an example we consider the collisional effect looking about two degrees from perpendicular to the field, where we predict an effect several times larger than simple collisional models predict. We show data from Jicamarca which agree with our predictions for both the angle and electron density variations.

G4-2
09:20

NUMERICAL SIMULATIONS OF THE ION-RAIN PROCESS AS VIEWED WITH INCOHERENT SCATTER RADAR

J. D. Mathews*
Communications and Space Sciences Laboratory
Penn State Un.
University Park, PA 16802
Q.-N. Zhou
Communications and Space Sciences Laboratory
Penn State Un.
University Park, PA 16802
Q.-H. Zhou
Arecibo Observatory
Arecibo, PR 00613

High resolution ISR observations of ion-rain (tendrils of ionization extending from the base of the F-region onto the evening intermediate tidal ion layer) and of certain intense spread-F events suggest the presence of E/F region electrodynamic coupling—E-fields mapped along the geomagnetic field "lines"—down to horizontal scales as small as a few kilometers. We further suggest that the ion-rain structures form due to horizontal organization of the plasma in the combined wind and E-field environment. These order 1 mV/m E-fields are hypothesized to be generated in a "field" of linear and/or non-linear Perkins-like instabilities embedded in the bottom-side nighttime F-region and are swept across the E-region with the F-region bulk motion. We present numerical simulations of 3-dimensional ion trajectories in wind and electric field structures similar to those implied by these observations. Further we employ a Monte Carlo-like technique to show how these structures would appear to a narrow-beam incoherent scatter radar. In this approach ions are randomly released into a large 4-D space-time volume with the antenna-beam forming the ensemble averager by recording the passage of an ion-trajectory through the beam at locations of fixed height and time resolution. Additionally, these simulations reveal details of a new horizontal convergence mechanism that occurs when the E-field appears to be almost motionless in the ion frame-of-reference allowing considerable E-field induced horizontal motion. These simulations also yield insight into formation of sporadic E and spread-F structures and we discuss instrumentation—including the Arecibo dual-beam radar system—and observational modes needed to further study electrodynamics on the suggested small scales.

G4-3
09:40

RECENT MESOSPHERIC WIND OBSERVATIONS FROM IDI MEASUREMENTS AT BEAR LAKE, HALLEY AND EISCAT

F. T. Berkey,* C. S. Fish
Space Dynamics Laboratory
Utah State University
Logan, UT 84322-4145

G. O. L. Jones
British Antarctic Survey
Cambridge, CB3 OET United Kingdom

M. T. Rietveld
Max-Planck-Institut für Aeronomie
D-37191 Katlenburg-Lindau, Germany

In order to conduct radar measurements of the mesosphere, an implementation of the imaging Doppler interferometer (IDI) technique (G.W. Adams et al., *Radio Sci.,* **20**(6), 1481-1492, 1985) was configured for the NOAA dynasonde operated by the British Antarctic Survey at Halley, Antarctica (G.O.L. Jones, K. Charles and M.J. Jarvis, *Radio Sci.*, **32**(6), 2109-2122, 1997). The initial results from these measurements have been encouraging (K. Charles and G.O.L. Jones, *J. Atmos. and Solar Terr. Phys.*, **61**, 351-362, 1999) and additional installations have been carried out for dynasondes operated at the USU Bear Lake Observatory and at the EISCAT facility near Tromsø, Norway.

The three currently operational dynasonde installations are sited at mid-latitude (Bear Lake), at a high geographic latitude in the Southern hemisphere (Halley) and at a high magnetic latitude in the Northern hemisphere (EISCAT). The mean and background winds, as well as the amplitude and period of the predominant tidal modes in the 50-115 km regime have been derived from the IDI measurements at each of these sites and the results will be discussed in this paper. Utilizing the inherent frequency agility of the NOAA dynasonde (R.N. Grubb, NOAA Technical Report, 1979), different sounding frequencies are used for IDI sounding at night and during the day at the Bear Lake Observatory. The impact of multiple frequency operation on the mesospheric sounding measurements will also be addressed.

A by-product of the dynasonde IDI implementation is the capability to detect echoes from the ionization created by meteors impinging on the ionosphere at heights from 60-115 km. A companion paper at this conference will discuss the results of these measurements, with particular emphasis on data obtained at the Bear Lake Observatory.

G4-4
10:00

COHERENT AND INCOHERENT SCATTER RADAR OBSERVATIONS OF STORMTIME IONOSPHERE MAGNETOSPHERE OSCILLATIONS

J. C. Foster* H. B. Vo E. V. Mishin
MIT Haystack Obs., Atmos. Sci. Group, Westford, MA 01886
A. P. Potekhin
Inst Solar Terr Phys, RAS, Box 4026, Irkutsk, 664033, Russia
F. J. Rich
AFRL, Hanscom AFB, MA 01731

A rare occurrence of coherent 150-MHz radar backscatter from two-stream E-region irregularities was observed near 55°Λ in the northward-directed sidelobes of the Irkutsk incoherent scatter radar (52.9 N, 103.3 E) during the September 25, 1998 magnetic cloud event. At such normally sub-auroral latitudes, polarization electric fields associated with ring-current injections result in regions of intense sunward convection (SAID) during enhanced geomagnetic activity. The occurrence of such conditions during this event has been confirmed by overflights of the DMSP satellites which observed polarization-jet convection electric fields in excess of 150 mV/m in the region of the radar backscatter.

The Irkutsk radar power profiles were dominated by sidelobe coherent contamination for more than 6 hours during the event. These were corrected for the effects of magnetic aspect sensitivity using a 90-min time-averaged power/range profile which was found to be qualitatively similar to the theoretical aspect sensitivity function calculated using antenna beam pattern, the IGRF 99 magnetic field, and a magnetic aspect angle sensitivity of -15 dB/deg. Correcting the power profile observations with this empirical aspect- angle function produces a relative variation of coherent power across a five-degree span of latitude for the course of the event. This reveals a 1000-s periodicity and latitude progression indicative of a wavelike modulation of the coherent backscatter conditions. Since the electric field is known to have greatly exceeded the threshold for the generation of two-stream irregularities across the region of interest, the observed variation in the coherent backscatter can be explained by a periodic modulation of the local magnetic field orientation. We calculate that a small(0.5 deg) change in the magnetic aspect angle will produce the 5-dB variation on backscattered power observed by the radar.

The oscillatory perturbation of the magnetic field in the Siberian sector near local midnight immediately followed a sharp impulse in the solar wind which produced an interval of globally enhanced activity. Ionospheric F-region density and vertical velocity above the Millstone Hill incoherent scatter radar (54°Λ), separated from the Irkutsk radar by 12 hours of local time, exhibited pronounced oscillations with a similar 20-min periodicity, while ground magnetic observations in both hemispheres revealed a similar oscillation. Radar observations define and confirm the global nature of the ionosphere/magnetosphere perturbations accompanying such impulsive events.

G4-5
10:40

INCOHERENT SCATTER MEASUREMENTS OF ION BEAM INJECTIONS INTO THE IONOSPHERE DURING SPACE SHUTTLE FLIGHT STS-93

P.A. Bernhardt
Plasma Physics Division
Naval Research Laboratory
Washington, DC 20375

M.P. Sulzer
Arecibo Observatory
Arecibo, PR 00613

E. Kudeki
Electric and Computer Engineering
UIUC, Urbana IL 61801

R.F. Woodman
Jicamarca Radio
Observatory, Jicamarca, Peru

R. Tsonuda
SRII
Menlo Park, CA 94025

In late July 1999 during the STS-93 flight of the Space Shuttle Columbia, the crew performed experiments with controlled ion injections over the incoherent scatter radar (ISR) facilities located at Arecibo, Puerto Rico; Jicamarca, Peru; and Kwajalein, Marshall Islands. Ion beams were formed by charge exchange in the ionosphere of the high velocity neutral molecules exhausted by the Orbital Maneuver Subsystem (OMS) engines on the Space Shuttle. Pick-up ions were produced with energies between 2 and 10 eV depending on the orientation of the OMS engines relative to the vehicle orbit. On this mission, the first ISR spectra were measured by reflection from electrons in the presence of the high-speed ions. The non-equilibrium ion distributions produced atypical ion-line spectra. These spectra were predicted by Bernhardt et al. [*J. Geophys. Res., 103*, 2239-2251, 1998]. Numerical fitting procedures were used to extract the ion beam parameters from the measured ISR spectra. The analysis shows relaxation from ring-beam distribution to a thermal distribution in the period of 30 seconds. The analysis of the spectra also indicates that collisional heating by the ion beams yields elevated temperatures in the background ions leading to enhanced radar echoes. Beam driven instabilities involving ions or charged dust in the OMS plume may produce turbulence that would also yield enhanced radar backscatter. This region of enhanced turbulence was postulated by Bernhardt et al. [*J. Geophys. Res., 100*, 23811-28818, 1995] but has not been observed in the radar data for the 2eV ion beam injections over Arecibo and Jicamarca. The 10 eV beam injections over Kwajalein may show the effects from irregularities produced by beam driven instabilities. These observations open up the possibility of conducting a new series of ion-beam instability and heating experiments using the Space Shuttle OMS engines as plasma beam generators.

G4-6
11:00

KHARKOV RADAR OBSERVATIONS OF HYDROGEN ION VARIATIONS DURING THE SOLAR ECLIPSE OF AUGUST, 1999

V. I. Taran V. N. Lysenko Ye. I. Grigorenko
Inst. of Ionosphere
Kharkov, 310002, Ukraine
J. C. Foster* L. P. Goncharenko
MIT Haystack Observatory
Atmospheric Sciences Group
Westford, MA 01886

Continuous observations of electron density, electron and ion temperatures, vertical plasma drift, and hydrogen ion density in the topside ionosphere were carried out at the Kharkov IS Radar during a 3-day interval centered on the August 11, 1999 partial solar eclipse. Maximum obscuration (83in the height range 200 - 1500 km with 1 min time resolution, but in this paper 15 minute integration intervals are considered. The main features of the ionosphere behavior during the August 11, 1999 eclipse are:

1. The eclipse caused a large and rapid increase in the hydrogen ion percentage concentration at all heights (40The lower boundary of H+ ions (10 800 km and the altitude, where H+ ions predominate over O+ ions, decreased from 1250 km to 1100 km.

2. Significant downward F-region plasma movement was observed during the eclipse. An upward drift of 5 m/sec was observed at altitude of 650 km before the eclipse. At eclipse maximum, the drift changed to 65 m/sec downward.

3. Eclipse effects on electron temperature Te were observed at all heights centered about the time of eclipse maximum and following closely the variation of the incident flux of solar radiation. There was a decrease in Te of more than 300 K at all heights above 220 km. The largest decrease (500 K) occurred at altitudes in the range 350 - 450 km.

4. During the eclipse there were changes in ion temperature Ti at all altitudes with an amplitude which increased with altitude. At 350 km, the temperature decreased by 100 K, at 550 km - by 300 K, and at 750 km by 500 K. The temperature change for the ions was much less than that of the electrons. One explanation might be that the ion=neutral coupling restricts the fall in Ti.

5. During the eclipse, electron densities and the altitude of the F layer maximum did not change appreciably.

G4-7
11:20

THIRD-GENERATION HF MODEM/PROTOCOL PERFORMANCE UNDER DEGRADED CONDITIONS

Tim Riley
National Telecommunications and Information Administration
Institute for Telecommunication Sciences
325 Broadway
Boulder, Colorado 80303

The amateur radio community traditionally has supplied a large reservoir of backup communications for the Federal and amateur radio emergency response communities. Due to the decreasing cost of HF modems, increasing numbers of HF radio operators are using modems for digital communications. In the interest of developing this resource, the National Communications System (NCS) sponsored the National Telecommunications and Information Administration (NTIA) to test various HF modems to establish a technical baseline of standardized performance data on HF modem protocols. It is intended that the Federal Emergency Management Agency (FEMA) use these test results to determine the protocols that could serve as an interchange with the amateur community in the event of a national emergency. The tests were conducted at NTIA s Institute for Telecommunication Sciences (ITS) laboratories in Boulder, Colorado. The controlled laboratory conditions enabled ITS to test the protocols under a well-defined, repeatable set of simulated ionospheric channel conditions. Although the extreme limits of degraded channel conditions used to test each protocol varied according to the robustness and implementation of the protocol, all of the protocols were subjected to the same set of degraded conditions. The performance of the various modems and their protocols were compared under the same conditions, establishing a baseline of modem protocol performance.

Earlier testing (Tim Riley, et. al., *A Comparison of HF Digital Protocols*, QST, pp. 35-39, July, 1996 and Tim Riley and Dennis Bodson, *HF Modems and Protocols: An Approach to Testing*, QEX, pp. 3-14, October, 1997) covered first, second and third-generation protocols such as AMTOR, PACTOR, G-TOR, CLOVER and PACTOR2. Follow-on testing compared the two predominant third-generation protocols: PACTOR2 and CLOVER 2000. This testing also utilized a new-generation atmospheric channel simulator, implementing the Watterson channel model on a DSP-based signal processing card with a NATO-approved algorithm. Since the PACTOR2 protocol was covered in both test phases, the results of both tests could be compared with confidence. Results of the tests are presented as throughput (in characters per second) versus channel conditions (CCIR good and poor with varying signal-to-noise ratios).

H3-1
09:00

LONGITUDINAL WAVE PROPAGATION IN A SLOWLY DECAYING MAGNETOPLASMA MEDIUM

V. R. Goteti
Department of Electrical Engineering
Alabama A&M University, Normal, AL 35762

Plasmas produced by solar flares, strong laser pulses or a nuclear explosion are typical examples of transient plasmas. The electron density rises rapidly to a peak value and decays slowly thereafter in such plasmas. Investigation of wave propagation under transient plasma conditions will provide information about creation of new waves, frequency modulation effects and plasma diagnostics.

This wave propagation problem is addressed by assuming that a right circularly polarized wave is propagating in the direction of the static magnetic field in a spatially homogeneous plasma medium (longitudinal propagation) for time $t < 0$. At time $t = 0$, the plasma is considered to start decaying slowly with time, its free electron density ultimately becoming zero. Conservation of wave number over the temporal discontinuity is used as a basis of analysis. The initial wave is shown to split into three new waves. Two of these constitute a pair of transmitted and reflected waves. The third wave appears due to the presence of the static magnetic field and it propagates as a transmitted wave only as long as the magnetoplasma exists. It vanishes when the plasma collapses completely and the entire space becomes free space.

A WKB type solution is developed to determine the frequencies and fields of these waves. A second order Riccati equation is derived as the zero order solution to determine the instantaneous frequencies of the waves. The first order solution is an improvement over the zero order solution in that complex instantaneous frequency functions are developed for the three waves. The fields of the waves are then completely obtained. In order for this solution to be valid, it is necessary that the number density of the plasma be a slowly varying function of time. A condition of validity of the solution is obtained. The proposed solution provides an identification of the individual waves and their fields as opposed to the total fields given by numerical solutions. An exponentially decaying number density profile is chosen as an illustration. The proposed solution compares well with numerical solutions for the total fields at $z = 0$. It is shown that in the absence of the static magnetic field, the proposed solution tallies with the solution for an isotropic plasma medium (D.K. Kalluri, and V. R. Goteti, *J. Appl. Phys.* **66**(8), 3472 - 75, 15 October 1989)

H3-2
09:20

ION BERNSTEIN WAVES DRIVEN BY MULTIPLE SHEAR LAYERS

M. A. Reynolds*
Department of Physics and Astronomy
Howard University
Washington, DC 20059
G. Ganguli
Beam Physics Branch, Plasma Physics Division
Naval Research Laboratory
Washington, DC 20375

For many years, observations of the auroral ionosphere have revealed fine scale structure in the transverse electric field (F. S. Mozer *et al.*, *Phys. Rev. Lett.*, **38**, 292, 1977; J. Bonnell, *Eos Trans. AGU*, **78**(46), Fall Meet. Suppl., F612, 1997). The overall effect of this structure is one of strong velocity shear, resembling many individual $\mathbf{E} \times \mathbf{B}$ flow layers in close proximity. The linear stability properties of waves in such nonuniform media are difficult to predict *a priori*: each situation must be studied individually, and evaluated on a case-by-case basis. Here, we study the effects that structured, nonuniform $\mathbf{E} \times \mathbf{B}$ flow has on the stability of ion Bernstein waves. Specifically, we investigate the case of three layers (whose thicknesses are on the order of the ion-cyclotron radius) with finite $\mathbf{E} \times \mathbf{B}$ flow, immersed in a background plasma that is stationary. In addition, we develop the formalism for a large number of layers, resembling a finely structured profile.

It has been shown that a single localized flow layer (with its associated velocity shear) can be unstable to ion Bernstein waves (G. Ganguli *et al.*, *Phys. Fluids*, **28**, 761, 1985), and that two layers can significantly couple to increase the growth rate of the instability (M. A. Reynolds and G. Ganguli, *Phys. Plasmas*, **5**, 2504, 1998). We generalize these single- and double-layer results to include the new effects due to the addition of a third layer.

The relevant results for one and two flow layers will be described, and for three layers we will investigate in detail two types of structures that are generic in character. The first type is characterized by flows in the same direction, with regions of zero velocity separating the layers. The second type is characterized by flows in opposite directions with little or no separation between the layers, resembling electrostatic shocks.

This work is supported by a New Faculty Grant from Howard University, and by grants from ONR and NASA.

H3-3
09:40

SOLITARY KINETIC ALFVEN STRUCTURES AND TURBULENCE

R. A. Treumann*
MPE
Garching
Germany
M. Berthomier and R. Pottelette
CETP
Saint-Maur des Fosses, Cedex
France

Kinetic Alfvén waves have long been known for their ability to evolve into solitary structures. In space plasmas of sufficiently large spatial extent one may expect that such structures may indeed evolve. Typical places for generation of kinetic Alfvén solitqry structures range from the solar corona close to solar loops to the foreshock of the bow shock of the earth, the magnetopause, the plasmasheet and the auroral magnetosphere. In the latter location it is probable that waves of this kind are excited not locally. Rather they propagate from the plasmasheet into the lower magnetosphere after having been generated at the reconnection site in the plasmasheet. There is little doubt that reconnection is a source of Alfvén waves; however, since it is limited in spatial extent to width of the order of the ion inertial length this is the ideal place for transformation into the kinetic regime. Further transformation is experienced when they travel down to the lower magnetosphere. When becoming large amplitude they evolve into solitons. A parametric investigation shows that those solitons exist over wide ranges of propagation velocities and for different conditions depending on the plasma being composed of a single or more electron components. In realistic cases one will always have a more-component electron plasma and hence the formation of modified kinetic Alfvénic solitary waves. Some of these waves may even propagate at superalfvénic speeds and represent themselves as density holes. the full structure is more complicated since the holes may be expressed in both components or even only in one component only. Either of these cases is of interest. In narrow ranges of parameter space they can be described by the ordinary Korteweg de Vries equations. In this case it is possible to develop a full turbulence theory of such waves that shows that a plasma containing kinetic Alfvén turbulence is energetically harder than when the plasma contains Alfvén waves only. Situations like this may arise in the plasma sheet of the magnetosphere. This turbulence may lead to cause energetic particle spectra. Leaking of some of the waves to the ionosphere will couple it to auroral processes.

H3-4
10:00

LOWER HYBRID SOLITARY STRUCTURES IN THE AURORAL IONOSPHERE

J. Bonnell* G. T. Delory
Space Sciences Laboratory
University of California
Berkeley, CA 94720
P. W. Schuck P. M. Kintner
School of Electrical Engineering
Cornell Univ.
Ithaca, NY 14853
K. Lynch
Univ. of New Hampshire, Durham, NH

Lower hybrid solitary structures (LHSS) are spatially localized regions of enhanced lower hybrid wave power that have been observed by many sounding rocket and satellites in the terrestrial auroral zone. We will present a review of the current observations of LHSS and attendent phenomena, the current success of the eigenmode interpretation of LHSS, as well as currently open and speculative questions about the nature of LHSS.

A hallmark of LHSS is the rotating electrostatic field structure observed within them. This rotating electric field is a coherent, non-plane wave structure, and has been quite successfully interpreted as an eigenmode of lower hybrid waves within a localized density depletion driven via linear scattering of the ambient, longer-wavelength VLF hiss. In addition, LHSS have been observed to be the locus of enhanced electric fields at frequencies below the local lower hybrid frequency. The presence and characteristic counter-rotating nature of the fields above and below the ambient lower hybrid frequrency is again successfully described via the eigenmode theory.

The question of the causal relation between the LHSS and the density depletions often observed in conjunction with them remains open. The original interpretation of LHSS as non-linear structures formed during the collapse of lower hybrid waves was found to be inconsistent with many of the observed properties of LHSS, but did allow for the self-consistent creation of the density depletions found in association with LHSS. The eigenmode interpretation makes no claims about the origin of the density depletions, and merely requires their presence at length scales around and below the ambient electron skin depth (c/ω_{pe}). Fluid simulations of LHSS have found that the ponderomotive effects of the enhanced lower hybrid electric fields are too small to dig density depletions on relevant time scales. Preferential heating of H+ by the enhanced lower hybrid waves has been invoked as a method to self-consistently seed the creation of LHSS. The LHSS are certainly observed to be the locus of perpendicular ion heating, but it is unclear if the expulsion of H+ from the region would allow for the necessary depletion in the electron density required to produce the observed electric field rotations.

H3-5
10:40

THEORY OF LOWER HYBRID SOLITARY STRUCTURES

P. W. Schuck* C. E. Seyler P. M. Kintner
Cornell University
J. W. Bonnell
Space Sciences Laboratory
J. L. Pincon
LPCE/CNRS

Lower hybrid solitary structures are isolated bursts of lower hybrid waves localized in plasma density depletions. Observations of this phenomena by seven sounding rockets and at least two satellites encompass an altitude range of 300-14,000 km. This phenomena is usually associated with bursts of transversely accelerated ions and consequently may contribute to the total outflow of heavy ions from the auroral ionosphere.

Previous theoretical works (Chang, *Phys. Fluids B*, **5**, 2646-2656, 1993; Shapiro et al., *Phys. Plasmas*, **2**, 516-526, 1993), have hypothesized that these observations are the direct result of lower hybrid wave collapse in self-consistent density depletions produced by the ponderomotive action of the waves. Freja observations of lower hybrid solitary structures (Pécseli et al., *Geophys. Res.*, **101**, 5299, 1996) are not consistent with the dynamical relations of lower hybrid collapse. Consequently, lower hybrid collapse is not directly responsible for the simultaneous observations of lower hybrid waves and density depletions.

This work considers the propagation characteristics of lower hybrid waves in the presence of a preexisting plasma density depletion and demonstrates that the observations of lower hybrid solitary structures can be explained in terms of the rotating eigenstates of a cylindrical density cavity. Inside a plasma density depletion, lower hybrid waves above the lower hybrid resonance rotate in a right-handed manner about the geomagnetic field, and lower hybrid waves below the lower hybrid resonance rotate in a left-handed manner about the geomagnetic field. Left-handed waves above the lower hybrid resonance are reflected from the density depletion.

A scattering formalism is developed to explain enhanced electric fields localized within the density depletion. Above the ambient lower hybrid resonance the wave spectrum is continuous and the total scattering cross section exhibits resonance phenomena for right-handed waves. The resonances result in enhanced electric fields localized within the cavity. Below the ambient lower hybrid resonance the states are trapped in the cavity, and in the context of the scattering formalism are three-dimensional bound states.

H3-6
11:00

HF CHIRPS: EIGENMODE TRAPPING IN DENSITY DEPLETIONS

K. L. McAdams*
Space and Atmospheric Sciences
Los Alamos National Laboratory
Los Alamos, NM 87545
R. E. Ergun
Space Sciences Laboratory
University of California at Berkeley
Berkeley, CA
J. LaBelle
Dept. of Physics and Astronomy
Dartmouth College
Hanover, NH 03755

We report high resolution measurements of the frequency-time structure of HF waves just above the electron plasma frequency in overdense conditions, $f_{pe} > f_{ce}$, in the auroral ionosphere. These observations were made on the PHAZE II sounding rocket, launched from Poker Flat, Alaska on Feb 10, 1997. Short duration narrowband emissions (HF chirps) are observed in the topside auroral ionosphere at altitudes of 299-320 km. They have frequencies of 1.8-2.3 MHz which is above the local plasma frequency ($f_{pe} \sim 1.7 - 2.2$ MHz). The emission frequencies of the HF chirps predominantly decrease with time. The most striking feature of the HF chirps is their narrow bandwidth, $\delta f \sim 300-600$ Hz. Typical HF Chirp amplitudes are 1 mV/m, typical durations are 100 ms, and typical frequency-time slopes are 50 kHz/s. The emissions often occur in flocks in which pairs of emissions appear simultaneously at frequencies 300-3000 Hz apart and drift in parallel (McAdams & LaBelle, *Geophys. Res. Lett.*,**26**, 1825-1828, 1999).

We put forth a model of the HF chirp emissions as quasi-trapped eigenmodes resonant in a density depletion (McAdams et al, Submitted to *Geophys. Res. Lett.*, 1999). The escaping waves retain the frequency structure of the eigenmodes when they leave the cavity and are observed as HF chirps. We show that this model is quantitatively consistent with observed characteristics of HF chirps, most notably the frequency spacing of the chirp emissions (0.1-4 kHz) and the fact that these are equally spaced independent of mode number. Several mechanisms for the escape of the waves from the cavity are presented including incomplete trapping, wave "tunnelling" and other non-linear wave mode conversion processes.

H3-7
11:20

REMOTE SENSING OF COHERENT STRUCTURES VIA ELECTROMAGNETIC RADIATION

J. LaBelle*
Department of Physics and Astronomy
Wilder Laboratory
Dartmouth College
Hanover, NH 03755

Recent satellite and rocket observations have shown that wave phenomena in the auroral ionosphere are often composed of coherent structures, such as solitary waves, wave packets, or eigenmodes imposed by pre-existing density structures. In some cases these structures have been confirmed by theoretical studies and plasma simulations. At the same time, ground-based and space-based measurements, sometimes with significantly improved frequency and time resolution, have highlighted previously unappreciated features of radio emissions of auroral origin. For example, auroral roar is a narrowband left-hand polarized emission near two and three times the ionospheric electron cyclotron frequency which exhibits fine structures as narrow as a few Hertz, often occurring in multiplets separated by the order of 1 kHz which drift up and down in frequency. These characteristics may be explained by wave trapping in density structures, as suggested by 1970's rocket measurements of cyclotron harmonic waves in an artificially induced density enhancement. Similarly, auroral HF chirps are narrow band emissions observed above the electron plasma frequency during a recent rocket flight, and these likewise may result from wave trapping in density structures. Other examples of possible remote sensing of coherent structures include auroral MF-burst, a broadband impulsive emission at 1.3-4.5 MHz composed of wave packets as short as 100-300 μs, and recent observations of highly structured whistler mode signals at ionospheric altitudes. The mechanisms for these radiations may be either direct or indirect (mode conversion). In the case of mode conversion radiation, either linear or nonlinear conversion processes may be significant. In either case, it is possible that the spectrum or the radiation reflects the source, potentially providing a means of remote sensing coherent structures in auroral wave phenomena and plasma properties associated with them.

B2-1
13:40

GENETIC ALGORITHM OPTIMIZATION OF A TRAVELING WAVE ARRAY OF LONGITUDINAL SLOTS IN A RECTANGULAR WAVEGUIDE

Anders Jensen* Sembiam Rengarajan
Department of Electrical and Computer Engineering
California State University
Northridge, CA 91330

Slotted waveguide arrays are an important class of microwave antennas with numerous applications in radar and communication systems.

While optimizing a slot array design with respect to any performance-parameter, one is confronted with a multidimensional problem due to a number of slots each having two variables, length and offset. This system exhibits many local minima. Therefore, local optimization techniques such as conjugate gradient and Fletcher-Powell minimization may not be well suited. We investigated the use of a genetic algorithm for optimizing the performance of traveling wave arrays of longitudinal slots and found that it is possible to escape from local minima. It is generally possible to obtain near-optimal designs, starting from an initial design.

We start with the analysis of a single longitudinal shunt slot in the broad wall of a rectangular waveguide. The equivalent shunt admittance of the slot is obtained from the moment method using entire domain expansion and weight functions for the fields in the slot aperture. (L. Josefsson, *IEEE Trans. Antennas Propag.*, **AP-35**, 1351-1357, 1987). The slot data obtained from the moment method are used in the analysis of a linear array by the direct method (M. Hamadallah", *IEEE Trans. Antennas Propag.*, **AP-37**, 817-823, 1989) taking mutual coupling into account (S. Rengarajan, *IEEE Trans. Antennas Propag.*, **AP-40** , 733-737, 1992).

We investigated the optimization of array performance with respect to a number of parameters, e.g. directivity, side lobe level, and input VSWR. For traveling wave arrays, the power dissipated into the load is also subject to minimization. The results of the optimizations show significant improvements with respect to all of those parameters, depending on the cost function that is minimized. We shall present several examples in the conference.

B2-2
14:00

PBG, PMC AND PEC SURFACES FOR ANTENNA APPLICATIONS: A COMPARATIVE STUDY

Zhan Li Yahya Rahmat-Samii
Department of Electrical Engineering
University of California, Los Angeles
Los Angeles, CA 90095-1594

In wireless communications, dipole antennas do not function effectively when positioned closely and parallel above a PEC (perfect electric conductor) ground plane due to the reverse image currents which reduce the radiation efficiency. Ideal PMC (perfect magnetic conductor) ground plane will create the positive image currents of the parallel dipole antenna above it. However, no natural material has ever been found to realize the magnetic conducting surface. In recent years, PBG (photonic band-gap) surface (D. Sievenpiper, C. Lam and E. Yablonovitch, *Applied Opt.*, 37, 2074-8, 1998) has drawn significant attention for its high surface impedance to prevent surface waves and allow in-phase reflection of the incident waves. Metallic photonic band-gap structure also has the advantage of low cost, which provides a good potential for building low-profile and high-efficiency antenna structure.

In this paper, a comparative investigation has been conducted to study the radiation characteristics of dipole antennas closely and parallel above an ideal PEC surface, an ideal PMC surface and a realistic metallic PBG surface. Because of the difficulty with other methods to accurately analyze the surface wave trapped in the PBG structure and the diffraction from the edge, Finite-Difference Time-Domain (FDTD) technique based on the Cartesian coordinate system discretization is chosen as the simulation tool. FDTD is capable of predicting the electromagnetic behavior of intricate antenna structures radiating in a complex environment (M. A. Jensen and Y. Rahmat-Samii, *IEEE Trans. Antennas Propagat.*, 42, 1106-1113, 1994). Since this technique readily handles planar conductors, thin wires and inhomogeneous dielectrics, it could be extended to analyze the effect of human tissue on the antenna structure with PBG surface.

For each case investigated, a finite ground plane is used and both the input impedances and the radiation patterns are computed and compared. As expected, an antenna at 0.02λ above the PEC surface will give very poor performance unless the distance between the antenna and the surface is increased to over 0.1λ. Although having better performance than that of PEC, an antenna at $0.02\lambda - 0.06\lambda$ above PMC surface still suffers from the mutual coupling with its positive image (R. Johnson and H. Jasik, *Antenna Engineering Handbook*, 1984), which will require a careful design of the feeding network. Finally, it is found that an antenna at 0.02λ above 0.04λ-thick PBG surface could have a very good input match to the normal 50Ω cable at the desired frequency. The input impedance properties and the radiation patterns will be presented for various representative cases.

B2-3
14:20

CPW-FED NOVEL WIDEBAND SLOT ANTENNA STRUCTURES

Christopher Holloway, Melinda Piket-May Alpesh Bhobe*
Department of Electrical and Computer Engineering
Campus Box 425
University of Colorado
Boulder, CO 80309

The need for antennas to cover wide bandwidths is of continuing importance, particularly in the field of electronic warefare and wideband radar and measurind systems. In the past fifteen to twenty years this subject has received considerable attention in microstrip antenna technology and as a consequence the bandwidth performance of microstrip antennas has been substantially improved, and it is now possible to design microstrip elements with impedance bandwidth ranging from 10-30 percent. The application of the log-periodic techniques to microstrip series fed arrays suggest that wideband action can be obtained. Operation of the microstrip antennas over multioctave bandwidths have been shown by using electromagnetically coupled patches in a log-periodic series fed array.

Radiation behaviour of slot can be used to create antenna structures. In the recent past considerable effort was spent on the study of slot antennas with coplanar waveguide (CPW) feeds because of numerous advantages like ease of shunt and series connections, low dispersion, low parasitic radiation, and avoidance of the need to for thin fragile substrates. Slot antenna structures have much wider bandwidth as compared to microstrip patch antennas. In this paper we will present some novel CPW fed wideband slot antennas stucrures and also the application of the log-periodic tecnique to CPW fed slot antennas. Method of Moments (MOM) and measured results will be presented.

B2-4
14:40

OPTIMIZATION OF MICROWAVE PARABOLIC ANTENNA SYSTEMS USING SWITCHED PARASITIC FEED STRUCTURES

G. J. Durnan D. V. Thiel* S. G. O'Keefe
Radio Science Laboratory
School of Microelectronic Engineering
Nathan Campus
Griffith University
Brisbane, Qld 4111 Australia

Beam switching in parabolic antenna systems has successfully been demonstrated for use in microwave communication systems to alleviate problems associated with fading events. Applying lateral offsets to parabolic feed points is well documented and the use of the parasitic feed structures has been discussed in this context (Durnan, Thiel, O'Keefe, *Microwave and Optical Technology Letters* , **Nov 20**, 1999). In addition, axial defocusing of feed positions give rise to loss of gain and a broadened main lobe.

In this presentation an examination of parasitic element positioning is performed for all angles of rotation and spacing for the first time. It can be envisaged that particular design requirements can be fulfilled by considering the combination of both axial and lateral offsetting of the parasitics.

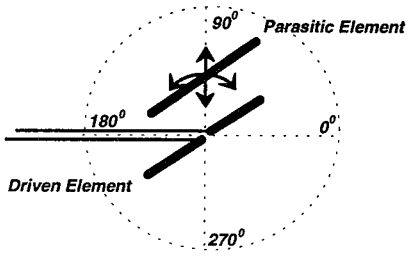

Arrangement of feed array element positioning

Modern optimization techniques are applied for the examination of parasitic element positioning. The methods employed consist of conjugate gradient methods for simple problem solutions and genetic algorithms for solutions where multiple requirements are considered. Simulations were performed at 1, 2 and 3 GHz. When optimized for maximum beam shift in a lateral plane a simple conjugate gradient method yields a parasitic element spacing of 0.6 wavelengths as being the ideal solution.

The switched parasitic technique has advantages in the design of low cost point to point microwave communications. These antennas, when implemented with symmetrical feed structures, feature simple implementation and constant input impedance.

B2-5
15:00

BEAM DIRECTION AND RIPPLE OF APERTURE DISTRIBUTION FOR A CYLINDRICAL SLOT ARRAY ANTENNA FED BY A COAXIAL WAVEGUIDE

Kyouichi Iigusa, Masato Tanaka
Communications Research Laboratory, M.P.T., Japan
E-mail: iigusa@crl.go.jp

We built a paired-slot array antenna on an oversized coaxial waveguide. The resulting antenna was omnidirectional in a plane perpendicular to the cylinder's axis. Using this antenna, we made several circular-polarized antennas whose beams were shaped along the cylinder axis. For example one had a cosecant beam and another had a conical beam with a 45-degree beam tilt and a 20-degree beam width. The radiation pattern along the axis was measured and an equivalent magnetic current distribution of an aperture along the axis was calculated, assuming a perfectly omnidirectional pattern, using the theory of cylindrical near-field antenna measurement. A ripple was observed in both the amplitude and phase. The origin and character of the ripple are analyzed below.

The model we used is shown in Fig. 1. Vertical and horizontal magnetic vectors are excited by the traveling wave in the coaxial waveguide at each pair of slots. We calculated the far-field pattern then recalculated the aperture distribution in the same way as was done for the experimental data. The same ripples as had been seen in the experimental results appeared in the calculated distribution. For a beam tilt antenna, however, the ripple period was different from the experimental results. We found that the calculated period is close to the experimental result if allowance is made for a reflected wave in the coaxial waveguide. For a broadside beam antenna, however, a reflection does not alter the ripple period.

To further study this ripple, we used a simpler model with elements arranged along the cylinder's axis along which a wave travels. We directly calculated the aperture distribution along a line parallel to the axis and at a distance equal to the radius of the cylindrical array antenna. The result is shown in Fig. 2 with dielectric constant ε_r, and reflection rate R as parameters. The ripple's period was found to depend on the tilt angle θ_t of the main beam and on the existence of reflection. The experimental result agrees with the result from this simple model.

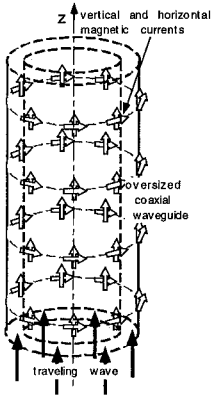

Fig.1 Cylindrical array model

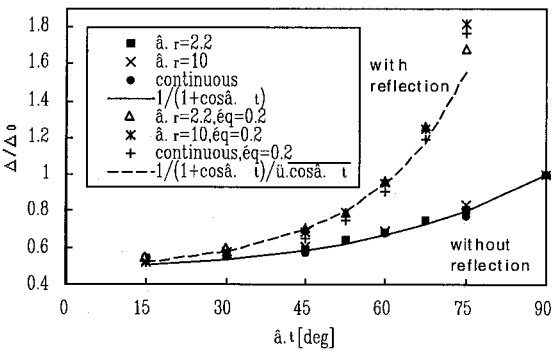

Fig. 2 Ripple period Δ/Δ_0 vs. beam tilt angle θ_t

B2-6 PARASITIC ACTIVE ARRAY ANTENNA FOR WIRELESS COMMUNICATION SYSTEM:
15:40 M. Murato, A. Kishi, S. Ohmori, T. Matsui, Communicatino Research Lab, Toyko, Japan

B2-7 16:00 THEORETICAL STUDY OF THE RESONANT FREQUENCIES OF TRIANGULAR MICROSTRIP RESONATORS

Esmat A.F. Abdallah, Mostafa El-Said, Essam A.Hashish
And Deena A.Salem
Electronics Research Institute, National Research Center Buildings, El Tahrir Street, Dokki, Cairo, Egypt.
Tel: 202 3368584, Fax: 202 3351631, E-mail: esmat@eri.sci.eg

Previous discussions on the resonant frequencies of the triangular microstrip resonators, presented various correction factors to the formula obtained using cavity model with perfect magnetic walls, are valid only for equilateral triangular resonators. In this study, a novel factor is used to cater for fringing field effect in triangular resonators. This factor is valid for both equilateral (symmetric) and non-equilateral (non-symmetric) triangular resonators. The side-lengths of the triangular resonator are replaced by its effective value. Besides, the effective value of the relative permittivity presented by Gang (X.Gang, IEEE-AP-37, No.2, pp.245-247, 1989) is used. In this paper, the problem of triangular resonators is solved using the variational technique. In which the stored energy in the circuit is minimized by imposing the Rayleigh-Ritz condition on a functional, F, which represents the total stored energy in the junction.

A trial function, $\phi_a'(\mathbf{r})$ is introduced as the function which causes the functional, F, to be minimized and should satisfy the Maxwell's equations and the boundary conditions of the original eigenfunction, and is expanded as $\phi_a'(\mathbf{r}) = \sum \mathbf{c}_i \mathbf{N}_i$, where $\mathbf{c}_i$ denote the complex expansion coefficients (eigen vectors) to be determined, $\mathbf{N}_i$ are real basis functions which are defined by the finite element method using quadrilateral isoparametric elements. The minimization process results into a set of simultaneous homogenous equations.

When the planar circuit has no coupling ports, i.e. in the case of an isolated resonator, the nontrivial condition of the obtained simultaneous equations give the resonant frequencies of the different modes that exist in the resonator. Considering the fact that it is always possible to inscribe a circle radius, R, in any triangle, using an empirical formula to account for the effective radius, $\mathbf{R}_{eff}$, (N. Kumprasert and W. Kiranon IEEE-AP-43, No.11, pp.1331-1333,1995) of the inscribed circle, and relating this effective radius to the effective side-lengths of the triangle yields the factor used in this paper to account for the fringing effect in triangular resonators.

To show the validity of this procedure the resonant frequencies of equilateral triangular resonators are first determined for different dielectric relative permittivity and several substrate thicknesses and the results are compared with previously published results (W. Chen, et. al, IEEE-AP-40, No.10, pp.1253-1256, 1992), from which it is observed that the difference between theory and experiment shows around 1% for $\varepsilon_r = \mathbf{2.32}$ and around 2% for $\varepsilon_r = \mathbf{10.5}$. Finally, the procedure is used to obtain the resonant frequencies of shapes other than equilateral triangular resonators, namely: 1. Equilateral triangular resonator with curved vertices for different curvature ratios (α). 2. Isosceles triangular resonators.
These results are the first published ones, to the knowledge of the authors, for these general shapes of the resonators.

Session H4, 13:55-Sat., Room 265
WAVES AND COHERENT STRUCTURES IN THE IONOSPHERE AND THE MAGNETOSPHERE

Chairperson: J. LaBelle, Dartmouth (jlabelle@einstein.dartmouth.edu)

H4-1
14:00

A STATISTICAL STUDY OF LARGE AMPLITUDE SOLITARY WAVE CHARACTERISTICS USING DATA FROM THE POLAR SATELLITE

C. Cattell J. Dombeck J. Wygant
School of Physics and Astronomy, University of Minnesota
Minneapolis, MN 55455
F. Mozer
Space Sciences Lab, University of California
Berkeley, CA 94720
C. Kletzing
Dept. of Physics and Astronomy, University of Iowa
Iowa City, IA

Large amplitude solitary waves, $e\phi/kT \sim 1$, have been observed in several distinct regions of the Earth's magnetosphere (Mozer et al.,*Phys. Rev. Lett.*,**79**,1281, 1997; Ergun et al., *Geophys. Res. Let.*,**25**, 2014,1998; Cattell et al., *Geophys. Res. Let.*,**26**,425,1999). These regions include the auroral zone, the high altitude cusp, at 5-9 Re, and the plasma sheet boundary, at 4-7 Re. In the low altitude auroral zone case, two different types have been identified. In the upward current regions, the observed solitary waves are believed to be rarefractive ion acoustic modes. This view is supported by the identification of these solitary waves as negative potential structures moving upward with associated ion beams at a few hundred km/s, near the ion acoustic speed. In contrast, solitary waves in the downward current regions move upward at several thousand km/s, are positive potential structures, and are associated with upward electron beams (Ergun et al., 1998; Bounds et al., *J. Geophys. Res.*, in press,1999). This evidence suggests an electron rather than an ion mode. Preliminary results of studies of large amplitude solitary waves in the high altitude regions, including velocities >1000 km/s, also seem to be consistent with an electron mode (Cattell et al., 1999). Analysis of amplitude versus parallel spatial width of solitary waves in the downward current auroral zone has indicated that these faster structures are more likely a BGK mode rather than a soliton (Ergun et al., 1998). Within a related family of solitary waves, the amplitude scales as the fourth power of the width for BGK modes while it scales inversely to the square of the width for acoustic modes (Muschietti et al., *Geophys. Res. Let.*,**26**,1093,1999). Such analysis, therefore, is extremely useful in distinguishing between BGK hole modes and acoustic solitons. We will describe the methodology and results of a statistical study of solitary wave characteristics in the upward current auroral zone. The results will be compared to compared with expectations from ion acoustic theory. Characteristics studied include amplitude versus parallel spatial width, parallel and perpendicular extent, and structure velocity. Similar studies of electron mode solitary wave at the high altitude plasma sheet boundary will also be described.

H4-2
14:20

THE ROLE OF SPATIALLY-COHERENT STRUCTURES IN THE AURORA

R. E. Ergun*
Space Sciences Laboratory
University of California
Berkeley, CA 94720

Large-amplitude, spatially-coherent, plasma structures known as fast solitary structures or electron phase space holes have been observed in several regions of the magnetosphere including the auroral zone, the plasma sheet boundary layer, and the bow shock. These recent observations have sparked several new theoretical investigations resulting with rapid progress in understanding these structures. Electron phase space holes can develop from bidirectional electron beams. Once developed, the one-dimensional properties, parallel to the magnetic field, can be adequately described by analytical treatment as BGK structures. The three-dimensional structures can lead to strong ion heating. There is evidence that the structures dissipate by radiating whistler waves. In this talk, we summarize observations of electron phase space holes from the Fast Auroral SnapshoT (FAST) satellite and discuss the role they play in the auroral acceleration processes. We show that ion acoustic turbulence, ion cyclotron emissions, and solitary structures can play an important role in modifying the current-voltage relationship in the downward current region of the aurora through heating electrons and ions. These two heating processes result from the same electromagnetic emissions but have differing effects on the parallel electric fields.The parallel electric fields in the downward current region arise to maintain a magnetosphere-driven current in a quasi-neutral plasma. Electron heating, parallel to the ambient magnetic field, causes a loss of electron momentum (and thus current) which acts to increase the parallel electric fields. Ion heating, perpendicular to the ambient magnetic field, results in escaping ion fluxes which can restructure the plasma density and ultimately acts to decrease the parallel electric fields. The resulting parallel electric fields are greatly influenced by these competing effects.

H4-3
14:40

ANALYSIS AND SIMULATION OF BGK ELECTRON HOLES

L. Muschietti* I. Roth, R.E. Ergun, C.W. Carlson
Space Sciences Laboratory
University of California
Berkeley, CA 94720

Recently, several satellites have reported the presence of rapidly-moving solitary potentials. The structures appear as positive potential spikes moving along the ambient magnetic field $\mathbf{B_0}$ with speeds much greater than the ion acoustic velocity; they have the electromagnetic signature of a positive charge surrounded by a negative cloud. These observations have been interpreted in terms of BGK electron holes.

The holes, also known as phase-space vortices, are exact, nonlinear solutions of the Vlasov-Poisson system of equations that involve a clump of trapped electrons. The associated density inhomogeneity creates a positive potential hump that self-consistently traps the electrons, resulting in a BGK mode. Such interesting plasma entities have been observed in simulations of the two-stream instability since the early days.

We construct a BGK electron hole which displays the characteristics of the potentials and electron distributions measured by the FAST satellite in the mid-altitude auroral zone. The distributions are "cigar-shaped" with $T_{\|} \gg T_{\perp}$ while the potentials have a gaussian profile parallel to $\mathbf{B_0}$. The nonlinear structure is tested in a two-dimensional particle-in-cell code. In particular, we exploit the code to investigate the role of the transverse direction (perpendicular to $\mathbf{B_0}$). Two questions need to be addressed. First, although the electrons are strongly magnetized and their motion restricted to the direction of $\mathbf{B_0}$, the potential structures observed by FAST have a definite transverse scale. What determines this scale is studied in various parameter regimes. Second, early simulations of electron holes associated with the two-stream instability suggested that the vortex structure is unstable in more than one spatial dimension. How stable is indeed the structure?

The electron hole is found to be very stable as long as the cyclotron frequency is larger than the bounce frequency of the trapped electrons, namely $\Omega_e > \omega_B \equiv \sqrt{q\psi/(m\Delta^2)}$ where ψ is the potential amplitude and Δ its half-width parallel to $\mathbf{B_0}$. On the other hand, when the reverse inequality is satisfied, $\omega_B > \Omega_e$, an undulation builds up in the transverse direction distorting the structure and leading to its destruction.

H4-4
15:00

LONG-TIME NONLINEAR EVOLUTION OF BIPOLAR ELECTRIC FIELD STRUCTURES IN THE AURORAL IONOSPHERE

D. L. Newman* M. V. Goldman M. Spector
CIPS, Campus Box 390
F. Crary
LASP, Campus Box 392
University of Colorado, Boulder, CO 80309
M. M. Oppenheim
Department of Astronomy,
Boston University, Boston, MA 02215

Bipolar electric field structures are a natural consequence of counter-streaming electrons in a magnetized plasma (M. V. Goldman, M. M. Oppenheim, and D. L. Newman, *Geophys. Res. Lett.*, **26**, 1821, 1999) such as the auroral ionosphere at the altitudes probed by FAST, where such bipolar fields have been measured (R. E. Ergun, et al., *Geophys. Res. Lett.*, **25**, 2044, 1998). Two-dimensional kinetic simulations (both PIC and Vlasov) show that these field structures, which early-on show significant coherence perpendicular to **B**, eventually break up in association with the production of electrostatic whistlers (M. M. Oppenheim, D. L. Newman, and M. V. Goldman, *Phys. Rev. Lett.*, **83** No. 12, 1999).

The interaction of the bipolar structures with the whistlers appears to result from a resonant coupling of the whistlers to normal "vibrational" modes of the electron phase-space holes associated with the bipolar electric fields. When the natural frequency of these vibrations is near the whistler frequency, both the vibrations and the whistlers can grow in amplitude. However, when the whistlers are suppressed, these vibrational modes are damped. Numerical and analytical support for such interactions will be presented, as well as a discussion of potential observational implications.

At still later times, other wave modes appear in the PIC simulations, including ion-cyclotron (Bernstein) modes driven by residual free energy in the particle distributions following the saturation of the initial two-stream instability. The frequencies of these waves are also consistent with spectra measured by FAST.

Research supported by NSF. Computations performed at the LANL Advanced Computing Laboratory and at the National Center for Atmospheric Research.

H4-5
15:40

NONLINEAR WAVES AND PROCESSES IN THE EXTERIOR CUSP

J. S. Pickett, J. D. Menietti, and D. A. Gurnett
Department of Physics and Astronomy
The University of Iowa
Iowa City, IA 52242

Nonlinear processes routinely occur in the turbulent boundary layer (TBL) that lies just outside the magnetopause current layer in the earth's exterior cusp. A greater understanding of these processes is being gained through analysis of waveform data obtained by the Plasma Wave Instrument (PWI) onboard the Polar spacecraft. Three orthogonal electric and magnetic field waveforms are captured simultaneously in the form of snapshots every few seconds by each of two PWI waveform receivers covering the frequency ranges of 1 to 25 Hz and 20 Hz to 25 kHz, respectively.

Examples of nonlinear waves and waves involved in nonlinear processes in the TBL will be presented and discussed, including low frequency turbulence (~1-10 Hz), electrostatic solitary pulses or coherent structures, and electrostatic wave bursts (2-12 kHz) associated with ~300-400 Hz whistler mode waves, and electron cyclotron harmonic waves. Various analysis techniques will be utilized in the time domain to gain information about these impulsive waves and processes, including minimum variance analysis to obtain the k-vector and polarization, direct calculation of the average Poynting vector, and wavelet analysis, which is localized in time and frequency space, since we are dealing with nonstationary time series. The results of these analyses will be used to help identify wave modes, instabilities, and location of wave generation. Some Polar spacecraft electron data will be presented in order to establish the possibility of electron anisotropies and wave-particle interactions as a means to wave generation.

H4-6
16:00

FIRST RESULTS FROM A NEW INTERFEROMETER USED TO STUDY AURORAL RADIO EMISSIONS

J.M. Hughes* J. LaBelle M.L. Trimpi
Department of Physics and Astronomy
Dartmouth College
Hanover, NH 03755

A Medium Frequency Interferometer (MFI) has recently been developed for the purpose of studying auroral radio emissions which occur in the frequency range from 2.5 to 3.0 MHz. In its standard operational mode, the MFI sweeps from 2.5 to 3.0 MHz in 1 kHz steps every 1.5 seconds, measuring the intensity of the recived signal and the relative phase at each of the 17 antennas in the array. The phase information can be used to determine the directon of arrival for any signal in the instrument bandwidth to within $\pm 5°$.

The MFI is located at the Sondrestrom Incoherent Scatter Radar site near Kangerlussuaq, Greenland and has recorded the directions of arrival for many auroral roar events which occured during the spring and fall of 1999. Auroral roar is a narrowband emission occuring near 2 and 3 times the local ionospheric electron gyrofrequency (f_{ce}). To date, all but two of the detected events originated to the south of the radar site, a result which is consistent with previous studies of the latitude dependence of auroral roar. Recent observations with the MFI have shown that individual events are often composed of signals which originate from multiple discrete source regions. On the night of April 28, 1999, ISR data are available for comparison and appear consistent with one proposed generation mechanism which postulates that auroral roar at $2f_{ce}$ is generated when the matching condition $f_{uh} = 2f_{ce}$ is met. These initial results are encouraging and indicate that the MFI is a valuable tool for studying auroral radio emissions. We present here a description of the instrument and show some example data from the first two seasons of operation.

Session H5, 13:55-Sat., Room 245
DUSTY PLASMAS
Chairperson: M. Horanyi, Univ. of Colorado (horanyi@styx.colorado.edu)

H5-1
14:00

DUSTY PLASMA EFFECTS IN PLANETARY MAGNETOSPHERES

M. Horanyi*
Laboratory for Atmospheric and Space Physics
University of Colorado
Boulder, CO 80309-0392

The study of dusty plasmas bridges traditionally separate subjects: celestial mechanics and plasma physics. Dust particles immersed in plasmas and UV radiation collect electrostatic charges and respond to electromagnetic forces in addition to all the other forces acting on uncharged grains. Simultaneously they can alter their plasma environment. Dust particles in plasmas are unusual charge carriers.They are many orders of magnitude heavier then any other plasma particles and they can have many orders of magnitude larger (negative or positive) time dependent charges. Dust particles can communicate non- electromagnetic forces (gravity, drag, radiation pressure) to the plasma that can represent new free energy sources. The Jovian magnetosphere shows a number of dusty plasma phenomena. The ring/halo region close to the planet, allows for the remote sensing of the fields and particles environment of the inner most regions of the magnetosphere. The dust streams, seen by Ulysses and Galileo, put constraints on the plasma properties of the Io torus, for example. The magnetosphere sculpts the size and spatial distribution of the small grains often resulting in capture, transport, energization and ejection of the dust particles. In this talk The analysis of the observations of the Galileo Dust Detector System (DDS) requires extensive computer simulations for the interpretation of the data. These simulations require a detailed description of the fields and particles environment and provide a unique consistency test of our models of the jovian magnetosphere.

The DDS observations indicate at least 3 different populations of dust grains in the jovian magnetosphere: 1) very small and very fast stream particles, 2) prograde big grains related to satellites and 3) big grains unrelated to satellites, some on retrograde orbits. In addition to the analysis and interpretation of these DDS observations we will also provide numerical models of the jovian ring/halo region. The SSI and NIMS observations provide detailed new information on the spatial structure and size distribution of small dust particles in this region. These observations will be used to infer the plasma conditions near Jupiter where no measurements are available.

H5-2
14:20

ATMOSPHERE-IONOSPHERE LASER PLASMA COLUMN GENERATION

R.F.Wuerker*
UCLA Plasma Physics Laboratory
Los Angeles, CA 90095-1547

We would like to present a method of using high power laser and a rotating liquid mirror to generate sufficient intensity in the atmosphere to effect the production of plasmas in the lower and upper atmosphere. The motivation is to generate a reproducible artificial ionosphere which will help us understand the physics of plasmas of large extent. Other applications include controlled modification of the conductivity and reproducible scattering by an ionosphere.

The laser breakdown of gases is greatly reduced by the presence of dust. Also the emission of plasma from solid targets occurs for laser fluxes greater than 100 MW per square cm (J.F.Ready, Effects of High Power Laser Radiation, Academic Press, 1971). Calculations show that such fluxes can be realized up to 100 km altitudes when infrared nanosecond laser radiation is focused by a 2.7 m diameter diffraction limited telescope, such as the Liquid Mirror Telescope already at the HIPAS Observatory in Alaska. Calculations also show that there is also enough meteor generated particulate to initiate laser breakdown up to 100 km altitudes. A theory of optical propagation through the atmosphere (T.S.McKechnie, Sky and Telescope, 36-38, August 1994) further predicts a diffraction limited core at either 1.52 or 2.2 micron wavelengths. Surplus NOVA 1.05 micron 100 J laser amplifiers could result in the assembly of a Raman shifted system that could create long plasma columns in the sky which could be used as plasma antennas, VLF/ELF generators, etc. Laboratory experiments will be presented which demonstrate that dusts can indeed be ionized at a certain distance determined by the focal length of the laser. The depth of focussed location can be varied and controls the length of ionization.

H5-3
14:40

DSD - A PARTICLE SIMULATION CODE FOR MODELING DUSTY PLASMAS

G. Joyce* M. Lampe G. Ganguli
Plasma Physics Division
Code 6790
Naval Research Laboratory
Washington, DC 20375

The NRL Dynamically Shielded Dust code (DSD) is a particle simulation code developed to study the behavior of strongly coupled, dusty plasmas. The model includes the electrostatic wake effects of plasma ions flowing through plasma electrons, collisions of dust and plasma particles with each other and with neutrals. The simulation model contains the short-range strong forces of a shielded Coulomb system, and the long-range forces that are caused by the wake. It also includes other effects of a flowing plasma such as drag forces. Magnetic fields may also be included in the formalism. In order to model strongly coupled dust in plasmas, we make use of the techniques of molecular dynamics simulation, PIC simulation, and the "particle-particle/particle-mesh" (P3M) technique of Hockney and Eastwood. We also make use of the dressed test particle representation of Rostoker and Rosenbluth. Many of the techniques we use in the model are common to all PIC plasma simulation codes. The unique properties of the code follow from the accurate representation of both the short-range aspects of the interaction between dust grains, and long-range forces mediated by the complete plasma dielectric response. If the streaming velocity is zero, the potential used in the model reduces to the Debye-Huckel potential, and the simulation is identical to molecular dynamics models of the Yukawa potential. The model basically represents the dust as simulation particles interacting via the dressed potential. The plasma appears only implicitly through the plasma dispersion function, so it is not necessary in the code to resolve the fast plasma time scales.

Research supported by NRL.

H5-4
15:00

NON-LINEAR VERTICAL OSCILLATIONS OF A DUST PARTICLE IN AN RF PLASMA SHEATH

A. Ivlev, V. Steinberg K. R. Sütterlin*
Max Planck Institut für extraterrestrische Physik
Giessenbachstraße
PO Box 1603
85740 Garching
Germany

For our experiments we used a Gaseous Electronics Conference (GEC) rf Reference Cell. Argon gas at pressure 0.5 Pa was used for discharge. A single spherical silica particle of 7.6 μm diameter was levitated in the sheath of the lower electrode. We excited the particle applying a sinosoidal potential to a wire parallel to the electrode.

We measured the dc offset and peak-to-peak voltage and the peak-to-peak current to the lower electrode. We did not measure any dependency of the lower electrode potential on U_w. Therefore, we conclude that the vertical oscillations are caused by a direct excitation from the wire.

For several wire positions we measured the amplitude-frequency dependence of particle oscillations for different values of U_w. The frequency was increased from 0.1 up to 40 Hz in 0.1 Hz steps, and then decreased to 0.1 Hz. The obtained curves for the vertical oscillations clearly exhibit non-linearity. Three maxima were observed: The main maximum corresponds to a resonance on the eigenfrequency $f_0 \simeq 17Hz$ of a small vertical oscillation, whereas the second and the third maxima lie close to $\frac{1}{2}f_0$ and $2f_0$. With increasing U_w, the main maximum shifts to smaller f, and when U_w reaches a certain value, hysteresis appears. The resonance at $2f_0$ exists only if the excitation voltage exceeds a threshold. In this case, the amplitude varies differently with increasing and decreasing f. For increasing f the amplitude jumps at a certain f_A from zero-level to a finite value, then continuously decreases to zero-level at f_B. On the way back, the oscillations start at f_B, the amplitude increases along the same branch till f_A, but then proceeds to increase further with decrease of f.

We fitted the obtained curves by the analytical expressions for the amplitude of anharmonic forced oscillations. This procedure allowed us to determine the profile of the sheath electric field in a relatively wide ($\simeq$ 10 mm) region around the particle levitation level. We suggest that the method of the non-linear particle oscillations is an effective way to study the sheath and sheath-presheath structure.

H5-5
15:40

CAPTURE OF INTERPLANETARY AND INTERSTELLAR DUST BY PLANETARY MAGNETOSPHERES

J. E. Colwell* M. Horányi
Laboratory for Atmospheric and Space Physics
Campus Box 392
University of Colorado
Boulder, CO 80309

Planetary magnetospheres are continuously pelted by a broad size distribution of interplanetary dust particles. In addition, the solar system moves through the interstellar medium which includes small (micrometer-sized) dust. These particles become charged in the solar wind and move under the influence of gravity, radiation pressure, and the Lorentz force. When these particles enter planetary magnetospheres, their charges are also affected by currents from the local plasma environment. As these particles traverse regions of the magnetosphere with rapidly varying plasma properties, they may exchange energy and angular momentum with the magnetosphere because their charges are not always in equilibrium with the local plasma. Some small grains may become trapped into long-lived orbits by this process. If the planets magnetic pole is co-aligned with the rotation axis, then the co-rotational electric field can help balance the gravitational force on the grains, leading to capture. At Jupiter, interstellar as well as interplanetary grains can be captured. At Jupiter, most captured grains are on retrograde orbits and some have been detected by the Galileo DDS (Colwell *et al.*, *Science* **280**, 88-91, 1998). The capture mechanism operates at Saturn as well, but less efficiently. Interstellar dust is not likely to be captured at Saturn due to high relative velocities between the dust and Saturn. The capture process is size-dependent, with very small grains prevented from penetrating the magnetosphere and larger grains relatively unaffected by non-gravitational forces. We describe the dynamics of captured exogenic dust at Jupiter and Saturn based on numerical integrations of test particle trajectories, beginning with realistic interplanetary and interstellar dust particle orbits.

H5-6
16:00

DUSTY PLASMA EXPERIMENTS RELATING TO MESOSPHERIC AEROSOLS

B. Smiley,* S. Robertson M. Horanyi Z. Sternovsky
University of Colorado, Boulder, CO 80309-0392

Rocket-borne probes in the polar mesosphere have seen charged aerosol layers at the locations of noctilucent clouds. These layers are thought to arise from plasma charging or photoelectric charging of nanometer-sized ice crystals which may have meteor dust as the nucleation center.

An experiment has been constructed to examine these charging processes. Ice crystals with 4 to 11 water molecules are generated by a supersonic nozzle and injected into an experimental chamber having energetic electrons, plasma or ultraviolet illumination. A magnetic mass analyzer is used to detect the charged clusters. Initial experiments have examined charging by energetic electrons and experiments on photoelectric and plasma charging are in progress. The typical expansion speed of the water vapor is on the order of 0.5 km/s, similar to a typical rocket speed through NLC layers at $\tilde{8}5$ km altitude. The nucleated ice crystals reach the bottom of the chamber with similar velocities, hence the experiment can be used in the future as an excellent calibration facility.

In a separate study, a new type of electrostatic probe with a magnetic field to prevent electron collection was launched into the ionosphere from White Sands, 2 November 1998, and a positively charged layer 0.5 km thick was observed at 86.5 km. This was probably a sporadic-E layer associated with ionized meteoric material.

In this talk we will report on the continuing analysis of the data from our first rocket flight and also on our future plans for rocket-borne experiments. We will also discuss the status of our experimental NLC chamber and the recent theoretical studies related to dusty plasmas in the mesosphere.

H5-7
16:20

EXPERIMENTAL PHOTOELECTRIC CHARGING OF DUST PARTICLES

A. A. Sickafoose* S. Robertson J. E. Colwell M. Horanyi
LASP
University of Colorado
Boulder, CO 80309-0392

Illumination of surfaces in space by solar ultraviolet light produces photoelectrons which form a plasma sheath near the surface. Dust particles on the surface can acquire a charge and be transported horizontally and vertically by electric fields within the sheath. On the moon, suspended dust grains have been observed on multiple occasions, and there is evidence for horizontal lunar dust transport. Understanding the photoelectric charging properties of dust can help explain the observed dynamics of lunar dust and help predict the behavior of dust on surfaces of planetary satellites, asteroids, planetary ring particles, and planetesimals. In addition, any human or spacecraft activity on planetary bodies is affected by dust dynamics near the surface.

We have examined the charging of dust 90-106 μm in diameter dropped through UV illumination and dropped past a UV illuminated surface having a photoelectron sheath. Experiments are performed in vacuum with illumination from a 1 kW Hg-Xe arc lamp having a spectrum extending to $\sim$ 200 nm ($\sim$ 6.2 eV), and the photoemitter is a 12 cm diameter zirconium plate. We present and compare the photoelectric charging properties of zinc, copper, graphite, lunar regolith simulant (JSC-1), and Martian regolith simulant (JSC Mars-1). We find that the charge on the elemental materials is consistent with the expected charge calculated from the work function of the materials, the energy of incoming photons or photoelectrons, and the capacitance of the grains. Dust dropped through UV illumination loses electrons due to photoemission, while dust dropped past an illuminated surface gains electrons from the photoelectron sheath. The results also suggest that JSC Mars-1 is more susceptible to photoelectric charging than JSC-1. This research is supported by NASA.

INDEX